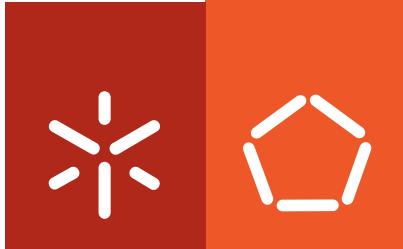Universidade do Minho
Escola de Engenharia

Daniela Fernandes Coutinho

Micro/nano-scale strategies for engineering in vitro the cellular microenvironment using biodegradable biomaterials

Outubro de 2011

Universidade do Minho
Escola de Engenharia

Daniela Fernandes Coutinho

Micro/nano-scale strategies for engineering in vitro the cellular microenvironment using biodegradable biomaterials

Programa Doutoral em Bioengenharia

Trabalho efectuado sob a orientação de:
Professor Nuno M. Neves
Professora Manuela E. Gomes
Professor Ali Khademhosseini

Outubro de 2011

Daniela Fernandes Coutinho

"Põe quanto és no mínimo que fazes."

Ricardo Reis

Although it is my name that comes on the front cover of this thesis, the work here described would have never been possible if it wasn't for the help and understanding of my supervisors, my friends and my family. To all the people that somehow were involved in making this thesis possible, I am deeply grateful. Although many names will be left unsaid, I need to highlight some of the people that directly contributed to my welfare during this period of my life.

I would like to start by acknowledging my supervisor, Professor Nuno Neves, for advising me throughout my PhD and for giving me the freedom to pursue my ideas, helping me on becoming a more independent researcher. Besides his obvious scientific input, he has always pushed me to excel and to think beyond the obvious. I would like to show my appreciation for his constant encouragement and guidance.

I am also deeply grateful to Professor Manuela Gomes, who has co-mentored me during these 3 years. I am thankful for her vision of a PhD being more than learning new techniques and finding new results, seeing it also as a way to broaden our horizons and as a preparation for the competitive scientific world. She was always prepared to assist me whenever needed and to pursuit what were the best interests for me. For all that I am truly grateful.

I would also like to acknowledge Professor Ali Khademhosseini for accepting to be my co-supervisor and for allowing me to work at his prestigeful lab. It is a pleasure to have been mentored by someone as passionate for science as him. I am deeply grateful for his guidance and for being a constant source of inspiration. His enthusiasm, strength and desire to do better and better have certainly motivated me to constantly give the best of myself in anything I do.

To Professor Rui Reis, the Director of 3B's Research Group, I express a special recognition for believing in me and for showing that only by working hard and by 'wearing the team's colors' one can succeed in science, as in life. I am truly grateful for the opportunity of doing my PhD at his internationally recognized lab and for all the important advices he gave me throughout these years.

A special word of appreciation goes to Professor Eugénio Ferreira. Despite his full agenda, he has always been helpful in solving all the bureaucratic issues related to my PhD. Finishing the thesis in due time was only possible because of his promptitude in solving those problems.

Doctor Shilpa Sant, who has not only been my lab mentor, but also my friend, also deserves a special acknowledgment. The work on this thesis would have never been possible if it wasn't for our long but fruitful discussions. Thank you for the constant help and useful scientific inputs.

Although evident, I would also like to thank all the co-authors of the works described in the thesis. It would have never been possible to accomplish the results and conclusions reported if it wasn't for the team-work, which I truly believe is crucial in any scientific project.

Although this journey has not been that long in time, it allowed me to meet incredible people who in their specific way helped me escaping from the frustrations faced throughout this PhD.

To my fellow students from the MIT-Portugal Program, thank you for all the fun moments we've had throughout our lovely country and overseas. I hope Melcões will be seeing us again shortly…

The period I've spent in Boston was certainly one of the best of my life, and the people I've met had for sure a major contribution for that. The names are too many to write here. In special to my friends Amir F., Javier, Nasser, Gülden and my dearest friend Onur, thank you for introducing me to the MIT drinks, for your friendship and for all your efforts for making me feel at home. I am particularly thankful to my roomies and friends João and Daniela. Thank you for making the time in Boston amazing, for all the small good surprises you've made me, for the walks next to the Charles river, and for all the moments we've shared in our cozy apartment with the craziest landlord.

To my 3B's colleagues, a word of appreciation for sharing with me your knowledge and time (and your patience). To the 'bar do Lip' gang, thank you for getting me back on board once I came back to Portugal. To the MT, especially to Joana, thank you for helping me with the bureaucratic questions that always took too much of our time.

I would like to thank the ones that have been fighting this battle along with me, Cristina, Ana Mendes, thanks for dealing with my meltdowns in these last few months… The moments of 'therapy' were crucial for writing this thesis. A special thank you to my dear friend Vitor who has been by my side since the beginning of this PhD. Even when 13 hours were separating

our craziness, we've managed to introduce each other to, let's say, peculiar songs. Thank you for all the silly moments we've had that always made me see the bright side of life.

To my dear 'old' friends… thank you for always being by my side! To Alexandrina, thank you for celebrating my achievements and for giving me strength in the hardest moments. For visiting me in Boston and, more importantly, for always managing a way to get us tickets for our FCPorto games.

I can't go on without expressing a warm appreciation for all the help, comprehension and friendship that I've always had from Mariana. Without any doubt, she is the responsible for keeping me sane during this PhD. *I see the ice is slowly melting… Here comes the sun…*

To my portista, '*cause you are my medicine when you're close to me*, thank you.

I am profoundly grateful to my mother, to my father and to my brother. This thesis is dedicated to them. Thank you for your unconditional support and love. There are no words to describe the luck I have for having a father, a mother and a brother like you.

MICRO/NANO-SCALE STRATEGIES FOR ENGINEERING IN VITRO THE CELLULAR

MICROENVIRONMENT USING BIODEGRADABLE BIOMATERIALS

Abstract

Biological tissues result of a specific spatial organization of cells, extracellular matrix (ECM) molecules, and soluble factors. These micro and nanoscaled biological entities organize into regional tissue architectures, creating highly complex and heterogeneous cellular microenvironments. To generate functional tissue equivalents *in vitro*, engineered biomaterials should mimic the structural, chemical and cellular complexity by recapitulating the unique native microenvironments. Thus, the main goal of this thesis was to engineer biodegradable polymers using various micro and nanofabrication techniques, with specific structural, biochemical and cellular cues for improved performance.

The main governing hypotheses of this thesis were: 1) substrates with improved structural properties can be engineered using biodegradable polymers that have previously shown good results in *in vivo* studies, 2) biochemical cues can be incorporated into biodegradable polymers, yielding biomaterials with integrated chemical cues for improved cellular performance, and 3) these structural and biochemical cues can be incorporated into a single system.

To develop biomaterials with structural cues, micromolding of poly(butylene succinate) (PBS) was performed to engineer surfaces with features at a microscale that induced the alignment of human adipose stem cells. Although this polymeric material has been processed at a macroscale into scaffolds, this was the first report on the engineering of this material at a microscale, demonstrated by the development of twenty features with different dimensions.

Improved substrates with structural cues were also engineered using the polysaccharide gellan gum (GG), which has been extensively studied at 3B's Research Group. Microcapsules of GG, aimed at being used as drug or cell carriers and/or delivery agents, were engineered using a two-phase system. The principle of hydrophobic-hydrophilic repulsion forces was combined with a microfabrication process by means of a needle/syringe pump system. Microcapsules with different diameters were produced by varying the system parameters. As an original proof-of-concept, fluorescent beads, cell suspensions and cell aggregates were encapsulated within this microfabrication system.

To develop biomaterials with enhanced biochemical cues, GG was chemically modified with ester bonds, yielding novel hydrogels crosslinkable by ultraviolet (UV) light. Methacrylated GG (MeGG) hydrogels were formed using physical and chemical mechanisms resulting in hydrogels with tunable mechanical properties, matching those of natural tissues from soft to hard, as the brain or collagenous bone. In a subsequent step, this material was combined

with chitosan (CHT), a natural polysaccharide, resulting in a polyelectrolyte complex (PEC) hydrogel that combined the most advantageous properties of CHT and MeGG. PEC hydrogels are commonly formed by the interaction between the chains of oppositely charged polymers and are thus held together by ionic forces, which can be disrupted by changes in physiological conditions. However, in our new system, the biochemical cues earlier introduced in GG, allowed to crosslink the MeGG-CHT hydrogel using UV light, stabilizing the structure of the hydrogel. This rather important property also enabled for the development of microgels by photolithography. The encapsulation of rat cardiac fibroblasts within MeGG before PEC hydrogel production, led to the fabrication of microgels with combined biochemical, structural and cellular cues.

The developed MeGG-CHT hydrogel was further engineered into a multi-hierarchical fibrous hydrogel by means of combining fluidics technology and chemistry principles of the interaction of two oppositely charged polymers. Two converging fluidic channels were used to extrude the MeGG-CHT hydrogel, formed by the assembly of the polymeric chains at the location where the channels converged. The resulting hydrogel closely mimicked the architecture of natural collagen fibers not only at a micro but also at a nanoscale. The developed hydrogel with relevant biological structural properties was enhanced by incorporating cell adhesive motifs (RGD peptides) into the MeGG backbone before processing.

The research work described in this thesis addresses strategies to mimic several parameters of the native microenvironment of tissues. Biochemical and cellular cues were incorporated into biomaterials that were microprocessed with relevant biological micro and nanoscale features. In summary, the works reported in this thesis show the importance of combining different areas of knowledge into the development of improved systems for biomedical engineering applications. Undoubtfully, chemistry and micro and nanofabrication technologies are two areas of knowledge that allow the fabrication of micro and nanostructured materials. Herein, this synergy was achieved with a top-down approach (by micromolding, photolithography or fluidics technologies) and/or with a bottom-up approach (by the assembly of polymer chains). The last work of this thesis is the result of the original combination of both approaches for the development of enhanced micro and nanostructured biomaterials, thus presenting significant improved features compared to currently developed systems to be successfully used in several regenerative medicine approaches.

Resumo

A funcionalidade dos tecidos biológicos está associada à organização espacial de células, à composição e distribuição de moléculas da matriz extracelular e a outros componentes solúveis. Estas entidades biológicas à escala micro/nanométrica organizam-se em arquitecturas locais específicas, criando micro-ambientes celulares complexos e heterogéneos. Existe portanto um grande interesse no desenvolvimento de equivalentes funcionais dos tecidos humanos usando biomateriais de modo a mimetizar a complexidade química, estrutural e celular. Acredita-se que estes biomateriais poderão recapitular as características únicas dos micro-ambientes dos tecidos, favorecendo a sua regeneração funcional. O objectivo principal desta tese consistiu em produzir e desenvolver polímeros biodegradáveis com estímulos químicos, estruturais e celulares de modo a obter uma elevada funcionalidade, usando para isso diferentes técnicas de micro/nano-fabricação.

As hipóteses científicas que estão na base do trabalho descrito nesta tese são: 1) é possível desenvolver substratos com estímulos estruturais usando polímeros biodegradáveis que já tenham demonstrado resultados promissores *in vivo*, 2) é possível incorporar estímulos bioquímicos em sistemas baseados em polímeros biodegradáveis, produzindo biomateriais com sinais bioquímicos integrados para o melhor desempenho biológico dos materiais, e 3) é possível combinar estes sinais estruturais e bioquímicos num único sistema.

O polímero polibutileno succinato foi micro-moldado de modo a desenvolver superfícies com topografias à escala micrométrica, visando o desenvolvimento de biomateriais com sinais estruturais, capazes de induzir o alinhamento de células do tecido adiposo humano. Embora este material tenha sido processado anteriormente sob a forma de estrutura 3D porosa, esta foi a primeira vez que foi descrito o processamento deste material à escala micrométrica, demonstrado pelo desenvolvimento de vinte padrões com diferentes dimensões.

O polissacarídeo goma gelana (GG), extensivamente estudado no Grupo de Investigação 3B's, foi usado para desenvolver substratos com sinais estruturais. Micro-cápsulas de GG foram fabricadas usando um sistema de duas fases, com o intuito de serem usadas para o transporte ou libertação de drogas ou células. O princípio de repulsão entre soluções hidrofóbicas e hidrófilas foi combinado com um processo de micro-fabricação, usando uma bomba de injecção. De modo a demonstrar o conceito, partículas fluorescentes, suspensões celulares e agregados celulares foram encapsulados usando este sistema.

Para desenvolver biomateriais com sinais bioquímicos, a GG foi modificada quimicamente com ligações éster, produzindo hidrogéis reticuláveis por radiação ultravioleta (UV). Os

hidrogéis de GG metacrilada (MeGG) são formados com mecanismos físicos e químicos, resultando em géis com propriedades mecânicas ajustáveis numa gama que se situa próximo da dos tecidos humanos moles e duros, como o cérebro e o osso. Este material foi posteriormente combinado com quitosano, um polissacarídeo de origem natural, resultando num complexo polieletrolítico (PEC) que combina as melhores propriedades do quitosano e da MeGG. A formação de hidrogéis de PECs resulta da interacção entre cadeias de polímeros com cargas opostas, sendo o mecanismo de ligação dependente de forças iónicas, as quais podem ser perturbadas por mudanças na composição da solução. Os sinais bioquímicos introduzidos anteriormente permitiram reticular o hidrogel MeGG-CHT com a radiação UV, estabilizando a estrutura do hidrogel. Este material permitiu também o desenvolvimento de micro-géis por fotolitografia. O encapsulamento de fibroblastos do coração de ratos na MeGG previamente à produção dos hidrogéis conduziu à fabricação de micro-géis com sinais bioquímicos, estruturais e celulares integrados num mesmo sistema.

O sistema de hidrogel MeGG-CHT foi usado para obter um hidrogel fibroso hierárquico, através da combinação de microfluídica e complexação polieletrolitica. Extrudiu-se o MeGG-CHT em dois canais convergentes com o objectivo de obter a complexação das cadeias poliméricas na forma de fibra. O hidrogel desenvolvido mimetiza a arquitectura das fibras de colagénio existentes no corpo humano, não só ao nível micrométrico mas também à escala nanométrica. O hidrogel desenvolvido foi funcionalizado através da incorporação de moléculas adesivas (péptidos RGD) na MeGG antes do seu processamento.

O trabalho de investigação descrito nesta tese demonstra o potencial de diferentes estratégias para mimetizar várias características do micro-ambiente existente nos tecidos. Sinais bioquímicos e celulares foram incorporados em biomateriais que foram posteriormente processados para obter estruturas biológicas relevantes à escala micro/nanométrica. Esta tese demonstra a importância de combinar diferentes áreas do conhecimento para o desenvolvimento de sistemas funcionais para aplicações biomédicas. É inquestionável que a química e as tecnologias de micro e nano-fabricação são duas áreas de conhecimento que se complementam e permitem a fabricação de materiais micro e nano-estruturados. Esta sinergia foi alcançada usando para o efeito uma abordagem *top-down* (através de fotolitografia, micro-moldação ou microfluídica) e/ou uma abordagem *bottom-up* (através da complexação de cadeias poliméricas). No último trabalho da tese estas duas abordagens convergem para o desenvolvimento de biomateriais micro e nano-estruturados. Este tipo de sistemas permitem a funcionalização de biomateriais até níveis de aproximação dos tecidos biológicos não tem paralelo nos sistemas convencionais, o que se traduz no desenvolvimento de sistemas de elevado desempenho para diferentes abordagens em engenharia de tecidos.

Table of Contents

A

AFM	Atomic Force Microscopy
ALG	Alginate
ANOVA	Analysis of variance
APT	A10 Aptamer
ASC	Adipose stem cells
ATR	Attenuated total reflection

B

BM-HSCs	Bone Marrow-Derived hematopoietic stem cells

C

Ca	Calcium
$CaCl_2$	Calcium chloride
Calcein AM	Acetomethoxy derivate of calcein
CCG	Chitosan–collagen–gelatin
CHT	Chitosan

D

D_2O	Deuterated water
DAPI	4',6-diamidino-2-phenylindole
DD	Degree of deacetylation
DIM	Dichloromethane
DS	Degree of substitution
dsDNA	Double stranded DNA
DMEM	Dulbecco's Modified Eagle's medium

E

EB	Embryoid bodies
ECM	Extracellular Matrix
EDC	1-ethyl-3-(3-dimethylaminopropyl) carbodiimide hydrochloride
EDTA	Ethylenediaminetetraacetic acid
ES	Embryonic Stem cells
EthD-1	Ethidium homodimer

F

FBS	Fetal bovine serum
FDA	Food and Drug Administration
FITC	Fluorescein isothiocyanate
FTIR	Fourier transform infrared spectroscopy

G

GAGs	Glycosaminoglycans
GG	Gellan Gum

K

K	Potassium

L

Low-MeGG	Low degree of methacrylation of MeGG

H

HA	Hyaluronic acid
hASC	Human adipose stem cells
HepG2	Human hepatocellular liver carcinoma cell line
High-MeGG	High degree of methacrylation of MeGG
^{1}H-NMR	Proton nuclear magnetic resonance
HSCs	Hematopoietic stem cells
hOBs	Primary Human Osteoblasts
hUVECs	Human Umbilical Vein Endothelial Cells

M

MA	Methacrylic anhydride
MEFs	Murine embryonic fibroblasts
MeGG	Methacrylated Gellan Gum
MeGG-CHT	Methacrylated Gellan Gum – Chitosan
MeGG-RGD	Modified MeGG with cell adhesive motifs (RGD)
Mg	Magnesium
MIN6	Insulinoma cell line
MSCs	Mesenchymal stem cells
M_w	Weight average molecular weight

N

Na	Sodium
NaOH	Sodium hydroxide
NIH-3T3	Fibroblastic cell line
NHS	N-hydroxysuccinimide
NSCs	Neural stem cells

P

PBS	Poly(butylene succinate)
PCL	Poly(ε-caprolactone)
PCLEEP	Poly(ε-caprolactone-co-ethyl ethylene phosphate)
PDMS	Polydimethylsiloxane
PEC	Polyelectrolyte complex
PECAM-1	Platelet/Endothelial cell adhesion molecule-1
PEG	Polyethylene glycol
PEO	Polyethylene oxide
PES	Polyethersulfone
PET	Polyethylene-terephthalate
pH	Measure of the acidity or basicity of an aqueous solution
PHBV	Poly(3-hydroxybutyrate-co-3-hydroxyvalerate)
pKa	Acid dissociation constant at logarithmic scale
PLGA	Poly(lactic-co-glycolic-acid)
PLLA	Poly(L-lactic acid)

P(LLA-CL)	Poly(L-lactid-co-ε-caprolactone)	**X**	
PU	Polyurethane	XPS	X-ray photoelectron spectroscopy

R

rCF   Rat cardiac fibroblasts

W

w/v   weight/volume

S

SAMs	Self-assembled monolayers
SAOS-2	Human Osteogenic Sarcoma Cells
SEM	Scanning electron microscopy
SMCs	Human coronary artery smooth muscle cells
SPCL	Starch/poycaprolactone
SPL	Scanning Probe Lithography
STM	Scanning tunneling microscopes
SVF	Stromal vascular fraction

Others

2D	Two-dimensional
3D	Three-dimensional
µCT	Microcontact Printing
µTM	Microtransfer Molding

U

UV   Ultraviolet

T

TCPS	Tissue culture polystyrene
TE	Tissue Engineering
TEM	Transmission electron microscopy
T_g	Glass transition temperature
TIM	Trichloromethane
T_m	Melting temperature
TMSPMA	3-[tris(trimethylsilyloxy)silyl]propyl methacrylate

V

VSMCs	Bovine Aorta Cells
v/v	Volume/volume

SECTION 1 – BACKGROUND
Chapter I - Micro and Nano Technology in Tissue Engineering

SECTION 2 - DETAILED DESCRIPTION OF EXPERIMENTAL MATERIALS AND METHODOLOGIES
Chapter II - Materials and Methods

poly(butylene succinate); rCF-rat cardiac fibroblasts; SEM-scanning electron microscopy; TEM-transmission electron microscopy; XPS-X-ray photoelectron spectroscopy.

SECTION 3 - DEVELOPING IMPROVED SUBSTRATES WITH STRUCTURAL CUES
Chapter III - Development of micro-patterned surfaces of poly(butylene succinate) by micromolding for guided tissue engineering

Chapter IV – An automated two-phase system for biodegradable microcapsule production

Schematics of the forces involved on the formation of the microcapsules: gravity (g), surface tension between the polymer and needle (F_{p-n}) and surface tension between the polymer and mineral oil (F_{p-o}).

SECTION 4 – DEVELOPING HYDROGELS WITH INTEGRATED CHEMICAL, BIOLOGICAL AND STRUCTURAL CUES
Chapter V – Modified gellan gum hydrogels with tunable physical and mechanical properties

immersed in water for 30 min. The weight and size of the samples varied with the presence or absence of ions in the solution.

Chapter VI - Microfabricated photocrosslinkable polyelectrolyte-complex of chitosan and methacrylated gellan gum

Chapter VII - Fabrication of collagen-mimicking hydrogel fiber bundles from the assembly of polyelectrolytes

Page

Daniela Fernandes Coutinho was born on the 20th of September 1984, in Viana do Castelo, Portugal. She is currently a PhD student at 3B's Research Group (Biomaterials, Biodegradables and Biomimetics), at University of Minho, Headquarters of the European Institute of Excellence on Tissue Engineering and Regenerative Medicine at Avepark, Caldas das Taipas - Guimarães, Portugal. This research unit has been classified by the Foundation of Science and Technology as excellent and is part of the Portuguese Associate Laboratory ICVS/3B's.

She received her MSc degree in 2007 in Biomedical Engineering, with a major in Biomaterials, Biomechanics and Rehabilitation, at University of Minho, Braga, Portugal, with a final grade of 17 (0-20 scale). In 2006 she spent 6 months at Centro de Biomateriales e Ingeniería Tisular, Universidad Politécnica de Valencia, Spain, developing biomaterials for tissue engineering, under the supervision of Professor José Luis Gomez Ribelles. In her master research project, she spent one year at the 3B's Research Group, working under the supervision of Professor Rui Reis and Professor Nuno Neves. Her Master thesis, entitled "The influence of the surface properties of chitosan-poly(butylene succinate) blends on protein adsorption and osteoblast-cell adhesion", was graded 18 (0-20 scale).

In October 2007, she started pursuing her PhD in Bioengineering Systems under the scope of the MIT-Portugal Program. The first year of the Doctoral Program was focused on providing strong knowledge in Innovation and Leadership, as other areas of Bioengineering from Biomaterials and Nanotechnology to Biomedical Devices. In this first year she was involved in an I-teams project (innovation project), in which students engaged in establishing a strategy for transferring technology from the lab to the market. She was one of the elements of the project entitled "DNAMiMics", submitted to the national innovation award START 2008, being one of the eight finalists of this contest. As part of the prize, she had the possibility of doing a course on management of startups given by IAPMEI, Inovcapital and the Nova School of Business and Economics.

In September 2008, she started her PhD research at the 3B's Research Group, at University of Minho, Portugal, under the supervision of Professor Nuno Neves and Professor Manuela Gomes. Between 2009 and 2010 she spent 18 months as a visiting student at the Khademhosseini Lab, at Harvard-MIT Division of Health Sciences and Technology (HST),

USA, studying microfabrication strategies for developing biomaterials at a micro-scale and controlling cellular behavior.

As a result of her research work, Daniela Coutinho has attended the most relevant conferences in her research field. She is the author of 5 papers in international refereed journals (4 submitted and 1 published), 2 book chapters and 9 communications in international conferences.

The work performed under the PhD work resulted in the publications listed below.

INTERNATIONAL REFEREED JOURNALS

1. **Coutinho DF**, Shilpa S, Shin H, Oliveira JT , Gomes ME, Neves NM, Khademhosseini A and Reis RL, 2010, Modified Gellan Gum hydrogels with tunable physical and mechanical properties, Biomaterials, 31:7494-7502.

2. **Coutinho DF**, Gomes ME, Neves NM, Reis RL, 2011, Development of poly(butylene succinate) micro-features for human adipose stem cell alignment. Submitted (2011).

3. **Coutinho DF**, Ahari AF, Kachouie N, Gomes ME, Neves ME, Reis RL, Khademhosseini A, 2011, An automated two-phase system for biodegradable microcapsule production. Submitted (2011).

4. **Coutinho DF**, Sant S, Shakiba M, Wang B, Gomes ME, Neves NM, Reis RL, Khademhosseini A, 2011, Photocrosslinkable polyelectrolyte-complex capsules of chitosan and methacrylated gellan gum for tissue engineering at a micro-scale. Submitted (2011).

5. **Coutinho DF**, Sant S, Neves NM, Gomes ME, Reis RL, Khademhosseini A, 2011, Fabrication of collagen-mimicking hydrogel fiber bundles from assembly of polyelectrolytes. Submitted (2011).

BOOK CHAPTERS

1. **Coutinho DF**, Costa P, Neves N, Gomes ME and Reis RL, Micro and Nano Technology in Tissue Engineering" for publication in the textbook, In The Tissue Engineering Book: State of the art, Visions and Limitations, Ed. N Pallua, Springer, (2010), *in press.*

2. Sant S, **Coutinho DF**, Sadr N, Reis R, Khademhosseini A, Tissue-analogs by the assembly of engineered hydrogel blocks, In Biomimetic approaches in the development of biomaterials, Ed. Mano J, Wiley-VCH*, in press.*

Oral Presentations

1. **Coutinho DF**, Sant S, Shakiba M, Wang B, Gomes ME, Neves NM, Reis RL and Khademhosseini A, Photocrosslinkable polyelectrolyte complex hydrogel with potential for tissue-engineering at micron scale, 9th International Symposium on Frontiers in Biomedical Polymers (FBPS 2011), Funchal, Madeira, Portugal, May 2011.

2. **Coutinho DF**, Sant S, Shakiba M, Gomes ME, Neves NM, Reis RL and Khademhosseini A, Fabrication of Hydrogel Fiber Bundles from Assembly of Polyelectrolytes, European Chapter of the Tissue Engineering and Regenerative Medicine International Society (TERMIS) 2011 Annual Meeting, Granada, Spain, June 2011.

3. **Coutinho DF**, Gomes ME, Neves NM and Reis RL, Development of poly(butylene succinate) micro-features for adipose stem cell alignment, European Chapter of the Tissue Engineering and Regenerative Medicine International Society (TERMIS) 2011 Annual Meeting, Granada, Spain, June 2011.

4. **Coutinho DF**, Sant S, Gomes ME, Neves NM, Reis RL, Khademhosseini A, Three-dimensional hydrogel mimics hierarchy and size of natural fiber bundles, ESAO-IFAO 2011, Porto, Portugal, October 2011.

5. **Coutinho DF**, Sant S, Gomes ME, Neves NM, Reis RL, Khademhosseini A, Natural-based photocrosslinkable polyelectrolyte complex hydrogel: development and microfabrication, ESAO-IFAO 2011, Porto, Portugal, October 2011.

Poster Presentations

1. **Coutinho DF,** Gomes ME, Neves NM, Khademhosseini A and Reis RL, Micro/Nano-processing strategies as a tool to clarify the biological performance of degradable biomaterials for biomedical applications, MIT-Portugal Program First Annual Conference, Lisbon, Portugal, July 2009.

2. **Coutinho DF,** Sant S, Shin H, Oliveira JT , Gomes ME, Neves NM, Khademhosseini A and Reis RL, Microfabrication of biomaterials for tissue engineering applications , MIT-Portugal 2nd Annual Conference, Porto, Portugal, September 2010.

3. **Coutinho DF**, Sant S, Shin H, Oliveira JT , Gomes ME, Neves NM, Khademhosseini A and Reis RL, Novel Methacrylated Gellan Gum Hydrogels with Tunable Mechanical Properties, BMES, Austin, United States of America, October 2010.

4. Sant S, **Coutinho DF**, Yamanlar S, Iyer D, Kashyap A, Wang B, Picart C, Gomes ME, Oliveira JT , Neves NM, Reis RL and Khademhosseini A, Biomimetic Biomaterials for

Tissue Engineering Applications, Wyss Institute for Biologically Inspired Engineering at Harvard University Retreat, Boston, United States of America, November 2010.

5. Mihaila SM, **Coutinho DF**, Reis RL, Marques AP, Gomes ME, Methacrylated kappa-carragenan as a photocrosslinkable biopolymer, Ninth International Symposium on Frontiers in Biomedical Polymers (FBPS), Funchal, Madeira, Portugal, May 2011.

INVITED LECTURES

1. Coutinho DF, Gomes ME, Neves NM and Reis RL, Estratégias de microfabricação para Engenharia de Tecidos, VI Jornadas de Engenharia Biomédica da Universidade do Minho, Braga, Portugal, March 2011.

2. Coutinho DF, Gomes ME, Neves NM and Reis RL, Natural Hydrogels and Micro-gels, 1st 3B's Symposium on biomaterials and stem cells in regenerative medicine, Guimarães, Portugal, April 2011.

The present thesis is divided into 5 sections containing 8 chapters. This structure was adopted to allow organizing the data presented in the various chapters, preceded by a general introduction and an overall materials and methods section. The main body of the thesis is based on a series of publications published in international journals or submitted for publication, identified in the first page of each chapter.

The first section is based on a published book chapter and consists on giving a comprehensive and detailed overview on the application of micro and nanofabrication techniques in tissue engineering applications.

A detailed analysis of the materials used, technologies applied for processing the materials, techniques used for the characterization of the developed structures and the biological assays performed is provided in Section 2/Chapter II. This chapter is aimed at complementing the information given in each of the experimental chapters.

The following five chapters are based on the experimental work, either published or submitted to international journals. Thus, each of the experimental chapter is presented as an adapted version of the published/submitted manuscript.

Section 3 is aimed at developing improved substrates with structural cues and for that polymers studied at 3B's Research Group were engineered into substrates with specific spatial configurations. Specifically, Chapter III is focused on developing biomimetic micropatterned surfaces of poly(butylene succinate) by micromolding and Chapter IV describes the development of a system capable of producing and stabilizing microcapsules in a single step, encapsulating bioentities for different applications.

The fourth section of the thesis reports on the incremental improvement of the properties of a hydrogel system by introducing chemical and biological cues and processing the hydrogel using top-down and/or bottom-up approaches. The first work of this section, described in Chapter V, studies the modification of the polysaccharide gellan gum in order to make it crosslinkable by physical and chemical methods. This material is further combined with chitosan, forming a polyelectrolyte complex hydrogel in Chapter VI. A comprehensive understanding on the interactions between both polymers behind the hydrogel formation is provided. The final work, presented in Chapter VII focuses on the fabrication of a multi-

hierarchical hydrogel by combining fluidics technology and polyelectrolyte-complexation, using both polymers.

The final section of the thesis presents the general conclusions and implications of the works described.

Section 1

BACKGROUND

Chapter I

MICRO AND NANOTECHNOLOGY IN TISSUE ENGINEERING

CHAPTER I [*]

MICRO AND NANOTECHNOLOGY IN TISSUE ENGINEERING

ABSTRACT

This manuscript provides an overview of the recent developments regarding micro and nanotechnologies and their applications in tissue engineering. Micro and nanotechnologies have been increasingly recognized as powerful tools for designing advanced tissue engineering strategies, both as production methods and as analysis tools. These technologies can be used to generate scaffolds with enhanced functionality that will not act as mere substrates for cellular adhesion but play as an active agent in the process of tissue regeneration. Moreover, these technologies can be used to study and control the phenomena occurring at the cellular microenvironment. Herein the main technologies developed/under development will be described and their diverse potential applications will be discussed.

1. INTRODUCTION

Tissue engineering (TE) is a rapidly growing scientific area [1] that aims to create, repair and/or replace tissues and organs by using combinations of cells, biomaterials and/or biologically active molecules [2, 3]. In this way, TE intends to help the body to produce a material that resembles as much as possible the body's own native tissue. By doing so, TE strategies promise to revolutionize current therapies and significantly improve the quality of life of millions of patients.

The classical TE strategy consists in isolating specific cells through a biopsy from a patient, to grow them on a biomimetic scaffold under controlled culture conditions, to deliver the resulting construct to the desired site in the patient's body, and to direct the new tissue formation into the scaffold that can be degraded over time [2, 3].

Most of the presently existing TE techniques rely on the use of macro-structured porous scaffolds, which act as supports for the initial cell attachment and subsequent tissue formation, both *in vitro* and *in vivo* [4-6]. This kind of approach has been successful to a certain extent in producing relatively simple constructs relying on the intrinsic natural capability of cells and tissues to self-regenerate, remodel and adapt. For this reason, cells have been the most significant factor in the generation of the tissue itself [7]. However, this natural capability of cells for adapting to its surrounding environment has limitations and that is the main reason why TE has not been able to generate complex thick tissues so far [8]. In fact, one of the most important drawbacks of currently available constructs in TE approaches is related to the lack of means to generate effective oxygen and nutrient dispersion pathways that can reach a whole construct homogenously and therefore enable the functionality/viability of the construct upon implementation.

In order to generate constructs capable of accurately mimicking/replacing structures as defined and organized as complex tissues and organs, novel kinds of scaffolds and devices have lately been developed which potentially allow obtaining a fine control over the cellular positioning, organization and interactions. For this, much has contributed the continuous technological development in the areas of micro and nano technologies, both in terms of production methods as also in analysis tools [9]. Developments in these areas may allow a finer control over the architecture of scaffolds, making them no longer simple substrates for cellular adhesion and proliferation, but most importantly, active agents in the process of tissue development [10]. Micropatterning integrated in a TE approach is a result of the combination of micro and nanofabrication techniques with materials science and surface engineering that result in a deep exploration of the microenvironment where cells are embedded [10, 11]. In TE, micro and nanotechnologies can also be applied to fabricate

biomimetic scaffolds with increased complexity to promote, for example, vascularization, also enabling to perform a series of high-throughput experiments (Figure I.1).
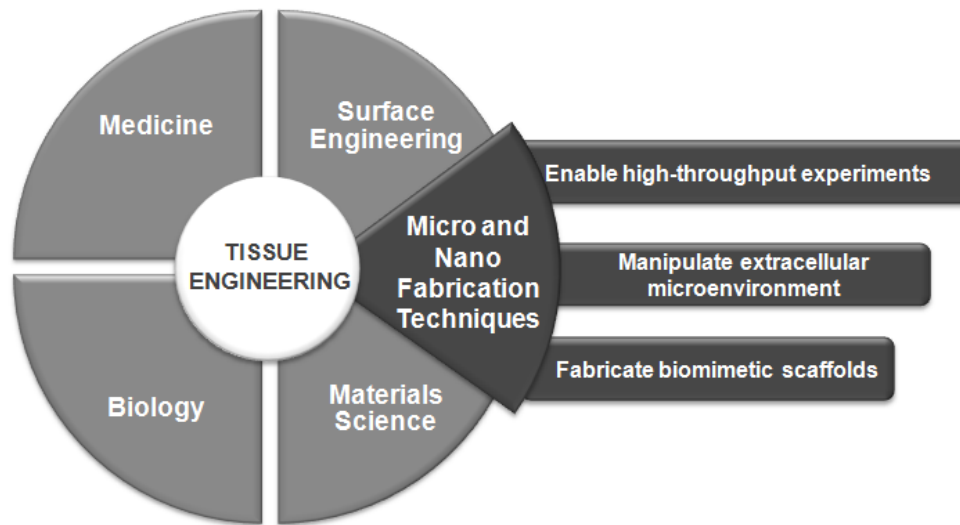
Figure I.1. Schematic representation of the different areas of expertise involved in a tissue engineering strategy. Highlight to the inputs brought by micro and nano fabrication techniques.

The main aim of this chapter is to shed new light on the use of micro and nanotechnologies in TE strategies, highlighting the need for new technologies to obtain an in depth understanding of the microenvironment at the implantation site. This chapter also reviews some of the most widely used and most promising micro and nanoscale technologies used in TE strategies follows. Subsequently, the most advanced applications of micro and nano fabrication techniques in different areas of TE will be described, showing their enormous potential for being applied to the improvement of the life quality of patients. Although the described techniques are usually applied for developing 2D structures, successful attempts to move towards 3D structures by means of micro and nanofabrication techniques will be explored. Finally, the application of micro and nanotechnologies into the development of cell/tissue culture systems (microbioreactors) will also be briefly discussed.

2. AIM OF THE DISCIPLINE

Micro and nanotechnologies consist on the design, characterization, production and application of structures, devices and systems by controlling their shape and size at micrometric or nanometric scales. The properties of materials at atomic, molecular and macromolecular scales are significantly different from those at a larger macroscopic scale and for this reason micro and nanosciences have been receiving increasingly scientific,

industrial and social attention. The development of those areas may revolutionize and change the world as we know it and as we see it. Materials science and health are among the various areas that may mostly benefit from the evolution of micro and nanotechnologies. The major challenge encountered in biomaterials science is the issue of biocompatibility. Given its vital role, the control of the biocompatibility has become a major challenge and a main focus of research in the process of developing new materials for TE applications. Micro and nanotechnologies previously used in other research areas, are now integrated onto the optimization of interactions occurring at the interface between materials and cells. By providing the possibility to tailor features such as micro and nanotopographies, these novel technologies allow for the development of new micro and nanostructured materials possessing unique properties allowing the development of solutions for the most complex end-applications.

Micro and nano technologies can be regarded and designed from two different perspectives: the top-down and the bottom-up approach. As these terms suggest, the top-down approach can be pictured as large entities creating small devices while the bottom-up approach consists of small entities generating large devices. Both perspectives are valid and interconnected and can lead to the development of new solutions for unmet needs in several fields.

3. THE NEED FOR MICRO AND NANOTECHNOLOGIES IN TISSUE ENGINEERING STRATEGIES

One of the major motivations for the increasing effort spent on designing and developing nano-structured materials for TE strategies is that natural tissues and the associated extracellular matrices are in fact composed of nanostructured materials [12-14] (Figure I.2).
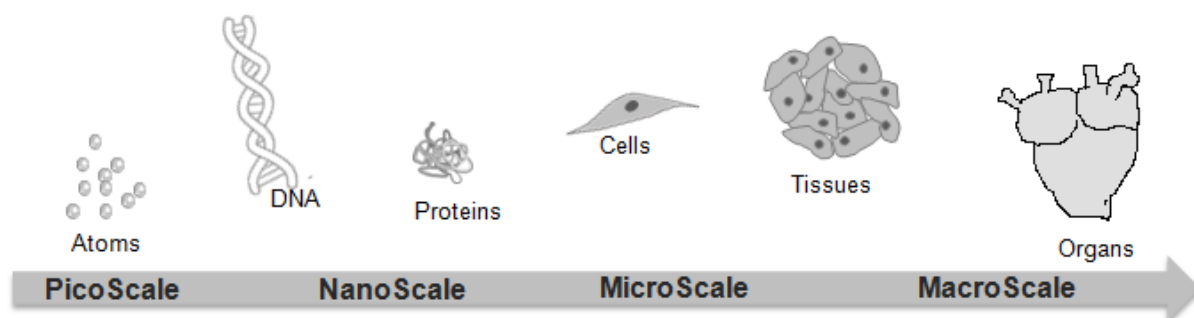
Figure I.2. Nano and Micro scales in Nature.

These highly organized and cooperative micro and nano-building blocks assemble in a controlled way to ultimately build healthy tissues. When an implant first contacts its host environment, proteins are the first biological entities to interact with the surface of the biomaterial [15, 16]. In fact, the surface of the material gets covered by a layer of proteins, just a few seconds after implantation in a competitive process. Since cells do not interact with naked surfaces, the proteic layer adsorbed onto the material's surface will interact with the cell receptors at the cell membrane surface [17]. Thus, the presence of specific molecules is mandatory for a suitable attachment and proliferation of cells onto the surface of a given substrate [18]. Proteins are the key elements creating a bridge between the non-biological surface of materials and cells [19]. Figure I.3 represents, in a simplified way, the cascade of events occurring at a biomaterial implantation site. The adsorption of proteins onto the surface of biomaterials from a surrounding environment is a rather complex process.
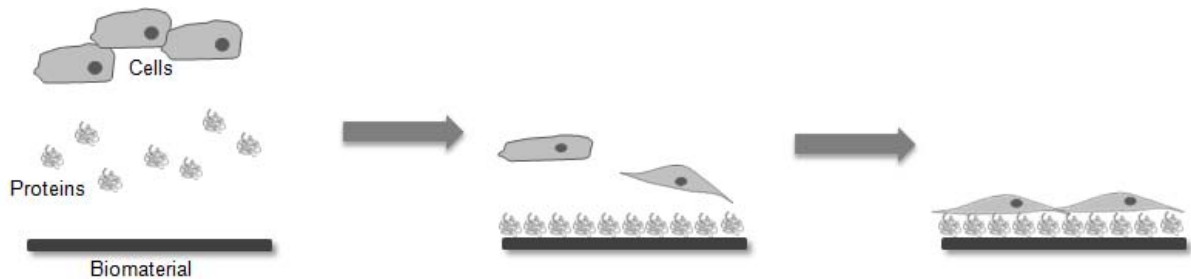
Figure I.3. A glimpse at the cascade of events occurring at the implantation site.

The adsorptive behavior of proteins is highly dependent on various surface properties such as chemistry, charge, topography, wettability and surface energy [20, 21]. These parameters of the implant's surface will determine not only the amount of proteins adsorbed but also their type and conformation. The protein net charge and charge distribution, size, conformation and hydrophobic domains are some of the characteristics of proteins that might have a profound effect on the implant surface properties and that could ultimately influence the cell response to the implant's surface [15, 16, 19, 22]. Therefore, whereas adsorbing to surfaces, these nano-scale entities can either retain their original conformation or may have it altered in response to the environment conditions [19]. This surface-specific adjustment can result in the presentation of different aminoacidic regions to cells [19].

The initial contact between anchorage-dependent cells and the biomaterial's surface involves various biological molecules, such as extracellular matrix (ECM) proteins, cell membrane proteins and cytoskeleton proteins [23]. Interactions between these biological molecules and their specific receptors induce signal transduction and consequently influence cell growth and differentiation [24, 25]. Thus, the surface micro and nano-structures are of huge importance as they will firstly dictate the pattern of protein adsorption, ultimately influencing

cell behavior through the motifs presented by those adsorbed proteins to the cells. Moreover, cells themselves are also capable of directing their own position and orientation through a process called mechanosensing [26]. It has been shown that cells can sense the topography of the surfaces to which they adhere and reposition themselves accordingly. Cells can respond both to the dimensions of the surface's roughness as also to its topography. Studies have revealed that cells can show a preference for adhering to surfaces within certain ranges of roughness, being this factor determinant in the amount of cellular proliferation over that surface [27]. As for the surface's geometry, studies have shown that, when seeded in linearly grooved surfaces, cells tend to preferably adhere and grow longitudinally over the grooved lines [28]. The cell alignment is also favored in surfaces exhibiting grooves within certain width ranges [29, 30]. Figure I.4 shows an example of a defined alignment of osteoblast-like cells (SaOs-2) on a patterned surface.
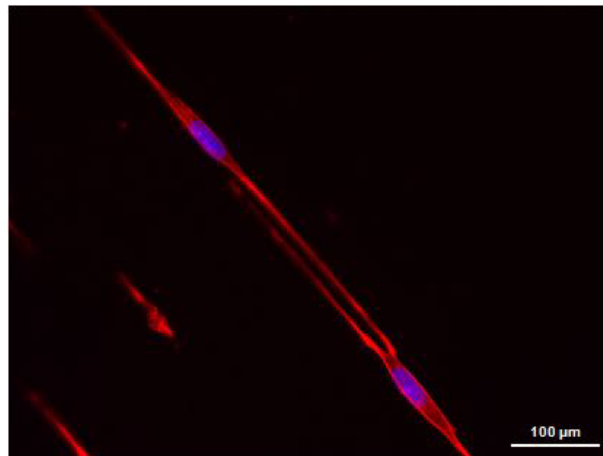
Figure I.4. Cell alignment of osteoblast-like cells (SaOs-2) on a patterned surface with the cytoskeleton stained with phalloidin and the nucleus counterstained with DAPI.

Still regarding geometry, studies have shown that cells tend to adhere preferably to randomly organized surfaces instead of geometrically organized ones. Thus, for the design of enhanced biomaterials to be used in TE strategies, it is of utmost importance to understand the cellular processes that lead to a more efficient tissue regeneration as well as those involved in the formation of new tissue avoiding triggering of undesired immunological or inflammatory responses. As referred, the interaction between polymeric biomaterials and biological elements is dictated by the processes occurring at the interface between these two phases. An approach to optimize the interaction of a biomaterial with its implantation site bioenvironment is by tailoring the properties of the material's surface with micro and nano-structures that could elicit the desired behavior on the biological entities. For that, micro and nanotechnologies can be used to overcome the limitations of the currently used techniques

to fabricate biomaterials with effective micro and nano-surface structures that could mimic as close as possible the micro and nano-bioenvironment.

4. MICRO AND NANO FABRICATION METHODS

Micro and nanofabrication is the general term used for describing processes of fabricating miniature micro or nano-scaled structures by using macroscale devices. The earliest microfabricated devices consisted of semiconductor integrated circuits and were fabricated by simple surface treatments or methods such as lithography or chemical vapor deposition [31, 32]. Apart from integrated circuits, which are mainly two-dimensional, these technologies are commonly used in the production of devices such as microelectromechanical systems (MEMS) [33, 34], laser diodes [35], flat panel displays [36] or fuel cells [37].

Different strategies have been utilized to apply two-dimensional micro and nano-featured devices to TE. Microfluidic devices can be produced through various surface treatments or lithographic methodologies. These methodologies consist in creating patterns on the surface of materials, into which cells can be cultured and positioned into specific locations by physical constraints. This physical constraint can also be used for controlling the interaction of cells with its surroundings, such as with other cells. The same grooves that are used for cellular constraint can also be used for selectively feeding cells by perfusing with cell culture medium using microfluidic systems [38].

As mentioned above, micro and nanofabrication methods can be roughly divided in two areas following radically different concepts: bottom-up or top-down (Figure I.5). The latter normally includes photolithography, microcontact printing, microtransfer molding, capillary force lithography, scanning probe lithography and electrospinning methods, which will be discussed in the following sections.
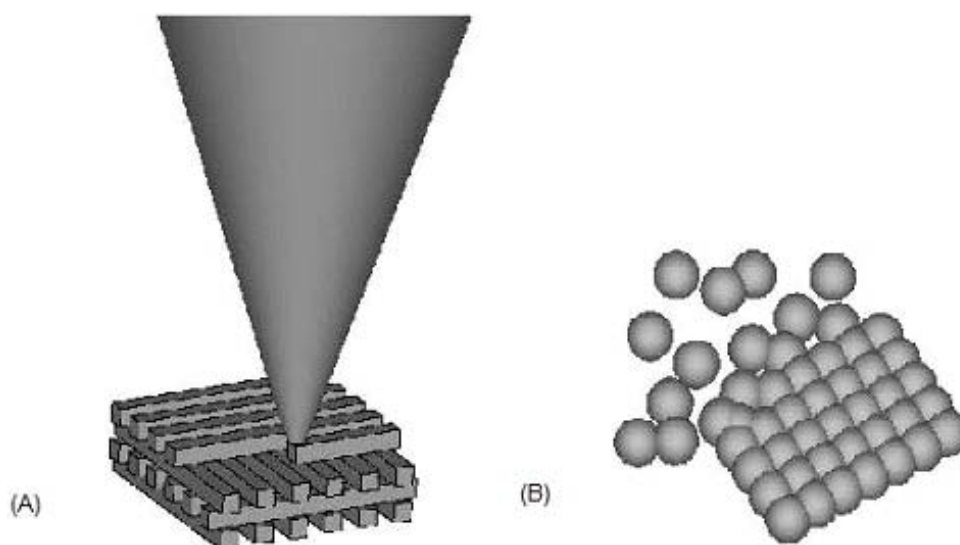
Figure I.5. Schematic diagram of the (A) top-down and (B) bottom-up nanotechnology approaches for tissue engineering.

Both approaches require a great know-how on the surface properties of materials. Besides having insights on the molecular events through thermodynamic and kinetic processes (bottom-up), researchers must also possess the skills to understand device miniaturization and fluidics, which are associated with top-down fabrication strategies. Interestingly, bottom-up and top-down approaches have in some cases merged to create systems more effective for tissue regeneration purposes. As an example, microfluidic devices have been used to act as vasculature systems and test the interaction of targeted particles with cells [39]. Also, 3D structures have been developed by combining bottom-up and top-down approaches. Hydrogels were micromachined by means of a top-down approach and then these patterned building blocks were assembled to form a more complex structure through a bottom-up approach [40, 41]. The next subsections are devoted to presenting an overview of the most used techniques of each approach.

4.1. Bottom-up Approach

The bottom-up approaches mainly rely on the natural assembly of atoms, molecules or other nano-sized building blocks like peptide residues (dimensions typically of 2 to 10 nm [42]). Nature has already perfectly controlled micro and nanoscale components by macromolecular recognition of various biological materials. Therefore, scientists are maintaining the trend of learning from nature how to design materials and systems using similar processes as the ones observed in nature [43]. The molecular assembly of building blocks by controlled reactions makes this technique more economic as compared to the conventional top-down methods [42].
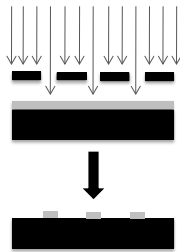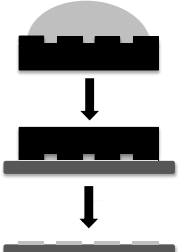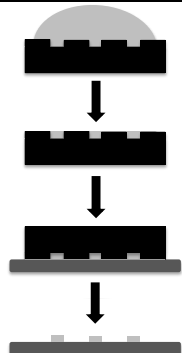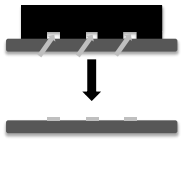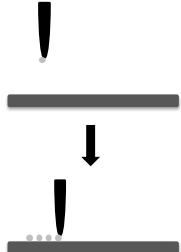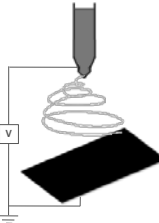
Indeed, biologically inspired self-assembly holds great promise in the development of nano-structures [44]. For instance, research has shown that amphiphilic peptides can self-assemble to form hydrogels with great potential for TE strategies [44]. Moreover, self-assembled scaffolds functionalized with specific peptide moieties can be produced by incorporating these functional groups into the initial building molecule.

Of great interest are also the self-assembled-monolayers (SAMs), well established for the study of surface modification [45]. The SAMs are produced when a substance spontaneously forms a molecular monolayer on a surface [46]. Work reported by Shuguang Zhang and collaborators [47, 48] has shown that by observing processes by which supramolecular structures are assembled in nature, the synthesis of novel synthetic materials can be developed. Thus, they have been able not only to coat surfaces by molecular assembly but also to develop nanofiber peptide and protein scaffolds with approximately 10 nm in diameter [44], which have proven to be suitable for applied studies in TE. Likewise, Frank Gu and collaborators [49] have successfully developed polymeric nanoparticles, which were formulated by the self-assembly of an amphiphilic triblock copolymer composed of end-to-end linkage of poly(lactic-co-glycolic-acid) (PLGA), polyethyleneglycol (PEG), and the A10 aptamer (Apt).

4.2. Top-down Approach

Most of the techniques used in the development of micro and nano-patterned surfaces for TE purposes follow this route. Frequently their origin is in other fields of research such as microelectronics fabrication. Nevertheless, all of these techniques are based on the development of micro and nanofeatures on a surface of a material by means of larger tools. In the next sections, we present an overview of the most relevant techniques used in micropatterning biological materials, as well as their advantages and limitations for this purpose. Photolithographic techniques are widely developed and optimized for patterning cells. Nonetheless, disadvantages of this technique, mainly regarding biocompatibility issues, have highlighted the interest on alternative techniques based on soft-lithographic methods, such as microcontact printing, microtransfer molding and molding in capillaries. Likewise, scanning probe lithographic methods based on Atomic Force Microscopy (AFM) are emerging as useful techniques for cell patterning applications. Additionally to these techniques, the development of micro and nano patterned surfaces by means of electrospinning method has demonstrated a notable importance in TE strategies, demonstrated by the exponentially increasing number of publications on this subject over the years. Table presents a summary of the technologies described in the next sections, concerning its resolution, materials that can be used, as well as their most advantageous and disadvantageous features.

Table I.1. Summary of the nano and micro-technologies most used.

| | Photolithography | Soft-lithography | | | | Electrospinning |
		Microcontact Printing	Microtransfer Molding	Molding in Capillaries	Scanning Probe Lithography	
Resolution	37 nm	35nm-1 µm	250 nm	50 µm	20 nm - 30 nm	5 nm - 1 µm
Scheme of the technique						
Most Advantageous Feature(s)	- Precise control of the features	- Simplicity - Flexibility - Allows for multi-pattern - Applied to non-planar surfaces	- Applied to non-planar surfaces - Allows to generate 3D structures - Pattern large areas	- Allows to produce in a parallel fashion different patterns - The use of wet patterns – broaden applications - Creation of gradients	- Precise control of the added groups	- Structures similar to ECM - High range of applicable materials
Most Disadvantageous Feature(s)	- Polymers added with photosensitive compounds	- Structural constraints of the stamp - Low control of the ligand density	- Microstructures have a thin film between the raised features	- Patterned geometries limiting	- Limited to a low range of patterned sizes	- Poor mechanical properties
Ref.	[50]	[51, 52]	[53]	[51]	[54]	[55]

4.2.1. Photolithography

Photolithography has been one of the first techniques to be applied in the micropatterning of surfaces [56] for various areas including for the biomedical field. Briefly, photolithography involves the placement of a precursor polymer solution and a UV light photo-initiator onto the substrate of choice, so that it forms a thin but uniform film (~ 1 μm thick) [57]. Photopolymerization is further performed under ultraviolet (UV) light using a mask to define selected exposure areas. Only the exposed regions of the pre-polymer, which are a result of a patterned mask that is placed in between the light source and the precursor polymer solution, are submitted to photopolymerization. The surface is washed, leaving the patterned projections. Even though there are several variations of photolithographic methods, all rely on the use of a photoresistant mask with the desired pattern and the exposure to UV radiation of a precursor polymer solution.

Despite the enormous potential offered by this technology, the application of photolithography to patterning in biomedical applications presents some drawbacks, such as: (1) the high costs associated with the necessary equipment, namely related with the fabrication of the photoresistant mask, (2) the need for clean-room facilities, (3) the extra expertise required from the biologists and (4) the use of chemical compounds which may be toxic to cells and induce denaturation of proteins.

4.2.2. Soft-lithography

As an attempt to overcome the limitations of photolitograpic methods, a set of techniques entitled soft-lithographic methods have been developed by Whitesides and his research group [51]. Like photolitography, these techniques also make use of a micropatterned surface to generate the pattern of interest in the desired substrate. In this case, an elastomeric mold is used to transfer the patterns into the surfaces, determining the term "soft". In soft lithography, a stamp is created by molding an elastomer, which is usually produced using polydimethylsiloxane (PDMS). It offers several advantages including being biocompatible and permeable to gases. Soft-lithography methods mainly comprise microcontact printing, microtransfer molding and molding in capillaries, also known as capillary force lithography.

The general advantages of the aforementioned methods comprise: (1) the lower costs of softer materials, (2) their potential biocompatibility, (3) PDMS surface can be replicated repeatedly from the microfabricated master and the (4) biopatterning does not damage the stamp surface.

4.2.2.1. Microcontact Printing

Microcontact printing (μCP) was pioneered by Whitesides and his group in 1994 [58] and allows for patterning molecules onto a surface, resulting in the control over the protein adsorption and cell behavior. Briefly, in this method, a stamp is produced by replica molding, which is usually made with PDMS. It involves inking the stamp with the substance to be transferred to the substrate. As the solvent evaporates, the molecules to be printed become deposited and by removing the stamp from the surface, a pattern is created [10]. The first major application of this contact-transfer based method in the biomedical field consisted on the stamping of alkanethiolate inks, resulting on the formation of self-assembled alkythiol monolayers [58, 59]. Nevertheless, efforts have been made towards the use of different ink solutions [60] to pattern polymers [61, 62], DNA [63, 64], proteins [65-68] or even cells [59, 69, 70]. However, the interactions between the stamp and the ink solution need to be controlled since PDMS is hydrophobic.

The stamp being deformable, allows detachment from the substrate without smearing the inked patterned. Moreover, because of its additive nature, it can be applied to non-planar surfaces and develop multi-protein patterns [68]. Also, μCP is convenient for printing large areas (100 cm^2) in a single stamping step. Once the stamp is available, multiple copies of the pattern can be produced. Even so, it possesses some inherent disadvantages: (1) the density of the stamped material is not easily controlled [10, 60], (2) the elastomeric stamp might swell leading to a change on the pattern geometry [10] and also (3) contamination of the patterns with unpolimerized low molecular weight siloxane from the elastomeric stamp my compromise the process [71, 72].

4.2.2.2. Microtransfer Molding

Microtransfer molding (μTM) was described for the first time in 1996 [53] and is a technique which allows for generating rather complex 3D structures. In μTM, an elastomeric mold usually made of PDMS, is produced by replica molding with the pattern of interest. A drop of the pre-polymer solution is poured onto the mold and the excess gently removed [71]. The filled mold is placed in contact with the substrate and the pre-polymer solution is cured either by thermal or photochemical processes. After the procedure, the mold is peeled off leaving the pattern on the polymer. By stacking layers, 3D structures can be produced by means of μTM. Moreover, it presents some other useful characteristics [53, 71]: (1) it allows for patterning non-planar surfaces, (2) for fabricating structures in large surface areas (3 cm^2) [71] in a short period of time, (3) it is possible to rapidly replicate microstructures from the mold, (4) two or more components can be used to uniformly create microstructures and (5) it is applicable to a wide range of materials. Depending on the applications, the main

shortcoming of this technique is due to the thin films that are formed between the raised features [71].

4.2.2.3. Molding in Capillaries (Capillary Force Lithography)

Microfluidic patterning using capillaries, also known as capillary force lithography, allows for patterning a surface of a material from the flow of a solution [73-75]. Microchannels (or capillaries) are formed by the void spaces when the PDMS structure is placed on top of the substrate. Thus, in opposition to the aforementioned techniques, the material is added to the surface in the areas where the stamp is not in contact with the surface. Through capillary forces, these microchannels deliver the targeted fluid to restricted areas of the substrate, allowing for a selective microfluidic patterning. The typical channel size is 50 µm, at which the fluids have a laminar flow with Reynolds Number ranging from 0.1 to 1 [51]. Therefore, if two streams coming from different inlets are to flow in a common channel, they will flow in parallel without turbulent mixing, and only with diffusion among both fluids at the interface. This characteristic makes of molding in capillaries a really interesting method for developing gradients. Lately, a great emphasis has been given towards the generation of gradients by using microchannels [76]. Nevertheless, this technique does not simply allow to be used as a vehicle to deposit compounds, but also as a manner to cure itself into the surface or to remove a material.

Microfluidic patterning is very useful since it allows for selective protein immobilization and selective cell adhesion. Moreover, if gradient systems are used, it is possible to analyze the influence that two or more different drugs or other different compounds have over a single cell. Also, capillary force lithography is often used for immunoassays. The small volume of reagents required by this technique makes it a very powerful and unique tool for screening tests. However, the patterns are limited to the channel geometries [10].

4.2.2.4. Scanning Probe Lithography

Scanning probe lithography (SPL) embraces a range of techniques that involve the surface modification at the nanoscale by means of scanning probes as atomic force microscopes (AFM) and scanning tunneling microscopes (STM) [50, 77]. By utilizing AFM and STM tips, SPL techniques enable for precisely pattern atoms or clusters of atoms onto a surface [50]. There are mainly three SPL sub-areas. The first one is entitled dip-pen nanolithography and allows for creating patterns of 15 nm. In this process, an AFM tip is inked with the material to be patterned, and while scanning a substrate, the tip transfers the material. For that, the humidity present plays an important role. Another area of SPL consists on the selective removal of a material from a surface. This is achieved by applying high pressure with the AFM tip onto the coated surface. Usually, the molecules that are removed from the surfaces

are SAMs. Finally, the third area is based on the localized chemical modification of the surface, either by electrochemical anodization or by using a conductive AFM or STM tip.

4.2.3. Electrospinning

Electrospinning is a well known and ubiquitous technique that enables the production of nanofibers and has been used by many researchers to make nanofibrous matrices for TE applications [55, 78-84]. The process of electrospinning results from the application of a high voltage electrostatic field operated between a metallic capillary of a syringe and a grounded collector. As a result from this electrostatic field, a solution drop deposited at the tip of the capillary tube elongates into long and thin fibers and projected over the grounded collector. The nanofibers produced by electrospinning are collected into a nonwoven web, which generally originate a random fiber orientation mesh with limited mechanical properties.

Scaffolds produced by this technique were shown to closely mimic the structure and morphology of native extracellular matrix (ECM) that consists of fibrilar structures with nano-sized diameters [85-87].

This technique also provides the possibility of producing nanofibrous scaffolds from native polymers such as collagen and elastin. TE constructs based on these materials produced by electrospinning have been widely reported [80, 88, 89], once they have been able to direct cell alignment and support cell growth (Figure I.6).
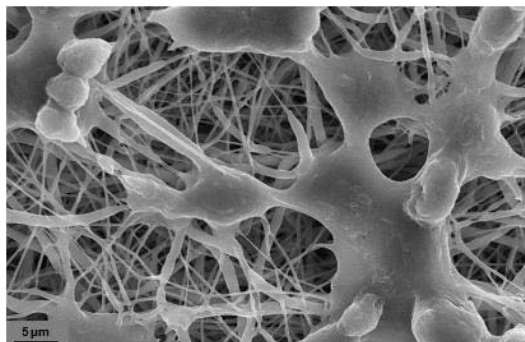
Figure I.6. Nanofiber mesh of polycaprolactone obtained by electrospinning cultured with SaOs-2.

5. APPLICATION OF MICRO AND NANOTECHNOLOGIES IN THE CONTROL OF CELL-MICROENVIRONMENT INTERACTIONS

Within a TE strategy, micro and nanotechnologies have been increasingly used either for studying or enhancing cell biology and biochemistry. To overcome the existing challenges in

TE strategies, micro and nano platforms have been developed to give inputs concerning: (i) cell behavior in different culturing conditions, (ii) cell-cell interactions in co-cultures, usually achieved by means of patterned surfaces, (iii) cell-ECM communication by high-throughput platforms, or (iv) analyze the influence of several soluble factors on specific cells through microfluidic systems (Figure I.7).

Cell-Microenvironment Interaction

Cell-Cell	Cell-ECM	Cell-Soluble Factors
Micro and Nano Patterned Surfaces	High-throughput systems (arrays)	Microfluidic Systems
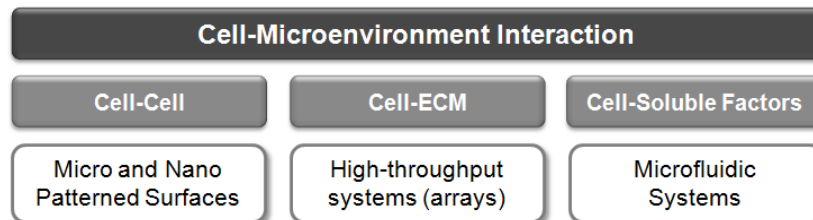
Figure I.7. Schematic representation of the micro and nano platforms used for tissue engineering applications.

Although much work still lies ahead, the ability to engineer the surface properties at a micro and nano scale has already proved to be useful for a wide spectrum of applications in TE. Engineered applications for TE by means of micro and nano technologies have been majorly focused on 2D structures. Nevertheless, besides the potential shown at a 2D level, micro and nanotechnologies have been successfully exploiting the 3D structured world. Since these support systems for tailoring cell behavior and for tissue regeneration have shown so promising results, efforts have been made towards mimicking with increased accuracy, the natural environment in tissues. Actually, microbioreactor systems are being developed that could enable tissue growth in a tightly controlled microenvironment. The next sections will highlight the interaction of biomaterials produced by micro and nano technologies with proteins and subsequently cells necessary for the regeneration of the abovementioned tissues, both at a 2D and 3D level. Moreover, a brief overview over the recent advances in the development of microbioreactors will be presented.

5.1. Micro and Nanotechnologies in the development of enhanced constructs for tissue engineering

In the development of constructs for TE strategy by means of micro and nanotechnologies, researchers must play attention to two important parameters: the design of the patterns should mimic as much as possible the native structural environment; and the biomaterial selected to be the groundwork of the patterned system should have appropriate characteristics for a specific application. During the last couple of decades, great efforts have been directed towards creating systems that could resemble the native environment of

tissues. In fact, important areas of tissue engineering have already taken advantage of such structures to understand the phenomena occurring at the interface biomaterial-biological entities, applying then the concepts into a tissue engineering strategy.

Several materials have been developed with osteoinductive and osteoconductive surface topographies intended to lead to the formation of new bone in the case of fracture or disease. Further investigations have shown increased osteoblast functions, such as cell proliferation and activity, when cultured onto nano-featured surfaces [90]. Moreover, reports have shown that the osteoclasts (bone-resorbing cells) activity [91, 92] was also influenced by the topographical micro and nano-sized cues. The coordination among osteoblasts and osteoclasts is of utmost importance for the effective maintenance of healthy bone. Therefore, results showing synergetic functions of osteoblasts and osteoclasts to ensure a healthy bone remodeling at the implant interface are of extreme importance. Recent studies have reported the successful application of microtopographies in improving the osteointegration and that microgrooves combined with chemical cues can guide selective rat mesenchymal stem cell-derived osteoblasts adhesion and alignment [93]. Further insights on the influence of patterns in the guidance of osteoblast cells were reported by S. Ber and colleagues, showing that through the appropriate choice of surface topography, both the cell alignment and bone formation by mesenchymal osteoprogenitor cells can be enhanced [94]. Polycaprolactone nanofiber meshes obtained from electrospinning have also shown enhanced cell attachment and proliferation when coated with biomimetic calcium phosphate (BCP) layer. [95]. In a different study is shown that the combination of nanofibers produced by electrospinning with micro fibers, originates scaffolds with enhanced characteristics for application in bone tissue regeneration [96]. The innovative structure of these scaffolds, inspired by extracellular matrix (ECM), simultaneously promotes cell adhesion through a nano-network and provides mechanical stability by means of the micro-fiber mesh. In another study, it was shown that the architecture of nano/micro-fiber-combined scaffolds elicited and guided the 3D distribution of endothelial cells without compromising the structural requirements for bone regeneration, demonstrating the potential of such structures to overcome the lack of vascularization that is associated with current bone TE constructs [97]. Figure I.8 shows this scaffold system embedded in a collagen gel, allowing to visualize Human Umbilical Vein Endothelial Cells (HUVECs) aligned both on the micro and nano polymeric fibers.
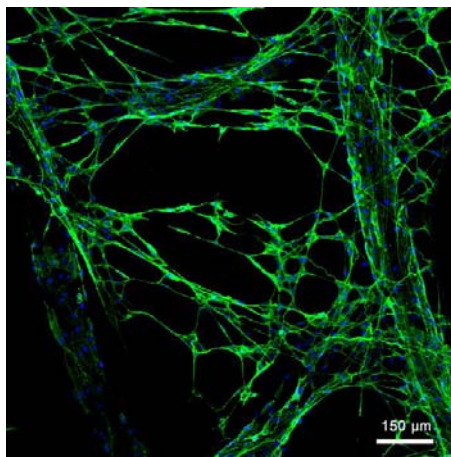
Figure I.8. Human Umbilical Vein Endothelial Cells (HUVECs) on collagen-nano and SPCL-micro fiber-combined scaffold after 7 days of culture. HUVECs were stained with endothelial-specific marker platelet/endothelial cell adhesion molecule-1 (PECAM-1) and nuclei were counterstained with DAPI.

The advent of micro and nanotechnologies associated with TE holds a great promise also for cartilage tissue regeneration. Currently, researchers suggest that TE strategies combined with nanopatterned materials can be useful for obtaining functional regeneration of cartilage tissue. The rationale is based on mimicking as closely as possible the natural composition and properties of cartilage. A study reports that micropatterned hyaluronic acid surfaces induced higher adhesion, migration and alignment of knee articular cartilage chondrocytes when compared to homogenous surfaces. Moreover, the patterned surfaces showed to promote cell differentiation into chondrocytes [98]. Similarly, Erik Petersen and his colleagues reported that cells cultured onto a microarray of micropatterned surfaces maintained their morphology and their ability to retain important phenotypic aspects of the chondrocytes [99]. Besides being applied into static cultures, micro and nano technologies have also been applied into the understanding of how cells respond to dynamic changes of the extracellular osmolality. P. Grace Chao and colleagues have described a system that yielded new information regarding the dynamic osmotic loading of chondrocytes, which could also contribute with new insights about the mechanisms of cellular homeostasis of other cell types [100]. Also, electrospinning has been successfully applied to the development of nanofiber meshes of starch-compounded PCL to act as a scaffold for cartilage tissue engineering [101].

The behavior of vascular cells (such as endothelial and smooth muscle cells) has shown to be enhanced on micro and nano structured surfaces. Microfluidic networks have been developed to produce highly uniform flows that mimic physiological patterns [102]. Sachin C. Daxini and colleagues have devoted efforts into testing the hypothesis that by creating well-defined micro-textured surfaces, low shear-stress regions could be created, which would

help on retaining endothelial cells. They have shown that endothelial cell retention was significantly improved on micropatterned surfaces when compared to unpatterned ones, which would be beneficial into reducing the thrombogenicity of implanted vascular grafts [103]. Another study went deeper into the analysis of how endothelial cells respond to the shear stress caused by the blood flow. This study helped on understanding the process of endothelial mechanotransduction, suggesting that the design of new substitutes for vascular tissue engineering, should not only consider the material and biological cues, but also the hemodynamic profiles, in order to improve tissue integration and regeneration [104]. An essential parameter in vascular tissue engineering is the recruitment of cells from the blood to the vascular wall in a situation of thrombosis or inflammation. In this context, Divya D. Nalayanda and colleagues have reported the development of microfluidic patterned surfaces that were successful in controlling the adhesion and rolling of endothelial cells under physiological flow [105].

The ability to direct cell attachment and orientation, jointly with the possibility to create fluidically isolated compartments, points out to the distinctive advantage of micro and nanotechnologies for neural tissue regeneration than the regular culture conditions. A very promising work that went deeper into the issue of synaptic signaling presented results that established that synapses forming on confining geometry of the micropattern are physiologically normal and capable of performing plastic modulations, demonstrating their usefulness as a model for signal processing by neuronal networks [106]. Essential parameters within a neural TE strategy are being further exploited by means of micro and nanotechnologies, such as the cell orientation, allowing for mimicking the microcircuitry that is encountered in the native tissue. A work of Christopher Bettinger and co-workers, reports the use of a flexible and biodegradable substrate of poly(glycerol–sebacate) with rounded features that could further elucidate the mechanism of cell alignment and contact guidance [30].

The liver is another well studied system in TE since the existing systems cannot fully mimic the synthetic and metabolic liver system. One option is the development of liver-like structures by means of micro and nanotechnologies. Recently, a very promising device was developed by scientists at the Harvard Medical School and the Massachusetts Institute of Technology that could eventually be used to create a functional liver organ. Basically, it involves the development of a network of microscopic tubes that branch out in a pattern similar to a vascularized system, to provide oxygen and nutrients to the liver cells. Indeed, 95% of the liver cells survived up to 2 weeks in this system [107]. Another system that combines microtechnologies and TE is the one described by Bhatia that consists on a miniaturized, multi-well culture system with a micropatterned architecture of collagen that has shown to maintain the phenotypic behavior of primary rat hepatocytes [108]. Recently, a

microfluidics bilayer device with a physiologically-based network was also described. The device showed to be able to maintain hepatic functions of both human hepatoma cells and primary rat hepatocytes [109].

The application of micro and nanotechnologies in the biology field has recently gone beyond the mainstream research for the engineering of a specific tissue. Stem cells and biomaterials that support their adhesion, proliferation and differentiation represents nowadays a very intense area of research. The use of micro and nano technologies for stem cell adhesion, proliferation and/or differentiation is a slightly different approach in comparison to the aforementioned tissue engineered approaches. By using stem cells, researchers aim, not only the regeneration of one specific tissue, but instead a wide variety of tissues and organs. In fact, micro and nano technologies are of extreme importance for studying stem cell differentiation since they allow generating a tightly tailored microenvironment according to the specificities of each tissue. Recently, Khademhosseini and collaborators have successfully developed cell-repellant poly(ethylene glycol) (PEG) wells that were used as templates for the formation of embryoid bodies (EB), which are cell aggregates of embryonic stem (ES) cells. This promising method showed that microwell techniques can be of great usefulness for initiating the differentiation of EB under controlled microenvironments [110]. Another study showed the successful application of micro and nanotechnologies to the maintenance of the undifferentiated state of human embryonic stem (hES) cells. The microwell patterned surfaces have proven to be effective in generating almost perfect aggregates for further differentiation studies [111]. Bhatia and co-workers have been devoting a great effort into the development of high-throughput platforms for the analysis of the signals and mechanisms that regulate stem cell fate [112]. Recently, a platform for assessing the interaction of ECM bioentities and growth factors and their effect on stem cell fate was developed [113]. This high-throughput technology allows for the simultaneous analysis of 1200 different experiments. The differentiation along cardiac lineage was assessed by means of a confocal microarray scanner. This technology represents a step further on the understanding of the microenvironment that dictates stem cell fate [113].

Besides the studies with embryonic stem cells, reports combining stem cells from other sources and micro and nanotechnologies have shown really promising results. An example is the work described by D. Zahor and colleagues [114], who have induced topography-guided alignment of mesenchymal stem cells by culturing them on micropatterned silicon surfaces. Another study evaluated the efficacy of a micropatterned surface in differentiating multipotent mouse bone marrow stromal precursors into fat tissue [115]. The results showed the positive influence of the patterns in the lipid production. Recently it was also reported the development of a biomimetic scaffold that could mimic a specific niche, where bone marrow-

derived hematopoietic stem cells (BM-HSCs) could healthily proliferate and differentiate [116].

Table I.2 summarizes the latest research studies in the area of TE that involve micro/nano structured surfaces. Examples are given regarding micro and nanotechnologies used to pattern surfaces aimed for vascular, bone, cartilage, neural and liver TE strategies, as well as for stem cell differentiation. Further information may be obtained in the references identified in the last column of the table.

Table I.2. Examples of controlling cell microenvironment using micro and nano technologies.

Application	Micro/Nano Technology	Cell-Microenvironment Interaction	Material	Features	Cells	Effect Observed	Ref.
Bone	Photolithography	Cell orientation and behavior	-	330nm deep and either 10, 25 or 100µm in width	HOBs	Groove/ridge topographies are important modulators of both cellular adhesion and osteospecific function and, critically, groove/ridge width is important in determining cellular response.	[117]
	Photolithography	Cell behavior	Photocrosslinkable chitosan	500-500 µm or 100-100 µm	SaOs-2	The method utilized allowed to create patterned cell co-cultures by using lysozyme or layer-by-layer surface switching.	[118]
	Photolithography combined with electrochemical micromachining	Cell shape and behavior	Titanium	Cavities with 100, 30 and 10 µm diameters	MG63 osteoblast-like cells	Cell attachment depends on cavity spacing, cell growth and aggregation depends on cavity dimensions, and cell morphology depends on the presence of sub-micron-scale structural features.	[119]
	Soft-lithography	Cell orientation and behavior	Collagen	groove width: 27 mm; groove depth: 12 mm; ridge width: 2 mm	Mesenchymal osteoprogenitor cells	Cell alignment can be significantly affected by the topography of the carrier surface; Appropriate surface topography can enhance bone formation.	[94]
	Microcontact Printing	Cell behavior	PHBV	1-10 µm groove width; 5-30 µm groove depth	Rat mesenchymal stem cell-derived osteoblasts	Microtopographies on PHBV can improve osseointegration when combined with chemical cues; microgrooves and cell adhesive protein lines on PHBV can guide selective	[93]

					osteoblast adhesion and alignment.	
	Microcontact printing combined with hot-embossing imprint lithography	Cell orientation and behavior	Polyimide; fibronectin	8 μm wide grooves 4 μm deep (hot-embossing printing); 10 μm wide (microcontact printing)	MC3T3-E1 osteoblast-like cells	Although chemical patterns induced stronger alignment than mechanical topography when presented separately, mechanical topography dominated alignment for all chemical patterns when combined.	[120]
	Electrospinning	Cell orientation and behavior	SPCL	Diameter of fiber 400 nm (average)	SaOs-2	The presence of the nanofibers induced the cell morphology to change into a more stretched and spread shape, increased cell activity and viability.	[96]
	Electrospinning	Cell orientation	PCL	Diameters of the fibers ranging between 200nm and 1.2 μm.	SaOs-2	The cells integrate with the surrounding fibers and migrate into the inner nanofibrous structure to form a three-dimensional cellular network.	[121]
Cartilage	Replica-molding	Controlled Microenvironment	PDMS; glass coverslip	Channels with 300 μm wide and 100 μm high	Chondrocytes isolated from articular cartilage	The method associated with an inverted microscope allowed to monitor real-time cell size changes; articular chondrocytes exhibited a trend of increasing changes in cell size with decreasing osmotic loading frequency.	[100]
	Photolithography	Cell behavior	HA on PET	Channels with 25 and 5 μm wide and with the same spacing	Articular knee chondrocyte	Micropatterned HA induced adhesion, migration, alignment and differentiation of chondrocytes.	[98]
	Photolithography	Cell shape and behavior	Agarose gel	15-65 μm wide; 40 μm deep	Chondrocytes isolated from	Micropatterned polymer gels were subsequently applied	[99]

				avian sterna	as scaffolds for chondrocyte culture and proved effective in maintaining key aspects of the chondrogenic phenotype (rounded cell morphology; production of type II collagen).	
Vascular	Soft-lithography	Controlled Microenvironment	PDMS	10 μm wide, 3 μm deep, 10 μm distance between each groove	MSCs	Microgroved patterns induced global gene expression changes (an increase in the smooth muscle marker calponin 1, a decrease in cartilage matrix markers, and alterations in cell signaling).	[122]
	Soft-lithography	Cell shape and behavior	PDMS and collagen	groove and ridge widths of 330 nm each; depth of 100 nm	VSMCs	Nanopatterns could successfully guide VSMCs along the pattern axes, improving collagen construct strength.	[123]
	Soft-lithography	Cell behavior under shear stress	PU	95 μm wide and 32 μm deep	Endothelial cells	Endothelial cell retention is improved on micropatterned surfaces, which could help on reducing the thrombogenicity of implanted grafts.	[103]
	Soft-lithography associated with melt molding and particulate leaching	Cell shape and behavior	PCL and PLGA	48 μm grooves; 5 μm deep; 12 μm spacing	VSMCs	VSMCs seeded into PLGA leached micro-patterned PCL scaffolds maintain similar degrees of alignment as seen on non-porous micro-patterned scaffolds (findings associated with promoting *in vivo* like VSMC morphology, enhanced ECM production and	[124]

					decreased proliferation).	
Microfluidic patterning	Cell shape and behavior	HA hydrogels			Cardiomyocytes	The linearly aligned myocytes detached from the surface and formed contractile cardiac organoids.	[125]
Microfluidic patterning	Cell-ligands	PEG	Gradient generation of tethered RGDS through a microfluidics/ photopolymerizatio n process		HUVEC	The adhesive ligand gradients modulated spatial distribution of attached endothelial cells.	[76]
Microfluidic patterning	Cell-ligands	PDMS	Width of 50–1000 µm and spacing between them of 50–100 µm; patterned adhesion molecules: P-selectin, E-selectin, von Willebrand Factor		Neutrophils, ChineseHamste r Ovary cells, platelets	The adhesion and rolling of three different cell types was controlled by patterning microfluidic channels with different ligands.	[105]
Electrospinning	Cell orientation and behavior	P(LLA-CL)	Diameters of the fibers ranging from 200 nm to 800 nm.		SMCs	The SMCs attached and migrated along the axis of the aligned nanofibers and expressed a spindle-like contractile phenotype.	[126]
Microcontact printing	Cell behavior	PDMS	Width of 20 and 115 Mm		Bovine aortic endothelial cells	The presented cell morphology may interfere with the mechanisms sensing the physical cues, therefore responding differently to shear stress.	[104]

	Microcontact printing	Cell-Cell; Cell behavior	Silicon oxide	3 to 20 µm in line width; 3.5 nm high of the layer	Rat hippocampal neurons	The immobilized neurons showed resting membrane potentials comparable with controls and were capable of eliciting action potentials after 1 day of culture.	[127]
	Microcontact printing	Cell orientation and behavior	Polystyrene; PDMS	4–6 µm wide lines	Rat embryonic cortical neurons	Cells comply well with the pattern and form synaptic connections along the experimentally defined pathways.	[106]
Neural	Replica-molding	Cell shape and behavior	Poly(glycerol–sebacate) on sucrose-coated microfabricated silicon	2-5 µm in wavelength; depth of 0,45 µm.	Bovine aortic endothelial cells	Cells cultured on substrates with smaller pitches exhibited a substantially higher frequency of cell alignment and smaller circularity index; this system showed to be appropriate for *in vivo* applications.	[30]
	Electrospinning	Cell orientation and behavior	PLLA	Average diameter of 300nm (concentration of 2% of PLLA) and of 1.5 µm (concentration of 5% of PLLA)	NSCs	The rate of NSC differentiation was higher for PLLA nanofibers than that of micro fibers and it was independent of the fiber alignment.	[128]
	Electrospinning	Cell orientation and behavior	PCL	Fiber diameter around 250 nm	hECs	When EBs cultured onto PCL nanofibers, they were capable of differentiating into mature neural lineage cells including neurons, oligodendrocytes and astrocytes. The aligned nanofibers prepared could also direct the neurite outgrowth.	[129]

	Photolithography	Cell-Cell (3D Structure)	PEG hydrogels	500 µm in width	Hepatocytes	Three-dimensional photopatterned constructs were cultured in a continuous flow bioreactor for 12 days where they performed favorably in comparison to unpatterned, unperfused constructs.	[130]
	Photolithography	Controlled Microenvironment	PDMS	through-holes (500 µm with 1200-µm center-to-center spacing)	Primary rat hepatocytes; Primary human hepatocytes; 3T3-J2 fibroblasts	The miniaturized, multiwall culture system for human liver cells with optimized microscale architecture was able to maintain phenotypic functions for several weeks.	[108]
Liver	Photolithography combined with robotic microarraying of proteins	Controlled Microenvironment	PEG	Collagen spots with 170 µm in diameter; 30 µm-30 µm PEG wells	Rat hepatocytes	When exposed to micropatterned surfaces, hepatocytes interacted exclusively with collagen-modified regions, attaching and becoming confined at a single-cell level within the hydrogel wells.	[131]
	Photolithography combined with anisotropic wet etching	Controlled Microenvironment	Titania ceramic	Circles with 200 µm in diameter; Heights ranging from 50-135 µm	Rat liver hepatocytes	The cells mainly aggregate within the cavities, and only single cells or small clusters are attached to the rims between the pits.	[132]
	Soft-lithography	Controlled Microenvironment	PDMS; polycarbonate	Branch pattern; main inlet and outlet channels are 2650 µm; the channels progressively branch and decrease to 35 µm in width	Hepatoma cell line HepG2/C3A; Primary liver cells	The design provides sufficient oxygen and nutrient mass transfer to support the viability and function of both a highly metabolic hepatoma cell line and primary rat hepatocytes.	[109]

	Electrospinning	Cell-Cell	PCLEEP	Diameters of the fibers ranging from 300nm to 1.5 µm.	Primary rat hepatocytes	Galactosylated PCLEEP nanofiber mesh exhibits the unique property of promoting hepatocyte aggregates within the mesh and around the fibers, forming an integrated spheroid–nanofiber construct.	[133]
Stem Cells	Photolithography	Cell orientation	Silicon	5 µm of width; 5 µm of spacing; 1.6 µm of depth	MSCs	The cells were shown to inhabit the grooves rather than ridges and exhibited an elongated shape, with unusually long processes.	[114]
	Photolithography	Cell behavior	PLLA	3 µm of width; 100 µm of spacing; 1.5 µm of depth	Mouse bone marrow stromal precursors	The microtopography showed to influence the differentiation of cells to adipocytes, also affecting the rate of lipid production.	[115]
	Soft-lithography	Cell shape and behavior	CCG blended membranes	200 µm in width and 80 µm in depth	hMSCs	Some of the cells formed a bridge-like structure between two adjacent ridges; the micropatterned CCG membranes could be used to regulate the distribution, alignment, proliferation and morphology of hMSCs during cell culture *in vitro*.	[134]
	Soft-lithography	Cell differentiation; Controlled Microenvironment	Cell-repellant PEG	150 µm – 40 µm diameter microwells	hECs	The microwell technique could be a useful approach for *in vitro* studies involving ES cells and, more specifically, for initiating the differentiation of EBs of greater uniformity based on	[110]

Soft-lithography	Cell-ECM	PDMS	3.5 mm in diameter bioreactors, arranged in a 4 x 3 array	hESCs	The microbioreactor array that combines the advantages of microarrays with those of bioreactors, provided means to study the growth and differentiation of hESCs under controlled conditions.	[135]
					controlled microenvironments.	
Soft-lithography	Controlled microenvironment	PDMS	cylinders 200 µm in diameter and 120 µm in height	hECs; MEFs	While exhibiting a similar viability and self-renewal profile as that of hES cells grown on flat surfaces, hES cells grown on microwell-patterned substrates show a greater level of homogeneity in aggregate size.	[111]
Electrospinning	Controlled microenvironment	Blend of poly(DL-lactide-co-glycolide) and collagen I	Diameter of fibers ranging from 100 nm to 500 nm in diameter.	BM-HSCs	Besides acting as an *in vitro* HSC culture system for supporting hematopoiesis purpose, the constructs may also act as an efficient captor and carrier for HSCs.	[116]
Electrospinning	Controlled microenvironment	PES	Fibers with an average diameter of 529 ±114 nm	HSPCs	Aminated nanofiber mesh could further enhance the HSPC-substrate adhesion and expansion of CFU–GEMM forming progenitor cells.	[136]

Legend: primary human osteoblasts (HOBs); Human osteogenic sarcoma cells (SAOS-2 cells); Poly(3-hydroxybutyrate-co-3-hydroxyvalerate) (PHBV); starch/poycaprolactone (SPCL); poly-caprolactone (PCL); Polydimethylsiloxane (PDMS); hyaluronic acid (HA); polyethylene-terephthalate (PET); Mesenchymal stem cells (MSCs); Bovine Aorta Cells (VSMCs); polyurethane (PU); polylactic-co-glycolic acid (PLGA); poly(ethylene glycol) (PEG); Human umbilical vein endothelial cells (HUVEC); poly(L-lactid-co-ε-caprolactone) P(LLA-CL); human coronary artery smooth muscle cells (SMCs); poly(L-lactic acid)

(PLLA); neural stem cells (NSCs); human embryonic stem (hECs) cells; poly(e-caprolactone-co-ethyl ethylene phosphate) (PCLEEP); chitosan–collagen–gelatin (CCG); Human mesenchymal stem cells (hMSCs); murine embryonic fibroblasts (MEFs); hematopoietic stem cells (BM-HSCs); polyethersulfone (PES); hematopoietic stem/progenitor cells (HSPCs)

5.2. Towards 3D micro and Nanofabricated structures

An effort has been made to push the domain of micro and nanotechnologies from bi-dimensionality to three-dimensionality [137] extending the applicability of these technologies. This transition to 3D structures can be achieved using micro and nano technologies to buildup three dimensional structures by stacking multiple two-dimensionally microfabricated layers. This kind of technology has been widely used in TE strategies for developing micro and nano-grooved three-dimensional microfluidic devices for the replication of several kinds of tissues [138]. Despite the high resolution achievable through those techniques, the basic two-dimensional nature of substrates used has not yet allowed to fully replicate the real three-dimensional structure of tissues and consequently to replicate their full functionality.

Some of the above mentioned techniques have already been successfully applied in the development of 3D supports for cell growth. For example, a method that combines the chemistry of bottom-up approaches with the engineering of top-down approaches was successfully employed to the development of 3D hydrogel structure [41]. Indeed, from the many synthetic materials being explored, hydrogels are amongst the most widely adopted for 3D cell cultures, due to their high water content and mechanical properties. Top-down TE approach allows for constructing 2D patterned hydrogels, either by photolithography or soft-lithography methods. A bottom-up approach is used further for the modular assembly of the small building blocks. A good example of this combined process is the packing of rod-shaped collagen microgels seeded with HepG2 hepatocytes and co-cultured with endothelial cells at the surface [139]. Langer and collaborators developed structures with defined shapes by micro-molding photocroslinkable hydrogels. Several cell types were encapsulated and the architecture tightly controlled [40, 140]. Using a different approach with photopolymerizable PEG hydrogels, it is possible, with tailored chemistry and architecture, to generate a 3D structure that can further support hepatocyte survival and liver-specific function [130].

Conceptually, 3D microfabricated objects should be created with three-dimensional resolution and ideally be freely manipulated (i.e. fabricated without any necessary attachments to the substrates). One of the challenging issues in TE strategies still is the uniform distribution of cells within 3D-scaffolds. As an attempt to surpass this challenge, it was studied the effect of three-dimensional, porous poly(L-lactide-co-glycolide) (PLGA) scaffolds modified with poly(ethylene oxide) (PEO) over cell behavior, within a bone TE strategy. This work showed that patterned regions of low and high cell adhesion were demonstrated on scaffolds fabricated with 1 mm thick stripes of PEO and non-PEO regions, respectively [141]. Another very promising work was recently reported [125], which is based on using microfluidic patterning for the development of 3D cardiac organoids. After seeding, the cardiomyocytes elongate along the hyaluronic acid (HA) patterns that serve as inductive

templates for organoid assembly. This study has further shown that only after 3 days of culture, the cardiomyocytes detach from the surface and start to show a contractile behavior. Many groups are now investigating the possibility of creating 3D objects through rapid prototyping techniques which consist of building up layer upon layer of material by printing methodologies. This approach is already successfully used in industrial large scale rapid prototyping by using techniques such as inkjet printing, stereolithography, selective laser sintering or fused deposition modeling. Such technologies are capable of generating objects with high geometry freedom and possessing highly complex three-dimensional architectures. Prototyping techniques based on the material selective deposition are also capable of building structures from actual living tissues/cells. The technology, so-called bioprinting, offers the ability to deposit cells and other biomolecules in a rapid layer-by-layer method, allowing creating three-dimensional tissue-like structures. A complex three-dimensional microfluidic system was fabricated with PDMS by rapid prototyping using two-level photolithography and replica molding. This method allows generating complex patterned microfluidic systems [142].

The 3D bioprinting technology is currently being studied by for possible use in TE applications where organs and body parts are intended to be built using inkjet techniques [143]. The above mentioned techniques, although capable of being fast and economic, are mostly limited by the scale factor since, in most cases, they are not capable of applying high printing resolutions.

Ultrasmall features may be achieved by the 3D microfabrication technique of 2-photon polymerization. In this approach, the desired 3D object is traced out in-situ (in the interior of a photopolymerizable liquid gel) by a focused laser beam. Unlike the commonly used lasers, the laser source used in this methodology is based on a visible light, ultra short pulse laser. The gel is cured to a solid only in the places where the laser is focused, due to the nonlinear nature of photoexcitation. When the process is finished the remaining gel is simply washed away. Feature sizes with 700 nm can be produced by this method that allows also the production of complex structures including moving and interlocked parts [144]. Another important feature on this technology is the nature of the polymerizable gel which can be made of a range of proteins such as fibrin, collagen and albumin which are very abundant in native human tissues.

5.3. Towards in vivo microenvironment - MicroBioreactors

Several recent studies demonstrate the importance of mimicking _in vitro_ certain critical aspects present in the native environment of tissues to be regenerated. Therefore, besides the basics of TE strategies, scaffolds and cells, it is of utmost importance to provide the cell-scaffold constructs with the appropriate microenvironment that will encourage the effective

organization among the elements of a tissue engineering strategy. The most widely used type of culturing system operates in static culture conditions. However, it is known that it may cause non-homogenous distribution of cells and nutrients and does not allow mimicking the flow stresses that are present _in vivo_. Bioreactors are systems that have shown to be successful in surpassing these challenges in culture systems. Bioreactors used in TE strategies not only allow for the growing of cells to higher densities but can also be used as extracorporeal devices for liver and kidney diseases. Moreover, in these systems, the biological and biochemical processes are closely monitored and the culturing conditions, such as the pH, temperature, pressure, shear stress, nutrients supply and waste removal, are tightly controlled.

Microbioreactors, also known as microfluidic bioreactors, offer further advantages for cellular applications. Besides providing large surface-area-to-volume ratio, they can offer microscale controllable fluid circuits [145, 146]. Indeed, microreactors have shown promising results in applications where conventional bioreactors have failed, since they act not as a mere culturing system but as a device for studying the mechanisms occurring at the tissue microenvironment. This allows designing better materials and/or culturing systems. For instance, a perfusion-based, micro 3-D cell culture platform was designed and fabricated based on SU-8 lithography and PDMS (poly-dimethylsiloxane) replication processes and used to study the loading of cell/agarose constructs. Moreover, this system was found to be particularly useful for cell-culture-based drug screening systems [147]. In fact, cell culture assays, combined with microbioreactors are now emerging as enabling tools for high-throughput cytotoxicity assays, since they allow for high controllability of operation and on-line monitoring/sensing [148]. A different system demonstrated the long-term culture (more than two weeks) of mammalian (human foreskin fibroblasts, HFF) cells in a microbioreactor under constant perfusion and the importance of understanding the relationship between design parameters (channel size, oxygen lever supply, shear stress, flow rate) and cell behavior (cell growth, cell morphology, perfusion rate) in microscale culture system [149]. In another approach, a microbioreactor with the size of a glass slide was used for studying the mechanisms involved in culturing _in vitro_ human embryonic stem cells (hESCs) [150]. A different microbioreactor with a PDMS treated surface was developed based on mass transport simulation. The elastomeric surface was treated with a surfactant in order to diminish the non-specific protein adhesion, keeping the culture conditions steady. This system helped on understanding what is the environment that better provides chondrocytes stable culture conditions over the culturing period [151]. Within a liver TE strategy, two types of PDMS microbioreactors containing a membrane, used as a scaffold for the attachment of cells, were developed. In this system, cells were immersed in the culture medium, expressing much higher functions and better mimicking the hepatocytes _in vivo_. After 15 days of culture,

the primary adult rat hepatocyte cultures have shown good cell attachment and reorganization, revealing to be promising tools for future liver TE [152]. Also aiming at promoting liver tissue regeneration, Linda Griffith and co-workers have developed a microbioreactor for perfused 3D liver culture. The reactor dimensions were designed so that the flow rates meet the estimated values of oxygen demand and also providing a shear stress at or below the physiological one. For 2 weeks, primary rat hepatocytes rearranged to form tissue-like structures, indicating that this system approximates the perfusion and architectural properties of an *in vivo* hepatic tissue [153, 154]. Recently, an array of twelve microbioreactors was reported [135]. With this technology, high-throughput assays can be performed, by assessing many factors that regulate cell behavior. The microbioreactor was fabricated by soft-lithography and each individual microbioreactor is perfused by culture medium. Moreover, this system allows for cells to be cultured onto the substrate or encapsulated in hydrogels, being the results followed by automated image analysis. As a prof-of-concept, researchers have cultured C2C12 cell line, primary rat cardiac myocytes and human embryonic stem cells (hESCs), illustrating the utility of the microbioreactors array for controlled studies.

A variety of large-scale bioreactors have been developed and optimized for TE strategies. Nevertheless, microfluidics has lead to the advent of a new generation of bioreactors aimed at mimicking *in vitro* the native microenvironment of tissues. Despite the already performed research in this area, microbioreactors are a relatively new direction in TE, leaving still plenty of room for new developments in human 3D models for studying the underlying mechanisms in cellular microenvironments.

6. CONCLUSIONS AND OUTLOOK

This chapter reviewed the recent developments regarding the use of micro and nano fabrication techniques as enabling technologies to tailor the characteristics of constructs aimed for tissue engineering. Technologies such as photolithography and soft-lithography, adapted from microelectronics, begun in the last couple of decades to provide opportunities for the tissue engineering area. Despite the already demonstrated potential of micro and nano technologies in some areas of the tissue engineering (bone, cartilage, vascular, neural, liver tissue engineering and stem cell research), the developments are still in an early stage. In fact, currently, although some of the described technologies are indeed capable of building structures with micro and nano architectures, these are mostly applied to build either micro or nano-sized devices. The major current challenge of micro and nano technologies in TE is therefore to extend the micro/nano architectures to macroscale devices which are large enough for substituting/regenerating tissues. To build those devices, the production

technologies need to be improved in order to become faster and more effective and at the same time not compromising the level of detail of the structures produced.

Nevertheless, given that the technology behind micro and nano fabrication techniques is already well established, that the creation of innovative biomaterials is developing at a rapid pace, and that the input from tissue and cell biology is continuously increasing, we believe that we are just on the verge of new opportunities that result from the synergies of the development of those areas.

Throughout the review some issues for future research are identified, hoping that technology can develop into those expanding areas. It is strongly expected that micro and nano technologies will have a major impact on TE, as they once had on microelectronics. Thus, key contributions regarding cell-microenvironment interactions are envisioned. Moreover, taking advantage of these new insights about the *in vivo* microenvironment, we expect the development of systems that could actually engage in healthy tissue regeneration.

REFERENCES

1.   CA V. The history of tissue engineering. J Cell Mol Med 2006;10(3):569-576.
2.   Gomes ME, RL R. Tissue Engineering: Key Elements and Some Trends. Macromolecular Bioscience 2004;4:737–742.
3.   Stock UA, Vacanti JP. TISSUE ENGINEERING: Current State and Prospects. Annual Review of Medicine 2001;52:443–451.
4.   Nair LS, Laurencin CT. Biodegradable polymers as biomaterials. Progress in Polymer Science 2007;32(8-9):762-798.
5.   Seal BL, Otero TC, A P. Polymeric biomaterials for tissue and organ regeneration. Materials Science and Engineering: R: Reports 2001;34(4-5):147-230.
6.   Ratner BD, SJ B. BIOMATERIALS:Where We Have Been andWhereWe Are Going. Annu Rev Biomed Eng 2004;6:41–75.
7.   Curtis A, M R. Tissue engineering: the biophysical background. Physics in Medicine and Biology 2001;46(4):R47-R65.
8.   Ikada Y. Challenges in tissue engineering. Journal of the Royal Society Interface 2006;3(10):589-601.
9.   Ryu W, Fasching RJ, Vyakarnam M, Greco RS, FB P. Microfabrication technology of biodegradable polymers for interconnecting microstructures. Journal of Microelectromechanical Systems 2006;15(6):1457-1465.
10.   Falconnet D, Csucs G, Grandin HM, M T. Surface engineering approaches to micropattern surfaces for cell-based assays. Biomaterials 2006;27(16):3044-3063.
11.   Nakanishi J, Takarada T, Yamaguchi K, M M. Recent advances in cell micropatterning techniques for bioanalytical and biomedical sciences. Analytical Sciences 2008;24(1):67-72.
12.   Aloy P, RB R. Structure-based systems biology: a zoom lens for the cell. FEBS Letters 2005;579(8):1854-1858.
13.   LeDuc PR, RM B. Nanoscale intracellular organization and functional architecture mediating cellular behavior. Annals of Biomedical Engineering 2006;34(1):102-113.
14.   MC R. Nanotechnology: convergence with modern biology and medicine. Current Opinion in Biotechnology 2003;14(337-346).
15.   M M. Formation of Adsorbed Protein Layers. Journal of Colloid and Interface Science 1998;207(2):186-199.
16.   Barbucci R, A. M. Conformation of human plasma proteins at polymer surfaces: the effectiveness of surface heparinization. Biomaterials 1994;15(12):955-962.
17.   Schoen FJ, RN M. Tissues, the Extracellular Matrix and Cell-Biomaterial Interactions. In: Ratner BDH, A.S.; Schoen, F.J.; Lemons, J.E., editor. Biomaterials science an introduction to materials in medicine. 2nd ed. New York: Academic Press, 2004.
18.   Jenney CR, JM A. Adsorbed serum proteins responsible for surface dependent human macrophage behavior. Journal of Biomedical Materials Research 2000;49(4):435-447.
19.   Castner DG, RD R. Biomedical surface science: Foundations to frontiers. Surface Science 2002;500(1-3):28-60.
20.   Nakanishi K, Sakiyama T, K I. On the adsorption of proteins on solid surfaces, a common but very complicated phenomenon. Journal of Bioscience and Bioengineering 2001;91(3):233-244.
21.   Boyan BD, Hummert TW, Dean DD, Z S. Role of material surfaces in regulating bone and cartilage cell response. Biomaterials 1996;17(2):137-146.
22.   Pincus MR, S N. Physiological Structure and Function of Proteins. Cell Physiology Source Book (Third Edition). San Diego: Academic Press, 2001. p. 19-42.
23.   Wozniak MA, Modzelewska K, Kwong L, PJ K. Focal adhesion regulation of cell behavior. Biochimica et Biophysica Acta (BBA) - Molecular Cell Research 2004;1692(2-3):103-119.
24.   Siebers MC, ter Brugge PJ, Walboomers XF, JA J. Integrins as linker proteins between osteoblasts and bone replacing materials. A critical review. Biomaterials 2005;26(2):137-146.
25.   AJ G. Get a grip: integrins in cell-biomaterial interactions. Biomaterials 2005;26(36):7525-7529.
26.   MA; S, DW D. Cell adhesion receptors in mechanotransduction. Current Opinion in Cell Biology 2008;20(5):551-556.
27.   Anselme K, Bigerelle M, Noel B, Iost A, P H. Effect of grooved titanium substratum on human osteoblastic cell growth. Journal of Biomedical Materials Research 2002;60(4):529-540.
28.   Zhu B, Zhang Q, Lu Q, Xu Y, Yin J, Hu J, Z W. Nanotopographical guidance of C6 glioma cell alignment and oriented growth. Biomaterials 2004;25(18):4215-4223.

29.   Clark P, Connolly P, Curtis AS, Dow JA, CD W. Cell guidance by ultrafine topography in vitro. J Cell Sci;99:73-77.
30.   Bettinger CJ, Orrick B, Misra A, Langer R, JT B. Microfabrication of poly (glycerol–sebacate) for contact guidance applications. Biomaterials 2006;27:2558–2565.
31.   Skladal P. Advances in electrochemical immunosensors. Electroanalysis 1997;9(10):737-745.
32.   Hierlemann A, Brand O, Hagleitner C, H B. Microfabrication techniques for chemical/biosensors. Proceedings of the IEEE 2003;91(6):839-863.
33.   Staples M, Daniel K, Cima MJ, Langer R. Application of micro- and nano-electromechanical devices to drug delivery. Pharmaceutical Research 2006;23(5):847-863.
34.   Christensen TB, Pedersen CM, Grondhal KG, Jensen TG, Sekulovic A, Bang DD, A W. PCR biocompatibility of lab-on-a-chip and MEMS materials. Journal of Micromechanics and Microengineering 2007;17(8):1527-1532.
35.   Zook JD, Burns DW, Herb WR, Guckel H, Kang JW, YC A. Optically excited self-resonant microbeams. 8th International Conference on Solid-State Sensors and Actuators (Eurosensors IX); 1995 Jun 25-29; Stockholm, Sweden: Elsevier Science Sa Lausanne; 1995. p. 92-98.
36.   Py C, Roth D, Levesque I, Stapledon J, Donat-Bouillud A. An integrated shadow-mask based on a stack of inorganic insulators for high-resolution OLEDs using evaporated or spun-on materials. Synthetic Metals 2001;122(1):225-227.
37.   Kjeang E, Djilali N, D S. Planar and three-dimensional microfluidic fuel cell architectures. International Mechanical Engineering Congress and Exposition 2007, Vol 11 Pt a and Pt B: Micro and Nano Systems 2008:941-943.
38.   Khademhosseini A, Langer R, Borenstein J, JP V. Microscale technologies for tissue engineering and biology. Proceedings of the National Academy of Sciences of the United States of America 2006;103(8):2480-2487.
39.   Wang F, Wang H, Wang J, Wang HY, Rummel PL, Garimella SV, C L. Microfluidic delivery of small molecules into mammalian cells based on hydrodynamic focusing. Biotechnology and Bioengineering 2008;100(1):150-158.
40.   Yeh J, Ling Y, Karp JM, Gantz J, Chandawarkar A, Eng G, Blumling III J, et al. Micromolding of shape-controlled, harvestable cell-laden hydrogels Biomaterials 2006;27(31):5391-5398.
41.   Du Y, Lo E, Vidula MK, Khabiry M, A K. Method of Bottom-Up Directed Assembly of Cell-Laden Microgels. Cellular and Molecular Bioengineering 2008.
42.   Mijatovic D, Eijkel JCT, A vdB. Technologies for nanofluidic systems: top-down vs. bottom-up - a review. Lab on a Chip 2005;5(492-500).
43.   Lee S, Chang W-J, Bashir R, Koo Y-M. "Bottom-up" approach for implementing nano/microstructure using biological and chemical interactions. Biotechnology and Bioprocess Engineering 2007;12(3):185-199.
44.   S Z. Fabrication of novel biomaterials through molecular self-assembly. Nature Biotechnology 2003;21(10):1171-1178.
45.   Senaratne W, Andruzzi L, CK O. Self-assembled monolayers and polymer brushes in biotechnology: Current applications and future perspectives. Biomacromolecules 2005;6(5):2427-2448.
46.   Gooding JJ, Mearns F, Yang WR, JQ L. Self-assembled monolayers into the 21(st) century: Recent advances and applications. Electroanalysis 2003;15(2):81-96.
47.   Zhang S, Marini DM, Hwang W, S S. Design of nanostructured biological materials through self-assembly of peptides and proteins. Current Opinion in Chemical Biology 2002;6(6):865-871.
48.   S Z. Building from the bottom up. Materials Today 2003;6(5):20-27.
49.   Gu F, Zhang L, Teply BA, Mann N, Wang A, Radovic-Moreno AF, Langer R, et al. Precise engineering of targeted nanoparticles by using self-assembled biointegrated block copolymers. Proceedings of the National Academy of Sciences of the United States of America 2008;105(7).
50.   Gates BD, Xu Q, Stewart M , Ryan D, Willson CG, GM W. New approaches to nanofabrication: molding, printing, and other techniques. Chemical Reviews 2005;105(4):1171-1196.
51.   Whitesides GM, Ostuni E, Takayama S, Jiang X, DE I. Soft Lithography in Biology and Biochemistry. Annual Review of Biomedical Engineering 2001;3:335-373
52.   Kumar A, GM W. Features of gold having micrometer to centimiter dimensions can be formed through a combination of stamping with an elastomeric stamp and an alkanethiol ink followed by chemical etching. Applied Physics Letters 1993;63(14):2002-2004.

53. Zhao XM, Xia YN, Whitesides GM. Fabrication of three-dimensional micro-structures: Microtransfer molding. Advanced Materials 1996;8(10):837-&.

54. Biebuyck HA, Larsen NB, Delamarche E, B M. Lithography beyond light: Microcontact printing with monolayer resists. IBM J Res Dev 1997;41(1-2):159-170.

55. Li WJ, Laurencin CT, Caterson EJ, Tuan RS, FK K. Electrospun nanofibrous structure: A novel scaffold for tissue engineering. Journal of Biomedical Materials Research 2002;60(4):613-621.

56. Wilbur JL, Kim E, Xin YN, GM W. Lithographic molding - a convenient route to structures with submicrometer dimensions. Advanced Materials 1995;7(7):649-652.

57. Albert F, T M. Microengineering of Cellular Interactions. Annu Rev Biomed Eng 2000;2:227-256.

58. Wilbur JL, Kumar A, Kim E, G W. Microfabrication by Microcontact Printing of Self-Assembled Monolayers. Advanced Materials 1994;6:600-604.

59. Mrksich M, Dike LE, Tien J, Ingber DE, GM W. Using Microcontact Printing to Pattern the Attachment of Mammalian Cells to Self-Assembled Monolayers of Alkanethiolates on Transparent Films of Gold and Silver. Experimental Cell Research 1997;235(2):305-313.

60. Ruiz SA, CS C. Microcontact printing: A tool to pattern. Soft Matter 2007;3:168 - 177.

61. Bajpai V, He P, Goettler L, Dong JH, Dai L. Controlled syntheses of conducting polymer micro- and nano-structures for potential applications. Synthetic Metals 2006;156(5-6):466-469.

62. Wang M, Braun HG, Kratzmüller T, E M. Patterning Polymers by Micro-Fluid-Contact Printing. Advanced Materials 2001;13(17):1312-1317.

63. Lange SA, Benes V, Kern DP, Horber JKH, A B. Microcontact printing of DNA molecules. Analytical Chemistry 2004;76(6):1641-1647.

64. Thibault C, De Berre V, Casimirius S, Trevisiol E, Francois J, C V. Direct microcontact printing of oligonucleotides for biochip applications. Journal of Nanobiotechnology 2005;3(1):7.

65. Rozkiewicz DI, Kraan Y, Werten MWT, de Wolf FA, Subramaniam V, Ravoo BJ, Reinhoudt DN. Covalent microcontact printing of proteins for cell patterning. Chemistry-a European Journal 2006;12(24):6290-6297.

66. Pla-Roca M, Fernandez JG, Mills CA, Martinez E, J S. Micro/nanopatterning of proteins via contact printing using high aspect ratio PMMA stamps and NanoImprint apparatus. Langmuir 2007;23(16):8614-8618.

67. Crozatier C, Le Berre M, Y C. Multi-colour micro-contact printing based on microfluidic network inking. Microelectronic Engineering 2006;83(4-9):910-913.

68. Bernard A, Renault JP, Michel B, Bosshard HR, E D. Microcontact Printing of Proteins. Advanced Materials 2000;12(14):1067-1070.

69. Thiébaud P, Lauer L, Knoll W, A O. PDMS device for patterned application of microfluids to neuronal cells arranged by microcontact printing. Biosensors and Bioelectronics 2002;17(1-2):87-93.

70. Singhvi R, Kumar A, Lopez GP, Stephanopoulos GN, Wang DI, Whitesides GM, DE I. Engineering cell shape and function. Science 1994;264(5159):696-698.

71. Xia Y, GM W. Soft Lithography. Angewandte Chemie International Edition 1998;37:550-575.

72. Quist AP, Pavlovic E, S O. Recent advances in microcontact printing. Analytical and Bioanalytical Chemistry 2004;381:591-600.

73. Suh KY, Lee HH. Formation of complex polymeric microstructures through physical self-organization and capillary dynamics. Journal of Micromechanics and Microengineering 2005;15(2):400-407.

74. Suh KY, Lee HH. Capillary force lithography: Large-area patterning, self-organization, and anisotropic dewetting. Advanced Functional Materials 2002;12(6-7):405-413.

75. Suh KY, Kim YS, Lee HH. Capillary force lithography. Advanced Materials 2001;13(18):1386-1389.

76. Burdick JA, Khademhosseini A, Langer R. Fabrication of Gradient Hydrogels Using a Microfluidics/Photopolymerization Process. Langmuir 2004;20(13):5153-5156.

77. Morrison D, Suh KY, A K. Micro and Nanopatterning for Bacteria- and Virus-Based Biosensing Applications. In: Zourob M, Elwary S, A T, editors. Principles of Bacterial Detection: Biosensors, Recognition Receptors and Microsystems, 2008.

78. Sundaray B, Subramanian V, Natarajan TS, Xiang RZ, Chang CC, WS F. Electrospinning of continuous aligned polymer fibers. Applied Physics Letters 2004;84(7):1222-1224.

79. Huang ZM, Zhang YZ, Kotaki M, S R. A review on polymer nanofibers by electrospinning and their applications in nanocomposites. Composites Science and Technology 2003;63(15):2223-2253.

80. Matthews JA, Boland ED, Wnek GE, Simpson DG, GL B. Electrospinning of collagen type II: A feasibility study. Journal of Bioactive and Compatible Polymers 2003;18(2):125-134.

81. Kidoaki S, Kwon IK, T M. Mesoscopic spatial designs of nano- and microfiber meshes for tissue-engineering matrix and scaffold based on newly devised multilayering and mixing electrospinning techniques. Biomaterials 2005;26(1):37-46.

82. Min BM, Lee G, Kim SH, Nam YS, Lee TS, WH P. Electrospinning of silk fibroin nanofibers and its effect on the adhesion and spreading of normal human keratinocytes and fibroblasts in vitro. Biomaterials 2004;25(7-8):1289-1297.

83. Martins A, Reis RL, Neves NM. Electrospinning: processing technique for tissue engineering scaffolding. International Materials Reviews 2008;53(5):257-274.

84. Martins A, Araujo JV, Reis RL, Neves NM. Electrospun nanostructured scaffolds for tissue engineering applications. Nanomedicine 2007;2(6):929-942.

85. Xu CY, Inai R, Kotaki M, S R. Electrospun nanofiber fabrication as synthetic extracellular matrix and its potential for vascular tissue engineering. Tissue Engineering 2004;10(7-8):1160-1168.

86. Robert L, Legeais JM, Robert AM, Renard G. Corneal collagens. Pathologie Biologie 2001;49(4):353-363.

87. Lanza RP, Langer R, J V. Principles of Tissue Engineering. 2nd ed. New York: Academic press, 2000.

88. Matthews JA, Wnek GE, Simpson DG, GL B. Electrospinning of collagen nanofibers. Biomacromolecules 2002;3(2):232-238.

89. Boland ED, Matthews JA, Pawlowski KJ, Simpson DG, Wnek GE, GL B. Electrospinning collagen and elastin: Preliminary vascular tissue engineering. Frontiers in Bioscience 2004;9:1422-1432.

90. Kunzler TP, Huwiler C, Drobek T, Vörös J, Spencer ND. Systematic study of osteoblast response to nanotopography by means of nanoparticle-density gradients. Biomaterials 2007;28(33):5000-5006.

91. Webster TJ, Ergun C, Doremus RH, Siegel RW, Bizios R. Enhanced osteoclast-like cell functions on nanophase ceramics. Biomaterials 2001;22(11):1327-1333.

92. Beatrice Sommer RF, Christoph Sprecher, Michael Leunig, Reinhold Ganz, Willy Hofstetter,. Wear particles and surface topographies are modulators of osteoclastogenesis in vitro. Journal of Biomedical Materials Research 2005;72A(1):67-76.

93. Kenar H, Kocabas A, Aydinli A, Hasirci V. Chemical and topographical modification of PHBV surface to promote osteoblast alignment and confinement. Journal of Biomedical Materials Research Part A 2008;85A(4):1001-1010.

94. Ber S, Torun Köse G, Haslrcl V. Bone tissue engineering on patterned collagen films: an in vitro study. Biomaterials 2005;26(14):1977-1986.

95. Araújo JV, Martins A, Leonor IB, Pinho ED, Reis RL, NM N. Surface controlled biomimetic coating of polycaprolactone nanofiber meshes to be used as bone extracellular matrix analogues. J Biomater Sci Polymer Edn 2008;19(10):1261-1278.

96. Tuzlakoglu K, Bolgen N, Salgado AJ, Gomes ME, Piskin E, Reis RL. Nano- and micro-fiber combined scaffolds: A new architecture for bone tissue engineering. Journal of Materials Science-Materials in Medicine 2005;16(12):1099-1104.

97. Santos MI, Tuzlakoglu K, Fuchs S, Gomes ME, Peters K, Unger RE, Piskin E, et al. Endothelial cell colonization and angiogenic potential of combined nano- and micro-fibrous scaffolds for bone tissue engineering. Biomaterials 2008;29(32):4306-4313.

98. Barbucci R, Torricelli P, Fini M, Pasqui D, Favia P, Sardella E, d'Agostino R, et al. Proliferative and re-defferentiative effects of photo-immobilized micro-patterned hyaluronan surfaces on chondrocyte cells. Biomaterials 2005;26(36):7596-7605.

99. Petersen EF, Spencer RGS, EW M. Microengineering neocartilage scaffolds. Biotechnology and Bioengineering 2002;78(7):801-804.

100. Chao PG, Tang ZL, Angelini E, West AC, Costa KD, CT H. Dynamic osmotic loading of chondrocytes using a novel microfluidic device. Journal of Biomechanics 2005;38(6):1273-1281.

101. Alves da Silva ML, Crawford A, Mundy J, Martins A, Araújo JV, Hatton PV, Reis RL, et al. Evaluation of Extracellular Matrix Formation in Polycaprolactone and Starch-Compounded Polycaprolactone Nanofiber Meshes When Seeded with Bovine Articular Chondrocytes. TISSUE ENGINEERING: Part A 2008;14.

102. Barber RW, Emerson DR. Optimal design of microfluidic networks using biologically inspired principles. Microfluidics and Nanofluidics 2008;4(3):179-191.

103. Daxini SC, Nichol JW, Sieminski AL, Smith G, Gooch KJ, Shastri VP. Micropatterned polymer surfaces improve retention of endothelial cells exposed to flow-induced shear stress. Biorheology 2006;43(1):45-55.
104. Lin X, Helmke BP. Micropatterned Structural Control Suppresses Mechanotaxis of Endothelial Cells. Biophysical Journal 2008;95(6):3066-3078.
105. Nalayanda DD, Kalukanimuttam M, Schmidtke DW. Micropatterned surfaces for controlling cell adhesion and rolling under flow. Biomedical Microdevices 2007;9(2):207-214.
106. Vogt AK, Wrobel G, Meyer W, Knoll W, A O. Synaptic plasticity in micropatterned neuronal networks. Biomaterials 2005;26(15):2549-2557.
107. Borenstein JT, Terai H, King KR, Weinberg EJ, Kaazempur-Mofrad MR, JP V. Microfabrication technology for vascularized tissue engineering. Biomedical Microdevices 2002;4(3):167-175.
108. Khetani SR, SN B. Microscale culture of human liver cells for drug development. Nature Biotechnology 2008;26:120 - 126
109. Carraro A, Hsu WM, Kulig KM, Cheung WS, Miller ML, Weinberg EJ, Swart EF, et al. In vitro analysis of a hepatic device with intrinsic microvascular-based channels. Biomedical Microdevices 2008;10(6):795-805.
110. Karp JM, Yeh J, Eng G, Fukuda J, Blumling J, Suh K-Y, Cheng J, et al. Controlling size, shape and homogeneity of embryoid bodies using poly(ethylene glycol) microwells. Lab on a Chip 2007;7:786 - 794.
111. Khademhosseini A, Ferreira L, Blumling III J, Yeh J, Fukuda J, R L. Co-culture of human embryonic stem cells with murine embryonic fibroblasts on microwell-patterned substrates Biomaterials 2007;27(36):5968-5977
112. Underhill GH, Bhatia SN. High-throughput analysis of signals regulating stem cell fate and function. Current Opinion in Chemical Biology 2007;11:357–366.
113. Flaim CJ, Teng D, Chien S, Bhatia SN. Combinatorial Signaling Microenvironments for Studying Stem Cell Fate. Stem Cells and Development 2008;17:29–39.
114. Zahor D, Radko A, Vago R, Gheber LA. Organization of mesenchymal stem cells is controlled by micropatterned silicon substrates. Materials Science & Engineering C-Biomimetic and Supramolecular Systems 2007;27(1):117-121.
115. Chaubey A, Ross KJ, Leadbetter RM, Burg KJL. Surface patterning: Tool to modulate stem cell differentiation in an adipose system. Journal of Biomedical Materials Research Part B-Applied Biomaterials 2008;84B(1):70-78.
116. Ma K, Chan CK, Liao S, Hwang WYK, Feng Q, S R. Electrospun nanofiber scaffolds for rapid and rich capture of bone marrow-derived hematopoietic stem cells. Biomaterials 2008;29(13):2096-2103.
117. Biggs MJP, Richards RG, McFarlane S, Wilkinson CDW, Oreffo ROC, MJ D. Adhesion formation of primary human osteoblasts and the functional response of mesenchymal stem cells to 330nm deep microgrooves Interface 2008;5(27):1231-1242.
118. Karp JM, Yeo Y, Geng WL, Cannizarro C, Yan K, Kohane DS, Vunjak-Novakovic G, et al. A photolithographic method to create cellular micropatterns. Biomaterials 2006;27(27):4755-4764.
119. Zinger O, Zhao G, Schwartz Z, Simpson J, Wieland M, Landolt D, B B. Differential regulation of osteoblasts by substrate microstructural features. Biomaterials 2005;26(14):1837-1847.
120. Charest JL, Eliason MT, Garcia AJ, King WP. Combined microscale mechanical topography and chemical patterns on polymer cell culture substrates. Biomaterials 2006;27(11):2487-2494.
121. Martins A, Cunha J, Macedo F, Reis RL, NM N. Improvement of Polycaprolactone Nanofibers Topographies: Testing the Influence in Osteoblastic Proliferation. Nanotech 2006 2006; 2006.
122. Kurpinski K, Chu J, Hashi C, Li S. Anisotropic mechanosensing by mesenchymal stem cells. Proceedings of the National Academy of Sciences of the United States of America 2006;103(44):16095-16100.
123. P. Zorlutuna NH, V. Hasirci,. Nanopatterned collagen tubes for vascular tissue engineering. Journal of Tissue Engineering and Regenerative Medicine 2008;2(6):373-377.
124. Sarkar S, Lee GY, Wong JY, Desai TA. Development and characterization of a porous micro-patterned scaffold for vascular tissue engineering applications. Biomaterials 2006;27(27):4775-4782.
125. Khademhosseini A, Eng G, Yeh J, Kucharczyk PA, Langer R, Vunjak-Novakovic G, M R. Microfluidic patterning for fabrication of contractile cardiac organoids Biomedical Microdevices 2007;9(2):149-157.

126. Xu CY, Inai R, Kotaki M, Ramakrishna S. Aligned biodegradable nanofibrous structure: a potential scaffold for blood vessel engineering. Biomaterials 2004;25:877-886.

127. Scholl M, Sprossler C, Denyer M, Krause M, Nakajima K, Maelicke A, Knoll W, et al. Ordered networks of rat hippocampal neurons attached to silicon oxide surfaces. Journal of Neuroscience Methods 2000;104(1):65-75.

128. Yang F, Murugan R, Wang S, S R. Electrospinning of nano/micro scale poly(L-lactic acid) aligned fibers and their potential in neural tissue engineering. Biomaterials 2005;26(15):2603-2610.

129. Xie J, Willerth SM, Li X, Macewan MR, Rader A, Sakiyama-Elbert SE, Y X. The differentiation of embryonic stem cells seeded on electrospun nanofibers into neural lineages. Biomaterials 2008;30:354-362.

130. VL Tsang, Chen AA, Cho LM, Jadin KD, Sah RL, DeLong S, West JL, et al. Fabrication of 3D hepatic tissues by additive photopatterning of cellular hydrogels. The FASEB Journal 2007;21(3):790-801.

131. Alexander R, Padmavathy R, Arno WT, Francüois B, Martin LY, T M. Designing a Hepatocellular Microenvironment with Protein Microarraying and Poly(ethylene glycol) Photolithography. Langmuir 2004;20:2999-3005.

132. Petronis S, Eckert KL, Gold J, E W. Microstructuring ceramic scaffolds for hepatocyte cell culture. Journal of Materials Science: Materials in Medicine 2001;12:523-528.

133. Chua K-N, Lim W-S, Zhang P, Lu H, Wen J, Ramakrishna S, Leong KW, et al. Stable immobilization of rat hepatocyte spheroids on galactosylated nanofiber scaffold. Biomaterials 2005;26:2537-2547.

134. Yu BY, Chou PH, Sun YM, Lee YT, TH Y. Topological micropatterned membranes and its effect on the morphology and growth of human mesenchymal stem cells (hMSCs). Journal of Membrane Science 2006;273(1-2):31-37.

135. Figallo E, Cannizzaro C, Gerecht S, Burdick JA, Langer R, Elvassore N, Vunjak-Novakovic G. Micro-bioreactor array for controlling cellular microenvironments. Lab on a Chip 2007;7:710 - 719.

136. Chua K-N, Chai C, Lee P-C, Tang Y-N, Ramakrishna S, Leong KW, H-Q M. Surface-aminated electrospun nanofibers enhance adhesion and expansion of human umbilical cord blood hematopoietic stem/progenitor cells. Biomaterials 2006;27(36):6043-6051.

137. A. Pietak AM, S. Gauthier, R. Oleschuk, S. D. Waldman,. Are micropatterned substrates for directed cell organization an effective method to create ordered 3D tissue constructs? Journal of Tissue Engineering and Regenerative Medicine 2008;2(7):450-453.

138. Vozzi G, Flaim CJ, Bianchi F, Ahluwalia A, S B. Microfabricated PLGA scaffolds: a comparative study for application to tissue engineering. Materials Science & Engineering C-Biomimetic and Supramolecular Systems 2002;20(1-2):43-47.

139. Uludag H, de Vos P, PA T. Technology of mammalian cell encapsulation. Advanced Drug Delivery Reviews 2000;42(1):29-64.

140. Khademhosseini A, Eng G, Yeh J, Junji F, James B-III, Robert L, AB J. Micromolding of photocrosslinkable hyaluronic acid for cell encapsulation and entrapment. Journal of biomedical materials research Part A 2006;79(3):522-532.

141. Koegler WS, LG G. Osteoblast response to PLGA tissue engineering scaffolds with PEO modified surface chemistries and demonstration of patterned cell response Biomaterials 2004;25(14):2819-2830

142. Anderson JR, Chiu DT, Jackman RJ, Cherniavskaya O, McDonald JC, Wu H, Whitesides SH, et al. Fabrication of Topologically Complex Three-Dimensional Microfluidic Systems in PDMS by Rapid Prototyping Analytical Chemistry 2000;72(14):3158 -3164.

143. Mironov V, Prestwich G, Forgacs G. Bioprinting living structures. Journal of Materials Chemistry 2007;17(20):2054-2060.

144. Kawata S, HB S. Two-photon photopolymerization as a tool for making micro-devices. Applied Surface Science 2003;208:153-158.

145. Li X, van der Steen G, van Dedem GWK, van der Wielen LAM, van Leeuwen M, van Gulik WM, Heijnen JJ, et al. Improving mixing in microbioreactors. Chemical Engineering Science 2008;63(11):3036-3046

146. Wu MH, Lin JL, Wang J, Cui Z, Z. C. Development of high throuput optical sensor array for on-line pH monitoring in micro-scale cell culture environment. Biomed Microdevices 2008.

147. Wu M-H, Huang S-B, Cui Z, Cui Z, G-B L. Development of perfusion-based micro 3-D cell culture platform and its application for high throuput drug testing Sensors and Actuators B: Chemical 2008;129(1):231-240

148. Yang ST, Zhang X, Y W. Microbioreactors for high-throughput cytotoxicity assays. Current Opinion in Drug Discovery & Development 2008;11(1):111-127.
149. Korin N, Bransky A, Dinnar U, S L. A parametric study of human fibroblasts culture in a microchannel bioreactor. Lab on a Chip 2007;7(5):611-617.
150. Cimetta E, Figallo E, Cannizzaro C, Nlvassore E, G V-N. Micro-bioreactor arrays for controlling cellular environments: Design principles for human embryonic stem cell applications Methods 2008;Article in Press, Corrected Proof
151. Wu MH, Urban JP, Cui Z, ZF C. Development of PDMS microbioreactor with well-defined and homogenous culture environment for chondrocyte 3-D culture. Biomed Microdevices 2006;8(4):331-340.
152. Ostrovidov S, Jiang J, Sakai Y, T F. Membrane-based PDMS microbioreactor for perfused 3D primary rat hepatocyte cultures. Biomed Microdevices 2004;6(4):279-287.
153. Powers MJ, Karel Domansky, Mohammad R. Kaazempur-Mofrad, Kalezi A, Capitano A, Upadhyaya A, Kurzawski P, et al. A Microfrabricated array bioreactor for perfused 3D liver culture. Biotechnology and Bioengineering 2002;78(3).
154. Powers MJ, Janigian DM, Wack KE, Baker CS, Stolz DB, LG G. Functional Behavior of Primary Rat Liver Cells in a Three-Dimensional Perfused Microarray Bioreactor. Tissue Engineering 2002;8(3):499-513.

Section 2

DETAILED DESCRIPTION OF EXPERIMENTAL MATERIALS AND METHODOLOGIES

Chapter II

MATERIALS AND METHODS

CHAPTER II

MATERIALS AND METHODS

The basis of scientific research is the constant formulation and testing of scientific hypotheses. In the field of tissue engineering, the challenges comprise the mimicry of the complex human systems through a number of simplifications. Thus, a wide spectrum of procedures and methods should be employed to validate the proposed hypotheses and to simulate as close as possible the *in vivo* conditions.

Under the scope of this thesis, several methodologies were used that either helped on understanding the mechanisms of the proposed systems or on assessing how far the developed systems can mimic the native microenvironments.

This chapter is aimed at giving an overview and also more detailed information on the materials used, the techniques applied for processing the materials, the characterization techniques used and the biological assays performed. It is expected that it will help on contextualizing and explaining the selection of materials and methods used throughout the thesis, complementing the information given on each chapter. Figure II.1 presents an overview of the materials studied and the respective processing and characterization methodologies used. Three materials were studied in the present thesis: poly(butylene succinate) (PBS), gellan gum (GG) and chitosan (CHT). PBS was processed by micromolding. GG was modified with chemical and biological cues and further processed into microcapsules or combined with CHT to produce hydrogels with improved properties.
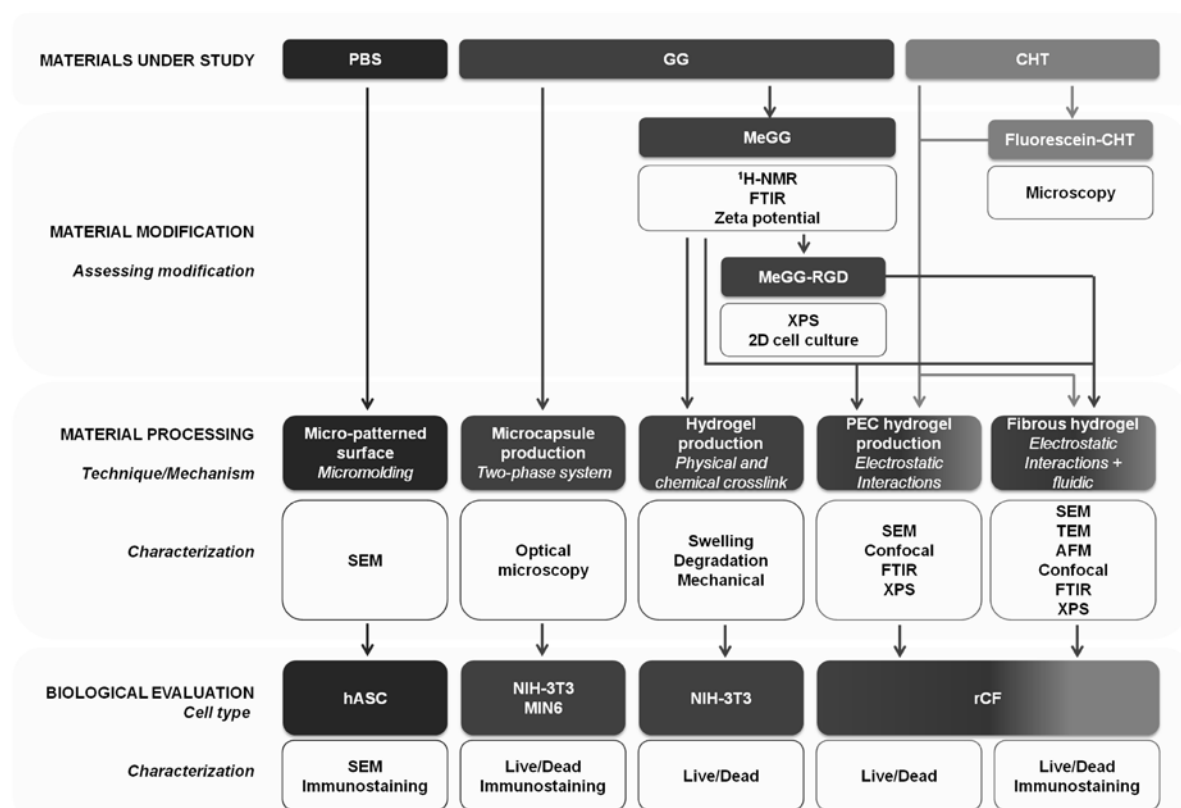
Figure II.1. Schematics overview of the materials and methodologies used to modify and process the studied materials. The techniques used to characterize the materials/structures are depicted within the white boxes. (legend in alphabetic order: ^{1}H-NMR-proton nuclear magnetic resonance; 2D-two-dimensional; AFM-atomic force microscopy; CHT-chitosan; FTIR-Fourier transform infrared spectroscopy; GG-gellan gum; hASC-human adipose stem cells; MeGG-methacrylated gellan gum; MeGG-RGD-modified MeGG with cell adhesive motifs (RGD); MIN6-insulinoma cell line; NIH-3T3-fibroblastic cell line; PBS-poly(butylene succinate); rCF-rat cardiac fibroblasts; SEM-scanning electron microscopy; TEM-transmission electron microscopy; XPS-X-ray photoelectron spectroscopy.

1. MATERIALS AND SOLUTIONS

1.1. Poly(butylene succinate)

Poly(butylene succinate) (PBS) is a commercially available aliphatic polyester under the trademark Bionolle®. It was first produced by Showa Highpolymer Co. Ltd. (Tokyo, Japan) and can be obtained by the polycondensation reaction of glycols with dicarboxylic acids [1]. The chemical structure of Bionolle® is depicted in Figure II.2. It presents a melting temperature (T_m) of 107.2 ºC [2] and a glass transition temperature (T_g) of -32 ºC [3]. It has been reported that PBS is biodegradable by hydrolysis, under physiological conditions, into water and carbon dioxide [4]. PBS has been processed at 3B's Research Group into several forms, such as injection molded discs [2] and fibrous scaffolds [5, 6], and mainly studied for

bone [6, 7] and cartilage [5] regeneration strategies. Its good biological properties, shown both *in vitro* and *in vivo*, and the lack of studies on the processing of this polymer at a microscale, have made it a good candidate for study under this thesis.

For the study described in this thesis (Chapter III), PBS was used in the form of pellets. The polymer was dissolved in two different solvents, previously reported to dissolve this polymer: dichloromethane (DIM, Sigma) or trichloromethane (TIM, VWR), also known as chloroform. The polymer solution was prepared with two concentrations: 0.5% and 2% (w/v) and further used for developing micro-structures (section 2.1).
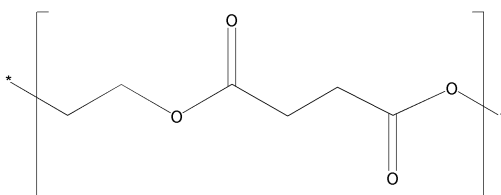
Figure II.2. Chemical structure of PBS.

1.2. Gellan Gum

Gellan Gum (GG, Gelrite®, Sigma, M_w=1.000.000) is an anionic polysaccharide composed of two β-D-glucose, one α-rhamnose and one β-D-glucuronic acid residues (Figure II.3) [8]. GG can be obtained as the product of the fermentation of the bacteria *Pseudomonas elodea* [8].
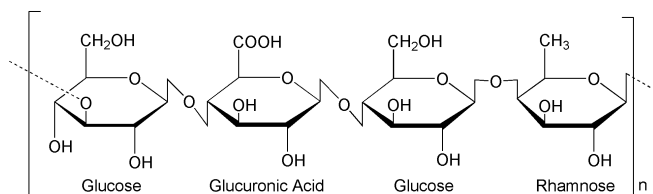
Figure II.3. Chemical structure of gellan gum (n: repeating unit).

GG can form hydrogels with different physical and mechanical properties depending on the mechanism used to crosslink the polymer chains. Upon temperature decrease, a random coil-helix transition occurs with further aggregation of the helices leading to the formation of junction zones [9]. The sol-gel transition of GG is ionotropic, as in alginate. Thus, the presence of cations is necessary for the formation of a stable hydrogel. However, this ionic crosslinking is highly dependent on the type of cations present, being stronger with divalent cations (such as Ca^{2+} and Mg^{2+}) than with monovalent ones (such as Na^+ and K^+) [10]. GG has FDA approval as a food additive and several associated patents for tissue engineering applications, namely for cartilage tissue engineering. GG can form hydrogels with different mechanical properties, being also heat and acid resistant [11]. GG has been firstly used in

biomedical applications as a drug delivery agent for ophthalmic treatments [12, 13]. *In vitro* and *in vivo* studies have demonstrated that GG is non-cytotoxic and that stem cells remain highly functional upon encapsulation in GG [14-17]. This natural polysaccharide presents a highly reactive group, the carboxylic acid (-COOH), that can be negatively charged if the pH of the solution is above its pKa value. Figure II.4 depicts the variation between the charged and uncharged states of GG.

Given its properties, GG appeared as an interesting polymer for the development of hydrogels under the present thesis (Chapters IV, V, VI and VII). The following sections (1.2.1.1 and 1.2.1.2) will focus on the chemical modification of GG first with chemical and then with biological cues.
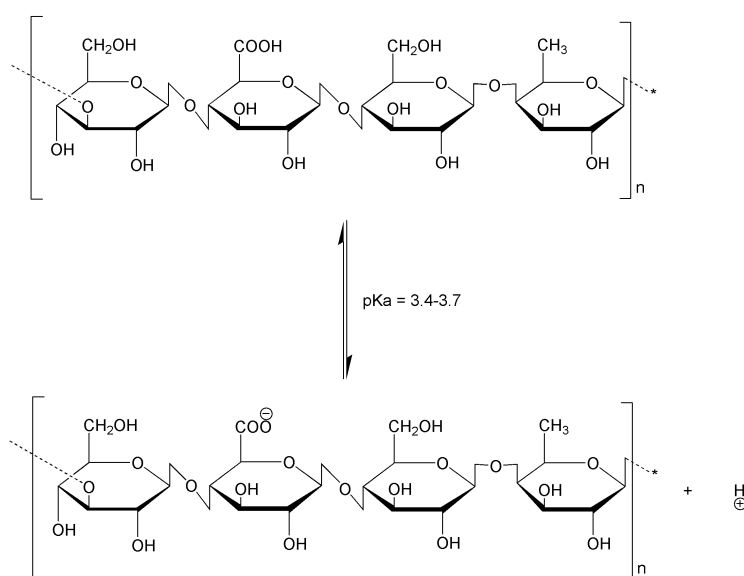
Figure II.4. Illustration of the protonation state of GG.

1.2.1. Introducing chemical and biochemical cues on gellan gum

1.2.1.1. Methacrylation of gellan gum

The major downside of the ionic crosslinking of GG is that it is highly dependent on the properties of the surrounding environment. Thus, once implanted *in vivo*, these ionotropic hydrogels might lose their stability due to the exchange of divalent cations with monovalent ones that are present in higher concentrations in the physiological environment. To overcome this disadvantage, chemical crosslinking of these hydrogels has been proposed [18]. Chemical crosslinking of hydrogels offer some advantages over the physical crosslinking mechanisms, mainly because it allows to better control the properties of the hydrogels, leading to a higher structural stability and to better mechanical properties [18, 19]. Several methods have been proposed for the chemical modification of GG in order to yield

hydrogels with more controllable characteristics [20, 21]. For instance, a chemical scissoring process has been used to adjust the molecular weight (M_w) of GG, and thus better control its properties [20]. A different study has functionalized GG with ester bonds using three different reagents (acrylic acid, acryloyl chloride or maleic anhydride) [21]. For the work described in this thesis, ester bonds were introduced in the GG backbone so that it could be chemically crosslinked by ultraviolet light (UV). Methacrylated Gellan Gum (MeGG) was synthesized by reacting GG with methacrylic anhydride (MA, Sigma) as depicted in Figure II.5. MA was the chosen reagent, since it has already shown promising results when used in the chemical modification of other polymers, namely hyaluronic acid [22]. Briefly, 1 g of GG was dissolved in 100 mL of dionized water at 90 ºC. Either 2 or 8 mL of MA were added to this solution at 50 ºC, in order to synthesize MeGG with low (Low-MeGG) or high (High-MeGG) degrees of methacrylation, respectively. The reaction was continued for 6 hours. Periodically, pH (8.0) was adjusted with 5.0 M NaOH solution. The modified MeGG solution was purified by dialysis (Fisher Scientific, membrane with molecular weight cutoff of 11-14 kD, USA) for at least 3 days against distilled water to remove the excess of MA. Purified MeGG was obtained by lyophilization and stored at a dry place protected from light.
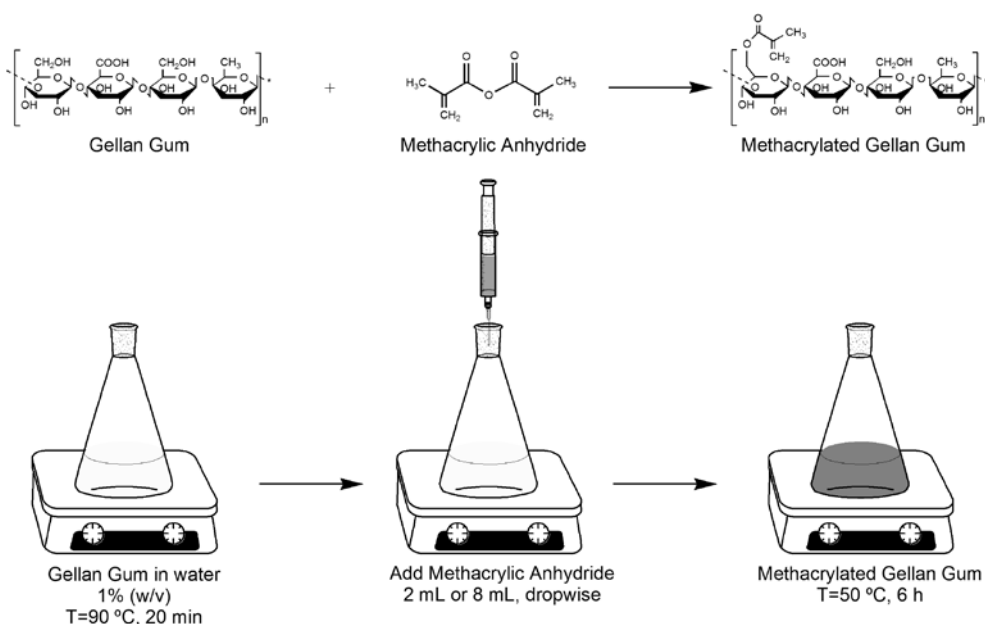
Figure II.5. Schematics illustration of the chemical reaction and the setup for the synthesis of MeGG.

1.2.1.2. Grafting adhesive sequences onto methacrylated gellan gum

Biomaterials aimed at being used as supports for cell attachment should present chemical and biological cues that cells would recognize. Cell attachment occurs through cell membrane receptors, such as integrins [23]. Proteins, such as fibronectin or vitronectin,

present in the extracellular matrix (ECM), contain specific amino-acid sequences, namely the RGD (Arg-Gly-Asp) sequence, which is recognizable by cell integrins [23]. The modification of biomaterials with specific adhesive amino-acid sequences has been reported as a way to improve the substrate properties [24-26]. However, the establishment of a covalent bond between the adhesive-sequences and the substrate is highly dependent on the functional groups present both on the peptides and on the polymeric material. Different coupling reagents and crosslinkers have been used to bind specific biomolecules on functional surfaces [27-29]. In the present thesis, a RGD sequence was covalently bonded to MeGG using a water soluble carbodiimide, often used to activate carboxylic acids. The procedure used for sequence immobilization was based on studies previously performed to immobilize amino-acid sequences on carboxylic-based substrates [30]. 1-ethyl-3-(3-dimethylaminopropyl) carbodiimide hydrochloride (EDC, Thermo Scientific) reacts preferentially with the carboxyl groups of MeGG, activating them. Then, activated -COOH of MeGG reacts with amine groups of the amino-acid sequence, creating a covalent bond. The chemical reaction and the schematics of the setup are depicted in Figure II.6. Briefly, the pH of MeGG solution was stabilized at 5.6. EDC (0.1 M) was added to 10 mL of MeGG and after 15 min, 0.2 M of N-hydroxysuccinimide (NHS, Sigma) was added to the reaction. After 1 h of reaction, 200 µL of RGD (2.4 mg/mL) were added. The reaction continued for 12 hours under agitation, at 4 °C. The solution was dialyzed for 2 days and kept at 4 °C after freeze drying.
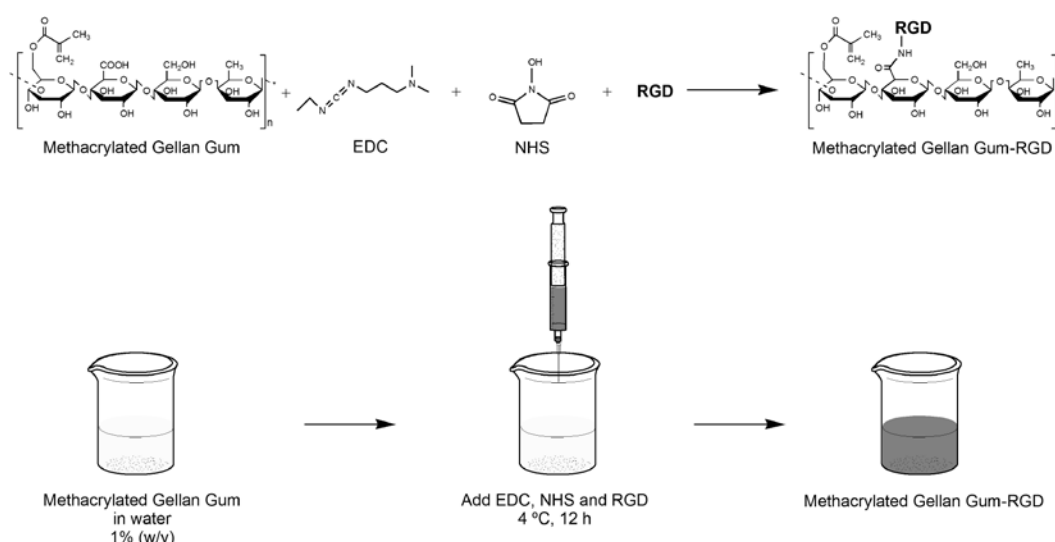
Figure II.6. Schematics illustration of the chemical reaction and the setup for the synthesis of MeGG-RGD.

1.3. Chitosan

Chitosan (CHT) is a linear polysaccharide composed of randomly distributed β-(1→4)-linked D-glucosamine (deacetylated unit) and N-acetyl-D-glucosamine (acetylated unit) [31] (Figure II.7). CHT can be obtained through the deacetylation of chitin, the second most abundant natural polysaccharide, which is the main component of the exoskeleton of crustaceans, insects, spiders or the cell walls of many algae or fungi [32]. The degree of deacetylation (% DD) of CHT is directly correlated with the amount of deacetylated and acetylated units, being 100% when no chitin residue is present on the polymer chain [33]. CHT has been reported to be biocompatible, biodegradable by human enzymes and to present antibacterial and wound-healing properties. This ability might result from the structural similarities with a variety of glycosaminoglycans (GAGs) present in different tissues in the human body.
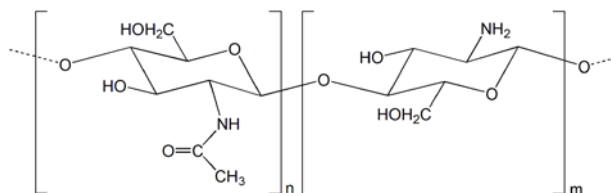
Figure II.7. Chemical structure of CHT (n: deacetylated repeating unit; m: acetylated repeating unit).

Membranes [34], capsules [35], scaffolds [36] and hydrogels [37] of CHT have been processed with different properties, according to the targeted biomedical application. Important parameters affecting the characteristics of CHT, and thus its processability, are the DD and the M_w. Due to the presence of amine groups, CHT is only soluble under pH 6.3, which corresponds to its pKa value, being positively charged under this state [38]. Figure II.8 depicts the protonation state of CHT. An acidic solution is needed to dissolve CHT. Given its good biological and processing properties, herein described, CHT was chosen to be combined with MeGG in chapters VI and VII of this thesis. The CHT (Sigma) herein used was dissolved in a 1% (v/v) acetic acid solution at 1% (w/v).
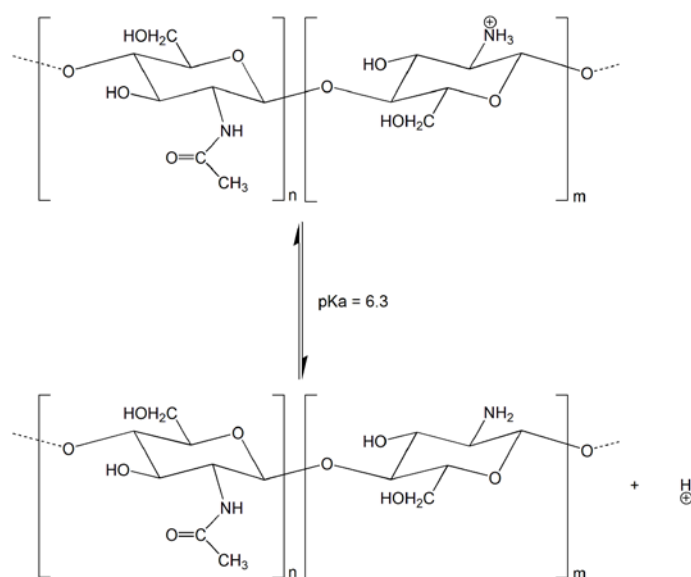
Figure II.8. Illustration of the protonation state of CHT.

1.3.1. Fluorescently labeled chitosan

To evaluate the distribution of CHT within the developed hydrogels (section 3), fluorescein-labeled CHT was synthesized. Fluorescein is widely used in different applications as a fluorescent tracer and presents a maximum absorption at 494 nm and maximum emission at 521 nm [39]. A well known derivative of fluorescein is fluorescein isothiocyanate (FITC), commonly used in flow cytometry. Fluorescein is pH-dependent, having the sharp green fluorescence that drops at pH lower than 5.5 [40]. As previously referred, the pH of CHT solution is approximately 4 and above its pKa value (6.3) the polymer precipitates. Thus, the pH of CHT solution was adjusted and kept at 6.0 with 5M NaOH in order to encompass the pH ranges of both CHT and fluorescein. Fluorescein-CHT conjugate was obtained as described elsewhere [41] by carbodiimide chemistry. This reaction is based on activating the carboxyl groups of fluorescein for coupling with the primary amines of CHT, yielding amide bonds. The chemical reaction is depicted in Figure II.9. A volume of 400 µL of 0.1% (w/v) fluorescein solution, previously dissolved in ethanol, was added to 10 mL of CHT solution (1%, w/v) at pH 6.0. To catalyze the formation of amide bonds, EDC was added to a final concentration of 0.05 M. The reaction was incubated for 12 h in the dark under stirring, at room temperature. The synthesized conjugate solution was purified by dialysis (Fisher Scientific, membrane with M_w cutoff of 11-14 kD, USA) for at least 3 days against distilled water to remove the unreacted fluorescein. Purified fluorescein-CHT was obtained by lyophilization and stored in a dry place protected from light.
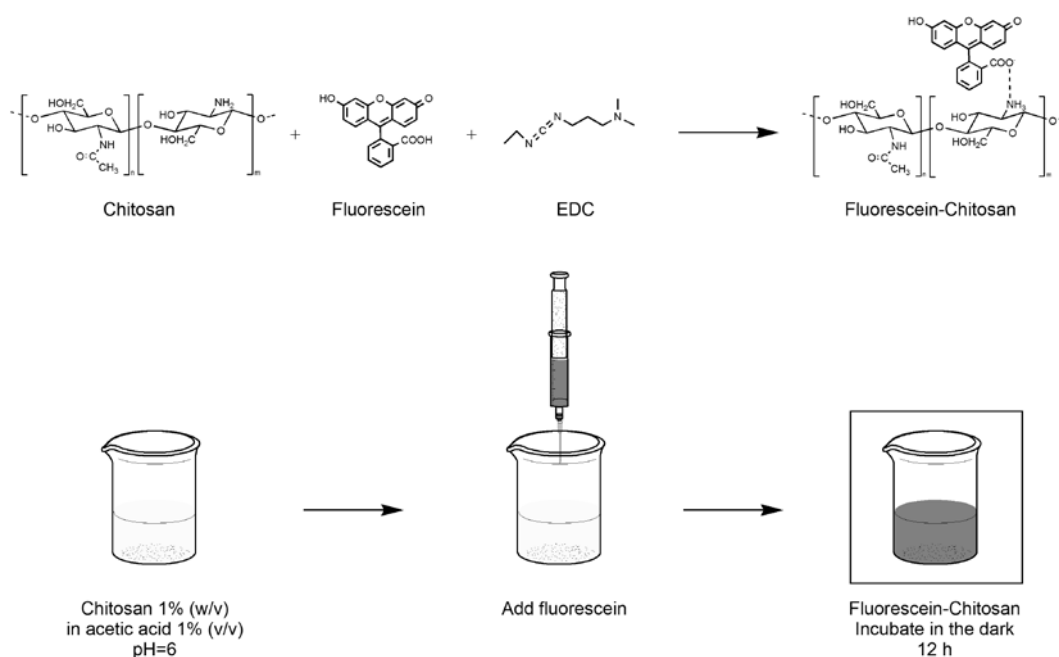
Figure II.9. Schematics illustration of the chemical reaction and the setup for the synthesis of fluorescein-CHT.

1.4. Alginate

Alginate, also known as alginic acid (ALG, Sigma-Aldrich), is an anionic polysaccharide present in the cell walls of brown algae. Alginates are linear unbranched polymers containing β (1→4) linked D-mannuronic acid (M) and α (1→4) linked L-guluronic acid (G) residues [42]. These monomers are arranged in alginate molecules in regions made up exclusively of one unit or the other, or as regions in which monomers alternate in sequence. Similarly to GG, ALG is ionotropic, forming insoluble hydrogels with divalent ions, especially Ca^{2+} cations. Given is wide use in tissue engineering approaches [43, 44], alginate was used as a control material in the study of the capsules production (Chapter IV).

2. MATERIAL PROCESSING: TECHNIQUES AND MECHANISMS USED

In order to recapitulate more closely the *in vivo* architectural features of tissues, a number of techniques have been employed to replicate them *in vitro* [45]. As discussed in the first chapter of the present thesis, fabrication techniques have been imported to tissue engineering from other areas, such as electronics [46]. These technologies have been optimized for the materials used in tissue engineering applications and combined with biological and chemical cues to engineer improved structures at micro- and nano-scales. The major focus of the present thesis was on enhancing the properties of the studied materials by

creating micro- and nano-scaled structures. Developing polymeric materials with specific micro- and nano-scaled cues allow instructing cells with specific stimuli that dictate their spatial arrangement, thus influencing cell properties, as proliferation [47] and differentiation [48]. For this purpose, a variety of techniques can be used that enable the development structures at a micro- and nano-scale. In this thesis, four relevant structures for tissue engineering were aimed: (i) development of micro-patterned surfaces, (ii) fabrication of microcapsules, (iii) development of hydrogels, and (iv) fabrication of a multi-scaled fibrous hydrogel system. More information on general techniques can be found on the first chapter of this thesis. The next sections describe with more detail the technique/mechanism selected for each work of the present thesis.

2.1. Micropatterned poly(butylene succinate) surfaces by micromolding

PBS has been processed at the 3B's Research Group in a variety of shapes, namely discs [2] and fibers [5]. However, no work has been reported regarding the processability of PBS at a micro-scale. Herein, we have processed this aliphatic polyester by micromolding. Pellets of PBS were dissolved at 0.5 and 2% (w/v), either in DIM or TIM. A polydimethylsiloxane (PDMS) mold was gently provided by Professor Hong Hong Lee (School of Chemical Engineering, Seoul National University). PDMS is an elastomeric silicon-based material widely used in microfabrication approaches since it can reproducibly replicate micro- and nano-features [49]. Since PDMS pre-polymer is liquid at room temperature, it can flow over nearly any micro- and nano-feature. Over time, PDMS cures, forming an elastic material. Elevated temperatures can increase the curing time of PDMS at expenses of dimensional stability. The PDMS mold was fabricated with 20 patterns with different combinations of groove and ridges sizes. Figure II.10 depicts the PDMS mold used in the present study. The lighter square regions correspond to the different patterns.
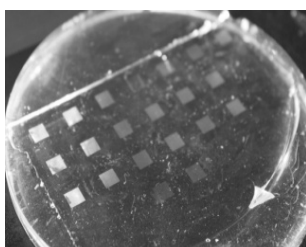
Figure II.10. PDMS mold used to develop PBS micro-patterns.

The PDMS mold and PBS solution were heated to the same temperature (~20 ºC or ~100 ºC). Then, 20 µL of PBS solution were pipetted on top of the pattern on the PDMS mold. An injection molded disc of PBS was placed over the PBS solution as a substrate for the PBS

pattern. A weight was used to facilitate the migration of the PBS solution by capillarity through the PDMS micro-patterns. As the solvent evaporates (~2 min), the micro-patterns of the PDMS were transferred to the PBS injection molded discs (substrate). Then, the PBS disc was gently removed from the surface of the PDMS mold, stamping the pattern of the mold into the PBS disc (Figure II.11). Three parameters of the system were varied in order to evaluate their influence over the fabricated micro-features: (i) the temperature of both the PDMS mold and the PBS solution (~20 ºC and ~100 ºC); (ii) concentration of the PBS solution (0.5 and 2%, w/v); and (iii) solvent used to dissolve PBS pellets (DIM or TIM). While varying one of the parameters, the others were kept constant. After optimizing the system parameters (see section 3.1.2.), twenty patterns with different groove/ridge size combinations were fabricated.
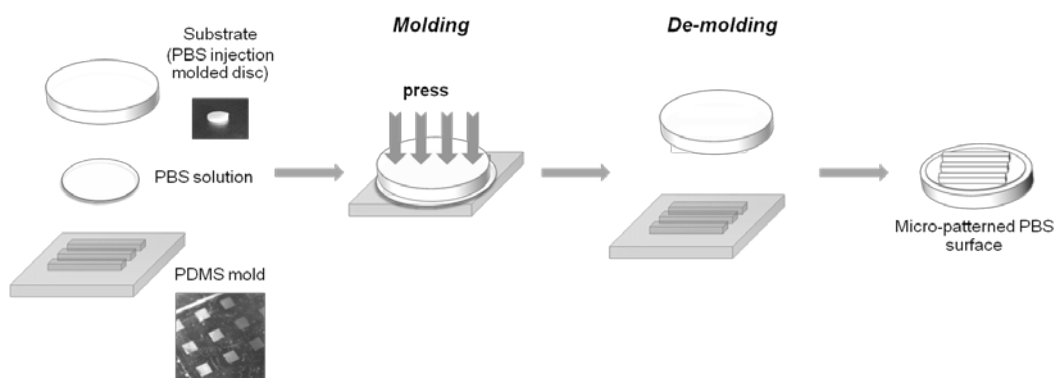
Figure II.11. Schematics of the procedure used for obtaining micro-patterned PBS surfaces.

2.2. Microcapsules production by a two-phase system

The development of microcapsules has been shown to be useful for the protection of bioactive agents such as drugs [50] and cells [51]. Polymeric capsules have the ability of surrounding the desired material, protecting it from the initial immune reaction of the human body, once it is implanted. Specifically, capsules of GG have already been produced by precipitation in an ionic bath [52]. However, the size of these capsules was reported to be in the order of a few millimeters. In the present thesis, capsules of GG at a micro-scale were developed using a two-phase system. GG solution was prepared as previously described [52]. Briefly, 1% (w/v) solution of GG was prepared by dissolving the powder in deionized water at 90 ºC for 20-30 min and stabilized at 40 ºC. GG microcapsules were produced in a single automated procedure, which comprised the formation and stabilization of the microcapsules. The schematic of the proposed automated microcapsule production system is depicted in Figure II.12. This system contained a controllable syringe pump device, a laboratory shaker and a beaker which was filled with a hydrophilic and a hydrophobic

solution. This two-phase system, formed by two distinct layers, was obtained by having mineral oil as the hydrophobic solution (with lower density) and cell culture medium as the hydrophilic solution (higher density). Polymeric droplets were dispensed by a syringe pump into the mineral oil. Agitation produced by the shaker increased the number of droplets generated. Due to the hydrophobicity of the mineral oil, perfectly spherical polymer drops were generated in this solution. When capsules passed through the mineral oil-medium interface, they started to chemically crosslink by the crosslinking agent present in the hydrophilic solution. Specifically, GG was crosslinked by calcium ions contained in the medium. Mineral oil could easily be removed and the capsules left suspended in the medium solution. Prior to use, the microcapsules were harvested from the medium and directly stored in an incubator.
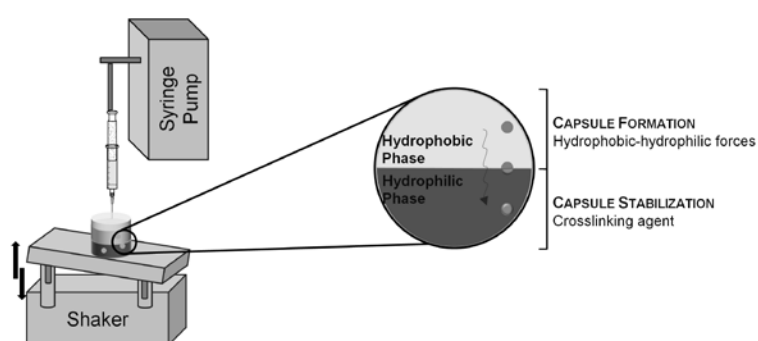
Figure II.12. Schematics of the system for microcapsule formation.

2.2.1. Microcapsule generation with encapsulated fluorescent beads

The encapsulation of fluorescent beads within the developed system is a widely employed method for evaluating the ability of the system to effectively distribute the encapsulated molecule/cell. In the present thesis, microbeads stock solutions containing microbeads with a diameter of 10 μm (with a solid fraction of 0.1% w/w) were suspended in the polymer solution at 37 °C. Two different bead concentrations, 0.01% (i.e., 4.55×10^5 beads/mL) and 0.1% (i.e., 4.55×10^6 beads/mL) of the original concentration (i.e., 4.55×10^7 beads/mL), were used to assess the influence of bead concentration on its distribution within the capsule. The protocol for generating encapsulated fluorescent beads was similar to that described for the simple microcapsules (section 2.2). Encapsulated fluorescent beads were imaged using a fluorescence microscope.

2.3. Fabrication of hydrogels of gellan gum and methacrylated gellan gum

There are a multitude of mechanisms that can be employed for the development of hydrogels. Generally, the mechanisms can be divided in two groups: physical and chemical

mechanisms. However, in both cases, the formation of a hydrogel consists on using an aqueous solution of a hydrophilic polymer, in which polymer chains are dispersed in low or moderate concentration. Once a crosslink agent is introduced, the polymer chains start to entangle, forming a three-dimensional (3D) polymeric network with large content in water [18]. Although hydrogels possess large water content, the presence of the crosslinking agent prevents the 3D structure from dissolving. Depending on the application, the crosslinking agent introduced can lead to the establishment of physical or chemical bonds on the network of the hydrogel. Physically crosslinked hydrogels are widely used in biomedical applications, mainly because they don't require the use of harsh chemical agents. However, the stability of the physically crosslinked hydrogels relies on cooperative bonding interactions that are relatively week, such as ionic bonds, hydrogen bonds and Van der Waals forces. The variation of the solution temperature and the addition of specific ions are some of the crosslinking agents that can be used to physically crosslink hydrogels. Since these hydrogels are formed by reversible bonds, the degradation and thus the stability of the hydrogels is highly dependent on the properties of the environment. Thus, chemically crosslinked hydrogels are used if a more stable hydrogel is required. Covalent bonds are established, usually between groups on the polymer backbone, resulting in a hydrogel with a stronger network.

In the present thesis, hydrogels of GG and MeGG were fabricated. As previously referred, hydrogels of GG can only be produced by physical mechanisms. GG hydrogels were used as a control for the evaluation of the properties of the MeGG hydrogels. Thus, for the development of GG hydrogels, GG was dissolved at 0.5, 1 and 2% (w/v) in dionized water, as described elsewhere [52]. The solution was progressively heated to 90 ºC and kept under agitation for 20-30 min, until complete and homogeneous dispersion of the material was obtained. Afterwards, calcium chloride ($CaCl_2$, Sigma, USA) was added to the dissolved material to fabricate physically crosslinked GG hydrogels. The final concentration of $CaCl_2$ solution was 0.08 mg/mL, unless mentioned otherwise, yielding a ratio of calcium equivalent/GG carboxylate moieties of 0.052 for 1% (w/v) solution of GG. The temperature was progressively decreased to 45 ºC and the solution casted into molds, allowing the temperature to cool to room temperature, thus crosslinking the hydrogel.

On the other hand, MeGG material developed is amenable to chemical crosslinking, due to the presence of the ester groups, introduced with the chemical modification (section 1.2.1). Similarly to GG, lyophilized Low-MeGG and High-MeGG were dissolved at 0.5, 1 and 2% (w/v) in deionized water under constant stirring at 50 ºC for 10 min. Afterwards, physically crosslinked MeGG hydrogels were fabricated by the addition of $CaCl_2$, under the same conditions as used for GG. Chemically crosslinked MeGG hydrogels were obtained by adding 0.5% (w/v) 2-hydroxy-1-[4-(2-hydroxyethoxy)phenyl]-2-methyl-1-propanone (Irgacure

2959, Ciba Specialty Chemicals) to the MeGG solution and exposing to light (320-500 nm, 7.14 mW/cm^2, EXFO OmniCure S2000) for 60 seconds. MeGG hydrogels crosslinked both by physical and chemical mechanism were obtained by combining the above described mechanisms. For all described experiments, polymer disks (1 mm thick, 4 mm in diameter) were punched from hydrogel slabs, unless stated otherwise. Figure II.13 depicts the formation of physically and chemically crosslinked MeGG hydrogels, as well as physically crosslinked GG hydrogels.
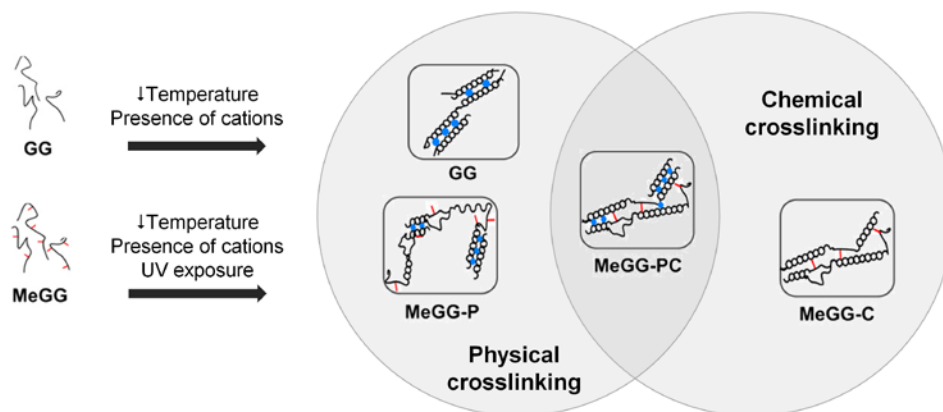
Figure II.13. Schematics of the formation of GG and MeGG hydrogels and the mechanisms behind physical and chemical crosslinking of these hydrogels. (Legend: MeGG-P-physical crosslinking; MeGG-C-chemical crosslinking; MeGG-PC-physical and chemical crosslinking; •-Cations; ▬-Methacrylate groups)

2.4. Micropatterned structures of methacrylated gellan gum-chitosan polyelectrolyte complex hydrogels by photolithography

Similarly to the procedure used for the fabrication of PBS patterns (section 2.1), micro-scaled structures were transferred to hydrogels, but instead of using micromolding as described previously, photolithography was the methodology used. The development of micro-scaled hydrogels was performed in a two-step procedure. In a first stage, micro-scaled hydrogels were developed by a physical mechanism, through ionic bonds established while mixing MeGG with CHT, creating a polyelectrolyte complex (PEC) hydrogel (MeGG-CHT). In a second step, a chemical crosslinking of the polyelectrolyte was performed, by exposing the hydrogel to UV, as previously reported for plain MeGG (section 2.3).

PEC hydrogels are formed as a result of the interaction between chains of polymers. This specific type of physical interaction is a result of the electrostatic interaction of polymer chains with opposite charge. A stronger and faster interaction occurs when both polymers are charged in their initial state. In the present thesis, both MeGG and CHT were used in

their charged state, respectively negatively and positively charged. Figure II.14 depicts the electrostatic interactions established between both polymers, which occur between the charged amino groups of CHT and the negatively charged carboxylic acid of MeGG.
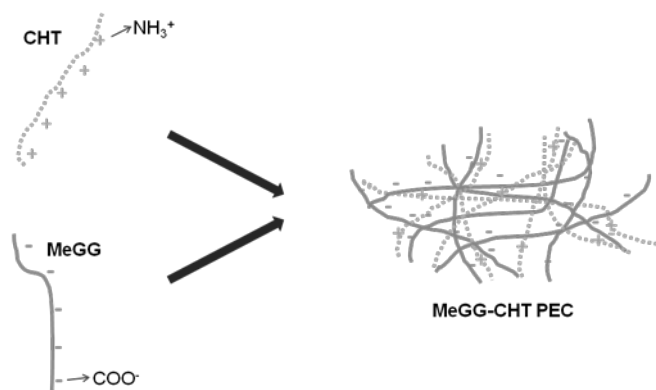
Figure II.14. Basic PEC interactions.

Chemical crosslinking of these hydrogels allowed not only to stabilize the physically established network, but also to develop micro-scaled hydrogel structures by photolithography. In fact, photopolymerizable biomaterials have been widely studied in the biomedical field, since they allow to spatially and temporally control their properties [53]. Briefly, photolithography involves mixing a precursor polymer and a photoinitiator and placing the mixture onto a substrate. A patterned mask, consisting on transparent regions that allow light to pass, and on dark regions that block the passage of light, is placed on top of the mixture. Spacers positioned in between the substrate and the patterned mask, impute a height to the micro-scaled structures. Only the exposed regions of the precursor polymer are submitted to photopolymerization. The rate of photopolymerization is dependent on several parameters, such as (i) the number of double bonds present in the photosensitive polymer used, (ii) the initiator efficiency, (iii) the initiator concentration, and (iv) the light intensity. Figure II.15 depicts in a simplistic way the photopolymerization reaction of a photosensitive polymer. Since the delivery/transportation of cells is one of the main aims of using hydrogels for tissue engineering, it may be necessary to polymerize the hydrogel in the presence of cells. Thus, it is necessary to select the proper parameters, in order to allow the maintenance of cell viability and function [53]. Cell encapsulation is only possible with water soluble precursors that form highly hydrated networks upon polymerization. The water soluble photoinitiator 2-hydroxy-1-[4-(hydroxyethoxy)phenyl]-2-methyl-1-propanone (Irgacure 2959) has been widely reported for the encapsulation of cells within photosensitive hydrogels due to its low cytotoxicity [54-56]. Also of importance is the light source and intensity. The type of light selected has to match the excitation wavelength of the photoinitiator used and its

intensity has to be considered, so that it is enough to initiate the reaction, without increasing too much the surface temperature [57].
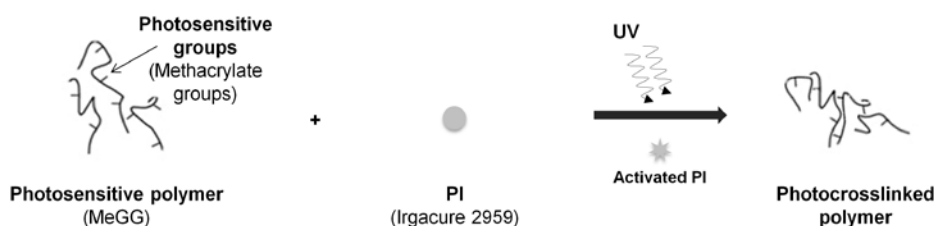
Figure II.15. Schematics of the photopolymerization reaction of a photosensitive polymer.

Specifically in this thesis, for the development of MeGG-CHT PEC hydrogels, CHT (1%, w/v) was dissolved in an aqueous solution of acetic acid (1%, v/v) and MeGG (1%, w/v) was dissolved in deionized water under constant stirring at 50 ºC for 10 min. 0.5% (w/v) of Irgacure 2959 was added as a photoinitiator for chemical crosslinking to the MeGG solution. The photocrosslinkable PEC hydrogel (MeGG-CHT) was formed by dispensing negatively charged MeGG into positively charged CHT. To visualize the formation of hydrogels, MeGG solution was colored with trypan blue and CHT solution with eosin Y (Figure II.16). Photocrosslinked MeGG-CHT PEC hydrogels were obtained by exposing to light (wavelength of 320-500 nm, 7.14 mW/cm^2, EXFO OmniCure S2000) for 60 sec. MeGG-CHT hydrogels with three different volume ratios (2:1, 1:1, 1:2) of the polymers were prepared by varying the volume of the polymer solution. These hydrogels were used for morphological and chemical characterization (section 3).
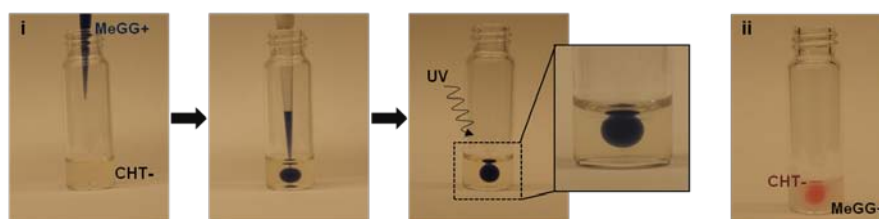
Figure II.16. Representation of a method to form photocrosslinkable PEC hydrogels by injecting (i) trypan blue stained MeGG in CHT or (ii) eosin stained CHT in MeGG solution.

In order to develop the micro-scaled MeGG-CHT hydrogels, the MeGG-CHT hydrogel described in Figure II.16 was formed onto a 3-[tris(trimethylsilyloxy)silyl]propyl methacrylate (TMSPMA) coated glass slides (see section 2.4.1. for further details on the surface modification) using photolithography. Briefly, 100 µL of MeGG prepolymer was pipetted into

the same volume of CHT previously placed on top of TMSPMA glass slide (Figure II.17). Untreated cover slip, placed on top of the MeGG-CHT hydrogel, was separated from treated glass slide by 150 µm spacers. The photomask (either with triangular or square shapes) was placed directly on top of the cover slip prior to exposure to light (wavelength 320-500 nm, 7.14 mW/cm^2, EXFO OmniCure S2000). Subsequently, the cover slip was removed and the remaining uncrosslinked prepolymer cell suspension was gently washed away with preheated Dulbecco's Modified Eagle Medium (DMEM).

Figure II.17. Schematic of process to create micro-patterned polyelectrolyte capsules by photolithography.

2.4.1. Preparation of TMSPMA treated glass slides

The surface modification of glass slides with TMSPMA allows the production of hydrophobic glass surfaces with highly reactive siloxane groups. Briefly, glass slides (Fisherbrand Plain Microscope Slides Precleaned, 25x75x1mm) were cleaned overnight with a sodium chloride solution (10%, w/v). After that period, glass slides were washed 6 times with deionized water. Each slide was afterwards rinsed 3 times with ethanol and left to dry. The TMSPMA treatment was performed overnight at 80 ºC. Cleaned glass slides were stacked in a clean beaker and the reagent poured over the glass slides. By capillarity the reagent covered both surfaces. The final step of the surface modification consisted on cleaning with ethanol (3 times) the TMSPMA treated surfaces and left to dry.

2.5. Multi-scale fibrous system of methacrylated gellan gum-chitosan by combining fluidics technology and polyelectrolyte complexes

The physical crosslinking of MeGG-CHT hydrogel described in section 2.4 was directed using a template. A bundle of aligned hydrogel fibers was generated by combining polyelectrolyte complexation and fluidics technology. Briefly, a fluidic device (Figure II.18) with two oblique channels (1 mm diameter) was fabricated using PDMS and template-based technology. PDMS pre-polymer was poured over a template made with needles of 18G.

MeGG solution (1% w/v, with or without cells) and CHT (1% w/v) solution were injected in each inlet of the microfluidic device and the flow maintained with a syringe pump. At the position where the two solutions merged, the oppositely charged chains of MeGG and CHT started to interact through electrostatic forces. The formed fibers were collected onto TMSPMA treated glass slides. The collected fibers were stabilized by exposure to light (320-500 nm, 1.2 mW/cm^2, EXFO OmniCure S2000) for 60 sec.
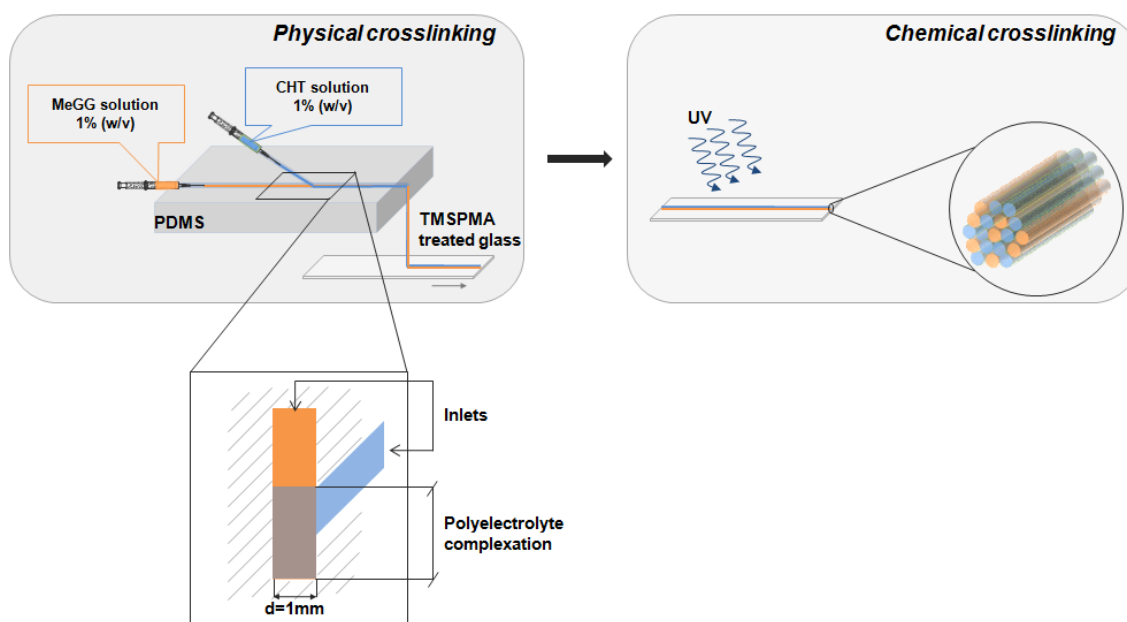
Figure II.18. Schematics of the process to develop the multi-scale fibrous hydrogel system of MeGG-CHT.

3. TECHNIQUES USED FOR CHARACTERIZING THE DEVELOPED MATERIALS/STRUCTURES

The next sections will give further details on the procedures and rationale for selecting the techniques used for the characterization (roughly divided into morphological, chemical and physical characterization) of the materials/structures developed and described in the previous sections.

3.1. Morphological Characterization

3.1.1. Optical and fluorescence microscopy

Optical and fluorescent microscopy was used to assess the size of the microcapsules developed in Chapter IV. The variation of the capsule diameters within each experiment was determined by examination under a standard inverted-light microscope. The size of the

microcapsules was measured using ImageJ software (http://rsbweb.nih.gov/ij/). Many parameters might affect the size of the microcapsules. In this study we characterized the effect of the syringe gauge (31, 27 and 25 G) and the syringe dispensing rate (0.002, 0.01 and 0.1 μL/hr), keeping constant, respectively, the solution pump rate at 0.01 μL/hr and the syringe gauge to 31 G. For that, some system parameters were kept fixed throughout all experiments including the speed and the maximum tilting angle of the shaker and the syringe volume (3 mL). To characterize the microcapsule size uniformity, three independent experiments were performed, each containing at least 15 replicates. Green fluorescence of encapsulated beads was evaluated using a blue filter.

Optical and fluorescent microscopy was also used to analyze the formation of the multi-scale fibrous hydrogel (Chapter VII). Fibrous hydrogel was engineered with fluorescein-CHT and plain MeGG and the distribution of CHT within the system was assessed with a blue filter. Also, the stabilization of the system was evaluated through the detection of green fluorescence of CHT, by immersing the system in phosphate buffer saline (PBS) for 7 days at 37 ºC.

3.1.2. Scanning electron microscopy

Scanning electron microscopy (SEM) was used to evaluate the morphology of the developed structures at a smaller scale than with optical microscopy. SEM micrographs can be obtained from secondary electrons emitted from the surface of the sample, as a result of the impact of a focused electron beam. This technique evaluates the surface of the samples with a penetration depth of 5 Å [58]. Micro-patterned PBS surfaces (Chapter III) were analyzed using a Leica Cambridge S-360 scanning electron microscope (Leica Cambridge, UK). Non-conductive samples are usually coated with a thin conductive metal layer in order to minimize charge accumulation. Thus, all specimens were pre-coated with a conductive layer of sputtered gold. SEM images were taken at an accelerating voltage of 15 kV at different magnifications. The size of the grooves and ridges of the patterns were calculated using an image analysis software (NIH Image J) and taking the groove as the lower section of the pattern and the ridge as the upper section, as depicted in Figure II.19.

Figure II.19. Definition of the groove and ridge of the PBS patterns.

SEM was also used to evaluate the morphology of the photocrosslinked MeGG-CHT PEC hydrogels (2:1, 1:1, 1:2 ratios and plain MeGG and CHT, Chapter VI) and of the MeGG-CHT fibrous hydrogels (Chapter VII). A Zeiss Ultra 55 scanning electron microscope was used under an accelerating voltage of 15 kV. Freshly prepared hydrogel samples were flash-frozen in liquid nitrogen, freeze-fractured and freeze-dried for 72 h as described previously [59]. Freeze-dried samples were sputter coated with palladium-platinum alloy target materials with 40 mA current for 80 sec using a sputter coater (SP-2 AJA Sputtering System) before SEM observation. The area of the pores of the photocrosslinked PEC hydrogels was calculated using an image analysis software (NIH Image J, n=40). The microstructure of the hydrogel fiber bundles (Chapter VII) was also observed under the same microscope. Similarly to PEC hydrogels, fibrous hydrogels were flash-frozen in liquid nitrogen and freeze-dried for 72 h.

3.1.3. Atomic force microscopy

Atomic force microscopy (AFM) is a high resolution type of scanning microscopy, allowing to obtain information about the topography of surfaces. It consists on a sharp tip fixed at the end of a flexible cantilever that moves across the surface of the sample. The tip deflects when it approaches the surface as a result of van der Waals and electrostatic repulsion and attraction forces between an atom of the tip and an atom of the surface of the material. The displacement of the tip is detected by a laser beam on the cantilever. AFM has a very high spatial resolution, thus allowing to obtain information of the surfaces at a micro- and nano-scale. In order to examine the microstructure of the hydrogel fiber bundles, AFM images were acquired by means of a Multimode Nanoscope V (Veeco). The microscope was placed on a table which protected the device from vibrations. A commercial Cantilever probe was used, with a thickness of 4 µm and a tip radius of 10-12.5 nm. The probe oscillation resonance frequency was ~100 kHz. All the samples were characterized using a set-point amplitude ratio of ~0.7. Images were captured at room temperature, at different locations and with an area of 25 µm^2. Images were processed and analyzed by multimode software Nanoscope V6.13.

3.1.4. Transmission electron microscopy

Transmission electron microscopy (TEM) is a microscopy technique that is based on the interaction of a beam of electrons that are transmitted through a thin sample. A micrograph is obtained from the interaction of the electrons with the specimen. TEM is capable of higher resolution than optical and scanning microscopy. Thus, this technique allows examining in

detail the structure at a nano-scale of the specimen. The TEM analysis of a biomaterial usually requires its sectioning, since a thin sample is needed for the analysis. Thus, embedding and sectioning of the material is necessary. The internal nanostructure of the hydrogel fiber bundles was analyzed by embedding freshly prepared samples and analyzing the transversal and longitudinal cross-sections of the hydrogel structure. The samples were prepared by fixing hydrated hydrogels in 2% gluteraldehyde/2% paraformaldahyde and treated with 1% osmium tetroxide. Samples were then dehydrated in acetone and embedded in epoxy resin. Ultrathin sections of 70 nm were placed on TEM grids and observed under TEM (Tecnai™ G² Spirit BioTWIN, FEI).

3.2. Chemical Characterization

3.2.1. Zeta potential

Zeta potential is widely used for the quantification of the electrical charge of particles, polymers or proteins. Although the electrical charge is not measured directly, it can be calculated using established theoretical models. The most widely used theory is the one developed by Marian Smoluchowski. In the present thesis, the zeta potential was measured in order to evaluate the electrical charge of the solutions of MeGG and CHT prior to PEC hydrogel formation (Chapter VI) and multi-scale fibrous hydrogel generation (Chapter VII). The charge of the initial solutions of MeGG and CHT (1% w/v) was determined using a Malvern Zetasizer® 3000 HS (Malvern Instruments, UK). Each analysis was performed for 120 sec at 25 ºC. Smoluchowski model was used. The experiments were performed in triplicates.

3.2.2. Fourier transform infrared spectroscopy

Fourier transform infrared spectroscopy (FTIR) is a standard technique used to obtain information about the chemical structure of the materials studied. Infrared (IR) light is adsorbed by the material, exciting specific molecular vibrations. Since it is known that discrete energy transitions are related to specific vibrational states of atomic and molecular units, one can identify the presence of chemical groups on the sample through the FTIR spectrum. The attenuated total reflection (ATR) sampling mode of FTIR can be used to increase the intensity of the signal obtained. However, since the penetration depth is high (1-5 µm), care should be taken while preparing the sample. The chemistry of the modified material reported on Chapter V and the developed PEC hydrogels reported on Chapter VI was analyzed by FTIR-ATR. The infrared spectra were recorded on a spectrophotometer Bruker Alpha FT-IR with a resolution of 2 cm^{-1} or 4 cm^{-1}, respectively for Chapter V and

Chapter VI. The results are presented as the average of 32 scans. PEC hydrogels were fabricated and freeze-dried before performing the FTIR analysis. Both the surface (2:1, 1:1 and 1:2 volume ratios) and the cross-section (1:1 ratio) of the MeGG-CHT hydrogels were evaluated. For that, a slice of the middle portion of the MeGG-CHT hydrogels was cut and freeze dried, in order to evaluate the cross-section of the hydrogels. For the surface analysis, the MeGG-CHT hydrogel was frozen immediately after preparation.

3.2.3. Proton nuclear magnetic resonance

The principle of proton nuclear magnetic resonance (^{1}H-NMR) is related to the magnetic properties of the hydrogen nuclei. The technique is based on the fact that, at a specific radio frequency, each hydrogen atom in a molecule will need a slightly different magnetic field to bring it to the resonance condition. This is dependent on the type of bonds the hydrogen atom is involved in the molecule. Thus, ^{1}H-NMR spectrum will give information regarding the hydrogen's atom environment in the molecule. Simple ^{1}H-NMR spectra are recorded in solution. Since protons from the solvent should not interfere in the analysis, deuterated solvents are usually preferred for the analysis. They consist on the use of deuterium (^{2}H), a stable isotope of hydrogen. The chemical modification to GG on Chapter V was assessed by ^{1}H-NMR spectroscopy. ^{1}H-NMR spectra were recorded with a Varian Inova 500 NMR equipped with a variable temperature system. Lyophilized materials were dissolved in deuterated water (D_2O) at a concentration of 10 mg/mL and at temperature of 50 ºC. Chemical shifts were referred to the methyl group of rhamnose as an internal standard, which is at δ 1.45 ppm [21]. The degree of substitution (DS, fraction of modified hydroxyl groups per repeating unit) was determined by the relative integration of the double bond proton peak (I_{DB}) of the methacrylate groups to the methyl protons of the internal standard (I_{CH_3rham}), according to Eq (1), as described elsewhere [21]. $n_{H_{DB}}$ and $n_{H_{CH_3rham}}$ corresponds to the number of protons in the double bond and the methyl group of rhamnose, respectively. $n_{OH_{monomer}}$ corresponds to the number of reactive -OH sites in the GG structure.

$$DS = \frac{\dfrac{I_{DB}}{n_{H_{DB}}} \Big/ \dfrac{I_{CH_3rham}}{n_{H_{CH_3rham}}}}{n_{OH_{monomer}}} \qquad (1)$$

3.2.4. X-ray photoelectron spectroscopy

X-ray photoelectron spectroscopy (XPS) technique is a quantitative spectroscopic technique based on the photoelectric effect. A focused beam of X-rays induces the emission of core-

level electrons from the material surface (10-250 Å) [60, 61] of characteristic kinetic energy. The survey spectrum provides the elemental composition of the material and the high resolution spectrum the environment of the atoms, thus giving information about its chemical and electronic state. XPS was performed to further characterize chemically both the surface and the cross-section of the photocrosslinked PEC hydrogels (Chapter VI). Analyzes were performed on a Kratos Axis Ultra XPS instrument using a monochromatic Al Kα X-ray source operating at 15 kV and 10 mA. The elements in the sample surface were identified from a survey spectrum at pass energy of 160 eV. The areas under the specific peaks were used to calculate the atomic percentages. High-resolution spectra were also recorded at pass energy of 20 eV and overlapping peaks were resolved into their individual components by CasaXPS software. Component energies (399.4 ± 0.4 eV, 400.5 ± 0.4 eV and 401.4 ± 0.4 eV, respectively for amine, amide and protonated amine), number of peaks and peak widths (full width at half-maximum, fwhm, fixed for 1.2 ± 1%) were fixed initially and refinement was performed for peak heights only. PEC hydrogels were fabricated as described in section 2.4.

3.3. Physical Characterization

3.3.1. Swelling study

Hydrogels are materials with the capacity to absorb high quantities of water. Thus, the study of the swelling kinetics of hydrogels when immersed in solutions is important to help on predicting their behavior *in vitro* and *in vivo.* To study the swelling kinetics of the developed hydrogels (Chapter V and VI), three solutions with different ionic content were used: distilled water (no ions); phosphate buffered saline (DPBS, Gibco, with monovalent ions); and media (Dulbecco's Modified Eagle's medium, DMEM, Gibco, with mono and divalent ions). Given that the formation of GG and MeGG hydrogels is dependent on the presence of ions, these three solutions with distinct ionic contents were selected in order to evaluate their possible effect over the hydrogel swelling kinetics. Hydrogel samples at 1% (w/v) were immersed in 2 mL of each solution at 37 ºC, under mild shaking. At different time points, the hydrogels (n=3) were removed from the solutions and gel surfaces were quickly blotted on a filter paper. Their wet weight was measured (w_t) and compared to the initial wet weight (w_0). The swelling ratio (S_k) was defined according to Eq (2).

$$S_k(\%) = \frac{w_t - w_0}{w_0} \times 100 \qquad (2)$$

3.3.2. Degradation study

Biodegradable polymers should be designed to degrade over time at the same rate as neo-tissue is formed. The products of the degradation should be non-toxic and be able to be removed from the organism. The biodegradation of materials requires the hydrolytic or enzymatic cleavage of polymeric bonds sensitive to those mechanisms. Biopolymers than are known to be susceptible to these degradation mechanisms can be tuned *in vitro*, in an attempt to predict their behavior *in vivo*. The degradation study performed in the present thesis was aimed at comparing the degradation profile between all the materials formulations. Thus, an accelerated hydrolytic degradation was performed using sodium hydroxide (NaOH). The effect of the degree of methacrylation, crosslinking mechanisms and polymer concentration over the *in vitro* degradation profile of MeGG hydrogels developed in Chapter V was studied. Weighed hydrogels (n=3) were hydrolytically degraded in a 0.1 mM NaOH solution at 37 ºC for 24 hours on a shaker. The samples were removed, freeze dried and weighed again to determine weight loss (WL), according to equation 3, where w_t corresponds to the dry weight of the sample at different time-points, and w_0 to the initial dry weight.

$$WL(\%) = \frac{w_t}{w_0} \times 100 \qquad (3)$$

3.3.3. Mechanical analysis

Biomaterials are subjected to different loads once implanted. The type and strength of these loads depend on the tissue in which they are implanted. Thus, when engineering biomaterials, one should consider the forces that they are designed to withstand and the type of deformation that they will be subjected to (elongation, compression, twist or break). In the present thesis, the developed hydrogels were tested for deformation by compression. The hydrogels developed in section 2.3 (Chapter V) were crosslinked through different mechanisms: physical, chemical, or a combination of both. To assess the effect of the degree of methacrylation, crosslinking mechanisms and polymer concentration on the mechanical properties of the developed hydrogels, compression tests were performed on an Instron 5542 mechanical tester. The setup is depicted in Figure II.20.A. Freshly prepared GG and MeGG hydrogels (1 mm thick, 8 mm in diameter, n=3) were compressed in the direction normal to the circular face of the cylindrical samples at a rate of 0.2 mm per minute until failure of the hydrogel. The stress-strain curve gives the representation of the hydrogel displacement (strain) as a function of the load applied to the hydrogel (stress). The Young's modulus was defined as the slope of the linear region of the stress-strain curve in the 5-15%

of the strain range. Ultimate stress and ultimate strain values were taken as the point where failure of the hydrogel occurred (Figure II.20.B).
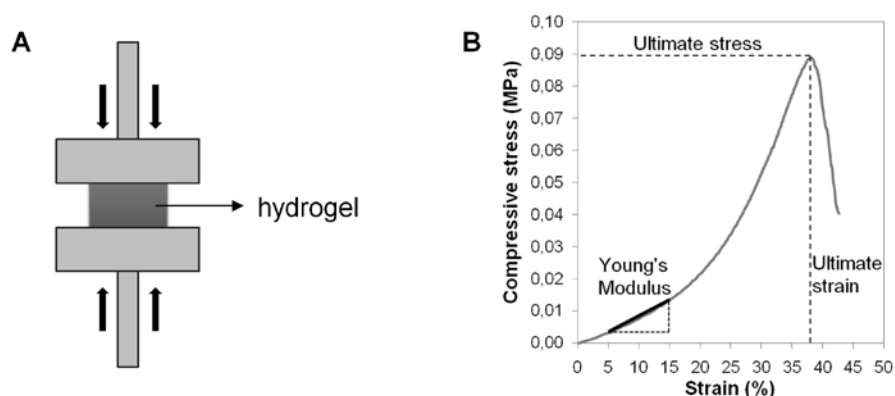
Figure II.20. (A) Schematics of the compression of the hydrogel. (B) Typical stress-strain curve with the Young's Modulus, Ultimate Stress and Ultimate Strain depicted on the graph.

4. BIOLOGICAL EVALUATION OF THE DEVELOPED MATERIALS/STRUCTURES

In order to validate the potential use of the developed materials and structures, they need to be submitted to a biological evaluation. Usually, this evaluation starts with simple *in vitro* studies that enable an initial screening of the biological performance of the materials/structures. Either cell lines or primary cell cultures are used for these analyzes, but for the initial studies a cell source is usually selected. After two-dimensional (2D) seeding or three-dimensional (3D) encapsulation, cell viability, proliferation and function can be evaluated through a series of different methodologies. With the outcomes from the *in vitro* analysis, materials/structures can be selected and/or optimized for further biological evaluation and/or for in *in vivo* studies. In the following sections it is described the cells, the seeding/encapsulation methodologies and techniques used for the biological evaluation of the materials developed in the scope of this thesis.

4.1. Cell sources

4.1.1. Cell lines

Cell lines are immortalized cultures of cells that present the ability to proliferate indefinitely, either due to a random mutation or a programmed modification. In the present thesis, two different cell lines were used: a fibroblast cell line (NIH-3T3, Chapter IV and V) and an insulinoma cell line (MIN6, Chapter IV).

NIH-3T3 is a standard fibroblast cell line, originally obtained from NIH Swiss mouse embryo fibroblasts. NIH-3T3 fibroblast cells were cultured in Dulbecco's Modified Eagle Medium (DMEM, Sigma-Aldrich) supplemented with 10% of heat-inactivated fetal bovine serum (FBS, Gibco) and 1% penicillin-streptomycin (Gibco) at 37 ºC, in a humidified atmosphere with 5% of CO_2.

The second cell line used in the present thesis was an insulinoma cell line (MIN6) derived from a transgenic mouse. Their ability to secrete insulin as a response to glucose stimuli, being this secretion concentration-dependent as observed in normal islets, makes them a useful model for studying normal pancreatic beta cells [62]. The MIN6 cell line used in this thesis was kindly provided by Dr. Donald Ingber, Wyss Institute of Harvard, Boston, MA, USA. MIN6 cells (passages 35-42) were maintained at 37°C and 5% CO_2 in DMEM supplemented with 10% FBS and 100 U/mL penicillin with 0.1 mg/mL streptomycin. The medium was changed every 3-4 days.

4.1.2. Primary cells

Primary cell cultures are usually obtained directly from a subject and have a limited lifespan. In the present thesis two different primary cell cultures were obtained: human adipose stem cells (hASC, Chapter III) and rat cardiac fibroblasts (rCF, Chapter VI and VII).

Adipose stem cells (ASC) have generated great enthusiasm for tissue engineering applications because of their easy harvesting procedures and wide availability as well as their ability to expand in culture and to differentiate into a variety of cell types such as endothelial cells [63], chondrocytes [64, 65], osteoblasts [66, 67] and neural cells [68, 69]. Adipose tissue is of mesodermic origin, consisting of a heterogeneous population of adipocytes and the stromal vascular fraction (SVF), which is comprised of vascular cells, smooth muscle cells, blood cells and fibroblast-like multipotential stem cells. Stem cells were isolated from human adipose tissue samples (collected from lipoaspiration procedures, under a protocol with Hospital da Prelada, Porto, Portugal), as described elsewhere [70], by the enzymatic digestion of the tissue with 0.2% collagenase type I A in phosphate buffer saline (PBS, Sigma) for 60 min at 37 ºC under gentle stirring. Digested tissue was filtered and adherent cells selected after centrifugation steps. Cells were expanded in Dulbecco's Modified Eagle Medium (DMEM, Sigma) supplemented with 10% heat-inactivated fetal bovine serum (FBS, Biochrom AG) and 1% of antibiotic (Gibco) at 37 ºC in a humidified atmosphere with 5% CO_2 until reaching enough number of cells for the study.

Cardiac fibroblasts used in this thesis were isolated from the heart of a 1 day old Sprague-Dawley rat, as described elsewhere [71]. Briefly, hearts (n=10) were washed with Hank's balanced salt solution (HBSS, Gibco Invitrogen) and were minced and incubated in 0.3

mg/mL collagenase solution containing 0.6 mg/mL pancretin (Sigma). Isolated cardiomyocytes and cardiac fibroblasts were plated in T75 flasks for 30 min in Dulbecco's Modified Eagles' medium (DMEM, Gibco Invitrogen) containing 10% of heat-inactivated fetal bovine serum (Sigma) and 1% penicillin-streptomycin (Gibco Invitrogen) at 37 ºC with 5% CO_2. Cardiac fibroblasts were purified by removing all non-adherent cells, including the cardiomyocytes.

4.2. Cell culture

4.2.1. Encapsulation of NIH-3T3 cell line

The effect of methacrylation and photocrosslinking on cell viability was assessed by encapsulating NIH-3T3 fibroblasts (Chapter V). A cell suspension of NIH-3T3 (10^7 cells/mL) was prepared by trypsinization (trypsin/EDTA solution, Gibco) and incorporated into the GG, Low-MeGG and High-MeGG polymer solutions prepared as described previously and stabilized at 40 ºC. After resuspension, the cell/polymer mixture was casted into molds. GG hydrogels with encapsulated cells were placed at room temperature for 1-2 minutes to form a solid gel. MeGG cell laden hydrogels were exposed to light (7.14 mW/cm^2) for 60 sec. Cell viability of cells encapsulated in the hydrogels under study was characterized 1h after preparation and after 1, 3 and 7 days of culture, by incubating cells with a Live/Dead (Invitrogen) assay (calcein AM/ethidium homodimer-1 in DPBS) for 20 min.

NIH-3T3 cells were also encapsulated within the generated microcapsules described in Chapter IV in order to demonstrate the ability of the system for keeping the viability of the cell suspension encapsulated A cell suspension of NIH-3T3 ($3x10^6$ cells/mL) was prepared by trypsinization (trypsin/EDTA solution, Gibco) and mixed with the GG polymer solution at 37 ºC. The protocol for generating capsules with NIH-3T3 cells was similar to that described for obtaining the simple microcapsules. The viability of the encapsulated cells in the hydrogels under study was characterized 1, 3, 5 and 7 days after culture, by incubating cells with a Live/Dead (Invitrogen) assay (calcein AM/ethidium homodimer-1 in DPBS) during 20 min.

4.2.2. Encapsulation of MIN6 cell aggregates

Cultured cells were passaged and used for MIN6 pseudo-islet formation when reaching 70% confluence (Chapter IV). MIN6 pseudo-islets (cell aggregates) were formed by seeding MIN6 cells with $6x10^6$ cells/mL concentration in poly(ethylene glycol) (PEG) microwells with a diameter of 300 μm for 3 days (Figure II.21). The MIN6 aggregates were harvested and preserved in medium immediately before encapsulation. MIN6 cell aggregates were suspended in GG polymer solution at 37 ºC and transferred to a 3 mL syringe for dispensing

and microencapsulation. MIN6-GG suspension was dispensed into the two-phase system (mineral oil-cell culture medium) and encapsulated pseudo-islets were formed. Insuline secretion from MIN6 cell aggregates was evaluated by immunostaining, as described in 4.3.5.
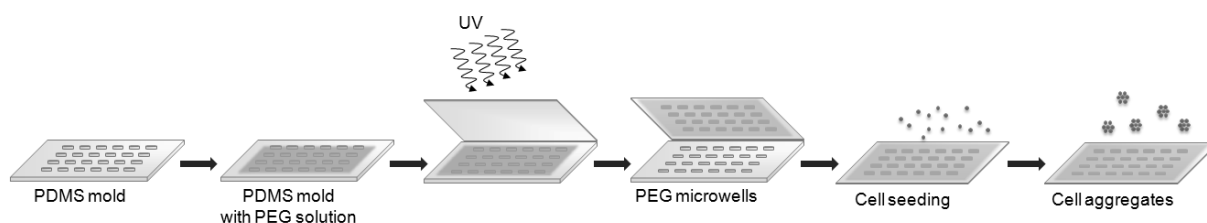
Figure II.21. Fabrication of cell aggregates of MIN6 using PEG microwells.

4.2.3. Seeding of Human adipose stem cells

Human adipose stem cells (hASCs) were cultured onto the PBS micro-patterned surfaces developed in Chapter III. Three sterile samples per pattern were placed in 24-well plates and 1.5 mL of the cell suspension was seeded onto the PBS micro-patterned surfaces using a density of 3.3×10^4 cells/mL, under the cell culture conditions referred in section 4.1.2. Seeded cells were incubated in a humidified atmosphere at 37 ºC and 5% of CO2 for 1 and 3 days. Tissue culture polystyrene (TCPS) was used as a control. After each time point, the metabolic activity, DNA content and morphology of the seeded cells were evaluated, as described below (section 4.3).

4.2.4. Encapsulation of rat cardiac fibroblasts

Primary cells isolated from rat hearts were encapsulated into the MeGG-CHT hydrogels developed in Chapters VI and VII. After reaching confluence, a cell suspension of rCF (107 cells/mL) was prepared by trypsinization (trypsin/EDTA solution, Gibco) and incorporated into the MeGG solution previously warmed to 37 ºC prior to the microfabrication process described in Chapter VI. The viability of encapsulated cells was evaluated by live/dead assay (section 4.3.1). The same cell source was encapsulated onto the fibrous hydrogel system. Similarly to the PEC hydrogels, rCF were suspended in MeGG-RGD solution (1.7x107 million cells/mL) and fibrous hydrogels prepared as described in section 2.5 using plain CHT and MeGG-RGD with suspended rCF. After stabilization with UV exposure, fibrous hydrogels were cultured for up to 7 days in 6-well-plates (Fisher Scientific) under standard culture conditions, with media exchanged every 48 h. The viability and cell morphology of encapsulated cells were evaluated as described in sections 4.3.1 and 4.3.5.

4.3. Evaluation of cell culture

The following sections give further details regarding the techniques used in the present thesis for evaluating cells (through analysis of cells viability, morphology, proliferation and activity/functionality) after seeding or encapsulation and culture onto the developed material/surfaces.

4.3.1. Live/Dead assay

The photoencapsulation of cells within hydrogels might be deleterious to cells as a result of the exposure to UV light and to the photoinitiator. The Live/Dead assay (Invitrogen) can be used to evaluate the viability of encapsulated cells. This assay provides a two-color fluorescence simultaneous visualization of live and dead cells. It is based on the use of acetomethoxy derivate of calcein (Calcein-AM) that is a non-fluorescent dye that easily permeates live cells. It can be hydrolytically converted to calcein, a strong green fluorescent dye (excitation~495 nm/emission~515 nm). On the other hand, dead cells are identified with ethidium homodimer (EthD-1). This dye passes the membrane of damaged cells and binds to the nucleic acids, increasing up to 40-fold its fluorescence intensity (excitation~495 nm/emission~635 nm). Cells with integrity of plasma membrane will exclude EthD-1. The detection of live/dead cells was performed on Chapters IV, V, VI and VII. After each culture period, hydrogels with encapsulated cells were gently washed with PBS. Calcein-AM/EthD-1 solution was prepared by mixing 20 µL of EthD-1 (2 mM) and 5 µL of Calcein-AM (4 mM) in 10 mL of PBS. Encapsulated cells were incubated with this solution for 20 min. After that period, the solution was removed and the excess of dye washed off with PBS. Hydrogels with encapsulated cells were then visualized under an inverted fluorescence microscope, as described in section 3.1.1.

4.3.2. Metabolic activity

Cell viability was evaluated during culture time (1 and 3 days) by quantifying the metabolic activity of hASC (Chapter III), using the Alamar Blue® (Invitrogen) assay. Alamar blue can be reduced in active cell mitochondria, changing the solution color from blue to a bright red color. Alamar blue stock solution was diluted with culture medium without phenol red. Analysis was performed according to the manufacture instructions. The plates were exposed to an excitation wavelength of 540-570 nm and the emission at 580-610 nm recorded in a microplate ELISA reader (BioTek, USA). The percentage viability was expressed as fluorescence in comparison to the non-patterned PBS surface.

4.3.3. DNA content

After each time-point, cells were lysed by osmotic and thermal shock and the supernatant used for double-stranded DNA (dsDNA) content analysis. Cell proliferation was evaluated by quantifying the DNA content on the hASC seeded PBS patterned surfaces using the Invitrogen/Molecular Probes PicoGreen dsDNA Quantification Kit. Probes PicoGreen dsDNA Quantification Kit. This assay allows measurement of the fluorescence produced when PicoGreen dye is excited by UV light while bounded to dsDNA. The protocol used is described below. Prior to DNA quantification, samples were thawed and sonicated for 15 min. Samples and controls were vortexed and 28.7 µL of each, plus 71.3 µL of PicoGreen solution and 100 µL of Tris–EDTA buffer was transferred into an opaque 96-well plate. Triplicates were made for each sample or assay standard. The plate was read on a microplate ELISA reader (BioTek, USA) using an excitation of 485 nm (excitation of the dye) and an emission wavelength of 528 nm (when the dye is bounded to the dsDNA). A standard curve was created (λDNA standard ranging between 0 and 2 µg/mL) and the DNA values of the samples were read off from the standard graph. The results are presented as µg DNA/cm^2 and allowed to evaluate the effect of the surface treatments over cell proliferation. The DNA amount was calculated from a standard curve.

4.3.4. Scanning electron microscopy of human adipose stem cells

SEM was performed as a means to evaluate the morphology of hASC seeded over PBS micro-patterned surfaces (Chapter III). After each culture period, samples were washed with PBS, fixed with 4% formaldehyde (Merck) and kept at 4 ºC in PBS until being prepared for SEM. For SEM analysis samples were dehydrated using graded ethanol solutions (50%, 70%, 90% and 100%, v/v) twice, 15 minutes each and let to dry overnight. SEM analysis was then carried out as described in section 3.1.2.

4.3.5. Immunostaining

Immunostaining was performed to obtain further details about the cell morphology. As described in 4.3.4, after each culture period, cells were washed with PBS, fixed with 4% formaldehyde and kept at 4 ºC until being prepared for immunostaining. Cytoskeleton of hASC cultured onto PBS micro-patterned surfaces (Chapter III) was stained with phalloidin and their nuclei counterstained with DAPI. The morphology of encapsulated rCF into the hydrogel fibers (Chapter VII) was also evaluated by staining the cell cytoskeleton with phalloidin and the cell nucleus with Hoechst.

Immunofluorescence was also used to assess the expression of insulin by encapsulated islets. Anti-Insulin receptor substrate 2 antibody produced in rabbit (Sigma-Aldrich) was coupled with a secondary antibody AlexaFluor 546-conjugated anti-rabbit (Sigma-Aldrich) in order to detect fluorescence.

5. STATISTICAL ANALYSIS

Statistical analysis was performed using GraphPad Prism 5 Software and all data were reported as a mean ± standard deviation.

Statistical differences between the means of two groups were analyzed with a Student t-test. The variance among at least three groups was evaluated using one-way analysis of variance (One-way ANOVA). Although one-way ANOVA measures significant effects of one factor only, two-way ANOVA measures the effect of two factors simultaneously. Thus, two-way ANOVA was used when two parameters were evaluated at the same time. Two-way ANOVA also assesses the interaction between the factors, thus generating three *p*-values, one for each parameter and one indicating the interaction between both parameters. Post-hoc analysis is commonly used for multiple comparisons among the groups, identifying patterns and limiting the probability of false positive significant differences. The Bonferroni's post-hoc test is one of the most used post-hoc tests and attempts to prevent data from incorrectly appearing statistically significantly. *P*-values lower than 0.05 were considered statistically significant in all the analysis. Table II.1 summarizes the statistical method selected to analyze the different data.

Table II.1. Summary of the statistical methods used and the data analyzed.

Statistical Analysis	Chapter	Data Analyzed
t-test	V	Swelling data
one-way ANOVA + Bonferroni's post-hoc test	IV	Microcapsules size
	VI	Hydrogel pore size (with SEM) and swelling data
two-way ANOVA + Bonferroni's post-hoc test	III	*In vitro* metabolic activity and dsDNA content
	V	Mechanical data

REFERENCES

1.   Fujimaki T. Processability and properties of aliphatic polyesters, 'BIONOLLE', synthesized by polycondensation reaction. Polymer Degradation and Stability 1998;59(1-3):209-214.
2.   Correlo VM, Boesel LF, Bhattacharya M, Mano JF, Neves NM, Reis RL. Properties of melt processed chitosan and aliphatic polyester blends. Mater Sci Eng A-Struct Mater Prop Microstruct Process 2005;403(1-2):57-68.
3.   Correlo VM, Boesel LF, Pinho E, Costa-Pinto AR, da Silva MLA, Bhattacharya M, Mano JF, et al. Melt-based compression-molded scaffolds from chitosan-polyester blends and composites: Morphology and mechanical properties. Journal of Biomedical Materials Research Part A 2009;91A(2):489-504.
4.   Correlo VM, Pinho ED, Pashkuleva I, Bhattacharya M, Neves NM, Reis RL. Water absorption and degradation characteristics of chitosan-based polyesters and hydroxyapatite composites. Macromol Biosci 2007;7(3):354-363.
5.   Oliveira JT, Crawford A, Mundy JL, Sol PC, Correlo VM, Bhattacharya M, Neves NM, et al. Novel Melt-Processable Chitosan-Polybutylene Succinate Fibre Scaffolds for Cartilage Tissue Engineering. J Biomater Sci-Polym Ed 2011;22(4-6):773-788.
6.   Martins A, Pinho ED, Correlo VM, Faria S, Marques AP, Reis RL, Neves NM. Biodegradable Nanofibers-Reinforced Microfibrous Composite Scaffolds for Bone Tissue Engineering. Tissue Eng Part A 2010;16(12):3599-3609.
7.   Pinto AR, Correlo VM, Bhattacharya M, Charbord P, Reis RL, Neves NM. Behaviour of human bone marrow mesenchymal stem cells seeded on fiber bonding chitosan polyester based for bone tissue engineering scaffolds. Tissue Engineering 2006;12(4):1019-1019.
8.   Jansson PE, Lindberg B, Sandford PA. Structural studies of Gellan Gum, an extracellular polysaccharide elaborated by pseudomonas-elodea. Carbohydr Res 1983;124(1):135-139.
9.   Miyoshi E, Takaya T, Nishinari K. Rheological and thermal studies of gel-sol transition in gellan gum aqueous solutions. Carbohydrate Polymers 1996;30:109-119.
10.   Singh BN, Kim KH. Effects of divalent cations on drug encapsulation efficiency of deacylated gellan gum. J Microencapsul 2005;22(7):761-771.
11.   Tako M, Teruya T, Tamaki Y, Konishi T. Molecular origin for rheological characteristics of native gellan gum. Colloid and Polymer Science 2009;287(12):1445-1454.
12.   Rozier A, Mazuel C, Grove J, Plazonnet B. Gelrite®: A novel, ion-activated, in-situ gelling polymer for ophthalmic vehicles. Effect on bioavailability of timolol. International Journal of Pharmaceutics 1989;57(2):163-168.
13.   Carlfors J, Edsman K, Petersson R, Jornving K. Rheological evaluation of Gelrite (R) in situ gels for ophthalmic use. European Journal of Pharmaceutical Sciences 1998;6(2):113-119.
14.   Oliveira JT, Santos TC, Martins L, Picciochi R, Marques AP, Castro AG, Neves NM, et al. Gellan Gum Injectable Hydrogels for Cartilage Tissue Engineering Applications: In Vitro Studies and Preliminary In Vivo Evaluation. Tissue Eng Part A 2009;16(1):343-353.
15.   Oliveira JT, Martins L, Picciochi R, Malafaya PB, Sousa RA, Neves NM, Mano JF, et al. Gellan Gum: A New Biomaterial for Cartilage Tissue Engineering Applications. Journal of Biomedical Materials Research-Part A 2010.
16.   Oliveira JT, Gardel L, Martins L, Rada T, Gomes ME, Reis RL. Injectable gellan gum hydrogels with autologous cells for the treatment of rabbit articular cartilage defects. Journal of Orthopedic Research 2010;in press.
17.   Oliveira JT, Santos TC, Martins L, Silva MA, Marques AP, Castro AG, Neves NM, et al. Performance of new gellan gum hydrogels combined with human articular chondrocytes for cartilage regeneration when subcutaneously implanted in nude mice. Journal of Tissue Engineering and Regenerative Medicine 2009;3(7):493-500.
18.   Hennink WE, van Nostrum CF. Novel crosslinking methods to design hydrogels. Advanced Drug Delivery Reviews 2002;54(1):13-36.
19.   Hoffman AS. Hydrogels for biomedical applications. Advanced Drug Delivery Reviews 2002;54(1):3-12.
20.   Gong YH, Wang CM, Lai RC, Su K, Zhang F, Wang DA. An improved injectable polysaccharide hydrogel: modified gellan gum for long-term cartilage regeneration in vitro. Journal of Materials Chemistry 2009;19(14):1968-1977.
21.   Hamcerencu M, Desbrieres J, Khoukh A, Popa M, Riess G. Synthesis and characterization of new unsaturated esters of Gellan Gum. Carbohydr Polym 2008;71(1):92-100.
22.   Oudshoorn MHM, Rissmann R, Bouwstra JA, Hennink WE. Synthesis of methacrylated hyaluronic acid with tailored degree of substitution. Polymer 2007;48(7):1915-1920.

23. Garcia AJ, Boettiger D. Integrin-fibronectin interactions at the cell-material interface: initial integrin binding and signaling. Biomaterials 1999;20(23-24):2427-2433.

24. Shu XZ, Ghosh K, Liu YC, Palumbo FS, Luo Y, Clark RA, Prestwich GD. Attachment and spreading of fibroblasts on an RGD peptide-modified injectable hyaluronan hydrogel. Journal of Biomedical Materials Research Part A 2004;68A(2):365-375.

25. Chollet C, Lazare S, Guillemot F, Durrieu MC. Impact of RGD micro-patterns on cell adhesion. Colloid Surf B-Biointerfaces 2010;75(1):107-114.

26. Neff JA, Caldwell KD, Tresco PA. A novel method for surface modification to promote cell attachment to hydrophobic substrates. J Biomed Mater Res 1998;40(4):511-519.

27. Ho MH, Wang DM, Hsieh HJ, Liu HC, Hsien TY, Lai JY, Hou LT. Preparation and characterization of RGD-immobilized chitosan scaffolds. Biomaterials 2005;26(16):3197-3206.

28. Pieper JS, Hafmans T, Veerkamp JH, van Kuppevelt TH. Development of tailor-made collagen-glycosaminoglycan matrices: EDC/NHS crosslinking, and ultrastructural aspects. Biomaterials 2000;21(6):581-593.

29. Sharon JL, Puleo DA. Immobilization of glycoproteins, such as VEGF, on biodegradable substrates. Acta Biomaterialia 2008;4(4):1016-1023.

30. Li LH, Wu JD, Gao CY. Gradient immobilization of a cell adhesion RGD peptide on thermal responsive surface for regulating cell adhesion and detachment. Colloid Surf B-Biointerfaces 2011;85(1):12-18.

31. Bhattarai N, Gunn J, Zhang MQ. Chitosan-based hydrogels for controlled, localized drug delivery. Advanced Drug Delivery Reviews 2010;62(1):83-99.

32. Malafaya PB, Silva GA, Reis RL. Natural-origin polymers as carriers and scaffolds for biomolecules and cell delivery in tissue engineering applications. Advanced Drug Delivery Reviews 2007;59(4-5):207-233.

33. Khor E, Lim LY. Implantable applications of chitin and chitosan. Biomaterials 2003;24(13):2339-2349.

34. Silva SS, Luna SM, Gomes ME, Benesch J, Pashkuleva I, Mano JF, Reis RL. Plasma surface modification of chitosan membranes: Characterization and preliminary cell response studies. Macromol Biosci 2008;8(6):568-576.

35. Malafaya PB, Santos TC, van Griensven M, Reis RL. Morphology, mechanical characterization and in vivo neo-vascularization of chitosan particle aggregated scaffolds architectures. Biomaterials 2008;29(29):3914-3926.

36. Duarte ARC, Mano JF, Reis RL. Preparation of chitosan scaffolds loaded with dexamethasone for tissue engineering applications using supercritical fluid technology. European Polymer Journal 2009;45(1):141-148.

37. Baran ET, Mano JF, Reis RL. Starch-chitosan hydrogels prepared by reductive alkylation cross-linking. Journal of Materials Science-Materials in Medicine 2004;15(7):759-765.

38. Sorlier P, Denuziere A, Viton C, Domard A. Relation between the degree of acetylation and the electrostatic properties of chitin and chitosan. Biomacromolecules 2001;2(3):765-772.

39. Sjoback R, Nygren J, Kubista M. Absorption and fluorescence properties of fluorescein. Spectrochimica Acta Part a-Molecular and Biomolecular Spectroscopy 1995;51(6):L7-L21.

40. Martin M, Lindqvist L. The pH dependence of fluorescein fluorescence. Journal of Luminescence 1975;10(6):381-390.

41. de Campos AM, Diebold Y, Carvalho ELS, Sanchez A, Alonso MJ. Chitosan nanoparticles as new ocular drug delivery systems: in vitro stability, in vivo fate, and cellular toxicity. Pharmaceutical Research 2004;21(5):803-810.

42. Gupta M, Raghava S. Smart systems based on polysaccharides. In: Reis R, Neves N, Mano J, Gomes M, Marques A, HS A, editors. Natural-based polymers for biomedical aplications. Cambridge: Woodhead Publishing, 2008.

43. Lee CSD, Moyer HR, Gittens RAI, Williams JK, Boskey AL, Boyan BD, Schwartz Z. Regulating in vivo calcification of alginate microbeads. Biomaterials 2010;31(18):4926-4934.

44. Chou AI, Akintoye SO, Nicoll SB. Photo-crosslinked alginate hydrogels support enhanced matrix accumulation by nucleus pulposus cells in vivo. Osteoarthritis and Cartilage 2009;17(10):1377-1384.

45. Nichol JW, Khademhosseini A. Modular tissue engineering: engineering biological tissues from the bottom up. Soft Matter 2009;5(7):1312-1319.

46. Xia YN, Whitesides GM. Soft lithography. Annu Rev Mater Sci 1998;28:153-184.

47. Schulte VA, Diez M, Moller M, Lensen MC. Surface Topography Induces Fibroblast Adhesion on Intrinsically Nonadhesive Poly(ethylene glycol) Substrates. Biomacromolecules 2009;10(10):2795-2801.

48. Guvendiren M, Burdick JA. The control of stem cell morphology and differentiation by hydrogel surface wrinkles. Biomaterials 2010;31(25):6511-6518.

49. Kumar A, Whitesides GM. Features of gold having micrometer to centimeter dimensions can be formed through a combination of stamping with an elastomeric stap and an alkanethiol ink followed by chemical etching. Applied Physics Letters 1993;63(14):2002-2004.

50. Santo VE, Frias AM, Carida M, Cancedda R, Gomes ME, Mano JF, Reis RL. Carrageenan-Based Hydrogels for the Controlled Delivery of PDGF-BB in Bone Tissue Engineering Applications. Biomacromolecules 2009;10(6):1392-1401.

51. Luna SM, Gomes ME, Mano JF, Reis RL. Development of a Novel Cell Encapsulation System Based on Natural Origin Polymers for Tissue Engineering Applications. J Bioact Compat Polym 2010;25(4):341-359.

52. Oliveira JT, Martins L, Picciochi R, Malafaya IB, Sousa RA, Neves NM, Mano JF, et al. Gellan gum: A new biomaterial for cartilage tissue engineering applications. Journal of Biomedical Materials Research Part A 2010;93A(3):852-863.

53. Ifkovits JL, Burdick JA. Review: Photopolymerizable and degradable biomaterials for tissue engineering applications. Tissue Engineering 2007;13(10):2369-2385.

54. Burdick JA, Anseth KS. Photoencapsulation of osteoblasts in injectable RGD-modified PEG hydrogels for bone tissue engineering. Biomaterials 2002;23(22):4315-4323.

55. Burdick JA, Chung C, Jia XQ, Randolph MA, Langer R. Controlled degradation and mechanical behavior of photopolymerized hyaluronic acid networks. Biomacromolecules 2005;6(1):386-391.

56. Nuttelman CR, Benoit DSW, Tripodi MC, Anseth KS. The effect of ethylene glycol methacrylate phosphate in PEG hydrogels on mineralization and viability of encapsulated hMSCs. Biomaterials 2006;27(8):1377-1386.

57. Burdick JA, Peterson AJ, Anseth KS. Conversion and temperature profiles during the photoinitiated polymerization of thick orthopaedic biomaterials. Biomaterials 2001;22(13):1779-1786.

58. White JR, Thomas EL. Advances in SEM of Polymers. Rubber Chemistry and Technology 1984;57(3):457-506.

59. Hwang CM, Sant S, Masaeli M, Kachouie NN, Zamanian B, Lee SH, Khademhosseini A. Fabrication of three-dimensional porous cell-laden hydrogel for tissue engineering. Biofabrication 2010;2(3).

60. McArthur SL. Applications of XPS in bioengineering. Surface and Interface Analysis 2006;38(11):1380-1385.

61. Delamar M. Recent aspects of chemical-analysis by photoelectron-spectroscopy (XPS, ESCA). Analusis 1988;16(8):419-427.

62. Ishihara H, Asano T, Tsukuda K, Katagiri H, Inukai K, Anai M, Kikuchi M, et al. Pancreatic beta-cell MIN6 exhibits characteristics of glucose-metabolism and glucose-stimulated insuline-secretion similar to those of normal islets. Diabetologia 1993;36(11):1139-1145.

63. N.C. Rivron, J. Liu, J. Rouwkema, J. de Boer, Blitterswijk CAv. Engineering Vascularised Tissues in vitro. European Cells and Materials 2008;15:27-40.

64. Ishimura D, Yamamoto N, Tajima K, Ohno A, Yamamoto Y, Washimi O, Yamada H. Differentiation of Adipose-derived Stromal Vascular Fraction Culture Cells into Chondrocytes Using the Method of Cell Sorting with a Mesenchymal Stem Cell Marker. Tohoku J Exp Med 2008;216(2):149-156.

65. Kim SK, Lee KC, Lee JH, Kwon YS. In Vivo Chondrogenesis of Adipose Tissue-Derived Stem Cells in Alginate Gel. Tissue Eng Regen Med 2009;6(1-3):155-164.

66. Kashani IR, Zaminy A, Barbarestani M, Hedayatpour A, Mahmoudi R, Vardasbi S, Nejad AF, et al. In vitro osteogenesis of rat adipose-derived stem cells: comparison with bone marrow stem cells. Arch Med Sci 2009;5(2):149-155.

67. Cho HH, Shin KK, Kim YJ, Song JS, Kim JM, Bae YC, Kim CD, et al. NF-kappa B Activation Stimulates Osteogenic Differentiation of Mesenchymal Stem Cells Derived from Human Adipose Tissue by Increasing TAZ Expression. J Cell Physiol;223(1):168-177.

68. Kokai LE, Rubin JP, Marra KG. The potential of adipose-derived adult stem cells as a source of neuronal progenitor cells. Plast Reconstr Surg 2005;116(5):1453-1460.

69. Huang TT, He DS, Kleiner G, Kuluz J. Neuron-like differentiation of adipose-derived stem cells from infant piglets in vitro. J Spinal Cord Med 2007;30:S35-S40.

70. Rada T, Reis RL, Gomes ME. Novel method for the isolation of adipose stem cells (ASCs). Journal of Tissue Engineering and Regenerative Medicine 2009;3:158–159.

71.   Khademhosseini A, Eng G, Yeh J, Kucharczyk PA, Langer R, Vunjak-Novakovic G, Radisic M. Microfluidic patterning for fabrication of contractile cardiac organoids. Biomedical Microdevices 2007;9(2):149-157.

Section 3

DEVELOPING IMPROVED SUBSTRATES WITH STRUCTURAL CUES

Chapter III

DEVELOPMENT OF MICRO-PATTERNED SURFACES OF POLY(BUTYLENE SUCCINATE) BY MICROMOLDING FOR GUIDED TISSUE ENGINEERING

DEVELOPMENT OF MICRO-PATTERNED SURFACES OF POLY(BUTYLENE SUCCINATE) BY MICROMOLDING FOR GUIDED TISSUE ENGINEERING

ABSTRACT

Native tissues present complex architectures at a micro and nano-scale that dictate their biological function. Several micro-fabrication techniques have been employed for engineering polymeric surfaces that could replicate *in vitro* those micro and nano-features. In this study, biomimetic surfaces of poly(butylene succinate) (PBS) were engineered by micromolding technique. After the optimization of the system parameters, twenty surfaces with different combinations of groove and ridge sizes were developed and characterized by scanning electron microscopy (SEM). The influence of the engineered micro-features over the viability and attachment of human Adipose derived adult stem cells (hASC) was evaluated. hASC cultured onto the engineered surfaces demonstrated to remain viable in all tested patterns. SEM and immunostaining showed adequate attachment and spreading of the stem cells for all the patterned groove/ridge combinations. This study indicated that it is possible to engineer micro-patterned surfaces of PBS and that the developed structures could have great potential for tissue engineering where cell alignment is an essential requisite.

KEYWORDS: poly(butylene succinate); micromolding; micro-features; human adipose stem cells.

1. INTRODUCTION

One of the major motivations for the increasing effort spent on designing and developing micro and nano-structured surfaces and materials for tissue engineering strategies is that natural tissues and the associated extracellular matrices (ECM) are composed of micro and nano-scaled elements [1, 2]. In fact, when an implant first contacts the host environment, a layer of proteins immediately covers the surface of the implant [3]. The adsorptive behavior of these proteins is highly dependent on the surface properties including its micro and nano-structure [4, 5] or the material chemistry [6, 7]. This surface-specific adjustment can result in the presentation of different regions of the proteins to cells, ultimately dictating the implant success.

The micro and nano-scale biological elements present in the ECM arrange themselves in specific architectures, essential for the normal tissue function. An outstanding example is the organization of fibroblasts and cardiomyocytes in the native myocardial tissue. These cells align themselves and assemble in parallel arrays in a way that is critical to obtain the electrical and mechanical properties of the heart [8]. Similarly, collagen fibers in the bone are aligned structures that provide bone with the tensile strength necessary to ensure the functionality of the tissue [9]. Thus, while developing engineered tissues it is of major importance to recapitulate the native micro-architecture, namely the controlled cellular alignment, and therefore to modulate *in vitro* the tissue function.

Several micro-fabrication techniques allow recapitulating the microarchitecture of tissues, modulating *in vitro* the cell shape, function or its differentiation. Specifically, several different methods have been reported for cellular alignment, namely micropatterning of molecules [10], fabricating fibrous scaffolds by electrospinning [11-13] or engineering microchannels using soft-lithography methodologies [14, 15]. Substrates with micropatterned adhesive proteins provide a tight control over the cell attachment process. However, these patterned surfaces consist of a two-dimensional (2D) substrate to culture cells. Three-dimensional (3D) structures with multiple opportunities for cell attachment have been developed using different technologies including electrospinning [11-13]. It has been reported that cells are able to align along the fibers within the 3D network [12]. In order to more precisely control the overall orientation of cells, microchannels have been fabricated using micromolding or photolithography methods. Cardiac organoids have been formed within micro-engineered channels as a result of the alignment of cardiomyocytes [14].

In this work we report a simple method to control the alignment of human adipose stem cells (hASC) by microengineering the surface of a poly(butylene succinate) (PBS) polymeric surface. PBS is an aliphatic polyester that has shown to be biodegradable [16, 17]. It has been processed by our group into discs [18] and fibers [19], showing promising results for

bone [20] and cartilage [21] tissue engineering, both *in vitro* [19, 21] and *in vivo* [20]. Herein, a micromolding technique was employed to fabricate micro-features with different groove/ridge sizes onto the polyester PBS surface. This system can be used as an *in vitro* model for the study of the biological performance of cells in different patterned surfaces. The described system is applicable to a variety of cell types and the lessons learnt from this system might be incorporated into device design of engineered tissues with specific cell shape and elongation *in vitro*, as observed in collagen fibers in bone.

2. MATERIALS & METHODS

2.1. Materials and solutions

The polymeric material used for the preparation of the substrates in this study was a commercially available poly(butylene succinate) (PBS, Bionolle 1050, Showa High Polymer Co. Ltd., Tokyo, Japan). Substrates for the micro-patterns of PBS were processed into circular discs (ø=10 mm, height=1.5mm) by conventional injection molding technology using optimized processing conditions, as described elsewhere [18]. For the development of the patterns, PBS pellets were dissolved at 0.5 and 2% (w/v), either in dichloromethane (DIM, Sigma) or trichloromethane (TIM, VWR). A polydimethylsiloxane (PDMS) mold was gently provided by Professor Hong Hong Lee (School of Chemical Engineering, Seoul National University). The PDMS mold was fabricated with 20 patterns with different combinations of groove and ridge sizes, enabling to characterize a range of scales of the patterns over the biological activity of cells on those substrates.

2.2. Preparation of micropatterned PBS surfaces

The PDMS mold and the PBS polymeric solution were heated to the same temperature. 20 µL of PBS solution were pipetted on top of the pattern present on the PDMS mold. An injection molded disc of PBS was placed over the PBS solution as a substrate for the PBS pattern. A weight was used to facilitate the migration of the PBS solution by capillarity through the PDMS micro-patterns. As the solvent evaporates (~2 min), the micro-patterns of the PDMS are transferred to the PBS injection molded discs (substrate) and the PBS disc gently removed from the surface of the PDMS mold (Figure 1). Three parameters of the system were varied in order to evaluate their influence over the fabricated micro-features: (1) the temperature of both the PDMS mold and the PBS solution (~20 ºC and ~100 ºC); (2) concentration of the PBS solution (0.5 and 2 %, w/v); and (3) solvent used to dissolve PBS pellets (DIM or TIM). Twenty patterns with different groove/ridge size combinations were fabricated. Micro-patterned PBS surfaces were analyzed using a Leica Cambridge S-360

scanning electron microscope (SEM, Leica Cambridge, UK). All specimens were pre-coated with a conductive layer of sputtered gold. SEM micrographs were taken at an accelerating voltage of 15 kV at different magnifications. The size of the grooves and ridges of the patterns were calculated using an image analysis software (NIH Image J, n=4). Six PBS micro-patterns from the twenty developed were selected for further biological studies (#3, #4, #6, #8, #15, #20) to obtain a good coverage of the range of dimensions that may have a stronger effect over the cells.

2.3. Attachment and proliferation of human adipose stem cells

2.3.1. Cell culture

In order to observe the cell response on the micro-patterned PBS surfaces, primary human adipose stem cells (hASC) were seeded on the engineered surfaces. hASC were isolated as described elsewhere [22]. Briefly, stem cells were isolated from human adipose tissue samples by the enzymatic digestion of the tissue with 0.2 % collagenase type I A in phosphate buffer saline (PBS, Sigma) for 60 min at 37 °C under gentle stirring. Digested tissue was filtered and adherent cells selected after centrifugation steps. Cells were expanded in Dulbecco's Modified Eagle Medium (DMEM, Sigma) supplemented with 10% heat-inactivated fetal bovine serum (FBS, Biochrom AG) and 1% of antibiotic (Gibco) at 37 °C in a humidified atmosphere with 5% CO_2 until reaching enough number for the study. Three samples per pattern were placed in 24-well plates and 1.5 mL of the cell suspension was seeded onto the PBS micro-patterned surfaces using a density of $3.3x10^4$ cells/mL. Seeded cells were incubated in a humidified atmosphere at 37 °C and 5% of CO_2 for 1 and 3 days in order to evaluate cell morphology upon spreading. TCPS was used as a control surface.

2.3.2. Cell viability assay

Cell viability was evaluated during culture time (1 and 3 days) by quantifying the metabolic activity of hASC, using Alamar Blue® (Invitrogen). Alamar blue can be reduced in active cell mitochondria, changing the solution color from blue to a bright red color. Alamar blue stock solution was diluted with culture medium without phenol red. Analysis was performed according to the manufacturer's instructions. The plates were exposed to an excitation wavelength of 540-570 nm and the emission at 580-610 nm recorded in a microplate ELISA reader (BioTek, USA). The percentage viability was expressed as the fluorescence measured in patterned surfaces in comparison to the non-patterned PBS surface.

2.3.3. DNA quantification

After each time-point, cells were lysed by osmotic and thermal shock and the supernatant used for DNA analysis. Cell proliferation was evaluated by quantifying the DNA content on the samples using the PicoGreen dsDNA kit (Molecular Probes). Analysis was performed according to the manufacturer's instructions. Fluorescence was read (485nm/528nm of excitation/emission) in a microplate ELISA reader (BioTek, USA). The DNA amount was calculated from a standard curve.

2.3.4. Cell morphology analysis

After each incubation period, samples were washed with phosphate buffer saline solution, fixed with 4% formaldehyde (Merck) and kept at 4 ºC in phosphate buffer saline solution until being prepared for SEM or immunostaining. For SEM analysis samples were dehydrated using graded ethanol solutions (50%, 70%, 90% and 100%, v/v). Immunostaining was performed to obtain further details about the cell morphology using an Axioplan 2 microscope (Zeiss, Germany). Cytoskeleton of cells was stained with phalloidin and their nuclei counterstained with DAPI.

2.4. Statistical analysis

All data were subjected to statistical analysis and were reported as mean ± standard deviation. Statistical significance in biological studies was determined by analysis of variance (two-way ANOVA) followed by Bonferroni's post-hoc test for multiple comparisons using GraphPad Prism 5 Software. The differences were considered statistically significant if $(*,\#)p<0.05$, $(**,\#\#)p<0.01$ or $(***,\#\#\#)p<0.001$.

3. RESULTS AND DISCUSSION

3.1. Fabrication of micropatterned poly(butylene-succinate) surfaces

In this study, micromolding was used to develop micro-patterned surfaces in a biodegradable polyester. Poly(butylene succinate) (PBS) pellets were dissolved in an organic solvent (DIM or TIM) and 20 µL of the solution was placed over the PDMS mold. Injection molded discs of PBS, previously fabricated as described elsewhere [18], were used as substrates for the micro-patterned PBS surfaces (Figure III.1).
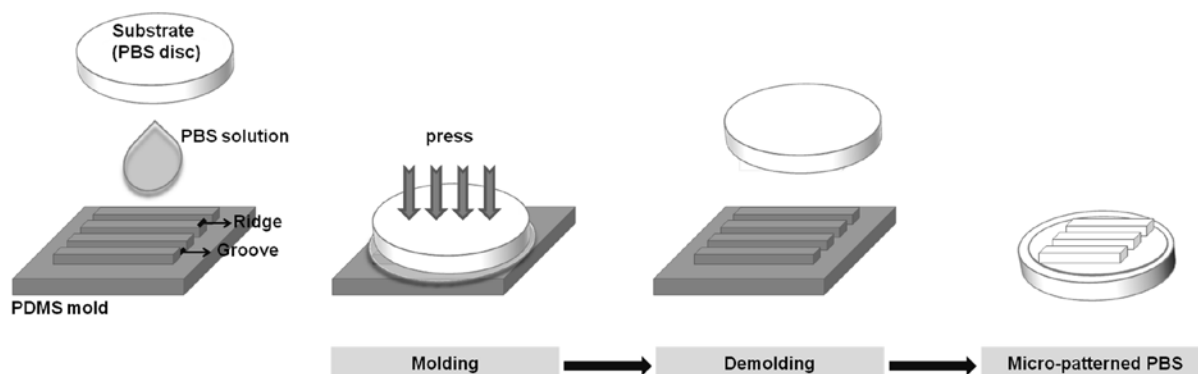
Figure III.1. Schematic representation of the preparation of micro-patterned PBS surface.

The most relevant parameters of the process of micromolding PBS surfaces were varied, while keeping the others constant: (1) temperature of the mold and of the solution (using DIM as solvent and 1% w/v of polymer solution), (2) concentration of the polymeric solution (using DIM as solvent and 100 ºC), and (3) solvent used to dissolve the PBS pellets (using a 1% w/v polymer solution at 100 ºC). SEM micrographs depicted in Figure III.2.A show that higher temperatures (~100 ºC) allow the polymeric solution to flow and fill easier by capillarity through the micro-patterns of the mold. The optimization shows that more defined patterns where obtained when the PDMS mold and the PBS solution were at the temperature of 100 ºC when compared to 20 ºC. Suh *et al* first described a variation of the micromolding methodology that is based on the flow of the polymeric solution by capillarity of the heated polymer, named capillary force lithography [23-25], supporting our results. The effect of polymer concentration over the definition of the PBS micro-patterns was also evaluated (Figure III.2.B). PBS pellets were dissolved at 0.5 and 2% (w/v) in DIM. Interestingly, sharp contours could be observed for both concentrations. It would be expected that the less concentrated solution would flow more easily through the micro-patterns of the mold as a result of its lower viscosity. However, no significant difference was observed at the studied length scale (µm). Thus the highest concentration (2%, w/v) was selected for the following studies. The third parameter analyzed was the solvent used for dissolving the PBS pellets (Figure III.2.C). Both DIM and TIM can dissolve the studied biodegradable polyester, being the former the less hazardous. Thus, micro-patterns were fabricated with solutions of PBS pellets dissolved in both solvents. Sharper edges were observed for the micro-patterns fabricated with DIM. Thus, DIM was the selected solvent for the subsequent studies. The evaluated system parameters presented a similar behavior when analyzed with other patterns (data not shown).
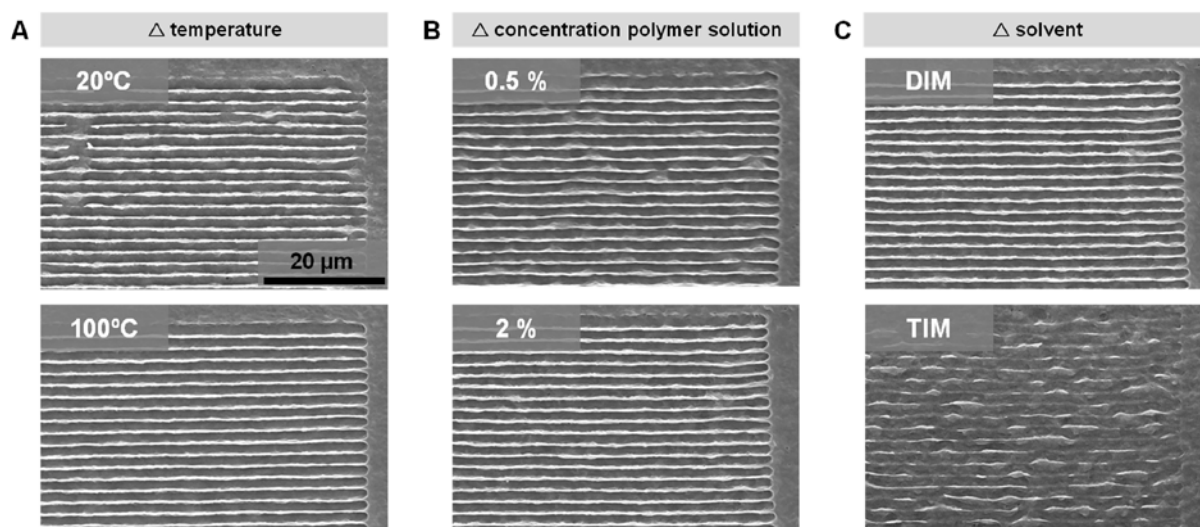
Figure III.2. Influence of the different parameters of the process on the fabrication of PBS micro-features. SEM of PBS micro-features using (A) two different temperatures, (B) two different polymer concentrations and (C) two different solvents.

Using the optimized parameters of 2% (w/v) solution of PBS pellets dissolved in DIM at 100 ºC, it was possible to engineer 20 different micro-patterns of PBS with a variety of groove and ridge sizes and groove/ridge ratios. Figure 3A shows the top-view of the PBS micro-patterns analyzed by scanning electron microscopy. The majority of the micro-patterns show quite defined surface features. However, some of them show the presence of a rough surface both on the grooves and in the ridges of the patterns. The volume of the solution used is small and the percentage of polymer within the total volume corresponds to a small fraction (2%, w/v), being 98% of the volume constituted by the solvent. Given that the solvent quickly evaporates at 100 ºC, it was expected the creation of a slight rough structure as observed in Figure III.3.A.

The dimensions of the patterns were measured from the SEM micrographs using image analysis software (NIH ImageJ). The groove and ridge sizes of each micro-patterned PBS surface are summarized in Figure III.3.B. Groove size ranged between 1.0 and 3.5 µm and ridge size varied from 0.4 to 4.2 µm. Patterns #19 and #20 present the highest groove size and pattern #6 the highest ridge size. Patterns #19 and #20 presented the highest values of both groove and ridge and #1 the smallest. The ratio between the groove and ridge sizes was calculated and it is shown in Figure III.3.C, showing that 10 patterns had a groove size larger than the ridge size. Roughly, the different patterns could be organized in 3 groups: (1) groove size bigger than ridge size (G>R, patterns #1, #2, #4, #7, #10, #13, #16, #18, #19, #20), (2) groove size smaller than ridge size (G<R, patterns #5, #6, #9, #11, #15, #17), and (3) similar groove and ridge sizes (G≈R, patterns #3, #8, #12, #14). Given these categories, six different patterns were selected for the biological studies. Patterns #3 and #4 were

selected since they presented the groove size bigger than the ridge size, being the difference higher for #4. Patterns #6 and #15 were selected because they presented a groove size smaller than the ridge size, being this difference more pronounced for pattern #6. Pattern #8 was selected as the pattern with the groove/ridge ratio closer to 1. Finally, pattern #20 was also selected since both features were larger than 2 μm, which is more within the range of the size that the cells under study sense with their filopodia [26].
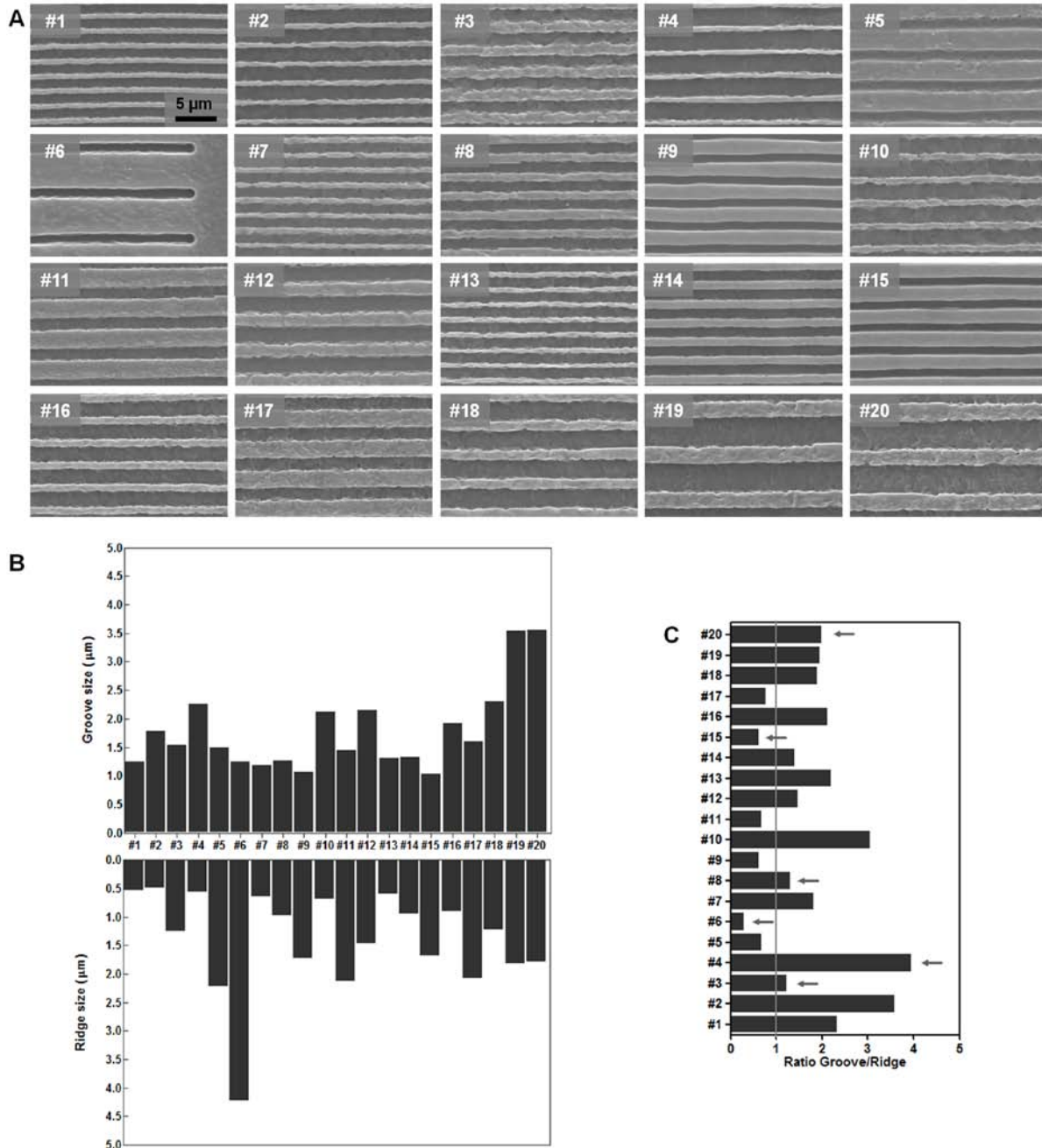
Figure III.3. (A) SEM of PBS micro-features using 20 different PDMS molds. (B) Dimensions in μm of the groove and ridge of the engineered micro-patterns of PBS (n=4) and (C) calculated ratio between the groove and ridge size of the micro-patterned PBS surfaces (arrows depict the selected patterns for the biological studies).

3.2. Cell behavior analysis

The *in vitro* biological performance of the engineered PBS micro-patterned surfaces was assessed after cell culture with hASC. Figure III.4 shows the viability of cultured hASC, compared to non-patterned PBS surfaces (control, 100%). Of significance is that the viability of hASC was similar for all patterned and non-patterned surfaces for both time-points. The exception was the pattern #3, which presented a significantly higher viability on day 3 (*$p<0.05$). The results showed that hASC are equally metabolically active in all the engineered and non-engineered surfaces, indicating that the engineered micro-surfaces do not influence negatively the mitochondrial metabolic activity of the studied cells.
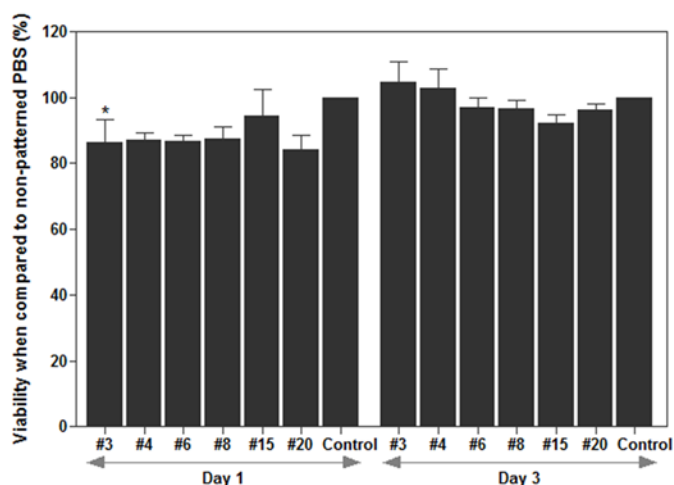
Figure III.4. Viability of hASC cultured onto micro-patterned PBS surfaces after 1 and 3 days of culture (*$p<0.05$ when compared to day 3).

Quantification of the amount of double stranded DNA (dsDNA) for the different time periods (Figure III.5) suggested that cultured hASC proliferated from day 1 to day 3 of culture, being this increase in DNA content statistically significant for patterns #15 (##$p<0.01$) and #20 (#$p<0.05$) and for the non-patterned PBS surface (control, ###$p<0.001$). Although at day 1 no statistically significant difference on the DNA content was observed among the patterns, at day 3 all the patterns, with exception of pattern #8, presented a significantly lower DNA content (*$p<0.05$, **$p<0.01$, ***$p<0.001$) than the non-patterned surfaces, suggesting that hASC would proliferate better on non-patterned surfaces. It has been reported that the average doubling time for hASC populations is 60 hours [27]. In this study we have analyzed the dsDNA content after 72 hours in culture. Thus, although the DNA content is lower in PBS micro-patterned surfaces, cells might still undergo cell division. These results suggest that hASC increase their dsDNA content faster on the non-patterned surfaces. However, on the micro-patterned surfaces cells undergo cytoskeleton rearrangement in response of the

micro-patterned substrate, which might be responsible for delaying the cell division mechanism.
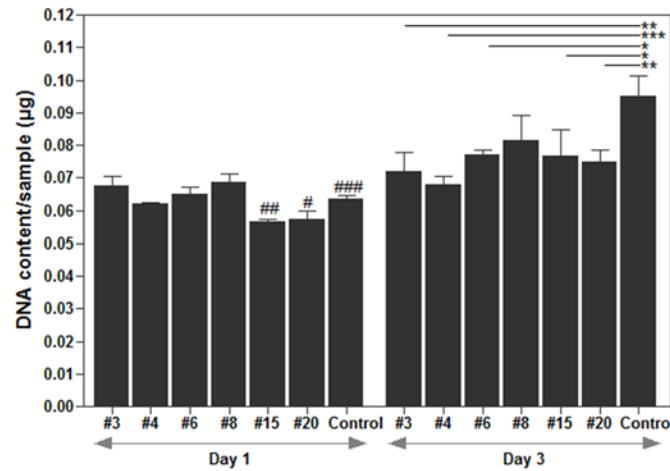
Figure III.5. DNA content of hASC cultured onto micro-patterned PBS surfaces after 1 and 3 days of culture (control corresponds to the non-patterned PBS surface, significantly different samples: #$p<0.05$, ##$p<0.01$, ###$p<0.001$ when compared to the respective surface at day 3; *$p<0.05$, **$p<0.01$, ***$p<0.001$ when compared to the control of day 3).

The SEM analysis of the adhered cells after 1 day of culture onto the different micro-patterned surfaces provided further information regarding the influence of the micro-patterns over the cell morphology (Figure III.6). After 1 day of culture the majority of cells were attached but not spread on the micro-patterned and non-patterned PBS surfaces. Cytoskeleton staining of cultured hASC further confirmed the SEM micrographs (Figure III.6.A.ii). For most of the micro-patterned surfaces the red staining of phalloidin overlapped the nucleus staining with DAPI, indicating that cells were attached but not spread, as the cytoskeleton was not stretched. However, cells appear to spread faster in patterns #15 and #20, given that after 1 day in culture the hASC seem more widen than on the other patterns. After 1 day culture, hASC seem to orient on the micro-patterned PBS surfaces along the direction of the patterns. On the other hand, on the non-patterned PBS surfaces, hASC were detected to form a uniform layer. This effect is more notorious after 3 days of culture (Figure III.6.B). Cells seem to elongate more along the micro-patterns on the PBS surfaces, being this behavior more obvious on patterns #3, #6, #8 and #20. Similarly to day 1 of culture, hASC appeared to be randomly oriented on the non-patterned PBS surfaces. Phalloidin staining of cell cytoskeleton and counterstaining of the nucleus with DAPI further confirms the SEM results. The cytoskeleton of hASC appears to be specially elongated on patterns #3 and #20.

Our results suggest that hASC can recognize the size of the patterns engineered on the PBS surfaces and align along their direction. Cells form cytoplasm extensions and cellular associations over different ridges instead of populating the groove of the patterns. This results from the fact that the size of hASC is within the range of 20-50 µm, while the size of the micro-patterns is under 5 µm width.
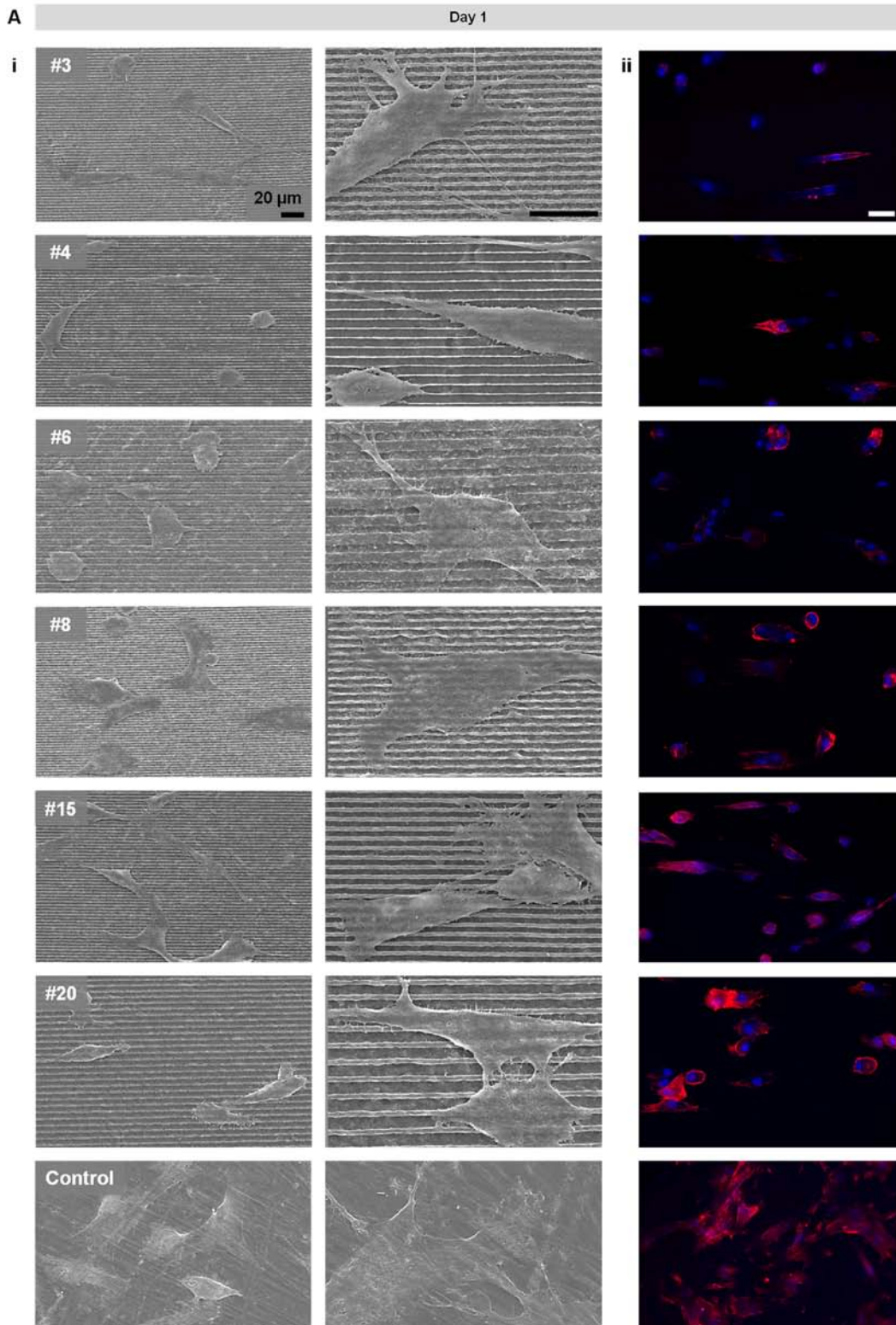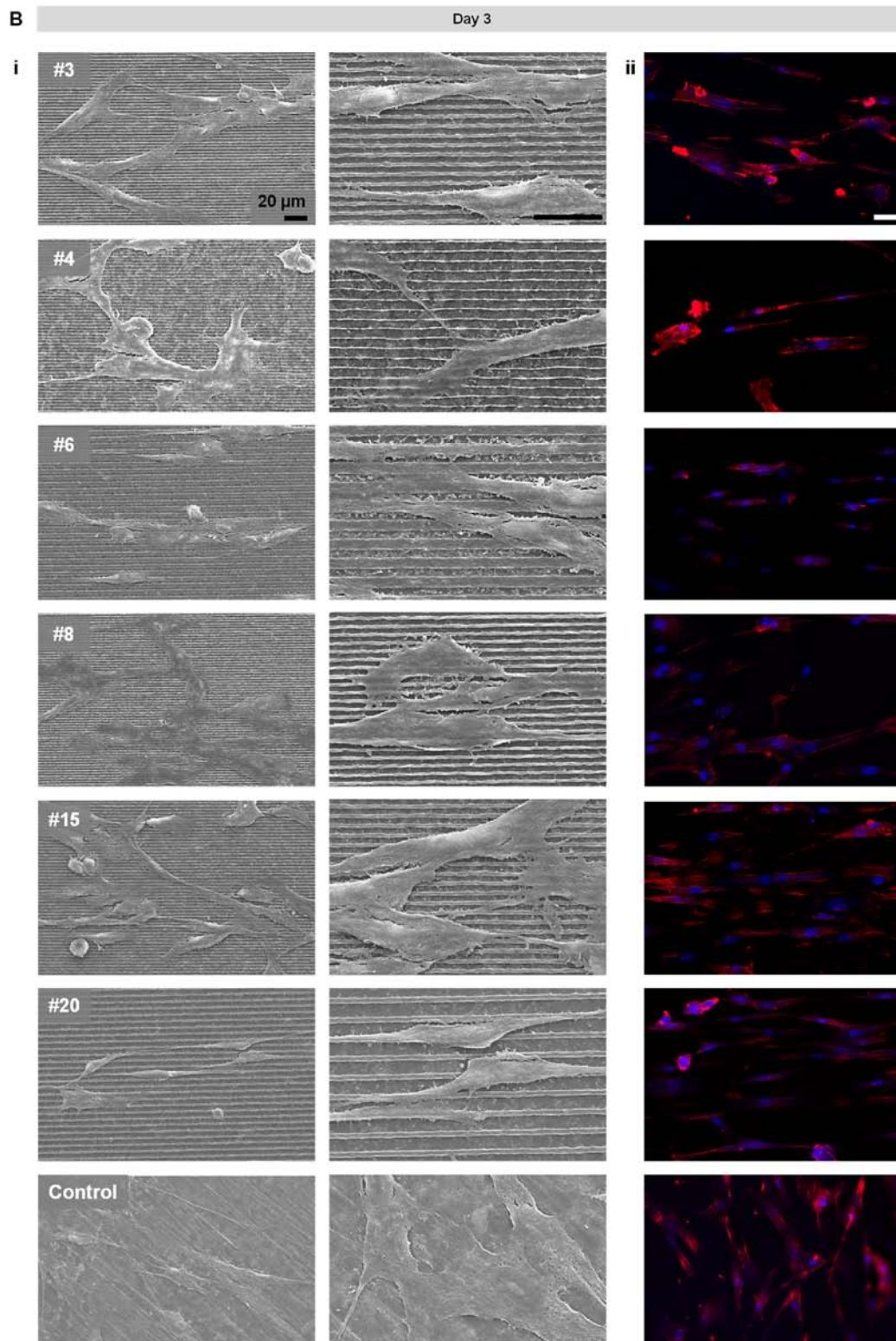
Figure III.6. Morphology of seeded hASC. (i) SEM with two magnifications and (ii) immunostaining of hASC cultured onto micro-patterned PBS surfaces after (A) 1 day and (B) 3 days of culture: cell cytoskeleton stained red with phalloidin and cell nucleus counterstained blue with DAPI.

4. CONCLUSIONS

Micro-patterned surfaces of the biodegradable polyester PBS were successfully micro-engineered by micromolding. The system parameters, namely the temperature of the mold and solution, the concentration of the polymer and the solvent used to dissolve the PBS pellets were optimized, allowing for the development of a variety of micro-patterns with different feature-sizes. The combination of different groove and ridge sizes resulted in the micro-fabrication of 10 patterns with groove size higher than the ridge, 6 patterns with groove size smaller than the ridge size and 4 patterns with similar groove and ridge sizes. The *in vitro* biological behavior of selected biomimetic micro-patterned surfaces revealed that the engineered surfaces were able to maintain a high viability of hASC. The engineered surfaces appear to direct the orientation of seeded hASC along the micro-patterned features of PBS. In contrast, cells appear to be randomly oriented on the non-patterned surfaces. This study combines micro-technologies and biomaterials to engineer a biomimetic surface at the micro-level using a polyester widely studied in our group. The importance of PBS micro-structure over the attachment and morphology of hACS, a stem cell source with a high degree of pluripotency, was demonstrated, indicating the potential of these surfaces as substrates for guided tissue engineering approaches.

REFERENCES

1.   Aloy P, Russell RB. Structure-based systems biology: a zoom lens for the cell. Febs Letters 2005;579(8):1854-1858.
2.   LeDuc PR, Bellin RM. Nanoscale intracellular organization and functional architecture mediating cellular behavior. Annals of Biomedical Engineering 2006;34(1):102-113.
3.   Malmsten M. Formation of adsorbed protein layers. Journal of Colloid and Interface Science 1998;207(2):186-199.
4.   Huang Y, Lu XY, Qian WP, Tang ZM, Zhong YP. Competitive protein adsorption on biomaterial surface studied with reflectometric interference spectroscopy. Acta Biomaterialia 2010;6(6):2083-2090.
5.   Kawamoto N, Mori H, Terano M, Yui N. Blood compatibility of polypropylene surfaces in relation to the crystalline-amorphous microstructure. Journal of Biomaterials Science-Polymer Edition 1997;8(11):859-877.
6.   Weber N, Bolikal D, Bourke SL, Kohn J. Small changes in the polymer structure influence the adsorption behavior of fibrinogen on polymer surfaces: Validation of a new rapid screening technique. Journal of Biomedical Materials Research Part A 2004;68A(3):496-503.
7.   Roach P, Farrar D, Perry CC. Surface tailoring for controlled protein adsorption: Effect of topography at the nanometer scale and chemistry. Journal of the American Chemical Society 2006;128(12):3939-3945.
8.   Papadaki M, Bursac N, Langer R, Merok J, Vunjak-Novakovic G, Freed LE. Tissue engineering of functional cardiac muscle: molecular, structural, and electrophysiological studies. American Journal of Physiology-Heart and Circulatory Physiology 2001;280(1):168-178.
9.   Skedros JG, Dayton MR, Sybrowsky CL, Bloebaum RD, Bachus KN. The influence of collagen fiber orientation and other histocompositional characteristics on the mechanical properties of equine cortical bone. Journal of Experimental Biology 2006;209(15):3025-3042.
10.   Fukuda J, Khademhosseini A, Yeh J, Eng G, Cheng JJ, Farokhzad OC, Langer R. Micropatterned cell co-cultures using layer-by-layer deposition of extracellular matrix components. Biomaterials 2006;27(8):1479-1486.
11.   da Silva M, Martins A, Costa-Pinto A, Costa P, Faria S, Gomes M, Reis RL, et al. Cartilage Tissue Engineering Using Electrospun PCL Nanofiber Meshes and MSCs. Biomacromolecules 2010;11(12):3228-3236.
12.   Santos MI, Tuzlakoglu K, Fuchs S, Gomes ME, Peters K, Unger RE, Piskin E, et al. Endothelial cell colonization and angiogenic potential of combined nano- and micro-fibrous scaffolds for bone tissue engineering. Biomaterials 2008;29(32):4306-4313.
13.   Martins A, Pinho ED, Faria S, Pashkuleva I, Marques AP, Reis RL, Neves NM. Surface Modification of Electrospun Polycaprolactone Nanofiber Meshes by Plasma Treatment to Enhance Biological Performance. Small 2009;5(10):1195-1206.
14.   Khademhosseini A, Eng G, Yeh J, Kucharczyk PA, Langer R, Vunjak-Novakovic G, Radisic M. Microfluidic patterning for fabrication of contractile cardiac organoids. Biomedical Microdevices 2007;9(2):149-157.
15.   Baran ET, Tuzlakoglu K, Salgado A, Reis RL. Microchannel-patterned and heparin micro-contact-printed biodegradable composite membranes for tissue-engineering applications. Journal of Tissue Engineering and Regenerative Medicine 2011;5(6):E108-E114.
16.   Tserki V, Matzinos P, Pavlidou E, Vachliotis D, Panayiotou C. Biodegradable aliphatic polyesters. Part I. Properties and biodegradation of poly(butylene succinate-co-butylene adipate). Polymer Degradation and Stability 2006;91(2):367-376.
17.   Tserki V, Matzinos P, Pavlidou E, Panayiotou C. Biodegradable aliphatic polyesters. Part II. Synthesis and characterization of chain extended poly(butylene succinate-co-butylene adipate). Polymer Degradation and Stability 2006;91(2):377-384.
18.   Correlo VM, Boesel LF, Bhattacharya M, Mano JF, Neves NM, Reis RL. Properties of melt processed chitosan and aliphatic polyester blends. Materials Science and Engineering a-Structural Materials Properties Microstructure and Processing 2005;403(1-2):57-68.
19.   Pinto AR, Correlo VM, Bhattacharya M, Charbord P, Reis RL, Neves NM. Behaviour of human bone marrow mesenchymal stem cells seeded on fiber bonding chitosan polyester based for bone tissue engineering scaffolds. Tissue Engineering 2006;12(4):1019-1019.
20.   Costa-Pinto A, Correlo V, Sol P, Bhattacharya M, Srouji S, Livne E, Reis R, et al. Chitosan–poly(butylene succinate) scaffolds and human bone marrow stromal cells induce bone repair in a mouse calvaria model. Journal of Tissue Engineering and Regenerative Medicine 2011.

21. da Silva MLA, Crawford A, Mundy JM, Correlo VM, Sol P, Bhattacharya M, Hatton PV, et al. Chitosan/polyester-based scaffolds for cartilage tissue engineering: Assessment of extracellular matrix formation. Acta Biomaterialia 2010;6(3):1149-1157.
22. Rada T, Reis RL, Gomes AE. Novel method for the isolation of adipose stem cells (ASCs). Journal of Tissue Engineering and Regenerative Medicine 2009;3(2):158-159.
23. Suh KY, Lee HH. Capillary force lithography: Large-area patterning, self-organization, and anisotropic dewetting. Advanced Functional Materials 2002;12(6-7):405-413.
24. Suh KY, Kim YS, Lee HH. Capillary force lithography. Advanced Materials 2001;13(18):1386-1389.
25. Khang DY, Lee HH. Pressure-assisted capillary force lithography. Advanced Materials 2004;16(2):176-179.
26. Rada T, Reis RL, Gomes ME. Adipose Tissue-Derived Stem Cells and Their Application in Bone and Cartilage Tissue Engineering. Tissue Engineering Part B-Reviews 2009;15(2):113-125.
27. Zuk PA, Zhu M, Mizuno H, Huang J, Futrell JW, Katz AJ, Benhaim P, et al. Multilineage cells from human adipose tissue: Implications for cell-based therapies. Tissue Engineering 2001;7(2):211-228.

Chapter IV

An automated two-phase system for biodegradable microcapsule production

CHAPTER IV *

AN AUTOMATED TWO-PHASE SYSTEM FOR BIODEGRADABLE MICROCAPSULE PRODUCTION

ABSTRACT

Polymeric capsules have been used for protection and delivery of bioactive materials such as drugs, enzymes, and cells for biomedical applications. A semi-permeable polymeric membrane can engulf a bioactive material, hampering the response from the immune system when implanted. Various methods have been proposed for the development of polymeric capsules including layer-by-layer, self-assembly and phase separation. The proposed approach in this paper is a generic two-phase system for polymeric microcapsule production. In the proposed system, gravity and mechanical forces along with hydrophilic-hydrophobic repulsion enforce the capsule formation and stabilization. Polymer droplets separate from the needle by surface tension and gravity, and form microcapsules passing through the hydrophobic material. Microcapsules cross through hydrophobic-hydrophilic interface, crosslinking and stabilizing in the hydrophilic material. This system was tested using gellan gum (GG) and alginate (ALG) for the production of the microcapsules. The proposed system can be adapted to other applications with different materials by replacing the bioactive material, the hydrophobic and/or the hydrophilic phases. The size of the microcapsules was dependent on the needle size and on the solution flow rate. The size and morphology of the microcapsules produced by the proposed system were uniform, when parameters were kept constant. This system was successfully used for generating polymeric microcapsules with encapsulated beads, cell suspensions and cell aggregates proving its capability for generating bioactive carriers that can potentially be used for drug delivery and stem cell therapy.

KEYWORDS: Capsule Formation; Encapsulation; Automated System; Ionic Polymers; Gellan Gum.

1. INTRODUCTION

Current therapeutic products often rely on the systemic injection of high doses of bioactive materials that may trigger an autoimmune response or cause other adverse effects in the human body. Hence, encapsulation of bioactive entities within immune-protective systems is an effective way to overcome these challenges. Microencapsulation of bioactive agents such as drugs [1], enzymes [2, 3], cell suspensions, [4] and cell aggregates [5, 6] has provided promising therapeutics for different diseases such as diabetes [7], hemophilia [8], and cancer [9, 10] and holds the potential to significantly improve the efficacy in the treatment of a variety of other diseases.

The proposed microcapsule production system provides a protective biocompatible polymeric layer by encapsulating the bioactive agent inside a permeable polymeric involucrum. The protective biocompatible polymeric layer is the primary surface to interact with the host immune system, significantly decreasing the risk of immune-rejection and maximizing the bioavailability at the target tissue. Alginate [11, 12], poly(lactic-co-glycolic) acid [13, 14], chitosan [15], carrageenan [16], and gellan gum [17, 18] are the most common polymers that have been proposed for the fabrication of micro and nanocapsules. The polymeric material should ensure the delivery of the bioentity to the host environment at the desired rate and during the intended duration of the treatment. Therefore, the selection of the appropriate polymeric layer for a specific therapy is of key importance and depends on different factors, namely the encapsulated bioactive material and the therapeutic target. Several clinical trials have demonstrated the viability and functionality of encapsulated cells [19, 20], motivating researchers to develop novel microencapsulation techniques with improved performance.

Several methods have been proposed to tailor the capsule size, morphology, and encapsulation efficiency for different applications [21-24]. The major challenges that must be addressed by new microcapsule production systems are uniform capsule fabrication along with maintaining the bioactivity of the encapsulated material throughout the process. Many different polymeric encapsulation techniques have been reported, such as electrostatic polymer interactions [11], phase separation [25] and *in situ* polymerization [26]. Polymerizing alginate droplets with divalent ions (such as Ca_2^+) is one of the most widely reported encapsulation methods [26, 27]. However, most of the proposed techniques require a two step procedure: i) capsule formation, and ii) capsule stabilization. Such processes depend on manipulation and are specifically designed for the polymer under study. Recently, the fabrication of bicompartmental microparticles with different shapes was reported [28]. However, due to the use of a strong electric field, the electrohydrodynamic co-jetting process

is not cell-friendly [28]. Thus, the encapsulation of some bioentities such as stem cells, which are extremely sensitive to the external forces, may be hindered since it might compromise their undifferentiated state during the encapsulation process. Thus, the establishment of an automated system that enables customized microparticle fabrication remains a key challenge in biomedical applications.

Herein, a new microcapsule production system is introduced to accomplish the capsule formation and stabilization in a single automated procedure. The proposed two-phase hydrophobic-hydrophilic system enables the formation and stabilization of the microcapsules in the hydrophobic and the hydrophilic phases, respectively. Microcapsules pass through the interface by gravity and by mechanical forces induced by a shaker. The system can be easily modified for different applications by replacing the bioactive material, hydrophobic, and/or hydrophilic solutions. Microcapsules with uniform shape, size, and morphology were successfully produced by the proposed system.

2. MATERIALS AND METHODS

2.1. Materials

The materials used in this study were a commercially available Gellan Gum (GG, Gelrite®, Sigma-Aldrich) and Alginic acid sodium salt (ALG, Sigma-Aldrich). The light mineral oil used was purchased from Sigma-Aldrich. 3 mL BD™ syringes with tip cap, clear (100/sp, 500/ca) and needles (31 G x 1 1/2 in, 27 G x 1 1/2 in, 25 G x 1 1/2 in gauge) were purchased from BD Biosciences. Fluoresbrite® Yellow Green (YG) fluorescent polystyrene latex microspheres (10.0 μm) packaged as 2.5% aqueous suspension with $4.55x10^7$ particles/mL were purchased from Polysciences (Warrington, PA). Calcium chloride ($CaCl_2$, M_w = 110.98 g/mol) was purchased from Sigma-Aldrich.

2.2. Preparation of solutions

GG solution was prepared as previously described [29]. Briefly, 1% (w/v) solution of GG was prepared by dissolving the powder in deionized water at 90 ºC for 20-30 min and stabilized at 40 ºC. Similarly, ALG solution was prepared at 1% (w/v) by dissolving 1 g ALG in 100 mL Dulbecco's Phosphate Buffer Saline (DPBS, Sigma).

2.3. Microcapsule generation

GG and ALG microcapsules were produced in a single automated procedure, which comprised the formation and stabilization of the microcapsules. The schematic of the proposed automated microcapsule production system is depicted in Figure IV.1.A and Figure

IV.1.B. This system contains a controllable syringe pump device, a laboratory shaker and a beaker which is filled with a hydrophilic and a hydrophobic solution. This two-phase system, formed by two distinct layers, is obtained by having mineral oil as the hydrophobic solution (with lower density) and cell culture medium as the hydrophilic solution (higher density). Polymeric droplets were dispensed by a syringe pump into the mineral oil. Agitation produced by the shaker increased the number of droplets generated. Due to the hydrophobicity of the mineral oil, perfectly spherical polymer drops were generated in this solution (Figure IV.1.C). When capsules pass through the mineral oil-medium interface, they start to chemically crosslink by the crosslinking agent present in the hydrophilic solution. Specifically, GG and ALG were crosslinked by calcium ions contained in the medium and $CaCl_2$ solution, respectively. Mineral oil can easily be removed and the capsules left suspended in the medium solution (Figure IV.1.D). Prior to use, the microcapsules were harvested from the medium and directly stored in the incubator. If sterile production is required, all the solutions and equipment can be sterilized by irradiation or by autoclaving.

2.3.1. Microcapsule generation with encapsulated fluorescent beads

Microbead stock solutions containing microbeads with a diameter of 10.0 µm (with a solid fraction of 0.1% w/w) were suspended with the polymer solution at 37 ⁰C. Two different bead concentrations, 0.01% (i.e., 4.55×10^5 beads/mL) and 0.1% (i.e., 4.55×10^6 beads/mL) of the original concentration (i.e., 4.55×10^7 beads/mL) were used to assess the influence of bead concentration over its distribution within the capsule. The protocol for generating encapsulated fluorescent beads was similar to that used for the simple microcapsules. Encapsulated fluorescent beads were imaged using a fluorescence microscope.

2.3.2. Microcapsule generation with encapsulated NIH-3T3 cells

NIH-3T3 fibroblast cells were cultured in Dulbecco's Modified Eagle Medium (DMEM, Sigma-Aldrich) supplemented with 10% of heat-inactivated fetal bovine serum (FBS, Gibco) and 1% penicillin-streptomycin (Gibco) at 37 ⁰C, in a humidified atmosphere with 5% of CO_2. A cell suspension of NIH-3T3 (3×10^6 cells/mL) was prepared by trypsinization (trypsin/EDTA solution, Gibco) and mixed with the GG polymer solution at 37 ⁰C. The protocol for generating capsules with NIH-3T3 cells was similar to that used for the simple microcapsules. The viability of the encapsulated cells in the hydrogels under study was characterized 1, 3, 5 and 7 days after culture, by incubating cells with a Live/Dead (Invitrogen) assay (calcein AM/ethidium homodimer-1 in DPBS) during 20 min.

2.3.3. Microcapsule generation with encapsulated MIN6 cell aggregates

A murine insulinoma cell line (MIN6) was kindly provided by Dr. Donald Ingber, Wyss Institute of Harvard, Boston, MA, USA. MIN6 cells (passages 35-42) were maintained at 37°C and 5% CO_2 in DMEM supplemented with 10% FBS and 100 U/mL penicillin with 0.1 mg/mL streptomycin. The medium was changed every 3-4 days and cultured cells were passaged and used for MIN6 pseudo-islet formation when reaching 70% confluence. MIN6 pseudo-islets were formed by seeding MIN6 cells with $6x10^6$ cells/mL concentration in poly(ethylene glycol) (PEG) microwells with a diameter of 300 µm for 3 days (more information on the supplementary Figure IV.S1 in the appendix of the present chapter). The MIN6 aggregates were harvested and preserved in medium immediately before encapsulation. MIN6 cell aggregates were suspended in GG polymer solution at 37 ºC and transferred to a 3 mL syringe for dispensing and microencapsulation. MIN6-GG suspension was dispensed into the two-phase system (mineral oil - cell culture medium) and encapsulated pseudo-islets were formed. Immunofluorescence was used to assess the expression of insulin by encapsulated islets. Anti-Insulin receptor substrate 2 antibody produced in rabbit (Sigma-Aldrich) was coupled with a secondary antibody AlexaFluor 546-conjugated anti-rabbit (Sigma-Aldrich) in order to detect fluorescence.

2.4. Microcapsule characterization

There are many parameters that might affect the size of the microcapsules. In this study we characterized the effect of the syringe gauge (31, 27 and 25 G) and syringe dispensing rate (0.002, 0.01 and 0.1 µL/hr), keeping constant, respectively, the solution pump rate at 0.01 µL/hr and the syringe gauge to 31 G. For that, some system parameters were kept fixed throughout all experiments including the speed and the maximum tilting angle of the shaker and the syringe volume (3 mL). To characterize the capsule size uniformity, three independent experiments were performed, each containing at least 15 replicates. The variation of the capsule diameters within each experiment was determined by examination under a standard inverted-light microscope. The size of the capsules was measured using ImageJ software (http://rsbweb.nih.gov/ij/).

2.5. Statistical analysis

All the data were subjected to statistical analysis and were reported as mean ± standard deviation. Analysis of variance (One-Way, $p<0.05$, and Two-Way ANOVA, p<0.0001) was used for statistical analysis.

3. RESULTS AND DISCUSSION

The proposed automated microcapsule production system was used to produce plain microcapsules, encapsulated microbeads, encapsulated cell suspensions and encapsulated cell aggregates.

3.1. Size-controlled microcapsule formation - Meet the demand

Capsules with uniform sizes and shapes have been made at the macro-level and have found several clinical and pharmaceutical applications [5, 10, 27]. However, the production of microcapsules for the incorporation of bioactive materials including drugs, cell suspensions and cell aggregates with uniform size and shape is very challenging and has not yet been fully met. Thus, there is an enormous demand for the development of an automated system with capability of continuous microcapsule production without manual intervention. Even more important is the need of a system that can be easily tuned according to the polymer, the encapsulated biological entity and therefore the therapeutic application. The system herein proposed is illustrated in Figure IV.1.
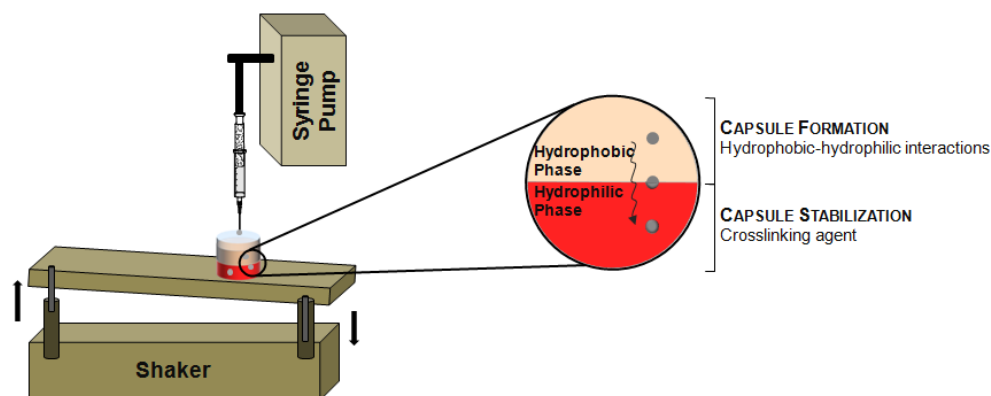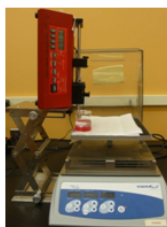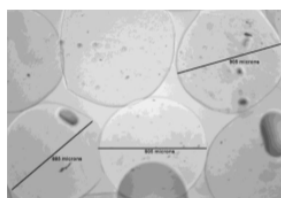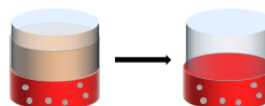
Figure IV.1. (A) Schematics of the system for microcapsule formation (not to scale). (B) Photography of the system setup. (C) Microscope image of capsules in medium depicting the non-assembly of the capsules. (D) Removal of the hydrophobic phase before sample incubation within the hydrophilic phase.

In a previous work [30], microcapsules were formed in a hydrophobic solution where oil was employed as a sheath fluid. In such cases, the remnant mineral oil on the microcapsule surface must be removed for the clinical and biological applications. The complete oil removal from the capsule surface is not an easy task as the polymerized hydrogel shell is fragile. In addition, the surface cleaning process may damage the encapsulated bio-active material. Hence, it is highly desired that the final step of capsule production (stabilization) occurs in a biocompatible hydrophilic solution. As illustrated in Figure IV.1.A, hydrogel droplets pass through a hydrophobic material (mineral oil) and polymerize in a hydrophilic solution (culture medium). The polymerization of encapsulated cells in cell culture medium conveys two important features: cleaning of mineral oil from microcapsule surface is not required; and manual manipulation for capsule harvesting and culturing in cell culture medium is avoided. These features not only contribute to damage-free capsule formation but also, indirectly, contribute to protect the biofunctionality of encapsulated bio-active materials. The effective stabilization of the microcapsules was confirmed by their non-aggregation when kept in cell culture medium (Figure IV.1.C). The cell-friendly characteristic of the proposed system is an important feature that has been the main concern of the authors in the process design and development. The viability and functionality of the encapsulated cell suspension and cell aggregates were investigated and are described in detail in the following sections.

3.1.1. Influence of system parameters over size of microcapsules

The size of microcapsules can be mainly controlled by the needle size, pump rate, material viscosity and tilt and speed of the shaker. By fixing four of these parameters the microcapsule size can be controlled by fine tuning the fifth parameter. In Figure IV.2 we have analyzed the influence of the pump rate and needle size over the size of the microcapsules, while the material viscosity and tilt and speed of the shaker were kept constant. GG at 1% (w/v) was used in all experiments. Polymer mass was stretched on the needle tip while the polymer solution was pumped with a specific rate through the needle, forming polymeric droplets. Four main forces contribute and drive the process of capsule formation: polymer-needle surface tension, polymer-mineral oil interfacial tension, mineral oil-cell culture medium interfacial tension and gravity (Figure IV.2.D).
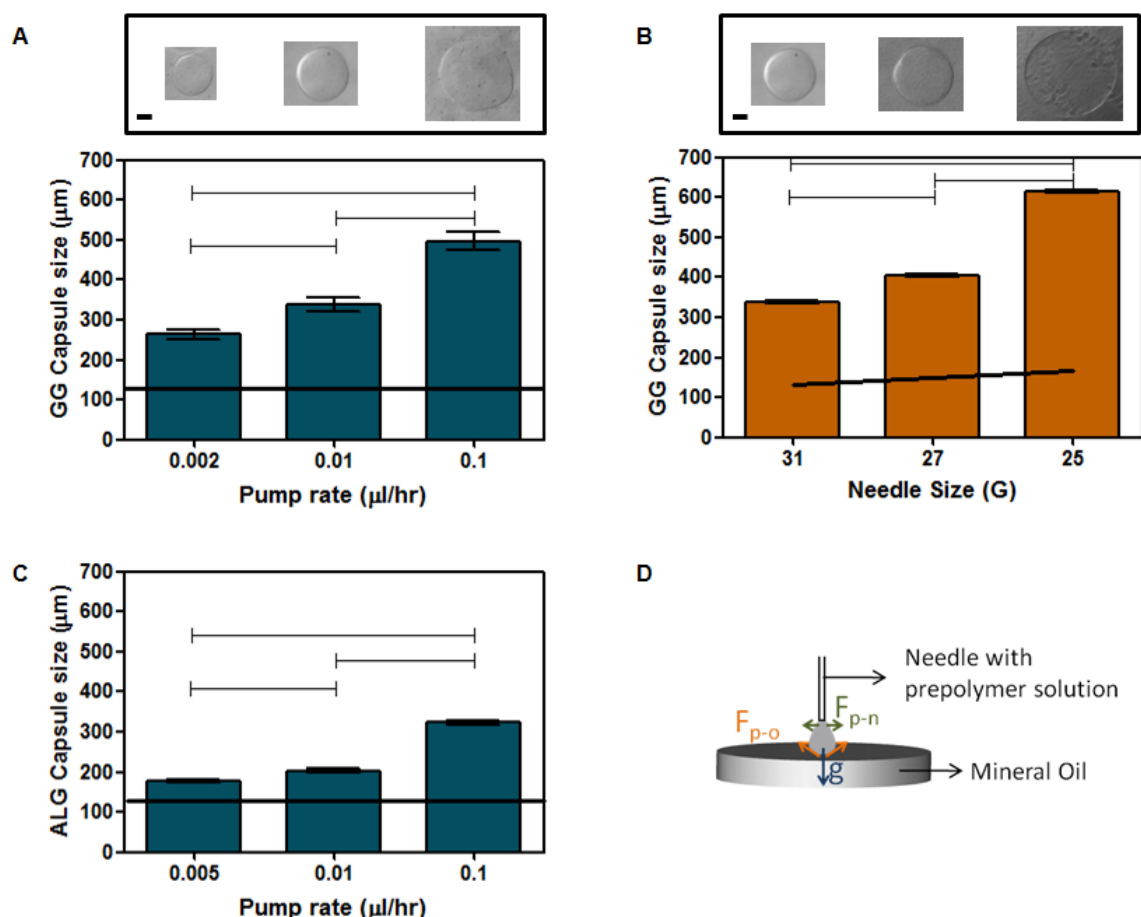
Figure IV.2. Influence of system parameters over capsule size of GG: (A) Pump rate (µL/hr) and (B) needle size (G) (p<0.05). Scale bar of the microcapsules is 100 µm. (C) Influence of pump rate over the microcapsule size using ALG (p<0.05). Black line corresponds to the inner diameter of the needle (µm). (D) Schematics of the forces involved on the formation of the microcapsules: gravity (g), surface tension between the polymer and needle (F_{p-n}) and surface tension between the polymer and mineral oil (F_{p-o}).

To analyze the effect of polymer solution dispensing rate on the capsule size, the needle size was fixed to 31G (approximately 135 µm of inner diameter) and the pump rate set to 0.002, 0.01 and 0.1 µL/h. As depicted in Figure IV.2.A, the microcapsules presented an average diameter of 270, 340, and 480 µm, significantly increasing with increasing pump rate value. The diameter of the produced microcapsules with three different pump rates was significantly different between each other (One-way Anova, *p*<0.05). Polymer adhered to the needle tip gained mass in such a way that, with a higher pump rate, the polymer volume dispensed for a specific period of time was higher. The mineral oil periodically met the stretched polymer because of the shaker movement and, as soon as the combination of gravity and polymer-mineral oil interfacial tension forces dominated the polymer-needle surface tension, the droplet could no longer bind to the needle. At this point, the polymer droplet separates from

the needle tip. Since the polymer volume dispensed by the pump is higher for a higher pump rate, larger capsules are formed when higher pump rates are used.

The influence of needle diameter on the size of the produced microcapsules (Figure IV.2.B) was investigated by fixing the pump rate at 0.01 µL/hr and varying the size of the needle (31, 27 and 25 G). Thus, the rate of the adhesion of the polymer to the needle tip was kept constant. It was observed that microcapsules showed increasing average size of 340, 400 and 600 µm, with increasing diameter of the needle, being significantly different between each other (One-way Anova, p<0.05). With a larger needle gauge, the polymer-needle surface tension is stronger, which is directly related to the increased surface area. As a result, stronger forces (gravity conjugated with polymer-mineral oil interfacial tension, directly related to the polymer mass) are needed to separate the stretched polymer solution from the needle tip. Regardless of the needle size used, the microcapsule diameter was higher than the diameter of the needle tip.

3.1.2. Versatility of the system and applicability to different polymeric materials

To investigate the versatility of the proposed system, we also analyzed the influence of the syringe pump rate over the capsule size using another well studied polymer in tissue engineering. ALG has been widely used in encapsulation systems due to its easy manipulation [12, 27]. Similarly to GG, Figure IV.2.C demonstrates that the size of the microcapsules of ALG was also dependent on the pump rate, significantly increasing (One-way Anova, $p<0.05$) as the pump rate increases. Interestingly, the diameter of the ALG microcapsules was significantly smaller (Two-way Anova, $p<0.0001$) than the one registered for the GG microcapsules. This might be a result of the different properties of the polymers used. We hypothesize that a higher viscosity of ALG reduced the stretching of the polymer by gravity. Thus, when the polymeric capsules were formed by contact with mineral oil, the polymer volume was lower, forming capsules with a smaller diameter.

3.1.3. Reproducibility of the system

To investigate the reproducibility and uniformity of the produced microcapsules by controlling either the pump rate or the needle size, experiments were repeated three times (Figure IV.3 A,B,C) for each condition (n=15). The uniformity of generated GG and ALG microcapsules can be easily observed for both parameters. Also, the size distribution of the microcapsules for the three needle sizes is shown in Figure IV.3.D,E,F. A relative increased polydispersity was observed with increasing needle gauge. These results demonstrated a precise control over the microcapsule size in the proposed continuous, stable and manipulation-free system for the production of the microcapsules.
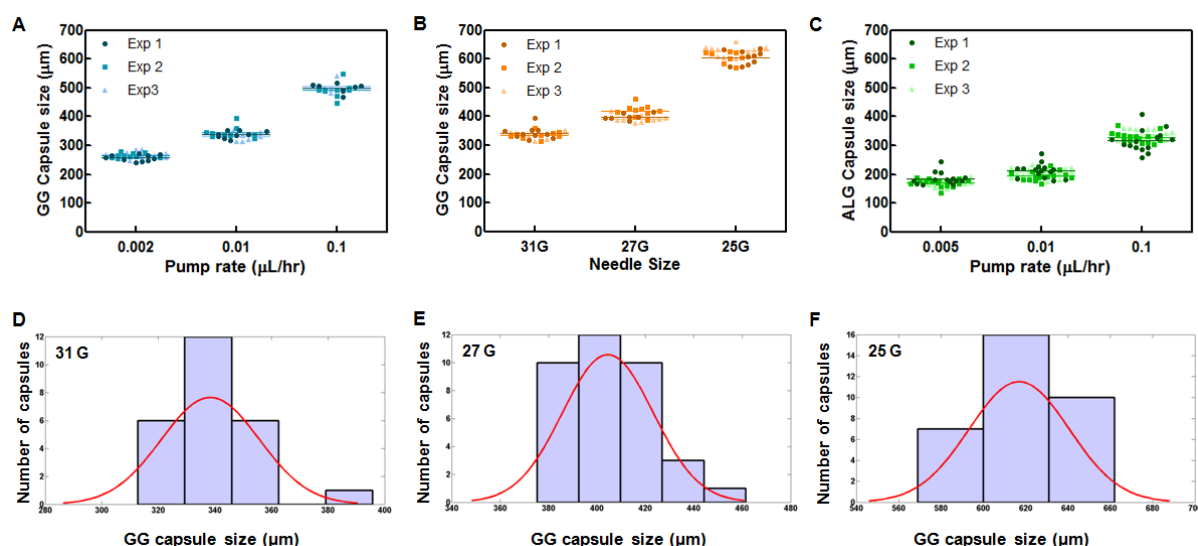
Figure IV.3. Capsule size uniformity at different (A) pump rates and (B) needle sizes for GG and for different (C) pump rates for ALG. Histogram of the distribution of capsule size for different needle sizes: (D) 31G, (E) 27G and (F) 25G.

3.2. System applications

Different types of polymers, including synthetic and natural polymers, have been used with considerable success for cell encapsulation. Herein, GG was the chosen ionic crosslinkable polymer to test the proposed system. GG has shown promising results both *in vitro* and *in vivo* as a scaffold for cartilage tissue engineering [18, 31, 32]. The ions in the cell culture medium, which was used in the proposed two-phase system for cell suspension and cell aggregate encapsulation, were sufficient for the crosslinking of this ionic polymer. For non-cell based capsules, including controlled release of drugs, culture medium can be replaced by some other ionic hydrophilic solutions such as phosphate buffered saline (PBS). Ions can also be added to non-ionic hydrophilic materials to optimize the microcapsule stabilization.

The ability to quickly generate microcapsules with encapsulated bio-entities within the proposed system was explored and is depicted in Figure IV.4. Our system was able to successfully encapsulate from simple microbeads to complex biological entities, such as cell aggregates. In the following sections, each application is described in detail.

A. Fluorescent beads encapsulation
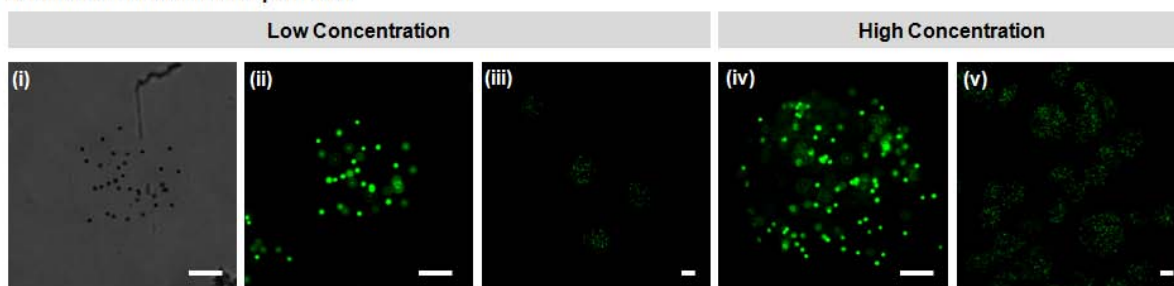
B. Viability of encapsulated NIH-3T3 cells
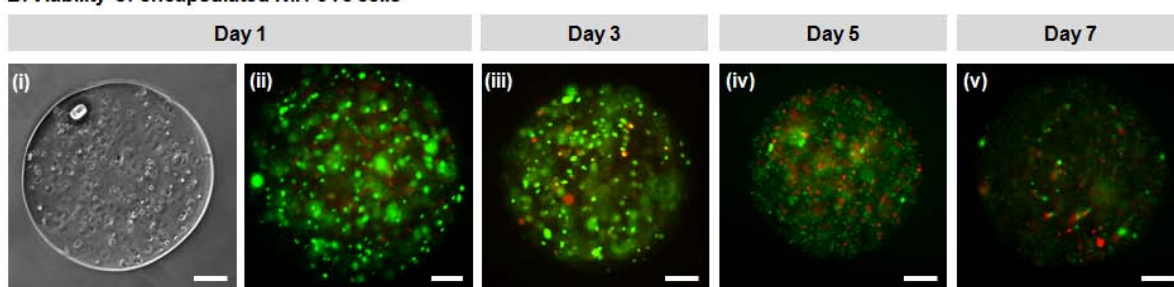
C. Insulin secretion of encapsulated MIN6 cell aggregates
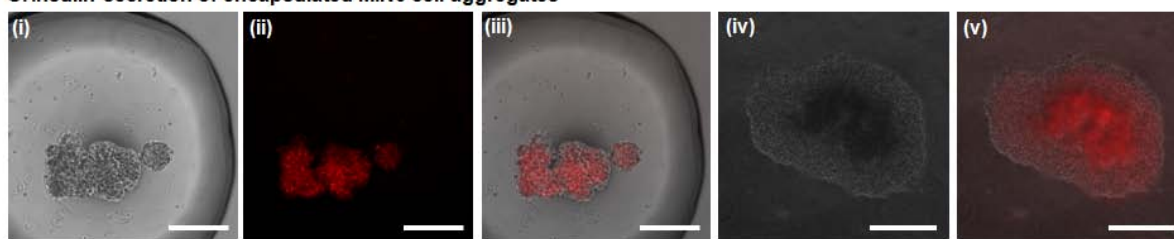
Figure IV.4. Potential applications of the proposed system: (A) fluorescent green microbead encapsulation with two concentrations: (i,ii,iii) low, and (iv, v) high. (B) Viability (live/dead) of encapsulated NIH-3T3 cells after: (i,ii) 1 day, (iii) 3 days, (iv) 5 days, and (v) 7 days in culture. (C) Insulin expression for testing the functionality of encapsulated cell aggregates using antibody staining (red). Scale bar: 100 μm.

3.2.1. Particle encapsulation

The proposed system can potentially be used for the incorporation of particles, such as drugs, being ultimately used for sustained drug release [33]. This application was investigated by encapsulating fluorescent microbeads in GG microcapsules by the proposed system. Green fluorescent spherical microbeads with 10 μm diameter were encapsulated within GG microcapsules and were imaged immediately after microcapsule formation, as depicted in Figure IV.4.A. Two different concentrations of encapsulated microbeads were used (low and high). This procedure can be used for potentially encapsulating particles with different sizes, shapes and biofunctionality for drug delivery applications.

3.2.2. Viability and stability of encapsulated cells

The proposed system is cell-friendly as harsh crosslinking processes such as UV and aggressive chemical crosslinking mechanisms are avoided. The proposed system allowed a good distribution of encapsulated NIH-3T3 cells within GG microcapsules (Figure IV.4.B). The viability of the encapsulated cells was investigated 1, 3, 5, and 7 days after culture, as depicted in Figure IV.4.B. NIH-3T3 fibroblast cells encapsulated within the microcapsules were stained with calcein AM, which is well retained in living cells, producing an intense uniform green fluorescence and with ethidium homodimer (EthD-1), which enters the damaged cell membrane (dead cell) and binds to nucleic acids. As it can be observed in Figure IV.4.B, even after seven days, most of the cells were alive. This not only demonstrated the biocompatibility of the microcapsules, but also showed the diffusion of cell culture medium into the microcapsules which enables the supply of oxygen and nutrients to the encapsulated cells, thus maintaining a high level of viability.

We should stress that the proposed system is a fast capsule production process where oil coated polymer droplets are immediately as they pass through the hydrophobic-hydrophilic interface. Additionally, the encapsulated cells can be easily incubated without further washing, filtering, transferring or any other manipulation or intervention. Those desirable attributes contribute to the higher cell viability and improved capsule biocompatibility.

3.2.3. Functionality of encapsulated cell aggregates

To investigate the functionality of encapsulated cells, aggregates of MIN6 cells were encapsulated in GG capsules and were analyzed to detect for insulin secretion. First, MIN6 cells were seeded in PEG-made microwells with 300 μm diameter and were incubated in cell culture medium for three days. The microwell fabrication and pseudo-islet production are explained in detail as supplementary data (Figure IV.S1). Cell aggregates were harvested on day three, mixed with the hydrogel solution (GG) and used to produce encapsulated pseudo-islets by the proposed system. As shown in Figure IV.4.C, cell aggregates were encapsulated in GG capsules and their functionality was assessed by immunostaining for insulin. The red fluorescence obtained demonstrated that the encapsulated cell aggregates were not only viable but also functional. These results showed that the system allowed not only producing microcapsules with viable encapsulated cells, but also enabled the production of microcapsules with functional cell aggregates.

4. CONCLUSIONS

We proposed a new mechanism for the production of microcapsules by using two distinct liquid phases. By means of a syringe pump, the polysaccharides GG or ALG were dispensed in the hydrophobic phase, leading to the formation of microcapsules. By gravity and mechanical forces the microcapsules crossed the solutions, falling down from the hydrophobic phase into the hydrophilic one. The crosslinking agent, intentionally dissolved in the hydrophilic phase, allowed obtaining the stabilization of the microcapsules. Encapsulated beads, cell suspensions and cell aggregates were successfully produced. By changing the hydrophobic and/or hydrophilic solution, the method is applicable to a broad range of microcapsule formulations. Our simple and functional system was successfully demonstrated by producing microcapsules with different materials, controlled size and morphology in a single step system.

REFERENCES

1. Cleland JL, Johnson OL, Putney S, Jones AJS. Recombinant human growth hormone poly(lactic-co-glycolic acid) microsphere formulation development. Adv Drug Deliv Rev 1997 Oct;28(1):71-84.
2. Cadenazzi G, Streitenberger S, Cerone S, Sansinanea A. Immobilization of enzymes: Micro-encapsulation of glutathione-s-transferase. Acta Bioquim Clin Latinoam 2003 Dec;37(4):401-404.
3. Lambert JM, Weinbreck F, Kleerebezem M. In vitro analysis of protection of the enzyme bile salt hydrolase against enteric conditions by whey protein-gum arabic microencapsulation. J Agric Food Chem 2008 Sep;56(18):8360-8364.
4. Orive G, Hernandez RM, Gascon AR, Calafiore R, Chang TMS, Vos PD, et al. Cell encapsulation: Promise and progress. Nat Med 2003;9(1):104-107.
5. Hasse C, Klock G, Schlosser A, Zimmermann U, Rothmund M. Parathyroid allotransplantation without immunosuppression. Lancet 1997;351:1296-1297.
6. Soon-Shiong P. Insulin independence in a type 1 diabetic patient after encapsulated islet transplantation. Lancet 1994;343:950-951.
7. Sun YL, Ma XJ, Zhou DB, Vacek I, Sun AM. Normalization of diabetes in spontaneously diabetic cynomologus monkeys by xenografts of microencapsulated porcine islets without immunosuppression. Journal of Clinical Investigation 1996 Sep;98(6):1417-1422.
8. Hortelano G, AlHendy A, Ofosu FA, Chang PL. Delivery of human factor ix in mice by encapsulated recombinant myoblasts: A novel approach towards allogeneic gene therapy of hemophilia b. Blood 1996 Jun;87(12):5095-5103.
9. Xu WM, Liu LZ, Charles IG. Microencapsulated inos-expressing cells cause tumor suppression in mice. Faseb Journal 2001 Dec;15(14):213-+.
10. Shi MQ, Hao S, Quereshi M, Guo WL, Zheng CY, Xiang J. Significant tumor regression induced by microencapsulation of recombinant tumor cells secreting fusion protein. Cancer Biotherapy and Radiopharmaceuticals 2005 Jun;20(3):260-266.
11. van Hoogmoed CG, Busscher HJ, de Vos P. Fourier transform infrared spectroscopy studies of alginate-pll capsules with varying compositions. J Biomed Mater Res Part A 2003 Oct;67A(1):172-178.
12. Koch S, Schwinger C, Kressler J, Heinzen C, Rainov NG. Alginate encapsulation of genetically engineered mammalian cells: Comparison of production devices, methods and microcapsule characteristics. J Microencapsul 2003 May-Jun;20(3):303-316.
13. Yin JH, Noda Y, Yotsuyanagi T. Properties of poly(lactic-co-glycolic acid) nanospheres containing protease inhibitors: Camostat mesilate and nafamostat mesilate. Int J Pharm 2006 May;314(1):46-55.
14. Emami J, Hamishehkar H, Najafabadi AR, Gilani K, Minaiyan M, Mahdavi H, et al. A novel approach to prepare insulin-loaded poly (lactic-co-glycolic acid) microcapsules and the protein stability study. J Pharm Sci 2009 May;98(5):1712-1731.
15. Taqieddin E, Amiji M. Enzyme immobilization in novel alginate-chitosan core-shell microcapsules. Biomaterials 2004 May;25(10):1937-1945.
16. Grenha A, Gomes ME, Rodrigues M, Santo VE, Mano JF, Neves NM, et al. Development of new chitosan/carrageenan nanoparticles for drug delivery applications. J Biomed Mater Res Part A 2010;92A(4):1265-1272.
17. Ohkawa K, Kitagawa T, Yamamoto H. Preparation and characterization of chitosan-gellan hybrid capsules formed by self-assembly at an aqueous solution interface. Macromol Mater Eng 2004 Jan;289(1):33-40.
18. Oliveira JT, Santos TC, Martins L, Picciochi R, Marques AP, Castro AG, et al. Gellan gum injectable hydrogels for cartilage tissue engineering applications: In vitro studies and preliminary in vivo evaluation. Tissue Engineering Part A 2009;16(1):343-353.
19. Soonshiong P, Heintz RE, Merideth N, Yao QX, Yao ZW, Zheng TL, et al. Insulin independence in a type-1 diabetic patient after encapsulated islet transplantation. Lancet 1994 Apr;343(8903):950-951.
20. Hasse C, Klock G, Schlosser A, Zimmermann U, Rothmund M. Parathyroid allotransplantation without immunosuppression. Lancet 1997 Nov;350(9087):1296-1297.
21. Landfester K, Musyanovych A, Mailander V. From polymeric particles to multifunctional nanocapsules for biomedical applications using the miniemulsion process. Journal of Polymer Science Part a-Polymer Chemistry 2010 Feb;48(3):493-515.

22. De Koker S, Lambrecht BN, Willart MA, van Kooyk Y, Grooten J, Vervaet C, et al. Designing polymeric particles for antigen delivery. Chem Soc Rev 2011;40(1):320-339.

23. Lensen D, Vriezema DM, van Hest JCM. Polymeric microcapsules for synthetic applications. Macromol Biosci 2008 Nov;8(11):991-1005.

24. De Cock LJ, De Koker S, De Geest BG, Grooten J, Vervaet C, Remon JP, et al. Polymeric multilayer capsules in drug delivery. Angew Chem-Int Edit 2010;49(39):6954-6973.

25. Roh IJ, Kwon IC. Fabrication of a pure porous chitosan bead matrix: Influences of phase separation on the microstructure. J Biomater Sci-Polym Ed 2002;13(7):769-782.

26. Zhang YJ, Wei Q, Yi CB, Hu CY, Zhao WF, Zhao CS. Preparation of polyethersulfone-alginate microcapsules for controlled release. J Appl Polym Sci 2009 Jan;111(2):651-657.

27. Calafiore R. Alginate microcapsules for pancreatic islet cell graft immunoprotection: Struggle and progress towards the final cure for type 1 diabetes mellitus. Expert Opin Biol Ther 2003 Apr;3(2):201-205.

28. Bhaskar S, Pollock KM, Yoshida M, Lahann J. Towards designer microparticles: Simultaneous control of anisotropy, shape, and size. Small 2010 Feb;6(3):404-411.

29. Coutinho DF, Sant SV, Shin H, Oliveira JT, Gomes ME, Neves NM, et al. Modified gellan gum hydrogels with tunable physical and mechanical properties. Biomaterials 2010 Oct;31(29):7494-7502.

30. Payne RG, Yaszemski MJ, Yasko AW, Mikos AG. Development of an injectable, in situ crosslinkable, degradable polymeric carrier for osteogenic cell populations. Part 1. Encapsulation of marrow stromal osteoblasts in surface crosslinked gelatin microparticles. Biomaterials 2002 Nov;23(22):4359-4371.

31. Oliveira JT, Gardel L, Martins L, Rada T, Gomes ME, Reis RL. Injectable gellan gum hydrogels with autologous cells for the treatment of rabbit articular cartilage defects. Journal of Orthopedic Research 2010;in press.

32. Oliveira JT, Santos TC, Martins L, Silva MA, Marques AP, Castro AG, et al. Performance of new gellan gum hydrogels combined with human articular chondrocytes for cartilage regeneration when subcutaneously implanted in nude mice. Journal of Tissue Engineering and Regenerative Medicine 2009;3(7):493-500.

33. Wang W, Liu XD, Xie YB, Zhang H, Yu WT, Xiong Y, et al. Microencapsulation using natural polysaccharides for drug delivery and cell implantation. J Mater Chem 2006;16(32):3252-3267.

APPENDIX

Supplementary Figure IV.S1

Figure IV.S1 provides supplementary information regarding the preparation of the cell aggregates using MIN6 cells.
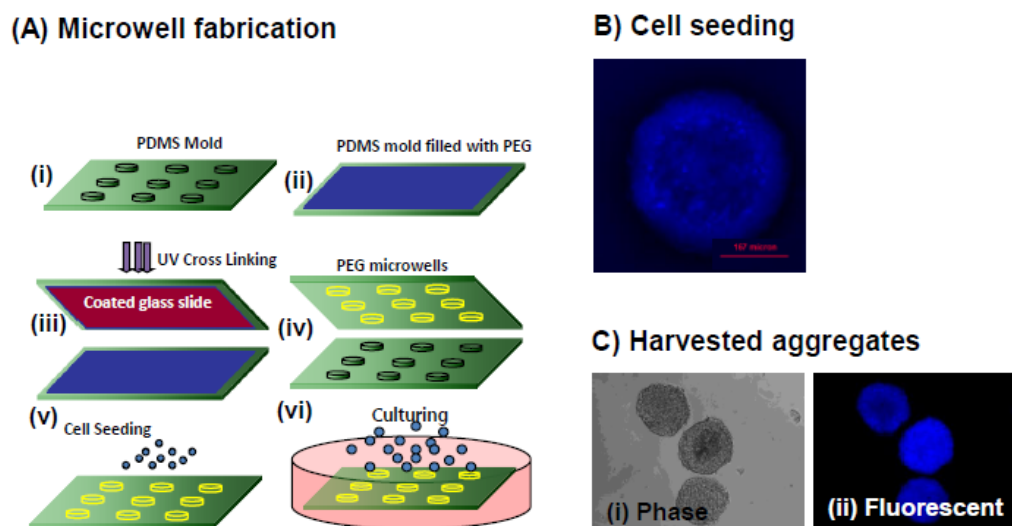
Figure IV.S1. Preparation of cell aggregates using MIN6 cells: (A) microwell fabrication; (B) cell seeding and (C) harvested cell aggregates.

Section 4

DEVELOPING HYDROGELS WITH INTEGRATED CHEMICAL, BIOLOGICAL AND STRUCTURAL CUES

Chapter V

MODIFIED GELLAN GUM HYDROGELS WITH TUNABLE PHYSICAL AND MECHANICAL PROPERTIES

CHAPTER V [*]

MODIFIED GELLAN GUM HYDROGELS WITH TUNABLE PHYSICAL AND MECHANICAL PROPERTIES

ABSTRACT

Gellan Gum (GG) has been recently proposed for tissue engineering applications. GG hydrogels are produced by physical crosslinking methods induced by temperature variation or by the presence of divalent cations. However, physical crosslinking methods may yield hydrogels that become weaker in physiological conditions due to the exchange of divalent cations by monovalent ones. Hence, this work presents a new class of GG hydrogels crosslinkable by both physical and chemical mechanisms. Methacrylate groups were incorporated in the GG chain, leading to the production of a methacrylated gellan gum (MeGG) hydrogel with highly tunable physical and mechanical properties. The chemical modification was confirmed by proton nuclear magnetic resonance (^{1}H-NMR) and Fourier transform infrared spectroscopy (FTIR-ATR). The mechanical properties of the developed hydrogel networks, with Young's modulus values between 0.15 and 148 kPa, showed to be tuned by the different crosslinking mechanisms used. The *in vitro* swelling kinetics and hydrolytic degradation rate was dependent on the crosslinking mechanisms used to form the hydrogels. Three-dimensional (3D) encapsulation of NIH-3T3 fibroblast cells in MeGG networks demonstrated *in vitro* biocompatibility confirmed by high cell survival. Given the highly tunable mechanical and degradation properties of MeGG, it may be applicable for a wide range of tissue engineering approaches.

1. INTRODUCTION

Hydrogels have received much attention in the field of tissue engineering, mainly due to their ability to be used as vehicles for drug delivery and as cell carriers [1-5]. Hydrogels are similar to natural extracellular matrix (ECM) molecules in that they have the ability to retain great quantities of water. One of the main advantages of hydrogels is their capacity to be formed *in situ* through a minimally invasive procedure. Both physical and chemical methods can be applied for the development of hydrogel networks [2, 6]. *In situ* forming physical hydrogels are usually spontaneously formed by weak secondary forces such as hydrogen bonding, van der Waals interactions and ionic bonding [6-8]. After injection, they instantaneously change from sol to gel state under physiological temperature, pH and ionic conditions. On the other hand, *in situ* forming chemical hydrogels can have their mechanical strength, integrity and swelling properties fine tuned by the degree of chemical crosslinking. These hydrogels have mainly been formed by the photo-irradiation of the vinyl groups of the injected pre-polymer [9, 10].

Physical and chemical crosslinking methods have been studied for several natural-origin hydrogels, such as hyaluronic acid (HA) [11-13], gelatin [14, 15] and alginate [16, 17]. Recently, the FDA approved Gellan Gum (GG) has been receiving particular attention for tissue engineering applications, namely cartilage regeneration [18-22], mainly due to its good mechanical properties and promising results as an ophthalmic drug vehicle [23, 24]. GG is an anionic microbial polysaccharide composed of a tetrasaccharide repeating unit of two β-D-glucose, one β-D-glucuronic acid and one α-L-rhamnose [25]. Upon temperature decrease, a random coil-helix transition occurs with further aggregation of the helices leading to the formation of junction zones [26]. The sol-gel transition of GG is ionotropic, as in alginate. Therefore, the presence of cations is necessary for the formation of a stable hydrogel. However, the gelation is greatly affected by the chemical nature of the cations present, being stronger with divalent ones. The rheological and physical properties of GG have been widely investigated [27-30]. Recently, Masakuni *et al.* proposed a gelation mechanism of deacylated GG in aqueous solution, with and without Ca^{2+} cations [31]. However, these physically crosslinked hydrogels tend to lose their stability *in vivo* after implantation due to the exchange of divalent cations with monovalent ones that are present in higher concentrations in physiological environment. In order to surpass this disadvantage, some chemical modifications to the GG backbone have been proposed. For instance, a chemical scissoring process has been used to adjust the molecular weight of GG [20]. Due to the properties of these formed GG hydrogels, they have been mainly proposed for cartilage tissue applications [20].

Although hydrogels closely mimic ECM and have great potential for tissue engineering applications, the major drawback is their weak mechanical properties. Thus, apart from *in vivo* stability, other important attributes of hydrogels for tissue engineering are their mechanical properties and degradation rate. Different tissues have different tissue regeneration rates and different mechanical properties. For instance, stiffness of solid tissues in the body can range from 1 kPa for the liver until 100 kPa for the collagenous bone [32]. Therefore, the materials used within a tissue engineering approach must have their degradation and mechanical properties finely tuned to match those of the native tissues.

In this present work, we present a simple method to functionalize GG with double bonds. We further used the photocrosslinkable methacrylated GG to prepare hydrogels using combination of physical and chemical crosslinking methods. It was hypothesized that physical and mechanical properties of hydrogels can be tuned by the crosslinking mechanisms applied. The described photocrosslinkable hydrogels can be used in various applications of tissue engineering due to their wide range of mechanical properties.

2. MATERIALS & METHODS

2.1. Synthesis of methacrylated gellan gum

Methacrylated Gellan Gum (MeGG) was synthesized by reacting Gellan Gum (GG, Gelrite®, Sigma, M_w=1.000.000) with methacrylic anhydride (MA, Sigma). Briefly, 1 g of GG was dissolved in 100 mL of deionized water at 90 ºC for 20-30 minutes, as described elsewhere [22]. To this solution, either 2 or 8 mL of MA was added at 50 ºC, in order to synthesize MeGG with low (Low-MeGG) or high (High-MeGG) degrees of methacrylation, respectively. The reaction was continued for 6 hours. Periodically, pH (8.0) was adjusted with 5.0 M NaOH solution. The modified MeGG solution was purified by dialysis (Fisher Scientific, membrane with molecular weight cutoff of 11-14 kD, USA) for at least 3 days against distilled water to remove the excess of MA. Purified MeGG was obtained by lyophilization and stored at a dry place protected from light.

2.2. Characterization of methacrylated gellan gum

The chemical modification to GG was assessed by proton nuclear magnetic resonance (^{1}H-NMR) spectroscopy. ^{1}H-NMR spectra were recorded with a Varian Inova 500 NMR equipped with a variable temperature system. Lyophilized materials were dissolved in D_2O at a concentration of 10 mg/mL and at temperature of 50 ºC. Chemical shifts were referred to the methyl group of rhamnose as an internal standard, which is at δ 1.45 ppm [33]. The degree of substitution (DS, fraction of modified hydroxyl groups per repeating unit) was determined

by the relative integration of the double bond proton peak (I_{DB}) of the methacrylate groups to the methyl protons of the internal standard $(I_{CH_3 rham})$, according to Eq (1), as described elsewhere [33]. $n_{H_{DB}}$ and $n_{H_{CH_3 rham}}$ corresponds to the number of protons in the double bond and the methyl group of rhamnose, respectively. $n_{OH_{monomer}}$ corresponds to the number of reactive –OH sites in the GG structure.

$$DS = \frac{\dfrac{I_{DB}}{n_{H_{DB}}} \Bigg/ \dfrac{I_{CH_3 rham}}{n_{H_{CH_3 rham}}}}{n_{OH_{monomer}}} \qquad (1)$$

The chemistry of the modified materials was further analyzed by Fourier transform infrared spectroscopy with attenuated total reflection (FTIR-ATR). The infrared spectra were recorded on a spectrophotometer Bruker Alpha FT-IR with a resolution of 2 cm^{-1}. The results are presented as the average of 32 scans.

2.3. Preparation of Hydrogels

The lyophilized Low-MeGG and High-MeGG were dissolved at 0.5, 1 and 2% (w/v) in deionized water under constant stirring at 50 ºC for 10 minutes. Plain GG was dissolved at the same concentrations, as described elsewhere [22]. Briefly, GG was dissolved in deionized water under constant stirring. The solution was progressively heated to 90ºC, under which complete and homogeneous dispersion of the material was obtained after 20-30 minutes. Afterwards, calcium chloride (CaCl$_2$, Sigma, USA) and/or 0.5% (w/v) 2-hydroxy-1-[4-(2-hydroxyethoxy)phenyl]-2-methyl-1-propanone (Irgacure 2959, Ciba Specialty Chemicals) were added to the dissolved materials to fabricate hydrogels with different crosslinking mechanisms. The final concentration of CaCl$_2$ solution was 0.08 mg/mL, unless mentioned otherwise, yielding a ratio of calcium equivalent/GG carboxylate moieties of 0.052 for 1% (w/v) solution of GG. After dissolution, the temperature of Low-MeGG, High-MeGG and plain GG was progressively decreased to 45 ºC. GG and physically crosslinked MeGG hydrogels were produced by casting the solutions into molds and allowing the temperature to cool to room temperature. Chemically crosslinked hydrogels were obtained by exposing to light (320-500 nm, 7.14 mW/cm^2, EXFO OmniCure S2000) for 60 sec. For all described experiments, polymer disks (1 mm thick, 4 mm in diameter) were punched from hydrogel slabs, unless stated otherwise.

2.4. Characterization of hydrogels

2.4.1. Swelling kinetics

To study the swelling kinetics of the developed hydrogels, three solutions with different ionic content were used: distilled water (no ions); phosphate buffered saline (PBS, Gibco, with monovalent ions); and media (Dulbecco's Modified Eagle's medium, DMEM, Gibco, with mono and divalent ions). Hydrogel samples at 1% (w/v) were immersed in 2 mL of each solution at 37 ºC, under mild shaking. At different time points, the hydrogels (n=3) were removed from the solutions and gel surfaces were quickly blotted on a filter paper. Their wet weight was measured (w_t) and compared to the initial wet weight (w_0). The swelling ratio (S_k) was defined according to Eq (2).

$$S_k(\%) = \frac{w_t - w_0}{w_0} \times 100 \qquad (2)$$

2.4.2. Mechanical properties

To assess the effect of the degree of methacrylation, crosslinking mechanisms and polymer concentration on the mechanical properties of the developed hydrogels, compression tests were performed on an Instron 5542 mechanical tester. Freshly prepared GG and MeGG hydrogels (1 mm thick, 8 mm in diameter, n=3) were compressed in the direction normal to the circular face of the cylindrical samples at a rate of 0.2 mm per minute until failure of the hydrogel. The Young's modulus was defined as the slope of the linear region of the stress-strain curve in the 5-15% of the strain range (the stress-strain curves for all the tested conditions can be find in Figure V.S1, in the appendix of the present chapter). Ultimate stress and ultimate strain values were taken as the point where failure of the hydrogel occurred.

2.4.3. *In vitro* degradation

The effect of the degree of methacrylation, crosslinking mechanisms and polymer concentration over the degradation profile of MeGG hydrogels was studied. Weighed hydrogels (n=3) were hydrolytically degraded in a 0.1 mM NaOH solution at 37 ºC for 24 hours on a shaker. The samples were removed, freeze dried and weighed again to determine mass loss.

2.4.4. *In vitro* cell encapsulation

The effect of methacrylation and photocrosslinking on cell viability was assessed by encapsulating NIH-3T3 fibroblasts. The cells were cultured in DMEM (Sigma) supplemented with 10% of heat-inactivated fetal bovine serum (FBS, Gibco) and 1% penicillin-streptomycin (Gibco) at 37 ºC, in a humified atmosphere with 5 % of CO_2. A cell suspension of NIH-3T3 (10^7 cells/mL) was prepared by trypsinization (trypsin/EDTA solution, Gibco) and

incorporated into the GG, Low-MeGG and High-MeGG polymer solutions prepared as described previously and stabilized at 40 ºC. After resuspension, the cell/polymer mixture was casted into molds. GG hydrogels with encapsulated cells were placed at room temperature for 1-2 minutes to form a solid gel. MeGG cell laden hydrogels were exposed to light (7.14 mW/cm^2) for 60 sec. Cell viability of cells encapsulated in the hydrogels under study was characterized 1h after preparation and after 1, 3 and 7 days of culture, by incubating cells with a Live/Dead (Invitrogen) assay (calcein AM/ethidium homodimer-1 in DPBS) for 20 min. Tissue culture polystyrene (TCPS) was used as a control.

2.5. Statistical Analysis

All the data were subjected to statistical analysis and were reported as a mean ± standard deviation. Statistical differences (***$p<0.0001$, **$p<0.001$, *$p<0.01$) were determined using Student's paired t-test between two groups and two-way ANOVA followed by Bonferroni post-hoc test for multiple comparisons in swelling and mechanical data.

3. RESULTS AND DISCUSSION

3.1. MeGG synthesis and characterization

GG hydrogels have been recently used in tissue engineering applications [18]. However, these hydrogels are produced only by means of physical crosslinking mechanisms. This crosslinking mechanisms yield to hydrogels that become weaker in physiological conditions due to the exchange of divalent cations by monovalent ones. To surpass this disadvantage we synthesized a new class of GG hydrogels crosslinkable by both physical and chemical mechanisms. MeGG was prepared by the methacrylation of GG polymer (Figure V.1.A). The spectra of GG obtained at 50 ºC (Figure V.1.B) showed the presence of four characteristic peaks that correspond to -CH of rhamnose (δ 5.29 ppm), -CH of glucuronic acid (δ 5.11 ppm), -CH of glucose (δ 4.88 ppm) and -CH$_3$ of rhamnose (δ 1.45 ppm). ^{1}H-NMR spectroscopy confirmed the methacrylation of GG by the appearance of distinctive peaks in the double bond region (δ 5.50-7.00 ppm) and a sharp peak that corresponds to the -CH$_3$ of the methacrylate groups (δ 2.09 ppm) on the modified GG spectra. Figure V.1.C and Figure V.1.D show the ^{1}H-NMR spectra of methacrylated GG with low and high degrees of methacrylation, respectively. Degree of methacrylation for Low-MeGG and High-MeGG was calculated by the ratio of average intensity of the methyl proton peaks of the methacrylate groups over the average intensity of the methyl groups of the rhamnose. For the Low-MeGG (Figure V.1.C), for each repeating unit on the polymer chain there is 0.15 methacrylate groups covalently linked to the polymer. On the other hand, 1.24 methacrylate groups were

found in each repeating unit for the High-MeGG of methacrylation material (Figure V.1.D). With the integral of the double bond peaks of the methacrylate group protons and the methyl protons of rhamnose, it is possible to approximate a percentage of degree of substitution (DS), as mentioned in Eq (1). Therefore, the average DS increased from 1.2% (Low-MeGG) to 11.25% (High-MeGG), when the volume of methacrylic anhydride added to the reaction was quadruplicated.
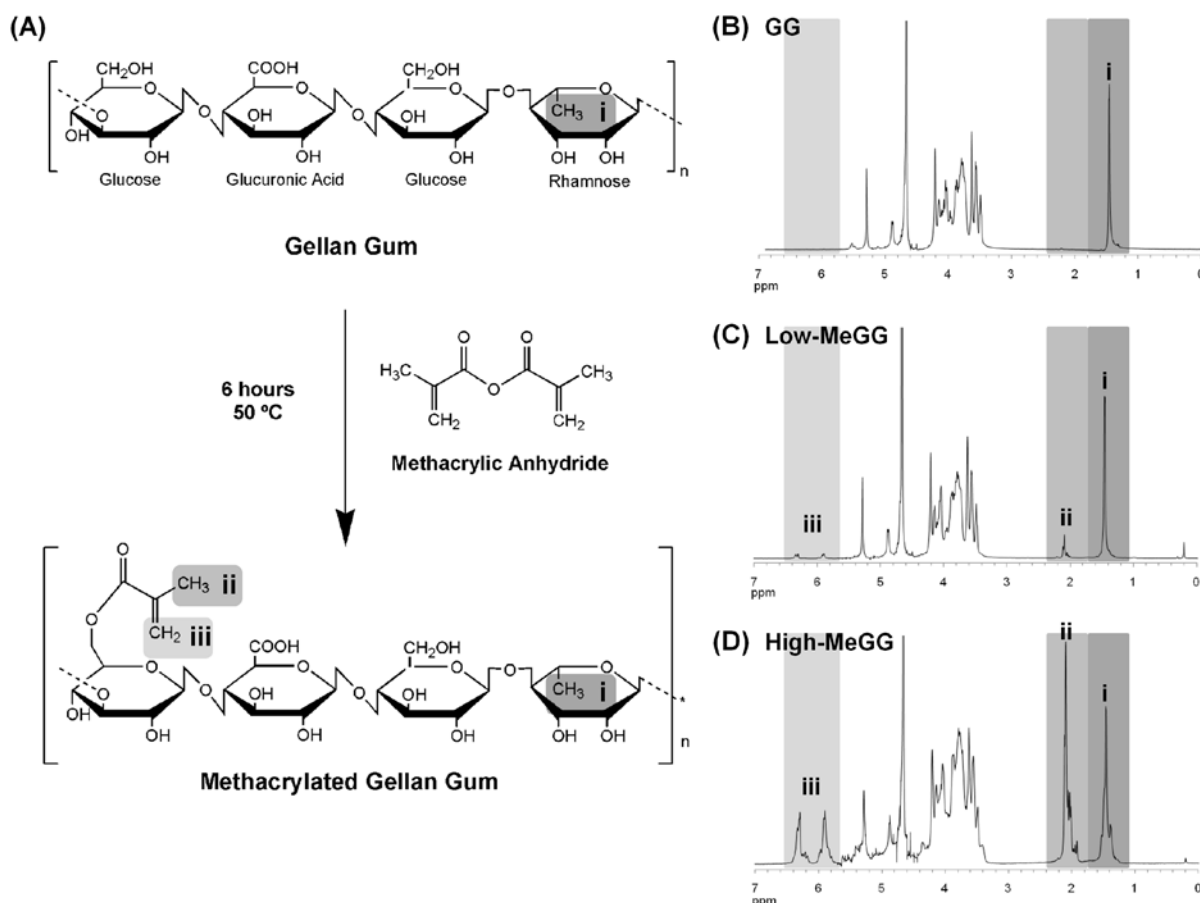
Figure V.1. (A) Schematic illustration of the synthesis of MeGG. ^{1}H-NMR spectra (T=50 °C) of (B) GG, (C) Low-MeGG and (D) High-MeGG recorder in D_2O. Methyl group of the MA (ii) was located at δ 2.09 ppm and vinyl groups of the MA (iii) were identified around δ 5.5-7 ppm.

The methacrylation of GG was also confirmed by FTIR-ATR by the appearance of the carbon double bond peak at 1640 cm^{-1}, known to be present in methacrylate groups but not in GG chains (Figure V.2). Moreover, the characteristic C=O peak of the ester bond appeared around 1770-1680 cm^{-1} and increased in intensity with increasing degree of methacrylation.
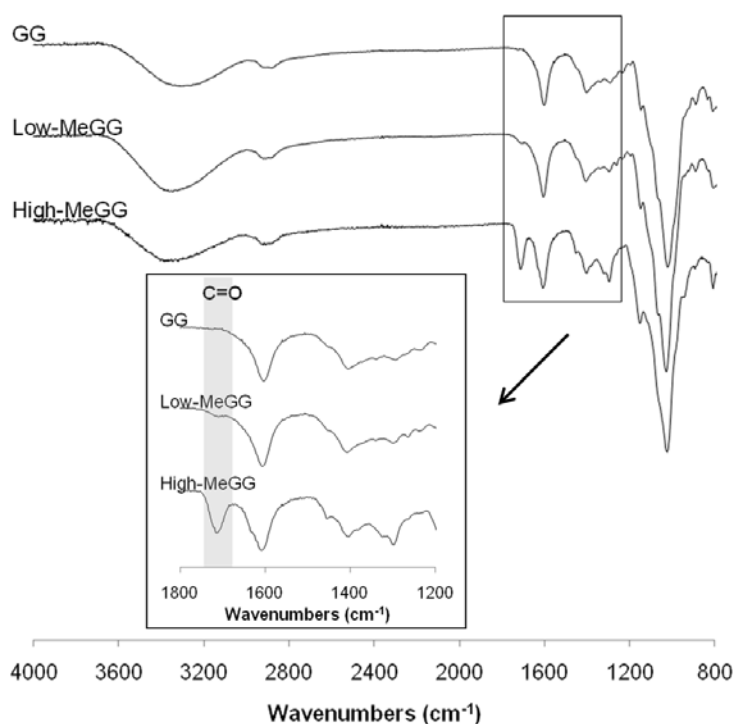
Figure V.2. FTIR-ATR spectra of GG, Low-MeGG and High-MeGG. The shoulder appearing around 1640 cm^{-1} corresponds to the C=C bond of the MA and is present on both Low-MeGG and High-MeGG. The absorption band present around 1770-1680 cm^{-1} corresponds to the C=O bond of the ester introduced in the chain.

3.2. Fabrication of MeGG hydrogels

GG is capable of physical gelation. As the temperature of a solution of the GG in water is decreased, GG chains undergo a conformational thermo-reversible change from random coils to double helices [26]. Then, the aggregation of the double helical elements occurs to form a three-dimensional (3D) network by hydrogen bonding with water. The gelation of GG is strongly affected by the presence of specific cations, namely Na$^+$, K$^+$, Ca^{2+} and Mg^{2+} although divalent cations promote a more efficient gelation than monovalent cations [29]. It was observed that after the methacrylation, Low-MeGG was still able to form a hydrogel in response to temperature decrease and in the presence of cations. Besides these physical crosslinking procedures, MeGG was also chemically crosslinked by UV exposure. Figure V.3 represents a schematics of the crosslinking mechanisms used in this study to produce each hydrogel: P for physical crosslinking by addition of Ca^{2+}; C for chemical crosslinking by UV exposure; and PC when samples were both physically and chemically crosslinked by addition of Ca^{2+} ions and by UV exposure. The physical crosslinking by temperature decrease was present for all samples.
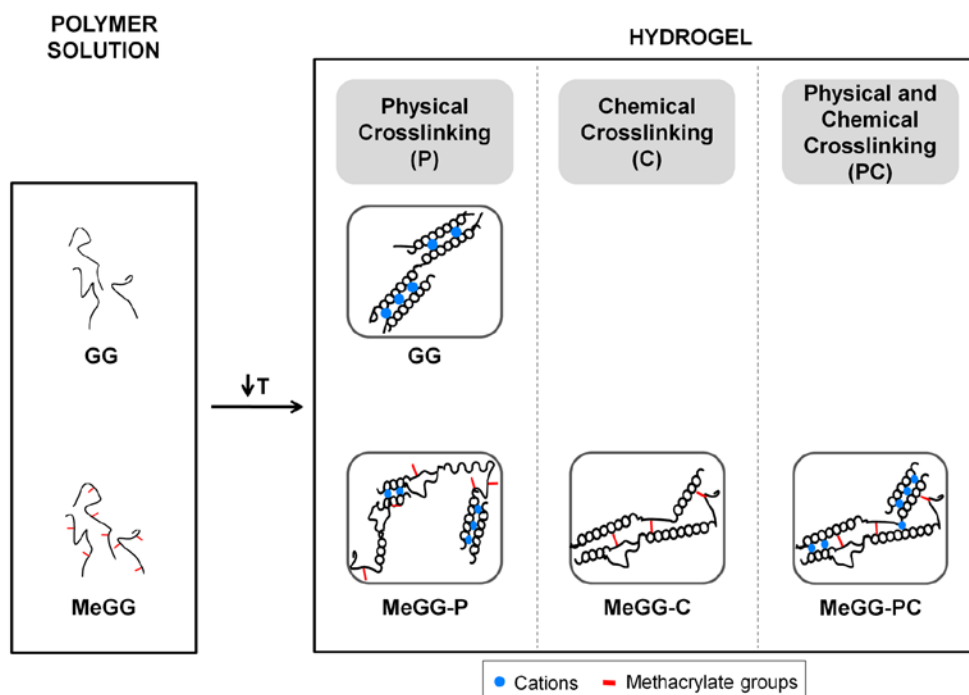
Figure V.3. Possible crosslinking mechanisms for GG, Low-MeGG and High-MeGG hydrogels. MeGG schematically represents both degrees of methacrylations. For all the materials, the physical crosslinking by temperature decrease was used. Upon temperature decrease, GG and MeGG chains randomly transit from a coil to a helix form. Physical crosslinking occurs when cations are present and a more stable hydrogel is formed through ionic bonding. Chemical crosslinking occurs if hydrogels are exposed to UV, allowing the double bonds of the methacrylate groups to react with each other. Physical and chemical crosslinking will occur when these mechanisms are combined.

3.3. Swelling kinetics of MeGG to ionic solutions

The swelling kinetics of MeGG hydrogels *in vitro* was assessed by immersing the hydrogels in solutions with different amounts and types of cations (Figure V.4). Crosslinked hydrogels were prepared with different types of crosslinking by combining the presence of cations and the exposure to UV. The difference in their wet weight over time reflects changes in their chemical and physical structure. Samples of plain GG were disintegrated after 30 min. Distilled water has no ions. Therefore, the less crosslinked hydrogel networks quickly uptake water, losing their integrity over time. On the other hand, modified hydrogels with the least crosslinked network (Low-MeGG-C) presented the highest swelling of almost 750% after 30 min of immersion in water (Figure V.4.A) (***$p<0.0001$). The High-MeGG hydrogels have more hydrophobic methacrylate groups in the chain. This, combined with a more crosslinked network due to photocrosslinking, led to a significantly lower water uptake for these hydrogels (***$p<0.0001$).

To study the effect of ionic solutions on MeGG and GG hydrogel swelling kinetics, hydrogels were immersed in both PBS (Figure V.4.B) and DMEM (Figure V.4.C) for 28 and 24 hours, respectively. In contrast to their behavior in water, all hydrogels rapidly shrank when immersed in solutions with cations. The presence of ions in these solutions increases the double helix formation and the establishment of junction zones, leading to the formation of more crosslinked networks [34]. When immersed in PBS, High-MeGG samples present a significant shrinking (***p<0.0001) as compared with the Low-MeGG samples, possibly because of the higher amount of hydrophobic methacrylic groups in the High-MeGG repulses water molecules from the bulk to outside of the hydrogel. Similarly, Qiang Li *et al* reported [35] a lower swelling ratio with increasing acrylate content in polyphosphoester hydrogels. A sharper decrease was registered for High-MeGG-PC, presenting a significant deswelling of nearly 60% after 30 min of immersion in PBS (**p<0.001 when compared to High-MeGG-C, ***p<0.0001 when compared to all other samples). Interestingly, when immersed in DMEM, where both mono and divalent cations are present, hydrogels showed lower shrinking (deswelling) than in PBS. This may be a result of the higher concentration of monovalent cations in media. Therefore, the divalent cations used to keep hydrogels physically crosslinked will be exchanged by monovalent ones, leading to the formation of less crosslinked networks, as described elsewhere [36].

We hypothesize that this is a result of an ionic crosslinking of the hydrogels with the cations present in the solutions. A similar result was reported with alginate hydrogels [36] where shrinking of the hydrogels occurred when immersed in a medium containing higher Ca^{2+} concentration. To further confirm the ionic nature of the hydrogel shrinking, samples were immersed in water for 30 min, followed by immersion in PBS for 20 hours to allow hydrogel crosslinking. Shrunken samples were again placed in water for 30 min allowing them to regain their original shape (Figure V.4.D). It was observed that hydrogels swelled in water, deswelled when immersed in PBS and swelled again when immersed in water. This experiment confirmed the ionic nature of swelling-deswelling behavior of MeGG hydrogels. It also shows the possibility to control the physical properties of the developed MeGG hydrogels, by changing the solution in which they are immersed.
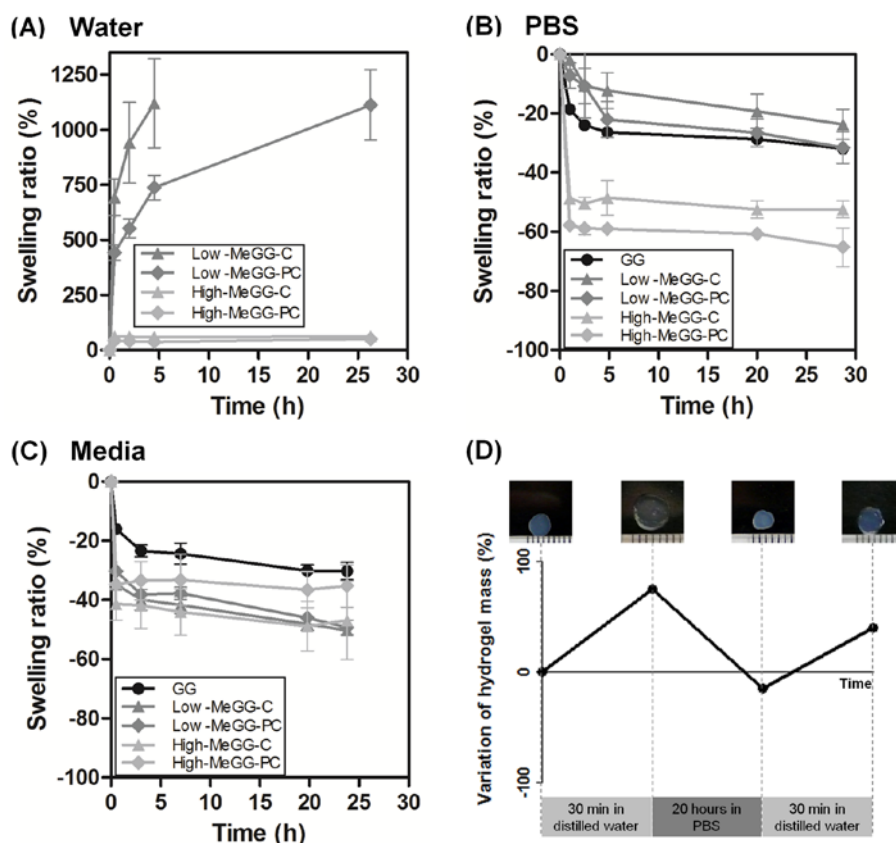
Figure V.4. Swelling kinetics of GG and MeGG hydrogels in solutions with different ionic content: (A) water (no ions), (B) PBS (monovalent ions) and (C) DMEM with 10% FBS (mono and divalent ions). GG was not stable in water and dissolves in 30 min. Hence, swelling could not be carried out. (D) Confirmation of the ionic nature of the hydrogel shrinking behavior when immersed in PBS. High-MeGG hydrogels were used has an example. Samples were immersed in water for 30 min, then placed in a PBS solution for 20 hours and again immersed in water for 30 min. The weight and size of the samples varied with the presence or absence of ions in the solution.

3.4. Tunable mechanical properties

The tissue stiffness can vary greatly depending on the function of the tissue in the body [37]. Therefore, when designing a biomaterial for enhancing tissue regeneration, it is of utmost importance to match the material stiffness with that of natural tissues. The use of both physical and chemical mechanisms to crosslink hydrogels gives the possibility to tune this property.

It is known that ionically crosslinked hydrogels exhibit weak mechanical properties [38]. This limitation can be overcome by the introduction of acrylate groups followed by photocrosslinking. Here we combined physical and chemical crosslinking mechanisms to fabricate MeGG with wide range of mechanical properties. The influence of three parameters over the mechanical properties was evaluated: ion concentration in the hydrogel fabrication

(Figure V.5.A), type of crosslinking mechanism (Figure V.5.B) and polymer concentration (Figure V.5.C), while keeping the other conditions constant. To study the mechanical properties of fabricated hydrogels, compression testing was performed on GG and MeGG hydrogels. Despite stable hydrogel formation, High-MeGG-P samples were too weak to test mechanically.
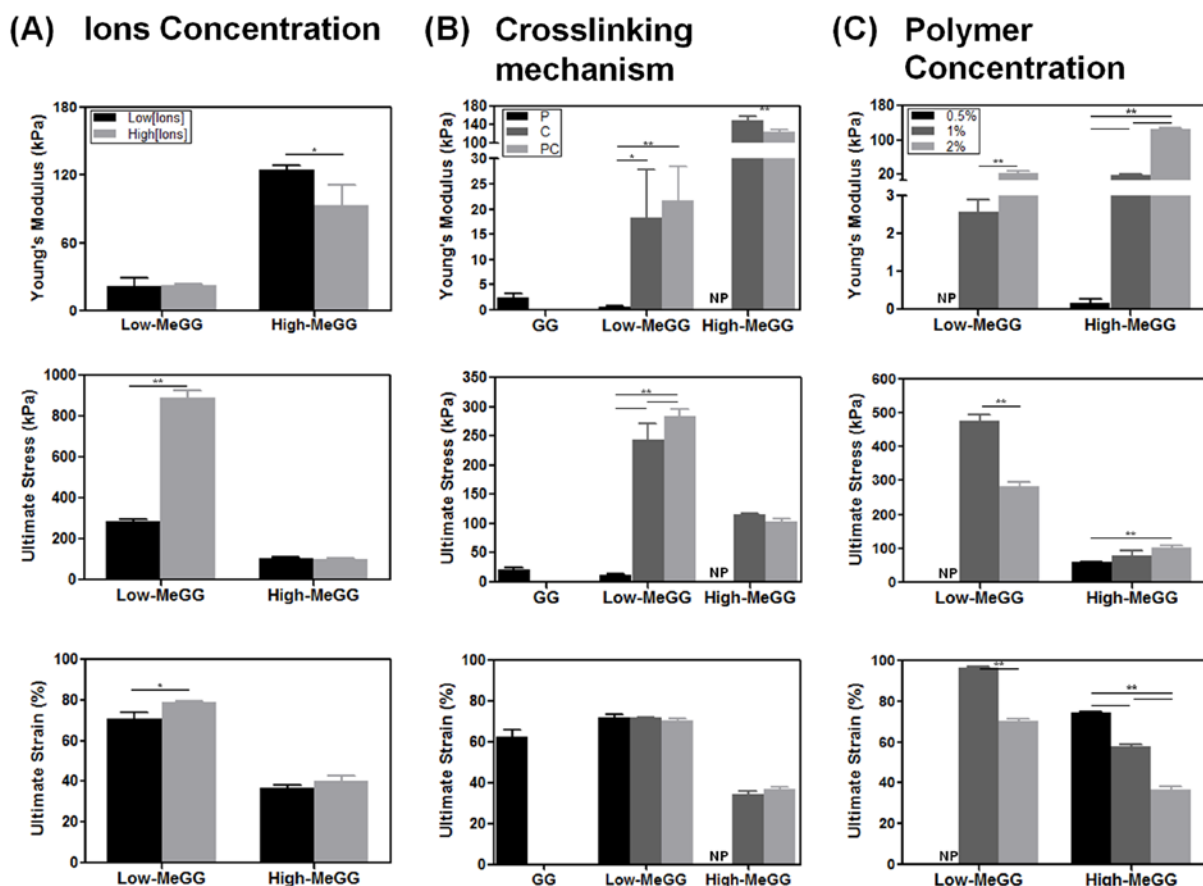
Figure V.5. Mechanical properties of GG and MeGG hydrogels: Young's Modulus, Ultimate stress and Ultimate strain. The influence of three parameters over the mechanical properties of the hydrogels was evaluated: (A) Concentration of ions in the hydrogel fabrication; (B) Type of crosslinking mechanism (P, C or PC); and (C) Polymer concentration. The mechanical properties of the developed hydrogels showed to be highly dependent on the ionic content, type of crosslinking, methacrylation degree and polymer concentration. Statistical analysis through two-way ANOVA and Bonferroni post-hoc test showed significant differences (***$p<0.0001$, **$p<0.001$, *$p<0.01$) between the analyzed groups. NP: not processable.

3.4.1. Effect of Ca²⁺ in the hydrogel fabrication

As assessed by the swelling kinetics assay, the hydrogel response was strongly influenced by the presence of cations in the solution. Hence, we tested the effect of varying the

concentration of Ca^{2+} ions present during hydrogel fabrication on the resulting gel's mechanical properties. Figure V.5.A shows the influence of the concentration of ions over the entanglement of the hydrogel network. For Low-MeGG hydrogels, the increase in concentration of ions from 0.08 mg/mL to 0.12 mg/mL showed no influence on the Young's modulus but a significant increase on the ultimate stress (**$p<0.001$) and ultimate strain (*$p<0.01$) of these hydrogels. On the other hand, a higher amount of Ca^{2+} ions used in the fabrication of the High-MeGG hydrogels significantly decreased the Young's modulus. Similarly, a marked decrease in the mechanical properties was observed in calcium-alginate hydrogels immersed in physiological baths of NaCl and $CaCl_2$ [39]. Moreover, the same ionic concentration on the fabrication process resulted in hydrogels with different stiffness depending on the degree of methacrylation. A significantly stiffer (***$p<0.0001$) hydrogel was obtained for High-MeGG in the presence of ions as compared to Low-MeGG. Interestingly, High-MeGG hydrogels were significantly less resistant (***$p<0.0001$) to fracture and to elongation compared to the Low-MeGG hydrogels. This might result from an excessive crosslinking of hydrogels due to their higher degree of methacrylation, leading to the formation of a brittle hydrogel [40]. These results demonstrate that the use of ions as a crosslinking agent affected Low-MeGG and High-MeGG hydrogels in opposite ways.

3.4.2. Effect of crosslinking mechanism

As previously described [41, 42], the crosslinking mechanisms used to fabricate the hydrogels significantly influenced their mechanical properties (Figure V.5.B). When only the physical mechanism was employed, the value of Young's modulus and ultimate stress of hydrogels significantly decreased (***$p<0.0001$) with increase in the degree of methacrylation of the materials. For higher degree of methacrylation, the sites available for ionic interactions between polymer chains are less, since the chain is occupied by methacrylate groups, as schematized in Figure V.3. Therefore, the ionic bonding may be weaker for the polymer chains with higher content of methacrylate groups.

The chemical crosslinking alone led to the development of hydrogels with significantly higher Young's modulus (**$p<0.001$) and ultimate stress (*$p<0.01$) values, when compared to those fabricated only with physical mechanism. Since GG is not chemically crosslinkable, only physical crosslinked GG is represented in Figure V.5.B.

The coupling effect of physical and chemical crosslinking mechanisms significantly decreased the stiffness of High-MeGG hydrogels, and did not influence the stiffness of the Low-MeGG hydrogels. A similar result was observed when the concentration of ions in the hydrogel production is increased (Figure V.5.A). Though, similar tendency was observed when the mechanisms are used alone, a significantly higher Young's modulus and lower

ultimate stress and strain values (***$p<0.0001$) were observed with the increase in the methacrylation degree.

3.4.3. Effect of polymer concentration

It is known that the polymer concentration exerts a great effect over the mechanical properties of hydrogels [41]. Therefore, three different concentrations (0.5, 1, 2% w/v) were tested for the PC samples of both low and high degree of methacrylation (Figure V.5.C). Stable hydrogels of 0.5% (w/v) of Low-MeGG could not be produced. The Young's modulus of the hydrogels significantly increased as the amount of polymer in the hydrogel network increased. Also, the capacity of High-MeGG samples to resist fracture significantly increased whereas significantly decreasing for the Low-MeGG hydrogels (**$p<0.001$). This increase of polymer concentration also led to a significant decrease on the elongation capacity of the materials (**$p<0.001$). Polymer concentration is known to influence the helix content in GG solutions [43]. As the concentration of GG polymer increases in solution, the helix content increases, leading to more intensive aggregation of the chains and to a stronger physical and chemical crosslinking.

Overall, combination of physical and chemical crosslinking mechanisms resulted in MeGG hydrogels with a wide range of mechanical properties. Therefore, hydrogels with biologically relevant stiffness values in the range of 0.15 to 148 kPa could be fabricated by means of physiologically feasible crosslinking mechanisms. Ultimate stress varied from 11.7 kPa to 889.5 kPa whereas ultimate strain values were in the range of 34.2 to 96.1%. Such tunable mechanical properties of hydrogels could be useful for tissue engineering applications ranging from soft tissues, as the brain to stiff tissues, as the collagenous bone [32].

3.5. Tunable degradation properties

The rate of tissue regeneration is dependent on the microenvironment and the tissue function [44]. Therefore, the development of a biomaterial that can degrade at a similar rate at which the new tissue is being formed is of utmost importance. Understanding the degradation behavior of polymers aimed to be used in tissue engineering applications is important to predict and ultimately tune their behavior in the *in vivo* environment. To our knowledge, so far no previous study has looked into the degradation mechanism of GG *in vitro*. However, hydrolytic degradation of polysaccharides as GG and MeGG can be usually achieved *in vivo* through the action of enzymes such as lysozyme or amylase. Moreover, the *in vivo* degradation of GG hydrogels was already assessed, showing that GG degrades *in vivo* [18]. Also, it was already reported that methacrylated hydrogels can be degraded *in vivo* [11]. In contrast with other hydrogels [45], GG and MeGG are quite stable in PBS due to the ionic

crosslinking, as described in a previous section, where we did not find any degradation in PBS. Hence, to compare the relative differences in mass loss over time between the different hydrogel networks the hydrolytic degradation was performed in accelerated condition with a sodium hydroxide 0.1 mM solution, as described previously [46]. Figure V.6 shows the *in vitro* accelerated hydrolytic degradation of GG and MeGG hydrogels. As expected, the crosslinking mechanisms used to produce the hydrogel led to different degradation profiles. Specifically, the physical crosslinking combined with chemical crosslinking mechanisms prolonged the rate of degradation as compared to only chemically crosslinked hydrogels. Moreover, High-MeGG hydrogels showed a slower degradation profile in comparison to Low-MeGG hydrogels, as reported by Oju Jeon *et al* for photocrosslinked alginate hydrogels [47].
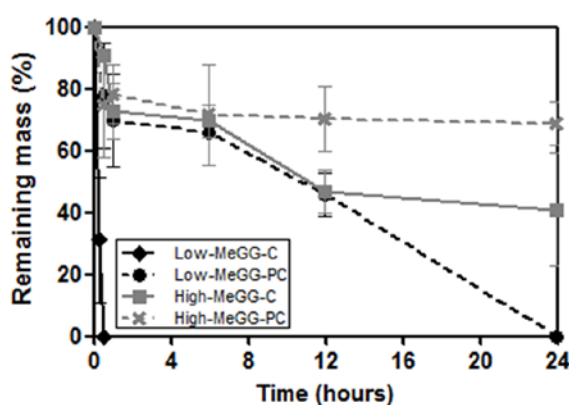
Figure V.6. *In vitro* hydrolytic degradation kinetics of the hydrogels in NaOH (0.1 mM) at 37 °C.

3.6. *In vitro* cell viability of NIH-3T3 cells encapsulated in MeGG

Previous studies [18, 21, 48] have demonstrated that GG hydrogels can adequately support the growth and ECM deposition of human articular chondrocytes *in vivo*. Here we studied the viability of photoencapsulated NIH-3T3 cells in the MeGG hydrogels by Live/Dead assay (Figure V.7). We evaluated the cell viability immediately after the fabrication to assess the effect of the crosslinking mechanisms on the cell viability. The UV exposure and the toxicity of the methacrylate groups of the modified GG showed no significant effect on the viability of encapsulated cells. These results further confirmed the biocompatibility of MeGG for cell encapsulation.
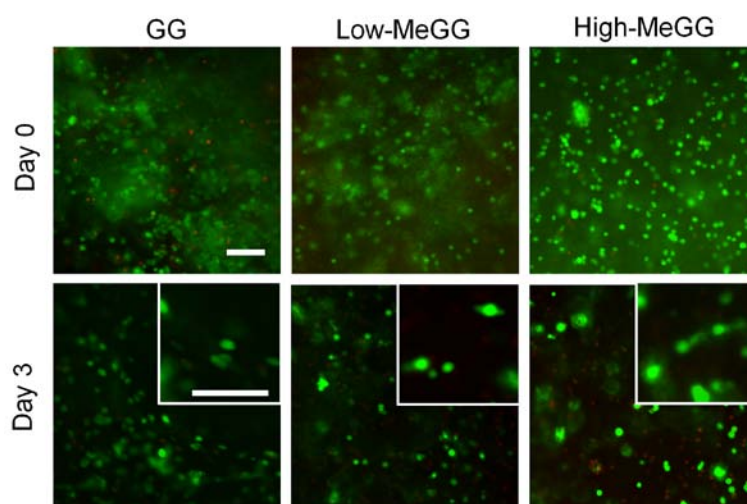
Figure V.7 Representative fluorescence micrographs of live (green) and dead (red) encapsulated NIH-3T3 cells in GG, Low-MeGG and High-MeGG immediately after encapsulation (day 0) and cultured *in vitro* for 3 days. The scale bars indicate 100 μm.

4. CONCLUSIONS

MeGG hydrogels were synthesized by reacting GG with different amounts of methacrylic anhydride, yielding to the development of hydrogels with two different degrees of methacrylation. The combination of physical crosslinking methods (temperature and the addition of cations) with chemical crosslinking approaches (through photocrosslinking), enabled the development of MeGG hydrogels with highly tunable physical and mechanical properties without affecting their biocompatibility. In summary, physiologically compatible crosslinking methods were used for the development of highly tunable hydrogels applicable for a wide range of tissue engineering applications.

REFERENCES

1. Qiu Y, Park K. Environment-sensitive hydrogels for drug delivery. Adv Drug Deliv Rev 2001;53(3):321-339.
2. Hoffman AS. Hydrogels for biomedical applications. Adv Drug Deliv Rev 2002;54(1):3-12.
3. Caldorera-Moore M, Peppas NA. Micro- and nanotechnologies for intelligent and responsive biomaterial-based medical systems. Adv Drug Deliv Rev 2009;61(15):1391-1401.
4. Peppas NA, Hilt JZ, Khademhosseini A, Langer R. Hydrogels in biology and medicine: From molecular principles to bionanotechnology. Adv Mater 2006;18(11):1345-1360.
5. Rabanel J, Bertrand N, Sant S, Louati S, Hildgen P. Polysaccharide hydrogels for the preparation of immunoisolated cell delivery systems. In: RH Marchessault, Ravenelle F, Zhu X, editors. Polysaccharides for Drug Delivery and Pharmaceutical Applications. Washington: Amer Chemical Soc, 2006. p. 305.
6. Chung HJ, Park TG. Self-assembled and nanostructured hydrogels for drug delivery and tissue engineering. Nano Today 2009;4(5):429-437.
7. Jeong B, Kim SW, Bae YH. Thermosensitive sol-gel reversible hydrogels. Adv Drug Deliv Rev 2002;54(1):37-51.
8. Hennink WE, van Nostrum CF. Novel crosslinking methods to design hydrogels. Adv Drug Deliv Rev 2002;54(1):13-36.
9. Van Tomme SR, Storm G, Hennink WE. In situ gelling hydrogels for pharmaceutical and biomedical applications. Int J Pharm 2008;355(1-2):1-18.
10. Ifkovits JL, Burdick JA. Review: Photopolymerizable and degradable biomaterials for tissue engineering applications. Tissue Eng 2007;13(10):2369-2385.
11. Hahn SK, Park JK, Tomimatsu T, Shimoboji T. Synthesis and degradation test of hyaluronic acid hydrogels. Int J Biol Macromol 2007;40(4):374-380.
12. Khademhosseini A, Eng G, Yeh J, Fukuda J, Blumling J, Langer R, Burdick JA. Micromolding of photocrosslinkable hyaluronic acid for cell encapsulation and entrapment. J Biomed Mater Res A 2006;79A(3):522-532.
13. Oudshoorn MHM, Rissmann R, Bouwstra JA, Hennink WE. Synthesis of methacrylated hyaluronic acid with tailored degree of substitution. Polymer 2007;48(7):1915-1920.
14. Van den Bulcke AI, Bogdanov B, De Rooze N, Schacht EH, Cornelissen M, Berghmans H. Structural and rheological properties of methacrylamide modified gelatin hydrogels. Biomacromolecules 2000;1(1):31-38.
15. Benton JA, DeForest CA, Vivekanandan V, Anseth KS. Photocrosslinking of Gelatin Macromers to Synthesize Porous Hydrogels That Promote Valvular Interstitial Cell Function. Tissue Eng Part A 2009;15(11):3221-3230.
16. Chou AI, Akintoye SO, Nicoll SB. Photo-crosslinked alginate hydrogels support enhanced matrix accumulation by nucleus pulposus cells in vivo. Osteoarthritis Cartilage 2009;17(10):1377-1384.
17. Chou AI, Nicoll SB. Characterization of photocrosslinked alginate hydrogels for nucleus pulposus cell encapsulation. J Biomed Mater Res A 2009;91A(1):187-194.
18. Oliveira JT, Santos TC, Martins L, Picciochi R, Marques AP, Castro AG, Neves NM, et al. Gellan Gum Injectable Hydrogels for Cartilage Tissue Engineering Applications: In Vitro Studies and Preliminary In Vivo Evaluation. Tissue Eng Part A 2009;16(1):343-353.
19. Oliveira JT, Santos TC, Martins L, Silva MA, Marques AP, Castro AG, Neves NM, et al. Performance of new gellan gum hydrogels combined with human articular chondrocytes for cartilage regeneration when subcutaneously implanted in nude mice. J Tissue Eng Regen Med 2009;3(7):493-500.
20. Gong YH, Wang CM, Lai RC, Su K, Zhang F, Wang DA. An improved injectable polysaccharide hydrogel: modified gellan gum for long-term cartilage regeneration in vitro. J Mater Chem 2009;19(14):1968-1977.
21. Oliveira JT, Gardel L, Martins L, Rada T, Gomes ME, Reis RL. Injectable gellan gum hydrogels with autologous cells for the treatment of rabbit articular cartilage defects. Journal of Orthopedic Research 2010;in press.
22. Oliveira JT, Martins L, Picciochi R, Malafaya PB, Sousa RA, Neves NM, Mano JF, et al. Gellan Gum: A New Biomaterial for Cartilage Tissue Engineering Applications. J Biomed Mater Res A 2010.
23. Carlfors J, Edsman K, Petersson R, Jornving K. Rheological evaluation of Gelrite (R) in situ gels for ophthalmic use. Eur J Pharm Sci 1998;6(2):113-119.

24. Rozier A, Mazuel C, Grove J, Plazonnet B. Gelrite®: A novel, ion-activated, in-situ gelling polymer for ophthalmic vehicles. Effect on bioavailability of timolol. Int J Pharm 1989;57(2):163-168.
25. Jansson PE, Lindberg B, Sandford PA. Structural studies of Gellan Gum, an extracellular polysaccharide elaborated by pseudomonas-elodea. Carbohydr Res 1983;124(1):135-139.
26. Miyoshi E, Takaya T, Nishinari K. Rheological and thermal studies of gel-sol transition in gellan gum aqueous solutions. Carbohydr Polym 1996;30:109-119.
27. Matricardi P, Cencetti C, Ria R, Alhaique F, Coviello T. Preparation and Characterization of Novel Gellan Gum Hydrogels Suitable for Modified Drug Release. Molecules 2009;14(9):3376-3391.
28. Caggioni M, Spicer PT, Blair DL, Lindberg SE, Weitz DA. Rheology and microrheology of a microstructured fluid: The gellan gum case. J Rheol 2007;51(5):851-865.
29. Singh BN, Kim KH. Effects of divalent cations on drug encapsulation efficiency of deacylated gellan gum. J Microencapsul 2005;22(7):761-771.
30. Ogawa E, Takahashi R, Yajima H, Nishinari K. Thermally induced coil-to-helix transition of sodium gellan gum with different molar masses in aqueous salt solutions. Biopolymers 2005;79(4):207-217.
31. Tako M, Teruya T, Tamaki Y, Konishi T. Molecular origin for rheological characteristics of native gellan gum. Colloid Polym Sci 2009;287(12):1445-1454.
32. Engler AJ, Sen S, Sweeney HL, Discher DE. Matrix elasticity directs stem cell lineage specification. Cell 2006;126(4):677-689.
33. Hamcerencu M, Desbrieres J, Khoukh A, Popa M, Riess G. Synthesis and characterization of new unsaturated esters of Gellan Gum. Carbohydr Polym 2008;71(1):92-100.
34. Miyoshi E, Takaya T, Nishinari K. Rheological and thermal studies of gel-sol transition in gellan gum aqueous solutions. Carbohydr Polym 1996;30(2-3):109-119.
35. Li Q, Wang J, Shahani S, Sun D, Sharma B, Elisseeff J, Leong K. Biodegradable and photocrosslinkable polyphosphoester hydrogel. Biomaterials 2006;27(7):1027-1034.
36. Kuo CK, Ma PX. Maintaining dimensions and mechanical properties of ionically crosslinked alginate hydrogel scaffolds in vitro. J Biomed Mater Res A 2008;84A(4):899-907.
37. Nemir S, West JL. Synthetic Materials in the Study of Cell Response to Substrate Rigidity. Ann Biomed Eng 2009;38(1):2-20.
38. Jagur-Grodzinski J. Polymeric gels and hydrogels for biomedical and pharmaceutical applications. Polym Adv Technol;21(1):27-47.
39. LeRoux MA, Guilak F, Setton LA. Compressive and shear properties of alginate gel: Effects of sodium ions and alginate concentration. J Biomed Mater Res 1999;47(1):46-53.
40. Tang Q, Sun X, Li Q, Wu J, Lin J. Fabrication of a high-strength hydrogel with an interpenetrating network structure. Colloids Surf A Physicochem Eng Asp 2009;346(1-3):91-98.
41. Brigham MD, Bick A, Lo E, Bendali A, Burdick JA, Khademhosseini A. Mechanically Robust and Bioadhesive Collagen and Photocrosslinkable Hyaluronic Acid Semi-Interpenetrating Networks. Tissue Eng Part A 2009;15(7):1645-1653.
42. Anseth KS, Bowman CN, BrannonPeppas L. Mechanical properties of hydrogels and their experimental determination. Biomaterials 1996;17(17):1647-1657.
43. Dai L, Liu XX, Liu YL, Tong Z. Concentration dependence of critical exponents for gelation in gellan gum aqueous solutions upon cooling. Euro Polym J 2008;44(12):4012-4019.
44. Liu CZ, Czernuszka JT. Development of biodegradable scaffolds for tissue engineering: a perspective on emerging technology. Mater Sci Technol 2007;23(4):379-391.
45. Meyvis TKL, De Smedt SC, Demeester J, Hennink WE. Influence of the degradation mechanism of hydrogels on their elastic and swelling properties during degradation. Macromolecules 2000;33(13):4717-4725.
46. Nijst CLE, Bruggeman JP, Karp JM, Ferreira L, Zumbuehl A, Bettinger CJ, Langer R. Synthesis and Characterization of Photocurable Elastomers from Poly(glycerol-co-sebacate). Biomacromolecules 2007;8(10):3067-3073.
47. Jeon O, Bouhadir KH, Mansour JM, Alsberg E. Photocrosslinked alginate hydrogels with tunable biodegradation rates and mechanical properties. Biomaterials 2009;30(14):2724-2734.
48. Oliveira JT, Santos TC, Martins L, Picciochi R, Marques AP, Castro AG, Neves NM, et al. Gellan Gum Injectable Hydrogels for Cartilage Tissue Engineering Applications: In Vitro Studies and Preliminary In Vivo Evaluation. Tissue Engineering: Part A 2009;15.

APPENDIX

Supplementary Figure V.S1

The values of the Young's Modulus, Ultimate stress and Ultimate strain represented in Figure V.5 were calculated using the stress-strain curves depicted in Figure V.S1, obtained during the compression mechanical analysis.
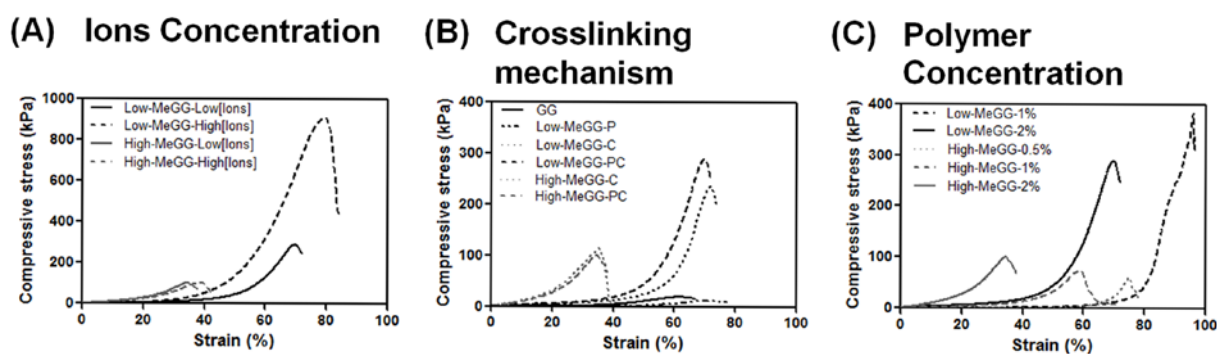
Figure V.S1. Stress vs. Strain curve of GG and MeGG hydrogels. The influence of three parameters over the mechanical properties of the hydrogels was evaluated: (A) Concentration of ions in the hydrogel fabrication; (B) Type of crosslinking mechanism (P, C or PC); and (C) Polymer concentration.

Chapter VI

*MICROFABRICATED PHOTOCROSSLINKABLE POLYELECTROLYTE-COMPLEX OF
CHITOSAN AND METHACRYLATED GELLAN GUM*

CHAPTER VI [*]

MICROFABRICATED PHOTOCROSSLINKABLE POLYELECTROLYTE-COMPLEX OF CHITOSAN AND METHACRYLATED GELLAN GUM

ABSTRACT

Chitosan (CHT)-based polyelectrolyte complexes (PECs) have been receiving great attention for tissue engineering approaches. These hydrogels are held together by molecular entanglements or ionic forces and can be disrupted by changes in physiological conditions, such as pH or ionic charges. In this study we present a new class of CHT-based PEC hydrogels amenable to stabilization by chemical crosslinking. The photocrosslinkable anionic polysaccharide methacrylated gellan gum (MeGG) was complexed with CHT and exposed to light, forming a PEC hydrogel. Experimental results revealed that with increasing MeGG content, fibrous structures were formed over the pores of the hydrogels. The chemical structure of the MeGG-CHT photocrosslinkable PEC hydrogels was analyzed using Fourier transform infrared spectroscopy (FTIR), revealing absorption peaks specific to the raw polymers. A significantly higher swelling ratio was observed for the PEC hydrogel with higher CHT content, when compared with MeGG hydrogel alone. The molecular interactions between both polysaccharides were evaluated by FTIR and X-ray photoelectron spectroscopy (XPS), indicating the diffusion of CHT to the interior of the hydrogel. Confocal and transmission electron microscopy (TEM) validated these findings. We hypothesized that the addition of MeGG to CHT solution first leads to a membrane formation around MeGG. Then, the migration of CHT inside the MeGG hydrogel occurs to balance the electrostatic charges inside and outside the PEC complex. The photocrosslinkable feature of MeGG further allowed the formation of cell-laden microscale hydrogel units with different shapes and sizes, indicating the possibility of replicating the *in vivo* microscale features of tissues. Overall, this system is potentially useful for a variety of applications including fabrication of cell encapsulated microscale hydrogel units for modular tissue engineering.

KEYWORDS: Hydrogel; Chitosan; Methacrylated Gellan Gum; Microfabrication; Polyelectrolyte complex; Modular tissue engineering.

---

1. INTRODUCTION

Hydrogels have been selected for the development of engineered tissues, either as scaffolds for supporting cell growth [1] or as cell carrier and delivery systems [2], mainly due to their structural similarity with the extracellular matrix (ECM) of tissues. Hydrogels resemble the ECM due to their highly hydrated three-dimensional (3D) structure and diffusive transport characteristics [3]. Additionally, they can be processed under cell-compatible conditions [4]. Hydrogels typically present many functional groups (amino, carboxylic and hydroxyl groups) available for chemical modification and/or conjugation with other molecules. This allows engineering their properties such as cellular attachment, molecular response, structural integrity, biodegradability, biocompatibility, and micro/nanoscale processing [5, 6].

Various hydrogels were shown to influence cell attachment [7], proliferation [8], and differentiation [9]. Hence, a new class of hydrogels are currently being synthesized with the focus on replicating the microenvironmental characteristics of tissues, such as cell attachment [4], mechanical properties [10], and biodegradability [11]. Natural and synthetic polymers were previously used for the production of hydrogels [12-14]. Among these, chitosan (CHT)-based hydrogels are attractive due to the high availability of CHT from naturally renewable and inexpensive sources, its reported biocompatibility, and biodegradability by enzymes present in human tissues [15-17]. CHT is a linear polysaccharide composed of randomly distributed β-(1-4)-linked D-glucosamine and N-acetyl-D-glucosamine units, being positively charged at a pH of 6.3 [18]. CHT can be obtained by the deacetylation of chitin and the number of amino groups is directly correlated with the degree of deacetylation [19]. CHT-based hydrogels can be formed either by chemical crosslinking through the addition of organic precursors or catalysts or by physical association with small anionic molecules or large negatively charged polymer chains [17, 20]. The advantages of the later class of hydrogels are significant since they reduce the cross-reactions of the precursors in the body [20]. These hydrogels are often designated as polyelectrolyte complex (PEC) hydrogels, as polyelectrolyte chains of one polymer complex with the chains of an oppositely charged polymer [21, 22]. CHT-based PEC networks have been developed with a number of anionic polymers, such as hyaluronic acid [23], carrageenan [13, 24], alginate [25], xanthan gum [26], and collagen [27]. Gellan gum (GG) is an anionic polysaccharide that has been applied in the clinic and showed potential for tissue engineering applications, mainly due to its tunable mechanical properties and promising results in cartilage tissue engineering [14, 28-30]. GG is composed of a tetrasaccharide repeating unit of two β-D-glucose, one β-D-glucuronic acid and one α-L-rhamnose [31]. PEC hydrogels of CHT and GG have been reported in the form of capsules and fibers [32, 33]. However, the stability of these PEC hydrogels is dependent on physicochemical properties of

the environment, such as charge density, pH and ionic strength. Thus, their behavior *in vivo* may be difficult to predict and their stability may be compromised upon implantation, as reported for other ionic hydrogels [34].

Although hydrogels allow replicating the 3D structure and viscoelastic properties of tissues, recapitulating the spatial distribution of biomolecules, the mechanical properties and the tissue microarchitecture is not straightforward. Microengineered hydrogels enable replicating these *in vivo* microscale features of tissues [35]. However, most of the available microfabrication techniques require the use of a photocrosslinkable polymer. Previous reports in the literature have exploited the advantages of different polymers for modular tissue engineering by developing composite hydrogels using a photocrosslinkable polymer [36, 37]. For example, poly(ethylene glycol) (PEG) was combined with methacrylated gelatin (GelMA), yielding a composite hydrogel with tunable mechanical properties [36]. Also, Xiao *et al.* developed a photocrosslinkable interpenetrating polymer network (IPN) based on GelMA and silk fibroin (SF) with tunable physical and mechanical properties [37].

Recently, we reported the chemical modification of GG with methacrylate groups (MeGG), yielding a hydrogel crosslinkable by both physical and chemical mechanisms [38]. Herein we present a simple way to prepare a robust photocrosslinkable PEC hydrogel using cationic CHT and anionic MeGG. It is hypothesized that carboxylate groups of MeGG would interact with the cationic amino groups of CHT, producing robust PEC hydrogels without the need for any harsh chemical precursors. To our knowledge, this is the first report on the combination of electrostatic interactions and the use of photosensitive polymer for the fabrication of a robust PEC hydrogel. Controlling the degree of complexation and thus the interactions at a molecular level would allow the development of customized hydrogels. The objective of this study is to fully characterize the developed hydrogels and the interactions between the two polymers in this system. We also investigate the fabrication of microscale hydrogels and assess the biocompatibility of encapsulated rat cardiac fibroblast cells in order to explore the applicability of these hydrogels for tissue engineering.

2. EXPERIMENTAL SECTION

2.1. Materials

All reagents were purchased from Sigma-Aldrich (USA), unless otherwise noted. Methacrylated gellan gum (MeGG) was synthesized as described previously [38]. Briefly, 1 g of gellan gum (GG, Gelrite®, Sigma-Aldrich, USA) was dissolved in 100 mL of deionized water at 90 ºC for 20-30 minutes, as described in detail elsewhere [14]. A volume of 8 mL of methacrylic anhydride (MA, Sigma) was added at 50 ºC to this solution. The reaction was

continued for 6 hours and the pH was adjusted to 8.0 periodically with 5.0 M NaOH solution. The modified MeGG solution was purified by dialysis (Fisher Scientific, membrane with molecular weight cutoff of 11-14 kD, USA) for at least 3 days against distilled water to remove the excess of MA. Purified MeGG was obtained by lyophilization and stored in a dry environment protected from light. Chitosan (CHT) was purchased from Sigma (degree of deacetylation of approximately 90% as determined by X-Ray photoelectron spectroscopy, XPS).

2.2. Preparation of photocrosslinkable PEC hydrogel

CHT (1%, w/v) was dissolved in an aqueous solution of acetic acid (1%, v/v) and MeGG (1% ,w/v) was dissolved in deionized water under constant stirring at 50 ºC for 10 min. 0.5% (w/v) 2-hydroxy-1-[4-(2-hydroxyethoxy)phenyl]-2-methyl-1-propanone (Irgacure 2959, Ciba Specialty Chemicals) was added to the MeGG solution. The photocrosslinkable PEC hydrogel (MeGG-CHT) was formed by dispensing negatively charged MeGG solution into positively charged CHT solution. To visualize the formation of hydrogels, MeGG solution was colored with trypan blue and CHT solution with eosin Y. Photocrosslinked MeGG-CHT PEC hydrogels were obtained by exposing to light (wavelength of 320-500 nm, 7.14 mW/cm^2, EXFO OmniCure S2000) for 60 sec. MeGG-CHT hydrogels with three different volume ratios (2:1, 1:1, 1:2) of the polymers were prepared by varying the volume of the two polymer solutions.

2.3. Characterization of hydrogels

2.3.1. Zeta potential measurement

The zeta potential of the initial solutions of MeGG and CHT (1% w/v) was determined using a Malvern Zetasizer® 3000 HS (Malvern Instruments, UK). Each analysis was performed for 120 seconds at 25ºC. The Smoluchowski model was used with a F(Ka) value of 1.50. Independent triplicate experiments were performed for obtaining statistical significance.

2.3.2. Morphological characterization

The morphology of the photocrosslinked MeGG-CHT PEC hydrogels (2:1, 1:1, 1:2 ratios and plain MeGG and CHT) was analyzed using a scanning electron microscope (SEM, Zeiss Ultra 55, Germany) with an accelerating voltage of 15 kV. Freshly prepared PEC and MeGG hydrogel samples were flash-frozen in liquid nitrogen, freeze-fractured and freeze-dried for 72 h as described previously [39]. The porous structure of CHT was obtained by flash-freezing and freeze-drying CHT solution (1%, w/v). Freeze-dried samples were sputter

coated with palladium-platinum alloy target materials with 40 mA current for 80 sec using a sputter coater (SP-2 AJA Sputtering System) before SEM observation. The area of the pores of the photocrosslinked PEC hydrogels was calculated using an image analysis software (NIH Image J, n=40).

2.3.3. Chemical characterization

The chemistry of the developed materials was analyzed by Fourier transform infrared spectroscopy with attenuated total reflection (FTIR-ATR). The infrared spectra were recorded on a Bruker Alpha FTIR spectrophotometer with a resolution of 4 cm^{-1}. The final result is presented as the average of 32 scans. X-ray photoelectron spectroscopy (XPS) enabled further chemical characterization of both the surface and the cross-section of the photocrosslinked PEC hydrogels. The analysis was performed on a Kratos Axis Ultra XPS instrument using a monochromatic Al Kα X-ray source operating at 15 kV and 10 mA. The elements in the sample surface were identified from a survey spectrum at pass energy of 160 eV. The areas under the specific peaks were used to calculate the atomic percentages (full XPS spectra of the studied materials, used to calculate the atomic percentages, can be found in Figure VI.S2, in the appendix of the present chapter). High-resolution spectra were also recorded at pass energy of 20 eV and overlapping peaks were resolved into their individual components by the CasaXPS software. The component energies (399.4 ± 0.4 eV, 400.5 ± 0.4 eV and 401.4 ± 0.4 eV, respectively for amine, amide and protonated amine), number of peaks and peak widths (full width at half-maximum, fwhm, fixed for 1.2 ± 1%) were fixed initially and a refinement was performed for the peak heights only. PEC hydrogels were fabricated and freeze-dried before performing the FTIR and XPS analyzes. Both the surfaces (2:1, 1:1 and 1:2 ratios) and the cross-section (1:1 ratio) of the MeGG-CHT hydrogels were evaluated. For that, a slice of the middle portion of the MeGG-CHT hydrogels was cut and freeze dried, in order to evaluate the cross-section of the hydrogels. For the surface analysis, the MeGG-CHT hydrogels were frozen immediately after preparation.

2.3.4. Swelling ratio measurement

To assess the influence of CHT content on the equilibrium swelling ratio of the photocrosslinked PEC hydrogels, MeGG-CHT hydrogels at 1% (w/v) with different ratios of MeGG:CHT (2:1, 1:1, 1:2) were immersed in 2 mL PBS at 37 ºC, under mild shaking. After 24 hours, hydrogels (n=4) were removed and hydrogel surfaces were quickly blotted on a filter paper. Their wet weight was measured (w_t) and compared to the initial wet weight (w_0). The equilibrium swelling ratio (S_{eq}) was defined in accordance to Eq (1).

$$S_{eq}(\%) = \frac{W_t - W_0}{W_0} \times 100 \qquad (1)$$

2.3.5. Distribution of MeGG and CHT polymers within the photocrosslinkable PEC hydrogel

The structure of the boundary region of the PEC hydrogels was observed at a nano-scale by transmission electron microscopy (TEM) immediately after preparation. PEC hydrogels were prepared (1:1 ratio) for analysis as described in section 2.2. The samples were prepared by fixing hydrogels in 2% gluteraldehyde/2% paraformaldehyde and 1% osmium tetroxide. Samples were then dehydrated in acetone and embedded in epoxy resin. Ultrathin sections of 70 nm thick were placed on TEM grids and analyzed under TEM (Tecnai™ G² Spirit BioTWIN, FEI).

To evaluate the distribution of the polymers in the bulk of the PEC hydrogels, fluorescein-labeled CHT was used for the formation of the MeGG-CHT PEC hydrogels. Fluorescein-CHT conjugate was obtained as described elsewhere [40]. The chemical reaction is shown in the supplementary Figure VI.S1 in the appendix of the present chapter. The pH of CHT solution (1%, w/v) was adjusted to 6.0 with the addition of 5M NaOH. A volume of 400 µL fluorescein solution (0.1%, w/v), previously dissolved in ethanol, was added to 10 mL of this solution. To catalyze the formation of amide bonds, 1-ethyl-3-(3-dimethylaminopropyl) carbodiimide hydrochloride (EDC, Thermo Scientific) was added to a final concentration of 0.05 M. The reaction was incubated for 12 h in the dark under stirring, at room temperature. The synthesized conjugate solution was purified by dialysis (Fisher Scientific, membrane with molecular weight cutoff of 11-14 kD, USA) for at least 3 days against distilled water to remove the unreacted fluorescein. Purified fluorescein-CHT was obtained by lyophilization and stored in a dry environment protected from light. PEC hydrogels (1:1 ratio) were prepared with fluorescein-CHT between two glass slides separated by 300 µm spacers. The distribution of fluorescein-CHT within the photocrosslinkable PEC hydrogel was evaluated by confocal laser scanning microscopy (CLSM) (Olympus FV300, Meville, NY) one hour after preparation. The imaging was initiated in the upper limit of the hydrogel and continued for a thickness of 400µm, using 5 µm z-intervals. Fluorescence of fluorescein-CHT was detected upon excitation at 488 nm, through a cut-off dichroic mirror and an emission band-pass filter of 505-530 nm.

2.4. Isolation of rat cardiac fibroblasts

Cardiac fibroblasts were isolated from the heart of a 1 day old Sprague-Dawley rat, following a procedure described in detail elsewhere [41]. Briefly, hearts (n=10) were washed with Hank's balanced salt solution (HBSS, Gibco Invitrogen) and were minced and incubated in

0.3 mg/mL collagenase solution containing 0.6 mg/mL pancreatin (Sigma). Isolated cardiomyocytes and cardiac fibroblasts were plated in T75 flasks for 30 min in Dulbecco's Modified Eagles' medium (DMEM, Gibco Invitrogen) containing 10% of heat-inactivated fetal bovine serum (Sigma) and 1% penicillin-streptomycin (Gibco Invitrogen) at 37 ºC with 5% CO_2. Cardiac fibroblasts were purified by removing all the non-adherent cells, including the cardiomyocytes. After reaching confluence, a cell suspension of rat cardiac fibroblasts (10^7 cells/mL) was prepared by trypsinization (trypsin/EDTA solution, Gibco) and incorporated into the MeGG solution previously warmed to 37 ºC prior to the microfabrication.

2.5. Microfabrication of cell-laden photocrosslinkable PEC hydrogels

The effect of PEC hydrogel formation and photocrosslinking on cell viability was assessed by encapsulating rat cardiac fibroblasts within microfabricated PEC hydrogels. MeGG-CHT hydrogels with encapsulated rat cardiac fibroblasts were micropatterned onto 3-[tris(trimethylsilyloxy)silyl]propyl methacrylate (TMSPMA) coated glass slides using photolithography methods, as previously reported [42]. Briefly, 100 μL of MeGG prepolymer containing cell suspension was pipetted into the same volume of CHT previously placed on top of TMSPMA glass slide. Untreated cover slip, placed on top of the MeGG-CHT hydrogel, was separated from treated glass slide by 150 μm spacers. The photomask (either with triangular or square shapes) was placed directly on top of the cover slip prior to exposure to light (wavelength 320-500 nm, 7.14 mW/cm^2, EXFO OmniCure S2000). Subsequently, the cover slip was removed and the remaining uncrosslinked prepolymer cell suspension was gently washed away with preheated DMEM. Micropatterned cell-laden hydrogels were cultured for 2 days in 6-well-plates (Fisher Scientific) under standard culture conditions. Viability of cells encapsulated in micropatterned MeGG-CHT hydrogels was assessed 1 h after preparation and after 2 days in culture, by incubating cells with a Live/Dead (Invitrogen) assay kit (calcein AM/ethidium homodimer-1 in DPBS) for 20 min.

2.6. Statistical Analysis

All the data were subjected to statistical analysis and was reported as a mean ± standard deviation. Statistical differences (*$p<0.05$, **$p<0.01$, ****$p<0.001$) were determined using one-way ANOVA followed by Bonferroni post-hoc test for multiple comparisons in SEM and swelling data.

3. RESULTS AND DISCUSSION

CHT is one of the few positively charged polysaccharides from natural origin [22] and has been widely used for the development of PEC hydrogels [13, 23]. Specifically, the development of GG-CHT PEC hydrogels has been reported by Yamamoto and collaborators [33]. However, the stability of these ionically crosslinked hydrogels cannot be assured *in vivo* since it is strongly dependent on the pH and ionic strength of the environment. Indeed, it has already been reported that ionic polymers, such as GG, can lose their stability as hydrogels due to the exchange of divalent ions by monovalent ions, present in higher concentrations in physiological environment [38]. In this study, we hypothesized that the use of photocrosslinkable MeGG for the formation of CHT-based hydrogels may improve the hydrogel performance by increasing the structural stability of the MeGG-CHT.

3.1. Photocrosslinkable PEC hydrogel formation

A new class of photocrosslinkable PEC hydrogels was developed by combining two oppositely charged polysaccharides of natural origin: cationic CHT (Figure VI.1.A) and anionic MeGG (Figure VI.1.B). CHT was dispersed in a solution of acetic acid (pH 4.06). The pH of MeGG solution, dissolved in deionized water, was 5.42. Given the pKa value of amine groups (6.4) of CHT [18] and of carboxylic acid groups (3.4-3.7) of MeGG [43], both polymers were charged in the initial solutions. This was confirmed by the measurement of the zeta potential of the initial solutions (Figure IV.1.C). CHT was positively charged with zeta potential value of about 38 mV, as a result of proton acceptance by the amino groups. MeGG was negatively charged with zeta potential value of -17 mV. When MeGG was added to CHT solution, the positively charged amino group interacted with the oppositely charged carboxylic group in MeGG by electrostatic interactions (Figure VI.1.D). Upon contact, a fast electrostatic interaction occurred, leading to an instant complexation. A solid membrane was formed at the interface of the two polymers (Figure VI.1.A), as previously reported in the literature [44]. The PEC hydrogel was then stabilized by UV exposure. Without the UV crosslinking it was not possible to handle the PEC hydrogels without leading to their disintegration, showing the importance of UV for their structural stability.
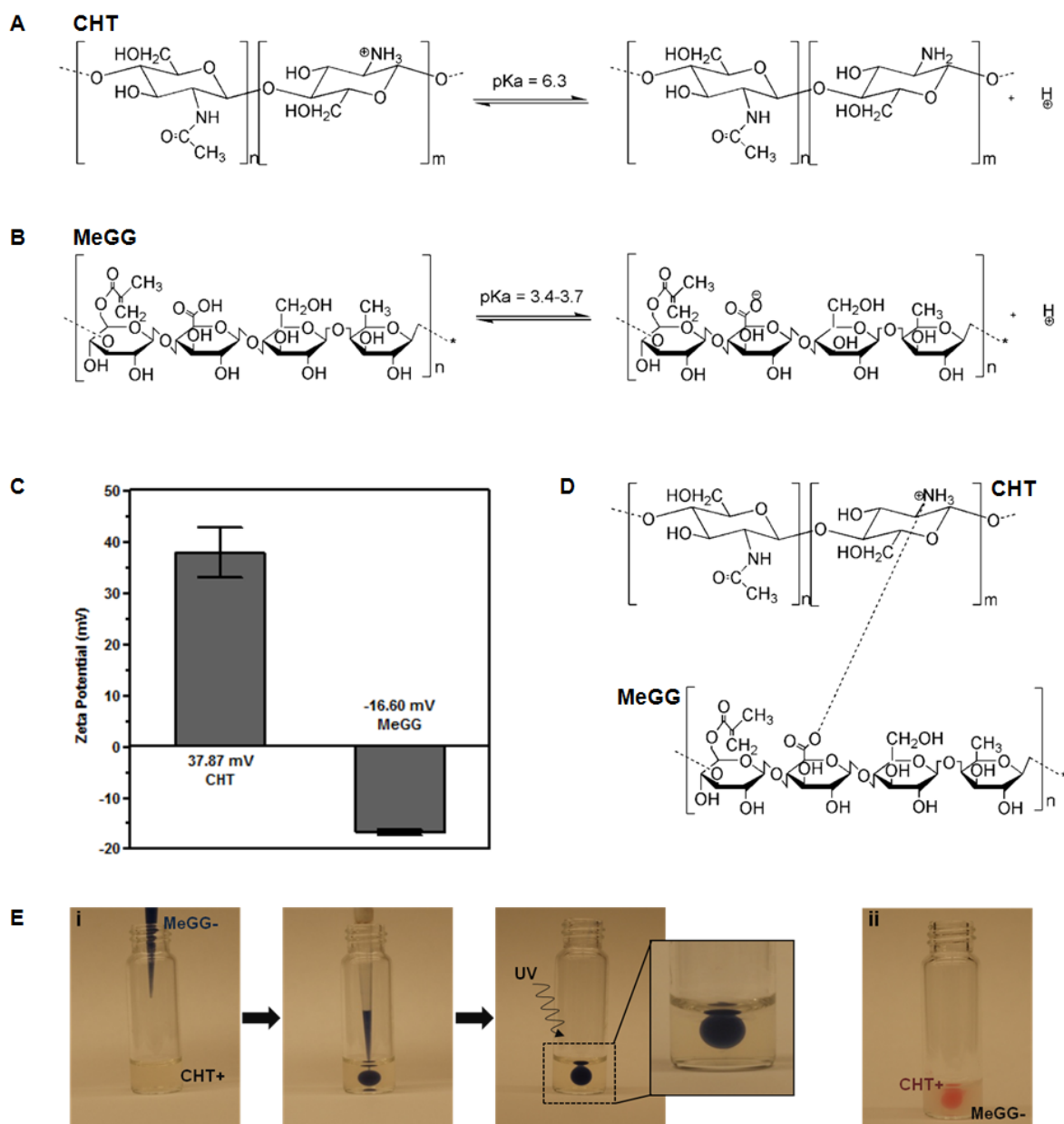
Figure IV.1. Chemical structures and illustration of the states of protonation of (A) CHT and (B) MeGG. (C) Zeta potential (mV) of CHT and MeGG in the initial solutions. (D) Representation of the possible electrostatic association between CHT and MeGG. (E) Representation of a method to form photocrosslinkable PEC hydrogels by injecting (i) trypan blue stained MeGG in CHT or (ii) eosin stained CHT in MeGG solution.

3.2. Morphological, chemical and swelling properties of MeGG-CHT PEC hydrogels

Various parameters that affect PEC formation include the polymer molecular weight, polymer charge, pH of the solution, temperature and solvent used [22, 45]. The effect of the ratio of the polymer on MeGG-CHT PEC formation was studied while keeping the other parameters constant. Thus, three different ratios of MeGG-CHT were studied by varying the volume of

the polymer solutions: excess of MeGG (2MeGG:1CHT), excess of CHT (1MeGG:2CHT), and equivalent polymer ratio (1MeGG:1CHT). It was observed for all the ratios that after PEC hydrogel formation, some amount of CHT solution would remain uncomplexed with MeGG, while all MeGG solution added would remain within the PEC hydrogel, as visualized in Figure VI.1.E. This can be explained by the zeta potential results, which showed higher charge amount on CHT than on MeGG. This suggests that the negative charges on the MeGG readily complexed with excess positive charges on CHT chains.

Figure VI.2.A shows the morphology of MeGG-CHT PEC hydrogels for MeGG:CHT ratios of 2:1, 1:1 and 1:2 and of the porous structure of the controls. Fibrous structures were detected along with the pores of the hydrogels for all conditions (highlighted with arrows). A similar behavior was reported by Shchipunov *et at.* when mixing CHT and xanthan gum at different ratios [26]. They observed that the morphology of the hydrogels changed from rod-like particles to a fibrillar-like structure with increasing amount of xanthan gum and thus, with higher charge ratio [26]. At the length scale analyzed, no significant change was observed in the area of the pores of the complexed hydrogels (Figure VI.2.B). Addition of CHT led to formation of smaller pores as compared to pure MeGG and CHT hydrogels. This may be due to interaction of oppositely charged polymer chains and their complexation.
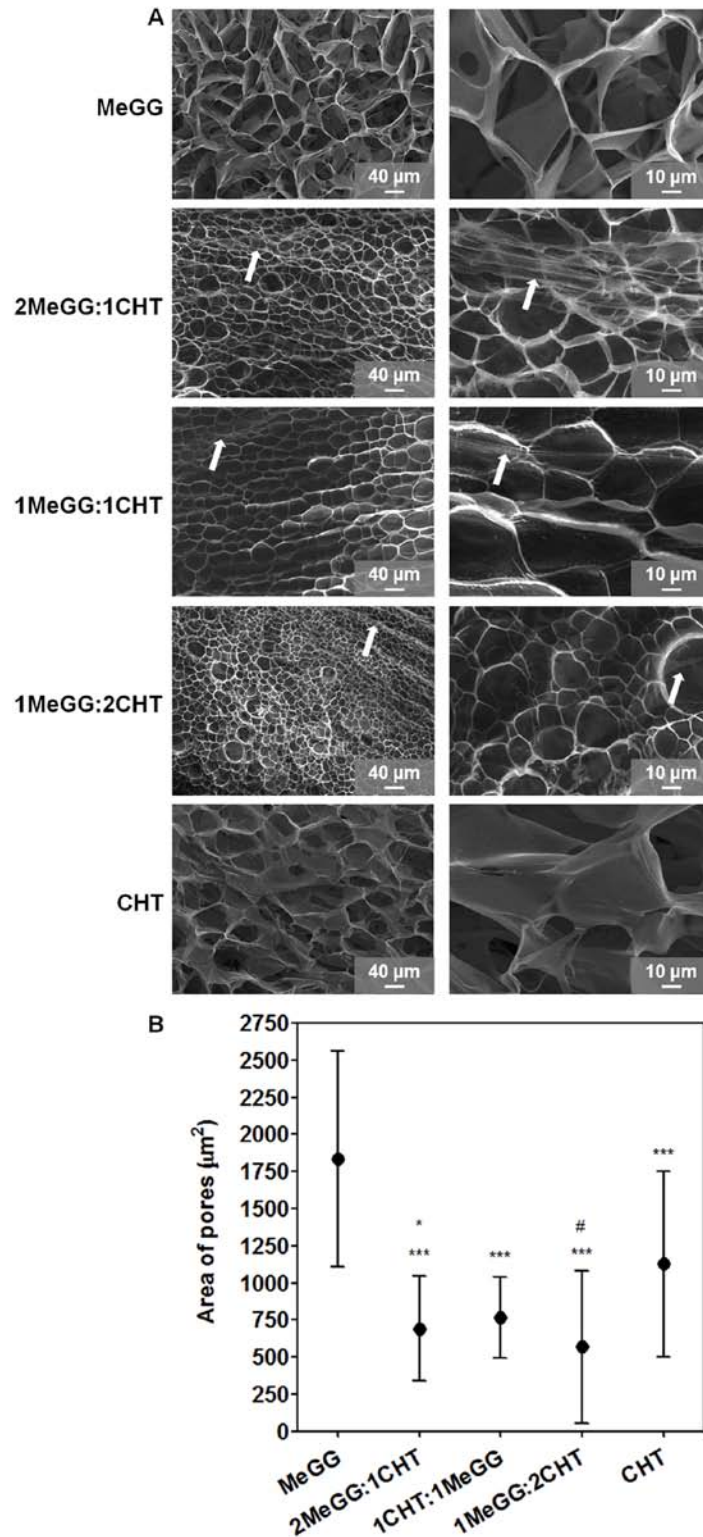
Figure VI.2. Morphological characterization of photocrosslinkable PEC hydrogels (1%, w/v) and of the controls: (A) SEM images of MeGG, 2MeGG:1CHT, 1MeGG:1CHT, 1MeGG:2CHT and CHT with two magnifications (arrows indicate the presence of fibers). (B) Average area of the pores (μm^2) of the MeGG, MeGG-CHT and CHT hydrogels (***$p < 0.0001$, statistical difference when compared to MeGG alone; *$p < 0.05$ and #$p < 0.0001$, statistical difference when compared to CHT alone).

FTIR-ATR of the lyophilized hydrogel was performed to characterize the chemical composition of the different polymer ratios. Figure VI.3 displays the FTIR spectra of all samples. The full peak assignment is provided in Table VI.1. FTIR spectrum of plain CHT displayed a band at 1548 cm^{-1} corresponding to the N-H bending vibration of the amine group. The absorption peak at 1409 cm^{-1} was assigned to the C-N stretch of the amide. The C=O stretch of the amide group of CHT was observed at 1652 cm^{-1} [46]. The spectrum of the raw MeGG showed absorption peaks at 1616 cm^{-1} and 1722 cm^{-1} corresponding, respectively, to the C=O stretch of the carboxylic and ester groups, as previously reported [38]. When MeGG was added to the CHT solution, the absorption peaks of both CHT and MeGG were present on the spectra of the MeGG-CHT PEC hydrogels for the different ratios tested. The peaks of the carbonyl group of the carboxylic acid of MeGG in the complexed hydrogels were shifted to lower wavenumbers and presented a narrower shape. The peaks of C=O of the amide and of the ester groups were displaced to higher wavenumbers, indicating a chemical interaction between the two polymers. The absorption peaks of the amine on the MeGG-CHT hydrogels were shifted to lower wavenumbers from 1548 cm^{-1} to 1537 cm^{-1}. On the complexed hydrogels a third peak appeared as a shoulder of the C=O of carboxylic acid peak around 1589 cm^{-1}, possibly corresponding to the deprotonated state of the carboxylic acid (COO$^-$). The absorption bands of C-N stretch of the amine and C-O stretch of the ester of the complexed hydrogel overlap. FTIR spectra revealed no major differences on the position of the peaks when compared among the different ratios of MeGG and CHT.
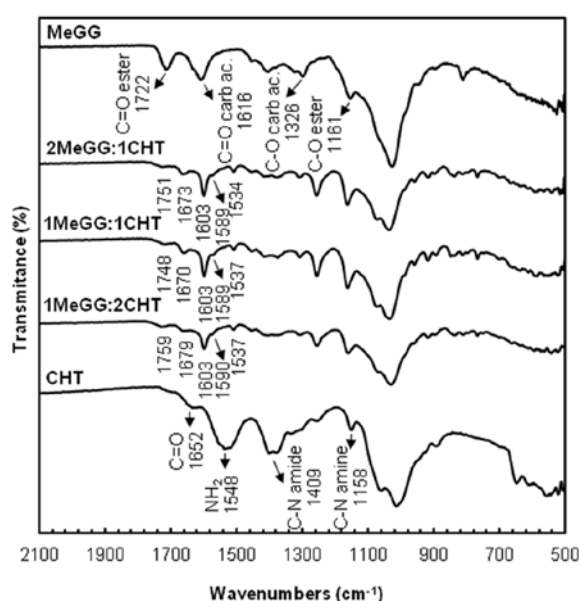
Figure VI.3. FTIR-ATR spectra of raw CHT and MeGG materials and of different volume ratios of the MeGG-CHT PEC hydrogels (2:1, 1:1 and 1:2).

Table VI.1. FTIR-ATR characteristic absorption bands of the components of raw CHT and MeGG and of different ratios of the MeGG-CHT PEC hydrogel (2:1, 1:1 and 1:2).

	Wavenumber (cm^{-1})				
Functional groups	**MeGG**	**2MeGG:1CHT**	**1MeGG:1CHT**	**1MeGG:2CHT**	**CHT**
C-N stretch amine		1168	1179	1167	1158
C-O stretch ester	1161				
C-O stretch carboxylic acid	1326	1261	1260	1263	
C-N stretch amide		1423	1428	1423	1409
NH$_2$		1534	1537	1537	1548
C=O carboxylic acid	1616	1603	1603	1603	
C=O amide		1673	1670	1679	1652
C=O ester	1722	1751	1748	1759	

It has been previously shown that MeGG hydrogels have tunable swelling properties [38], presenting a rapid shrinking when immersed in ionic solutions. In the presence of ions, the formation of junction zones increases, creating more crosslinked networks and reduced degree of swelling [47]. We further investigated this behavior by immersing MeGG-CHT PEC hydrogels in PBS (containing monovalent ions) in order to assess the influence of the presence of CHT on the swelling behavior of these hydrogels (Figure VI.4). After 24h of immersion, hydrogels with higher CHT content presented a significantly higher (*p<0.05) swelling ratio compared to MeGG alone. As previously reported [38], the ionic crosslinking of MeGG in ionic solutions is established through the carboxylic acid group of MeGG. In the PEC hydrogel complex, carboxylic acid group is involved in the electrostatic interactions with CHT. Thus, it is expected that with higher CHT content, the number of available groups for ionic crosslinking is reduced, thus decreasing the hydrogel shrinking when compared with MeGG alone.
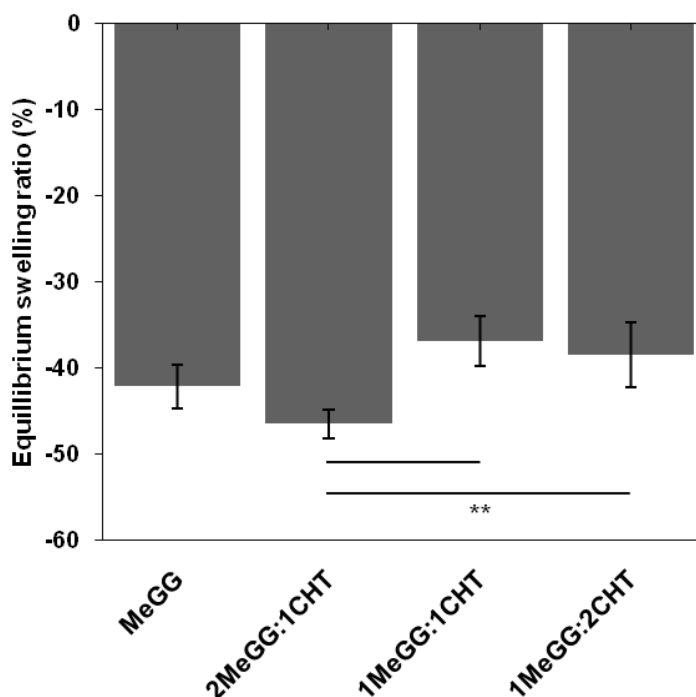
Figure IV.4. Equilibrium swelling ratio (%) of MeGG alone and MeGG-CHT hydrogels in different ratios (2:1, 1:1, 1:2) in PBS (**$p < 0.01$).

3.3. Interactions between MeGG and CHT within the MeGG-CHT PEC hydrogel

When MeGG was added to CHT solution, an apparent membrane started to form at the interface between both polymers. The membrane closed, forming a jellified capsule (Figure VI.1.E). Although CHT was involved in the formation of the membrane at the interface of the polymers, it was not clear whether CHT remained at the surface or infiltrated inside the MeGG phase. It was previously reported that when the negatively charged hyaluronic acid is added to a solution of oppositely charged peptides, a hydrogel is formed. After the hydrogel formation, the polymer chains and the peptides rearrange in order to balance the charge differences [44]. To gain more insight on the interactions between MeGG and CHT in our photocrosslinkable PEC hydrogel, the interactions at the boundary and in the bulk of the MeGG-CHT PEC hydrogel were analyzed. Only hydrogels with the same polymer ratio (1:1) were analyzed in this section.

PEC hydrogels were prepared for TEM immediately after fabrication. The analysis of the boundary region of the hydrogel at a nanoscale showed the presence of a membrane (Figure IV.5.A). To confirm the presence of CHT within the bulk hydrogel, PEC hydrogels were prepared with fluorescently labeled CHT using fluorescein. Confocal microscopy throughout the hydrogel thickness (xz section) one hour after hydrogel preparation confirmed the presence of CHT throughout the MeGG-CHT PEC hydrogel (Figure VI.5.B).
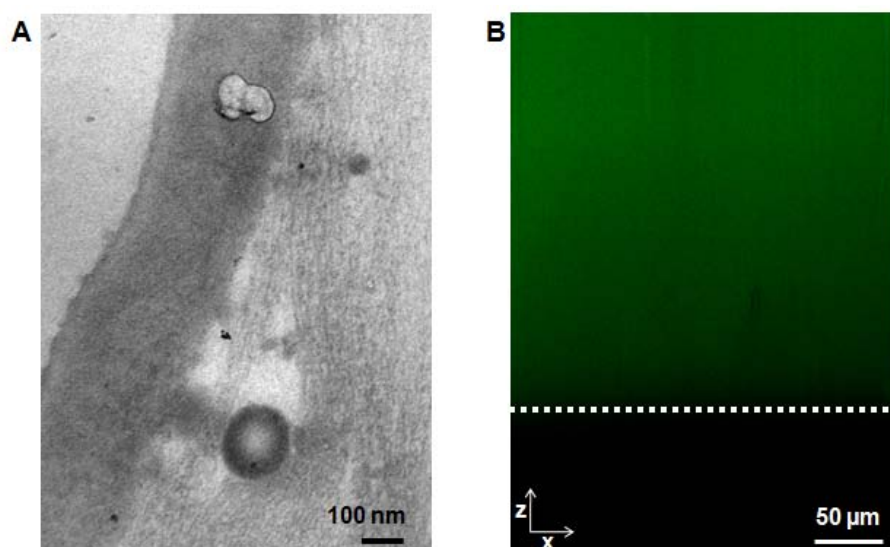
Figure VI.5. (A) TEM micrograph of photocrosslinkable MeGG-CHT PEC immersed in CHT. (B) Distribution of fluorescein-labeled CHT within the xz axis of the PEC MeGG-CHT capsules (white line depicts the limit of the hydrogel).

We further studied the interaction of MeGG and CHT within the PEC hydrogel by FTIR-ATR and XPS. Figure VI.6.A shows the FTIR-ATR spectra performed both to the surface and to the cross-section of the MeGG-CHT PEC hydrogel. The major absorption peaks of MeGG-CHT reported in Figure VI.3 were also present in the cross-section of the hydrogel (Figure VI.6.A), indicating that the internal structure of the hydrogel had the same chemical composition as the surface. XPS chemically validated these findings.
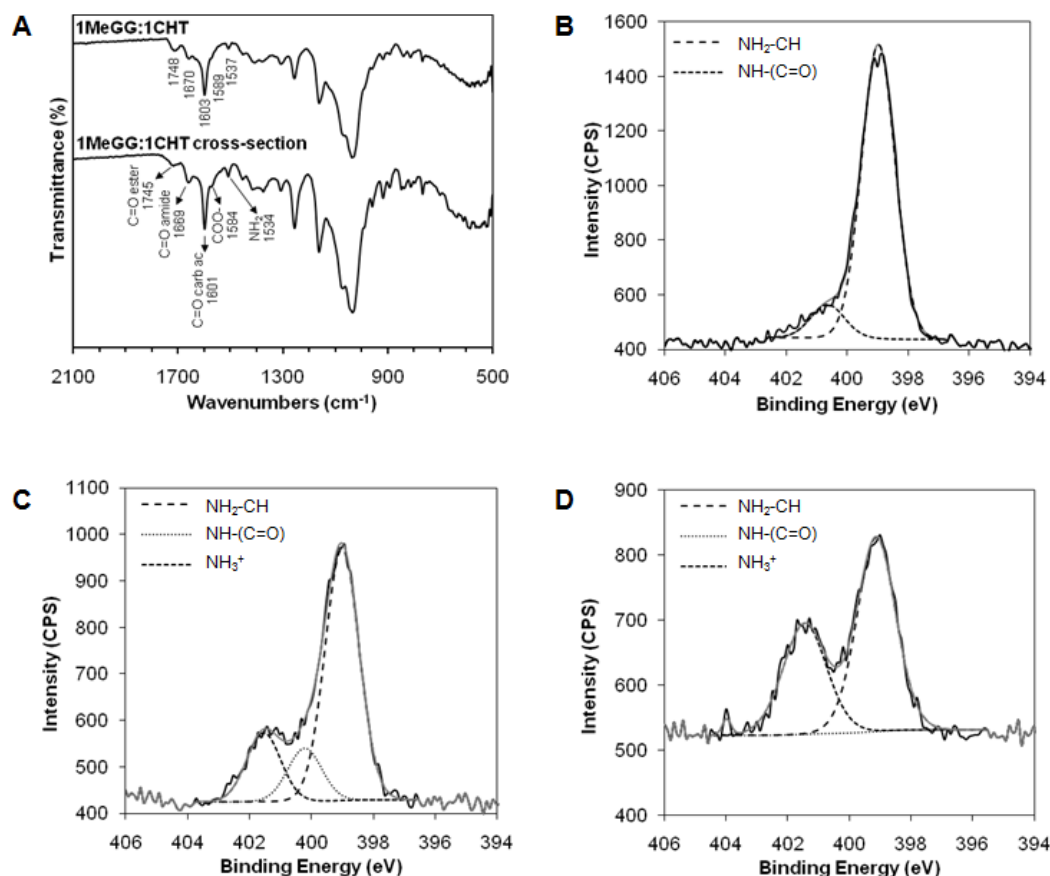
Figure VI.6. Chemical analysis of the cross-section of the MeGG-CHT PEC hydrogel with 1:1 ratio. (A) FTIR-ATR spectra of the surface and cross-section of PEC hydrogel. XPS N 1s narrow scans with curve fit of (B) CHT, (C) surface and (D) cross-section of MeGG-CHT hydrogel. Binding energies: 399.4 ± 0.4 eV (amine), 400.5 ± 0.4 eV (amide) and 401.4 ± 0.4 eV (protonated amine).

Table VI.2 summarizes the XPS survey scan of carbon, oxygen and nitrogen peaks of the samples. Nitrogen element was present on CHT, in agreement with the molecular structure, and also at the surface and cross-section of the MeGG-CHT PEC hydrogels. High-resolution spectrum of nitrogen was recorded to assess the presence of different nitrogen species on the samples, namely amide, amine and protonated amine. The high-resolution spectrum of CHT could be fitted with two peaks (Figure VI.6.B) corresponding to the amine and amide groups of CHT, at 399.00 eV and 400.67 eV, respectively. The atomic ratios of these peaks indicated a degree of deacetylation of CHT close to 90% (Table VI.2). The N1s peaks of both the surface (Figure VI.6.C) and section (Figure VI.6.D) of the MeGG-CHT PEC hydrogel were deconvoluted with a third peak corresponding to the protonated amine (401.5 eV). The presence of this peak at the surface and cross-section of the hydrogel indicated the migration of charged CHT to the interior of the hydrogel.

Table VI.2. Elemental analysis of the studied materials. Atomic percent of various nitrogen species was determined through curve fitting to the N1s peak in the XPS spectra. N1 - amine (399.4 ± 0.4 eV); N2 – amide (400.5 ± 0.4 eV); N3 - protonated amine (401.4 ± 0.4 eV).

Materials	Elemental Analysis (%)			Nitrogen Species (%)		
	C1s	O1s	N1s	N1	N2	N3
CHT	68.62	24.85	6.53	89.96	10.04	
MeGG	70.59	29.41				
MeGG-CHT section	70.06	27.34	2.60	51.61	16.36	32.03
MeGG-CHT surface	70.19	25.48	4.32	67.25	14.26	18.50

3.4. Mechanism of photocrosslinkable PEC hydrogel formation

Based on the discussed results, we have formulated a possible mechanism for the PEC hydrogel formation using two large polysaccharide chains (Figure VI.7). When MeGG is immersed in CHT solution, we expect the polymer chains to immediately interact upon contact. As confirmed by zeta potential measurement, both solutions were charged in the initial state. Thus, the complexation and hydrogel formation is triggered immediately once the polymer chains contact. As the electrostatic attraction between the positively charged CHT and negatively charged MeGG starts taking place, each protonated amine of CHT complexes with a charged carboxylic acid of MeGG polymer, forming a physical barrier at the interface of both polymers. This physical separation between two polymers creates a diffusion barrier for the long, coiled-shape, MeGG polymer [31]. CLSM, FTIR and XPS revealed the presence of CHT in the interior of the hydrogel, indicating that upon the barrier formation, the polymer with lower molecular weight would diffuse inside the hydrogel capsule. There are several parameters influencing this behavior, namely the size and configuration of the polymer chains and the charges associated with each polymer chain. The zeta potential of CHT showed to have nearly twice as much charge as that of MeGG. We hypothesize that the highly charged CHT will migrate inside the bulk of the hydrogel in order to balance the electrostatic charges inside and outside the hydrogel. However, in each MeGG monomer, only one of the saccharides has a charged group, while CHT has, theoretically, nearly 90% of the polymeric chain charged. Thus, even though CHT migrates to the interior of the hydrogel capsule to balance the ionic charge, the atomic percent of protonated amine inside the capsule (32%) suggests that the amount of charges of MeGG is not enough to complex with all charged amine groups of CHT. TEM revealed the formation of membrane-like barrier when the PEC complex was analyzed immediately after the addition of the two polymers. The hypothesized mechanism based on the results obtained from the chemical and

microscopic characterizations gives understanding over the hydrogel formation and the presence of CHT inside the bulk of the hydrogel. The structure of the MeGG-CHT PEC hydrogel can be stabilized by photocrosslinking. After light exposure, the ester groups from MeGG chains covalently bond, creating a highly stable network.
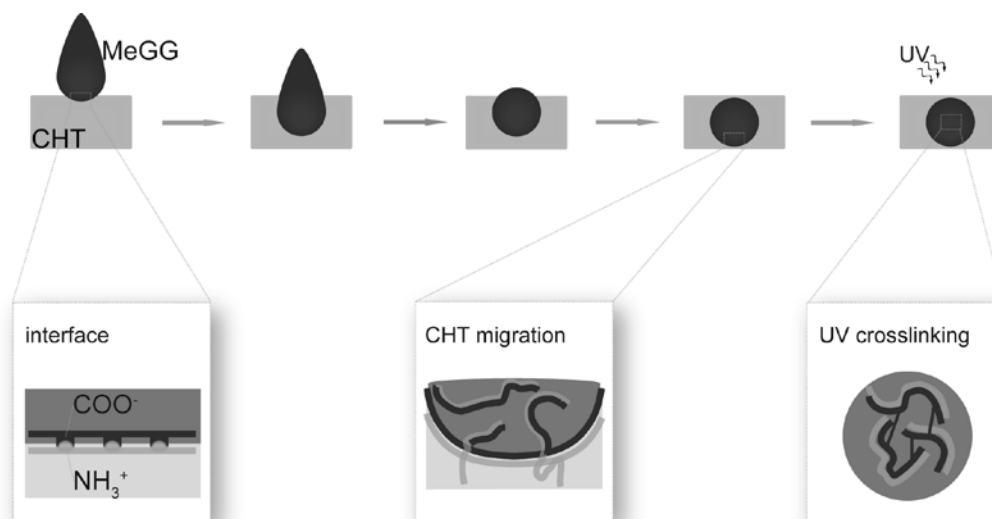
Figure VI.7. Hypothesized mechanism for the formation of a photocrosslinkable hydrogel capsule.

3.5. Microfabrication of fibroblast encapsulated MeGG-CHT PEC hydrogel

Microengineered blocks have been developed and assembled in order to mimic the native functional units [42]. To achieve this, different materials have been blended, forming composite hydrogel networks [36, 37], where at least one of the polymers is photocrosslinkable. We have reported a photocrosslinkable PEC that combines electrostatic interactions with photosensitive properties of polymers to develop a robust PEC hydrogel amenable to microfabrication. To demonstrate the advantage of the photocrosslinkable PEC hydrogels for tissue engineering at a microscale, MeGG-CHT hydrogels were microfabricated by photolithography into triangles and squares as an example of microfabrication into shape-specific structures. A number of microgel units could be developed merely by employing masks with different shapes (Figure VI.8). The ability to wash way with pre-heated DMEM the uncrosslinked MeGG-CHT demonstrates the instability of the PEC hydrogel without the UV crosslinking. We further studied the viability of encapsulated primary fibroblasts isolated from neonatal rat hearts in micropatterned MeGG-CHT hydrogels by a Live/Dead assay. The processing method showed no significant effect over the viability of the encapsulated cells. The use of MeGG as a cell carrier protected the cells from acidic pH of CHT, allowing encapsulation of cells inside MeGG-CHT hydrogels. It

is envisioned that different types of cells can be encapsulated employing this methodology, enabling building heterogeneous tissues.
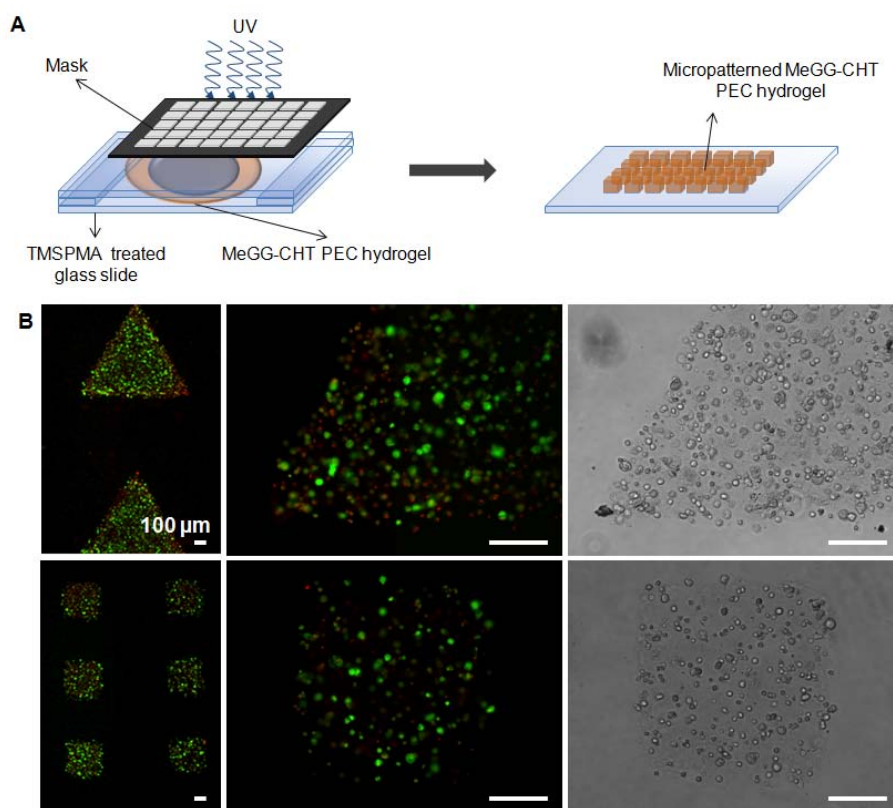
Figure VI.8. (A) Schematic of process to create micropatterned polyelectrolyte capsules by photolithography. (B) Fluorescence images of live (green)/dead (red)fibroblasts from rat heart encapsulated in the PEC microgels microfabricated into triangles and squares (scale bar corresponds to 100 μm).

4. CONCLUSIONS

Robust CHT-based PEC hydrogels were developed by combining CHT with the photocrosslinkable anionic polysaccharide MeGG. The PEC hydrogels contained fibers over the porous structure and improved the swelling behavior as compared to MeGG alone. When MeGG was added to CHT solution, rapid electrostatic interaction occurred between the polymers at the interface, forming a membrane between both solutions. We also demonstrated the chemical interaction between CHT and MeGG in the interior of the hydrogel, indicating that CHT diffuses through the formed membrane into the bulk of the hydrogels. The ability to photocrosslink these PEC hydrogels conferred additional stability and enabled fabrication of shape-specific, cell-laden, microscale building blocks that can be used for modular tissue engineering.

ACKNOWLEDGEMENTS

REFERENCES

1. Hunt NC, Grover LM. Cell encapsulation using biopolymer gels for regenerative medicine. Biotechnology Letters 2010;32(6):733-742.
2. Rabanel J, Bertrand N, Sant S, Louati S, Hildgen P. Polysaccharide hydrogels for the preparation of immunoisolated cell delivery systems. In: RH Marchessault, Ravenelle F, Zhu X, editors. Polysaccharides for Drug Delivery and Pharmaceutical Applications. Washington: Amer Chemical Soc, 2006. p. 305.
3. Mather ML, Tomlins PE. Hydrogels in regenerative medicine: towards understanding structure-function relationships. Regenerative Medicine 2010;5(5):809-821.
4. Brandl F, Sommer F, Goepferich A. Rational design of hydrogels for tissue engineering: Impact of physical factors on cell behavior. Biomaterials 2007;28(2):134-146.
5. Zuidema JM, Pap MM, Jaroch DB, Morrison FA, Gilbert RJ. Fabrication and characterization of tunable polysaccharide hydrogel blends for neural repair. Acta Biomaterialia 2011;7(4):1634-1643.
6. Lutolf MP, Hubbell JA. Synthetic biomaterials as instructive extracellular microenvironments for morphogenesis in tissue engineering. Nature Biotechnology 2005;23(1):47-55.
7. Schneider GB, English A, Abraham M, Zaharias R, Stanford C, Keller J. The effect of hydrogel charge density on cell attachment. Biomaterials 2004;25(15):3023-3028.
8. Hadjipanayi E, Mudera V, Brown RA. Close dependence of fibroblast proliferation on collagen scaffold matrix stiffness. Journal of Tissue Engineering and Regenerative Medicine 2009;3(2):77-84.
9. Betz MW, Yeatts AB, Richbourg WJ, Caccamese JF, Coletti DP, Falco EE, Fisher JP. Macroporous Hydrogels Upregulate Osteogenic Signal Expression and Promote Bone Regeneration. Biomacromolecules 2010;11(5):1160-1168.
10. Kloxin AM, Benton JA, Anseth KS. In situ elasticity modulation with dynamic substrates to direct cell phenotype. Biomaterials 2010;31(1):1-8.
11. Anderson SB, Lin CC, Kuntzler DV, Anseth KS. The performance of human mesenchymal stem cells encapsulated in cell-degradable polymer-peptide hydrogels. Biomaterials 2011;32(14):3564-3574.
12. Brigham MD, Bick A, Lo E, Bendali A, Burdick JA, Khademhosseini A. Mechanically Robust and Bioadhesive Collagen and Photocrosslinkable Hyaluronic Acid Semi-Interpenetrating Networks. Tissue Eng Part A 2009;15(7):1645-1653.
13. Grenha A, Gomes ME, Rodrigues M, Santo VE, Mano JF, Neves NM, Reis RL. Development of new chitosan/carrageenan nanoparticles for drug delivery applications. J Biomed Mater Res A 2010;92A(4):1265-1272.
14. Oliveira JT, Martins L, Picciochi R, Malafaya PB, Sousa RA, Neves NM, Mano JF, et al. Gellan Gum: A New Biomaterial for Cartilage Tissue Engineering Applications. J Biomed Mater Res A 2010.
15. Chen SC, Wu YC, Mi FL, Lin YH, Yu LC, Sung HW. A novel pH-sensitive hydrogel composed of N,O-carboxymethyl chitosan and alginate cross-linked by genipin for protein drug delivery. J Control Release 2004;96(2):285-300.
16. Bhattarai N, Ramay HR, Gunn J, Matsen FA, Zhang MQ. PEG-grafted chitosan as an injectable thermosensitive hydrogel for sustained protein release. J Control Release 2005;103(3):609-624.
17. Berger J, Reist M, Mayer JM, Felt O, Peppas NA, Gurny R. Structure and interactions in covalently and ionically crosslinked chitosan hydrogels for biomedical applications. Eur J Pharm Biopharm 2004;57(1):19-34.
18. Sorlier P, Denuziere A, Viton C, Domard A. Relation between the degree of acetylation and the electrostatic properties of chitin and chitosan. Biomacromolecules 2001;2(3):765-772.
19. Gomes ME, Azevedo HS, Malafaya PB, Silva SS, Oliveira JM, Silva GA, Sousa RA, et al. Natural Polymers in tissue engineering applications. In: C Van Blitterswijk, A Lindahl, P Thomsen, D Williams, J Hubbell, Cancedda R, editors. Textbook on tissue engineering. Amsterdam: Elsevier, 2007.
20. Bhattarai N, Gunn J, Zhang MQ. Chitosan-based hydrogels for controlled, localized drug delivery. Adv Drug Deliv Rev 2010;62(1):83-99.
21. Ii'ina AV, Varlamov VP. Chitosan-based polyelectrolyte complexes: A review. Appl Biochem Micro 2005;41(1):5-11.
22. Bhatia SR, Khattak SF, Roberts SC. Polyelectrolytes for cell encapsulation. Curr Opin Colloid Interface Sci 2005;10(1-2):45-51.

23. Feng Q, Zeng GC, Yang PH, Wang CX, Cai JY. Self-assembly and characterization of polyelectrolyte complex films of hyaluronic acid/chitosan. Colloids Surf, A 2005;257-58:85-88.
24. Granero AJ, Razal JM, Wallace GG, Panhuis MIH. Conducting gel-fibres based on carrageenan, chitosan and carbon nanotubes. J Mater Chem 2010;20(37):7953-7956.
25. Lawrie G, Keen I, Drew B, Chandler-Temple A, Rintoul L, Fredericks P, Grondahl L. Interactions between alginate and chitosan biopolymers characterized using FTIR and XPS. Biomacromolecules 2007;8(8):2533-2541.
26. Shchipunov Y, Sarin S, Kim I, Ha CS. Hydrogels formed through regulated self-organization of gradually charging chitosan in solution of xanthan. Green Chem 2010;12(7):1187-1195.
27. Deng C, Zhang PC, Vulesevic B, Kuraitis D, Li FF, Yang AF, Griffith M, et al. A Collagen-Chitosan Hydrogel for Endothelial Differentiation and Angiogenesis. Tissue Eng Part A 2010;16(10):3099-3109.
28. Carlfors J, Edsman K, Petersson R, Jornving K. Rheological evaluation of Gelrite (R) in situ gels for ophthalmic use. Eur J Pharm Sci 1998;6(2):113-119.
29. Oliveira JT, Santos TC, Martins L, Picciochi R, Marques AP, Castro AG, Neves NM, et al. Gellan Gum Injectable Hydrogels for Cartilage Tissue Engineering Applications: In Vitro Studies and Preliminary In Vivo Evaluation. Tissue Eng Part A 2009;16(1):343-353.
30. Rozier A, Mazuel C, Grove J, Plazonnet B. Gelrite®: A novel, ion-activated, in-situ gelling polymer for ophthalmic vehicles. Effect on bioavailability of timolol. International Journal of Pharmaceutics 1989;57(2):163-168.
31. Jansson PE, Lindberg B, Sandford PA. Structural studies of Gellan Gum, an extracellular polysaccharide elaborated by pseudomonas-elodea. Carbohydr Res 1983;124(1):135-139.
32. Amaike M, Senoo Y, Yamamoto H. Sphere, honeycomb, regularly spaced droplet and fiber structures of polyion complexes of chitosan and gellan. Macromol Rapid Commun 1998;19(6):287-289.
33. Ohkawa K, Kitagawa T, Yamamoto H. Preparation and characterization of chitosan-gellan hybrid capsules formed by self-assembly at an aqueous solution interface. Macromol Mater Eng 2004;289(1):33-40.
34. Kuo CK, Ma PX. Maintaining dimensions and mechanical properties of ionically crosslinked alginate hydrogel scaffolds in vitro. J Biomed Mater Res A 2008;84A(4):899-907.
35. Khademhosseini A, Langer, R. Microengineered hydrogels for tissue engineering. Biomaterials 2007;28:5087–5092.
36. Hutson C, Nichol J, Aubin H, Bae H, Yamanlar S, Al-Haque S, Koshy S, et al. Synthesis and Characterization of Tunable Poly(Ethylene Glycol): Gelatin Methacrylate Composite Hydrogels. Tissue Engineering Part A 2011.
37. Xiao W, He J, Nichol JW, Wang L, Hutson CB, Wang B, Du Y, et al. Synthesis and characterization of photocrosslinkable gelatin and silk fibroin interpenetrating polymer network hydrogels. Acta Biomaterialia 2011;7(6):2384-2393.
38. Coutinho DF, Sant SV, Shin H, Oliveira JT, Gomes ME, Neves NM, Khademhosseini A, et al. Modified Gellan Gum hydrogels with tunable physical and mechanical properties. Biomaterials 2010;31(29):7494-7502.
39. Hwang CM, Sant S, Masaeli M, Kachouie NN, Zamanian B, Lee SH, Khademhosseini A. Fabrication of three-dimensional porous cell-laden hydrogel for tissue engineering. Biofabrication 2010;2(3).
40. de Campos AM, Diebold Y, Carvalho ELS, Sanchez A, Alonso MJ. Chitosan nanoparticles as new ocular drug delivery systems: in vitro stability, in vivo fate, and cellular toxicity. Pharmaceutical Research 2004;21(5):803-810.
41. Khademhosseini A, Eng G, Yeh J, Kucharczyk PA, Langer R, Vunjak-Novakovic G, Radisic M. Microfluidic patterning for fabrication of contractile cardiac organoids. Biomedical Microdevices 2007;9(2):149-157.
42. Du YA, Lo E, Ali S, Khademhosseini A. Directed assembly of cell-laden microgels for fabrication of 3D tissue constructs. PNAS 2008;105(28):9522-9527.
43. Mao R, Tang J, Swanson BG. Gelling temperatures of gellan solutions as affected by citrate buffers. J Food Sci 1999;64(4):648-652.
44. Capito RM, Azevedo HS, Velichko YS, Mata A, Stupp SI. Self-assembly of large and small molecules into hierarchically ordered sacs and membranes. Science 2008;319(5871):1812-1816.
45. Ulrich S, Seijo M, Stoll S. The many facets of polyelectrolytes and oppositely charged macroions complex formation. Curr Opin Colloid Interface Sci 2006;11(5):268-272.

46.   Osman Z, Arof AK. FTIR studies of chitosan acetate based polymer electrolytes. Electrochimica Acta 2003;48(8):993-999.
47.   Grasdalen H, Smidsord O. Gelation of Gellan Gum. Carbohydr Polym 1987;7(5):371-393.

APPENDIX

Supplementary Figure VI.S1

Figure VI.S1 shows a schematic representation of the chemical reaction followed to produce fluorescein-labeled CHT. Fluorescein-CHT was used for analyzing the distribution of CHT throughout the xz axis of PEC MeGG-CHT hydrogel, as depicted in Figure VI.5.
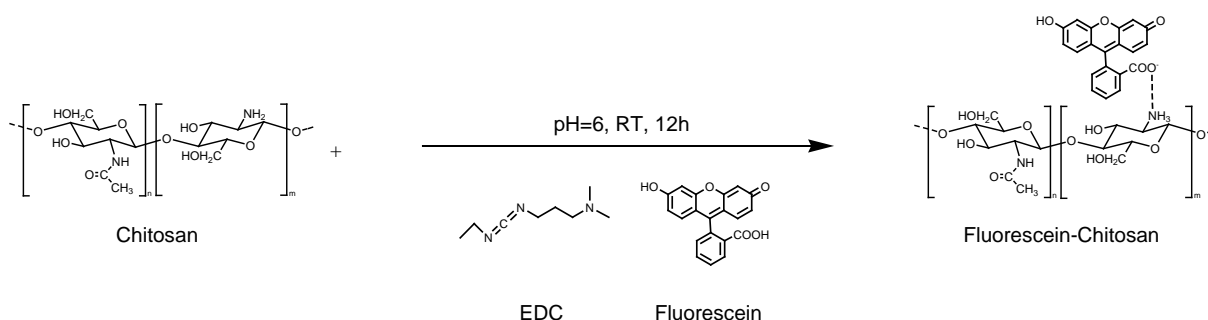
Figure VI.S1. Schematic representation of the chemical reaction for producing fluorescein-labeled CHT (fluorescein-CHT).

Supplementary Figure VI.S2

The elemental analysis summarized in Table VI.2 was calculated based on the survey spectra depicted in Figure VI.S2. The percentages of the elements were calculated by the areas under the specific peaks.
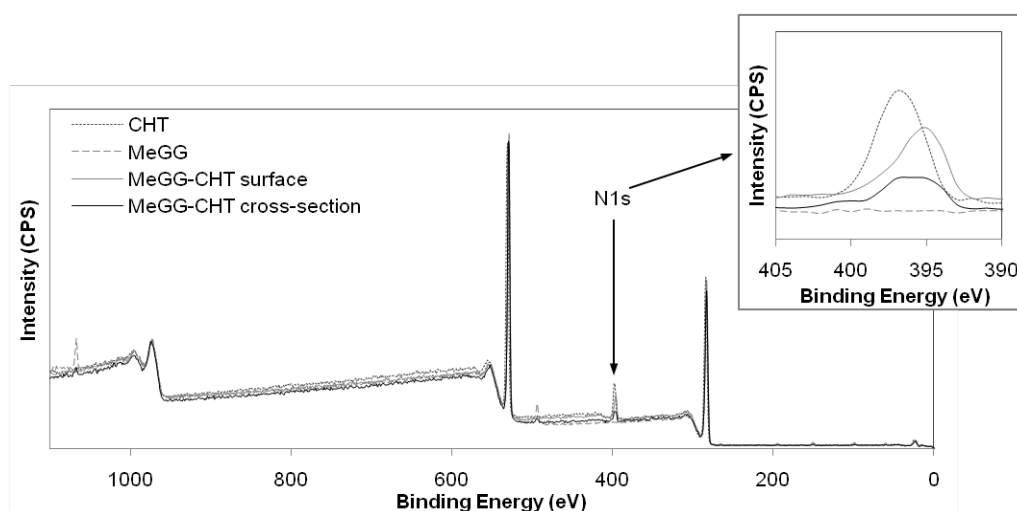
Figure VI.S2. Survey spectra of CHT, MeGG and the surface and cross-section of MeGG-CHT PEC hydrogel.

Chapter VII

FABRICATION OF COLLAGEN-MIMICKING HYDROGEL FIBER BUNDLES FROM THE ASSEMBLY OF POLYELECTROLYTES

ABSTRACT

Fiber bundles are the main structural component in many tissues throughout the body. In most cases, collagen subunits spontaneously self-assemble into a fibrillar structure that provides ductility to bone and constitutes the basis of muscle contraction. Translating these natural architectural features into a biomimetic scaffold is very challenging. Here we propose a simple strategy to engineer biomimetic fiber bundles that replicate the hierarchy and size of natural collagen fibers. The simple interaction of a polyelectrolyte solution of methacrylated gellan gum (MeGG) with a countercharged chitosan (CHT) polymer solution leads to the complexation of the polyelectrolytes. This polyelectrolyte complex was extruded through a polydimethylsiloxane (PDMS) channel, forming a fibrous hydrogel with hierarchical organization and structure similar to that of collagen fibers and in which encapsulated cells were shown to elongate. The striations along the longitudinal axis of the fibrous hydrogel resemble the *D*-periodic bands present in native collagen. In order to confirm if these findings may be applied to other materials/applications, a comprehensive understanding of the mechanism beyond this interaction is needed. We herein propose a tentative exploration of the process of formation of those fiber bundle striations. This fibrous hydrogel system can potentially be used as a scaffold for tissue engineering, as a drug delivery agent or even as an *in vitro* three-dimensional model for the study of collagen-fiber-related diseases.

KEYWORDS: Hydrogel microfibers; self-assembly; hierarchical architecture; collagen mimicking; chitosan; methacrylated gellan gum.

---

1. INTRODUCTION

In biological systems, fibrous structures self-assemble into a three-dimensional (3D) hierarchical system and are present in a variety of tissues. In the heart [1], brain [2], bone [3] or skin [4], bundles of fibers, usually composed of collagen molecules as building blocks, are responsible for providing tensile strength to tissues. Abnormalities in fiber formation or lack of collagen synthesis can lead to clinical scenarios where a serious reduction of tissue strength is observed. Osteogenesis imperfecta and arterial aneurysms are just two known examples of collagen-related diseases [5]. Collagen is the most abundant protein in the human body [6], thus receiving a great attention from the scientific community. Hodge and Petruska [7] first proposed a 3D model for the structure of fibrillar collagen. Three left-handed helix polypeptide chains are twisted together into a right-handed coiled-coil triple helix, forming the collagen molecule, also known as tropocollagen. The internal hydrogen bonding between the nitrogen and carboxyl residues of the amino-acids allows for the stabilization of the tropocollagen structure, which is nearly 300 nm long. These tropocollagen molecules undergo self-assembly linearly and laterally through electrostatic interactions, and the final structure is stabilized by both hydrogen bonds and hydrophobic interactions. These structures result in collagen microfibrils (~100 nm in diameter) with periodic striations, called D-bands (D=67nm) [8] that result from the preferential linear organization and by the staggered orientation of the tropocollagen triple helix. Finally, these microfibrils assemble in parallel bundles, forming fibers of ~10 μm in diameter. Engineering a tissue that replicates the ability of collagen to form hierarchical assemblies with precise linearly defined periodic features of collagen fibers in the body is therefore of great biomedical relevance. Numerous strategies for the development of synthetic fiber bundles have been proposed [9-12]. Electrospinning has been widely reported for fiber formation [9, 13, 14]. However, the high shear stress that cells are subjected to as a result of the polymer stretching may reduce the viability of encapsulated cells. Extrusion of polymers from microfluidic channels into aqueous solutions is an alternative system for the production of fibers [10, 15, 16]. Although it allows cell encapsulation, the need for long incubation times for the material crosslinking, can decrease cell viability and functionality. While these technologies allow for mimicking the hierarchical organization at a micro-scale, the most characteristic feature of collagen fibers, their axial D-periodicity, is not easily achieved by these means. A highly popular alternative consists of using self-assembly systems based on peptides [17], proteins [18], nucleic acids [19] or polysaccharides [20], allowing for a bottom-up design. Peptides have been the most investigated building blocks for the formation of collagen-like fibrous systems [11, 12, 17, 21, 22]. For instance, Rele *et al.* have reported on the synthesis of peptides capable of fibrillogenesis, forming striations with D-bands of approximately 18 nm [21], which is

considerably smaller than that reported for native collagen [8]. These peptides were composed of positive and negatively charged amino-acids that self-assembled when incubated in buffer solution for 9 days. Although able to mimic at a nano-scale the collagen structure, for most of the peptide-based systems, a fiber coarsening process is required to further thicken the initially formed fibers. This process is time consuming and consists on an extra step in the process of engineering a synthetic fibrous system that requires external control. Moreover, the peptide synthesis itself is a quite laborious and expensive process.

Most of the existing engineered fiber bundles fail to replicate simultaneously the micro-bioenvironment, achieved through cell encapsulation into hydrogel systems, and the structural organization into multiple length scales within a cell-friendly, water-soluble system. Thus, the ability to replicate the nano to micro scale hierarchical structure, including periodic D-bands of collagen fibers, along with its biological properties to mediate the interactions between cells and the extracellular-matrix (ECM) may be of extreme relevance for biomedical applications.

A less studied approach is the self-assembly of polysaccharides into fibrous systems [20, 23]. We herein report the successful production of a self-assembled fibrous hydrogel with two natural-based polysaccharides with opposite charges: anionic methacrylated gellan gum (MeGG) and cationic chitosan (CHT). A convenient microfluidic-based approach was used to direct the formation and processing of the hydrogel. Although we applied this approach to MeGG and CHT, it could be generalized to most charged biopolymers.

2. EXPERIMENTAL SECTION

2.1. Materials and solutions

Chitosan (CHT) was purchased from Sigma-Aldrich (USA) and methacrylated gellan gum (MeGG) was synthesized as described in detail elsewhere [24]. Briefly, 1 % (w/v) of gellan gum (GG, Gelrite®, Sigma-Aldrich, USA) was dissolved in deionized water at 90 ºC for 20-30 minutes [25]. Methacrylic anhydride (MA, 8 %, v/v) was added at 50 ºC and the reaction continued for 6 h at pH (8.0). The modified MeGG polymer was dialyzed (Fisher Scientific, membrane with molecular weight cutoff of 11-14 kD, USA), freeze dried and stored in a dry place protected from the light. CHT and MeGG were dissolved (1%, v/v), respectively, in an aqueous solution of acetic acid and in deionized water under constant stirring at 50 ºC for 10 min. The photoinitiator 2-hydroxy-1-[4-(2-hydroxyethoxy)phenyl]-2-methyl-1-propanone (Irgacure 2959, Ciba Specialty Chemicals) was added (0.5%, w/v) to MeGG for obtaining the chemical crosslinking. All other reagents were purchased from Sigma-Aldrich unless specifically mentioned.

2.2. Hydrogel fiber bundle fabrication

A bundle of aligned hydrogel fibers was generated by combining polyelectrolyte complexation and fluidics technology. Briefly, a fluidic device (Figure VII.1.A) with two converging channels (1 mm diameter) was fabricated using polydimethylsiloxane (PDMS) and template-based technology. A MeGG solution (1%, w/v, with or without cells) and CHT solution (1%, w/v) were injected at each inlet channel of the fluidic device and the flow rate was maintained constant by the action of a syringe pump. When the two solutions are mixed in the confluence of the two channels, the oppositely charged chains of MeGG and CHT started to form a complex through electrostatic forces. The fibers were collected onto 3-(trimethoxysilyl) propyl methacrylated (TMSPMA) surface treated glass slides. The collected fibers were stabilized by exposure to light (320-500 nm, 1.2 mW/cm^2, EXFO OmniCure S2000) for 60 sec to obtain the photocrosslinking of MeGG.

2.3. Hydrogel fiber bundle characterization

2.3.1. Distribution of CHT within the hydrogel fiber bundle

Fluorescein-labeled CHT was used in the development of the hydrogel fiber bundle in order to evaluate the distribution of CHT within the hydrogel structure. Fluorescein-CHT conjugate was synthesized as described elsewhere [26]. Briefly, the amine groups of CHT were reacted with the carboxylic groups of fluorescein, forming amide bonds (chemical reaction illustrated in supplementary Figure VII.S1, in the appendix of the present chapter). The pH of the solution was adjusted to 8 by adding 5.0 M NaOH. Fluorescein, previously dissolved in ethanol (0.1%, w/v), was added to the CHT solution at 4% (v/v). 1-ethyl-3-(3-dimethylaminopropyl) carbodiimide hydrochloride (EDC, Thermo Scientific) was added until reaching a final concentration of 0.05 M to catalyze the formation of amide bonds. The reaction continued for 12 h under permanent stirring in the dark and at room temperature. The fluorescein-CHT conjugate was purified by dialysis (Fisher Scientific, membrane with molecular weight cutoff of 11-14 kD, USA) for at least 3 days against distilled water to remove the unreacted fluorescein. Purified CHT was obtained by lyophilization and stored at a dry place protected from light. Confocal laser scanning microscope z-stacks of the hydrogel fiber bundle were taken with an Olympus FV300 (Meville, NY) and fluorescence detected upon excitation at 488 nm through a cut-off dichroic mirror and an emission band-pass filter of 505-530 nm.

The hydrogel fiber bundles prepared with fluorescein-CHT were kept in phosphate buffer saline solution (PBS, Gibco) at 37 ºC for 7 days in order to evaluate the stability of CHT within the hydrogel structure. Hydrogel fiber bundles were analyzed under an inverted fluorescence microscope (Nikon TE 200-U, Nikon Instruments Inc., USA).

2.3.2. Scanning electron microscopy (SEM)

The microstructure of the hydrogel fiber bundles was further analyzed using a scanning electron microscope (Zeiss Ultra 55, Germany). Hydrogels were flash-frozen in liquid nitrogen and freeze-dried for 72 h, as previously described [27]. The images were captured at 15 kV. Samples were sputter-coated (SP-2 AJA Sputtering System) with a palladium-platinum alloy with 40 mA current for 80 sec before SEM observation.

2.3.3. Atomic force microscopy (AFM)

Atomic force microscopy images (AFM) were acquired by means of a Multimode Nanoscope V (Veeco) in order to examine the microstructure of the hydrogel fiber bundles. It was used a commercial Cantilever probe, with a thickness of 4 µm and a tip radius of 10-12.5 nm. The probe oscillation resonance frequency was ~100 kHz. All the samples were characterized using a set-point amplitude ratio of ~0.7. Images were captured at room temperature, at different locations and with an area of 25 µm^2. Images were processed and analyzed by multimode software Nanoscope V6.13.

2.3.4. Transmission electron microscopy (TEM)

The internal nanostructure of the hydrogel fiber bundles was analyzed by embedding freshly prepared samples and analyzing the transverse and longitudinal cross-sections of the hydrogel structure. The samples were prepared by fixing hydrated hydrogels in 2% gluteraldehyde/2% paraformaldahyde and 1% osmium tetroxide. Samples were then dehydrated in acetone and embedded in epoxy resin. Ultrathin sections of 70 nm thick were placed on TEM grids and observed under TEN (Tecnai™ G² Spirit BioTWIN, FEI).

2.4. Biofunctionalization of the hydrogel fiber bundle

RGD sequence was covalently bound to MeGG using a water soluble carbodiimide. The procedure used for sequence immobilization was based on studies previously performed to immobilize amino-acid sequences on carboxylic-based substrates [28]. EDC reacts preferentially with the carboxyl groups of MeGG, activating them. Then, activated COOH of MeGG reacts with amine groups of the amino-acid sequence, covalently binding. Briefly, the pH of MeGG solution was stabilized at 5.6. 1-ethyl-3-(3-dimethylaminopropyl) carbodiimide hydrochloride (EDC, Thermo Scientific, 0.1 M) was added to 10 mL of MeGG and after 15 min, 0.2 M of N-Hydroxysuccinimide (NHS, Sigma) were added to the reaction. After 1 h of reaction, 200 µL of RGD (2.4 mg/mL) were added. The reaction continued for 12 hours under agitation, at 4 ºC. The solution was dialyzed for 2 days and kept at 4 ºC after freeze drying. Further information on the reaction followed and on the characterization of the resulting

material can be found in supplementary Figure VII.S3, in the appendix of the present chapter.

2.5. Rat cardiac fibroblasts encapsulation

Rat cardiac fibroblasts were isolated from the heart of a 1 day old Sprague-Dawley rat [29]. Briefly, hearts (n=10) were washed with Hank's balanced salt solution (Gibco Invitrogen Co., USA) in order to remove the excess of blood inside. Tissues were minced and incubated in a solution of 0.3 mg/mL of collagenase and 0.6 mg/mL of pancreatin (Sigma Chemical Co., USA). Isolated cells were pre-cultured for 30 min in Dulbecco's modified Eagles' medium (DMEM, Gibco Invitrogen), supplemented with 10% of heat-inactivated fetal bovine serum (Sigma) and 1% penicillin-streptomycin (Gibco Invitrogen), at 37 ºC in air with 5% CO_2. Rat cardiac fibroblast population was purified by changing the medium and removing the non-adherent cells, namely the cardiomyocytes. Once confluence was reached, rat cardiac fibroblasts were trypsinized (trypsin/EDTA solution, Gibco) and suspended (17 million cells/mL) in the MeGG-RGD solution, previously warmed to 37 ºC. Fibrous hydrogels were prepared as described before, using plain CHT and MeGG-RGD with suspended rat cardiac fibroblasts. After stabilization with UV exposure, fibrous hydrogels were cultured for up to 7 days in 6-well-plates (Fisher Scientific) under standard culture conditions, with media exchanged every 48 h. Viability of cells encapsulated after 7 days of culture was evaluated by incubating cells with a Live/Dead (Invitrogen) assay (calcein AM/ethidium homodimer-1 in DPBS) for 20 min. Cell alignment was assessed by immunostaining of the cell cytoskeleton with phalloidin and counterstaining their nuclei with DAPI.

3. RESULTS AND DISCUSSION

To replicate the structural hierarchy of the collagen fibers, we took advantage of the electrostatic interaction that is known to occur between two charged polyelectrolytes. A fibrous hydrogel structure was fabricated by flowing aqueous solutions at 1 % (w/v) of MeGG and CHT through two distinct but confluent channels engineered in polydimethylsiloxane (PDMS). The gelation of the polymers was triggered when one polymer came in contact with the countercharged polymer, at the junction of the channels (Figure VII.1.A). After polymer complexation, the common channel directed the polyelectrolyte complex (PEC) to the outlet of the PDMS channel, where the fibrous hydrogel was collected. CHT was used owing to its previously shown potential for biomedical applications [26]. It is derived from chitin, the second most abundant natural polysaccharide, and it has been widely studied for the development of PECs [30-32]. CHT contains amine groups that are protonated at the pH (~4)

of the solution used (1% v/v, acetic acid) (supplementary Figure VII.S2 in the appendix of the present chapter shows the zeta potential measurement of CHT solution). GG has recently been shown to have great potential *in vivo* for cartilage tissue engineering [33] and can be easily synthesized from the natural polymer gellan gum (GG) [24]. MeGG is a photocrosslinkable polymer and thus can form hydrogels by exposure to UV light. Also, it can be crosslinked by physical mechanisms (temperature and in the presence of ions), forming a double helix [34]. This polymer was negatively charged under the conditions used (supplementary Figure VII.S2 in the appendix of the present chapter shows the zeta potential measurement of MeGG solution). In fact, we have shown in a recent work the strong interaction between these two charged polymers while forming a PEC hydrogel (Chapter VI of this thesis). It has been reported that PEC hydrogels have poor hydrolytic stability since they are dependent on the physicochemical properties of the environment. Thus, in order to obtain a stable fibrous hydrogel, MeGG was photocrosslinked by UV exposure, stabilizing the fibrous hydrogel. Given the small dimensions of these fibers they were collected onto siloxane treated glass slides (TMSPMA glass slides) (Figure VII.1.A). The presence of siloxane groups on the treated glass slide allowed the methacrylated polymer to covalently bond to it, facilitating the handling and the cell culture studies of this fibrous hydrogel. The reported fluidic system allowed to produce aligned structures, as observed in Figure VII.1.B, in contrast with the randomly formed fibers when both polymers were mixed outside a channel (Figure VII.1.C). Since the pH of the solutions of both polymers was different, we examined the possibility of the formation of the fibrous hydrogel due to the precipitation of one of the polymers as a result of pH change. To rule out this possibility, MeGG was allowed to interact with an acetic acid solution (1% v/v) without CHT while in another experiment, CHT solution in acetic acid was allowed to interact with deionized water without MeGG. For both cases where one of the polymers was replaced only with the solvent, no fibers were formed. This result confirmed that the formation of the fibers is uniquely a result of the complexation of both polymers.
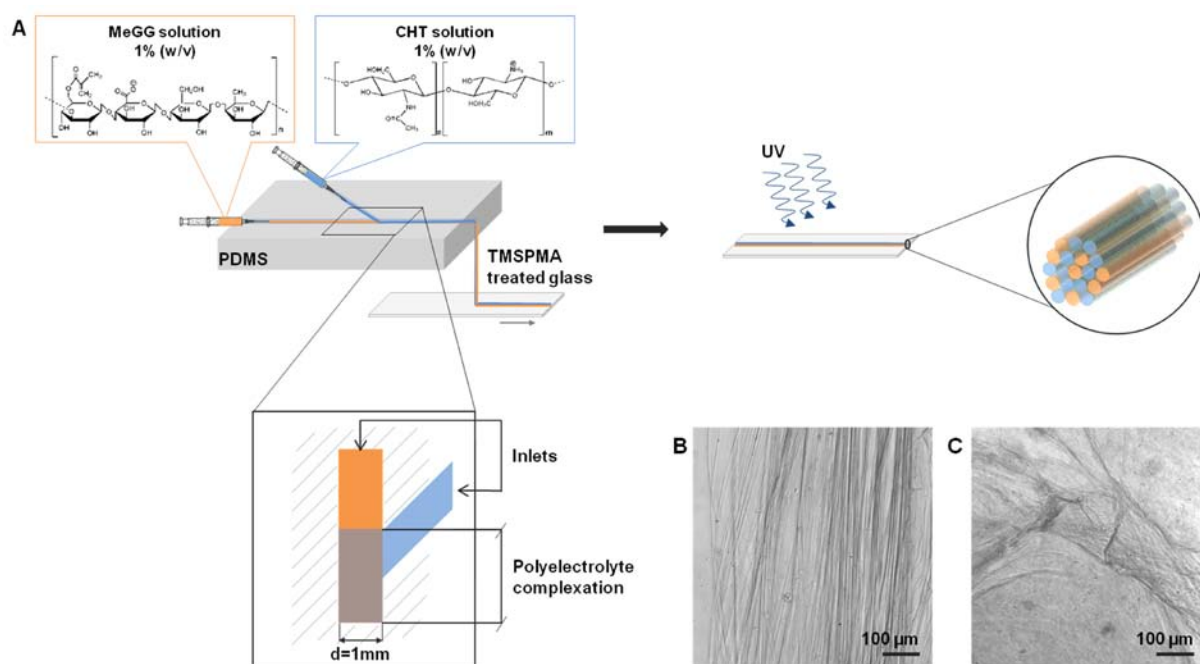
Figure VII.1. Fabrication of an aligned fibrous hydrogel. (A) Schematics of fabrication of hydrogel fiber bundle with methacrylated gellan gum (MeGG) and chitosan (CHT). Both solutions are flowed through separate channels within the PDMS mold. In the region where both solutions meet, complexation of the polyelectrolytes occurs. The hydrogel fiber bundle is collected onto a TMSPMA treated glass slide and MeGG crosslinked with UV light. (B) Optical microscopy images of aligned engineered hydrogel fiber bundles and (C) optical microscopy images of unaligned fibers, obtained by mixing both polymers randomly.

We next examined the distribution of both polymers within the fibrous hydrogel system. CHT was fluorescently labeled with fluorescein in a reaction depicted in Figure VII.S1 (in the appendix of the present chapter). The distribution of CHT in the hydrogel fiber bundle was evaluated by producing fibrous hydrogels as described above using MeGG and fluorescein-CHT. Confocal microscopy of fluorescently labeled CHT (Figure VII.2.A) in the xyz planes of the fiber bundle showed that CHT was present throughout the fibrous hydrogel, as expected. Using the same fluorescent system, we evaluated the stability of the fibrous hydrogel. Optical and fluorescent microscopy revealed that fluorescein-CHT was present even after 7 days when the fibrous hydrogel was incubated in phosphate buffer saline (PBS) at 37 °C (Figure VII.2.B). This showed that, although only MeGG is covalently bonded to the treated glass slide, CHT is kept within the system for up to 7 days. These observations suggest that the electrostatic interactions between MeGG and CHT are strong enough, not only to form the fibrous hydrogel, but also to hold both polymers together in a stable system after 7 days.
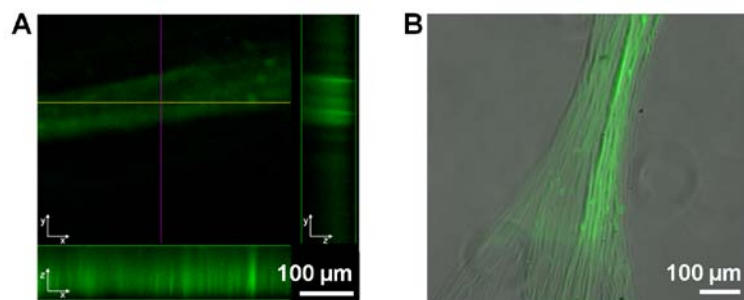
Figure VII.2. Distribution of both polyelectrolytes within the hydrogel fiber bundle. (A) Confocal image of the distribution of fluorescein-CHT within the hydrogel. (B) MeGG-CHT hydrogel fiber bundle with fluorescein-labeled CHT after incubation in PBS for 7 days at 37 ºC.

We further evaluated the microstructure of the hydrogel fibers. The micro-scale structure of the fibrous hydrogel showed a similar organization to that observed in natural collagen fibers. Scanning electron microscopy (SEM) of the top and side views of the system revealed that the fibrous hydrogel is constituted by several fibrils aligned in parallel and packed together in a bundle (Figure VII.3.A and B). The diameter of the fiber under the top view was larger than that observed in the side view. This may be caused by the spreading of this aqueous system once it was collected onto the treated glass slide. The morphology of the fibrous hydrogel was further confirmed by atomic force microscopy (AFM), indicating that the fibril size varied from 1 to 5 µm (Figure VII.3.C). As in natural collagen fibers, we could observe a hierarchical organization of several fibrils assembled into a fiber. This structure, although architecturally similar to the natural one, is considerably larger than that observed in human tissues [35]. This was expected, since the channels of the fluidic system were 1 mm in diameter; however, other dimensions of fibers may be obtained by modulating the channel diameter.
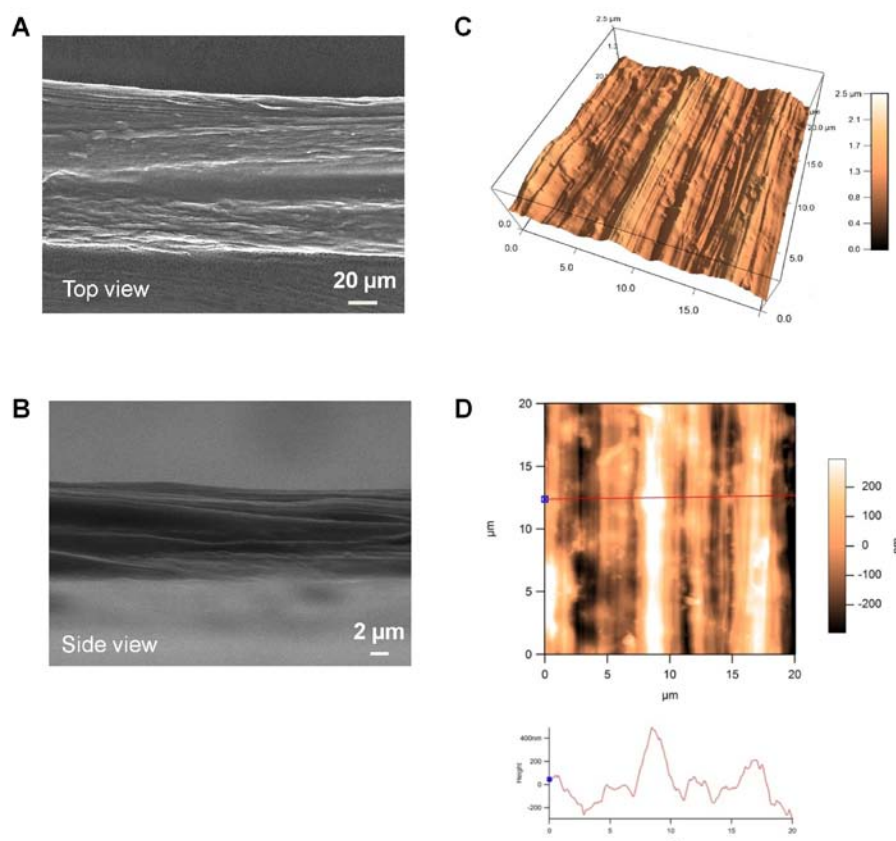
Figure VII.3. Characterization of aligned hydrogel fiber bundle. Scanning electron microscopy of the (A) top and (B) side views of the hydrogel fibers. (C) 3D atomic force microscopy of the hydrogel fiber bundle. (D) Height image of the hydrogel fibers and respective cross-section.

Of interest is the structure of the hydrogel fiber bundle analyzed at the nano-scale. Transmission electron microscopy (TEM) performed in transversal cross-sections of the fibrous hydrogel showed the presence of several circular structures packed together into a more complex structure (Figure VII.4). This result showed that a hierarchical organization observed at a micro-scale is also present at a smaller scale on the engineered fibers. The full structural hierarchy of the collagen fibers was recapitulated by the presence of D-periodic bands, observed under TEM of the longitudinal section of the fibrous hydrogel. Interestingly, the size of this periodic band is just slightly higher ($D\approx100$ nm) than that reported for natural collagen fibers ($D=67$ nm) [8], whereas D-periodic bands reported when using self-assembling peptides were in the range of 18 nm [21]. As seen from TEM micrographs, the well defined periodic light and dark patterns were present along the fiber axis and across the entire width, orthogonal to the longitudinal fiber axis. In natural collagen, these features occur as a result of the staggered repetition of tropocollagen molecules, linearly self-assembled by electrostatic interactions and laterally packed through hydrogen bonds and hydrophobic forces [8]. Similarly, the results herein obtained suggest that the observed striations

correspond to the longitudinal repetition of polymer chains along the fiber main axis. This might be a result of the similar molecular configuration of both CHT and MeGG to the natural collagen molecules. The proposed structure for hydrated CHT chains is a 2-fold helix stabilized by two hydrogen bonds, one intra- and another inter-molecular [36]. On the other hand, plain GG molecular structure was proposed as a left-handed double helix, stabilized with three intra-chain hydrogen bonds per tetrasaccharide unit, involving the glucuronate residue. The double helix is further stabilized by another three inter-chain hydrogen bonds in the interior of the molecule [37]. We propose a mechanism for the presence of striations perpendicular to the fiber axis. We hypothesize that the chains of MeGG and CHT are staggered linearly by electrostatic interactions occurring between the charged carboxylic acid of MeGG and the protonated amine of CHT. The polymeric chains might assemble laterally by the effect of hydrogen bonds. The stabilization of the fibrous hydrogel is further achieved by photocrosslinking of the MeGG and thus covalently bonding parallel chains of complexed MeGG. To the best of our knowledge, the level of architectural organization that we have observed has not yet been reported for other polysaccharides. Mimicry of the hierarchical structure of native collagen fibers by directing the self-assembly of two polysaccharides in a relative simple hydrogel system is of extreme importance for several biomedical and biotechnological applications. Of relevance is that this system can be used to fabricate fibrous hydrogels using other polysaccharides, possibly more relevant for other applications. However, the selected polysaccharides must present a minimum of common characteristics shared with the present system. Of extreme importance is to have two polysaccharides with opposite charges and that the pH of the solutions is compatible with the pKa values of both polymers. Another important requirement is the ability of the polymers to stabilize the structure through the establishment of hydrogen bonds. We also believe that the similarity of the molecular configuration in α-helix of the polymers to the collagen molecule might positively influence the formation of the striations.
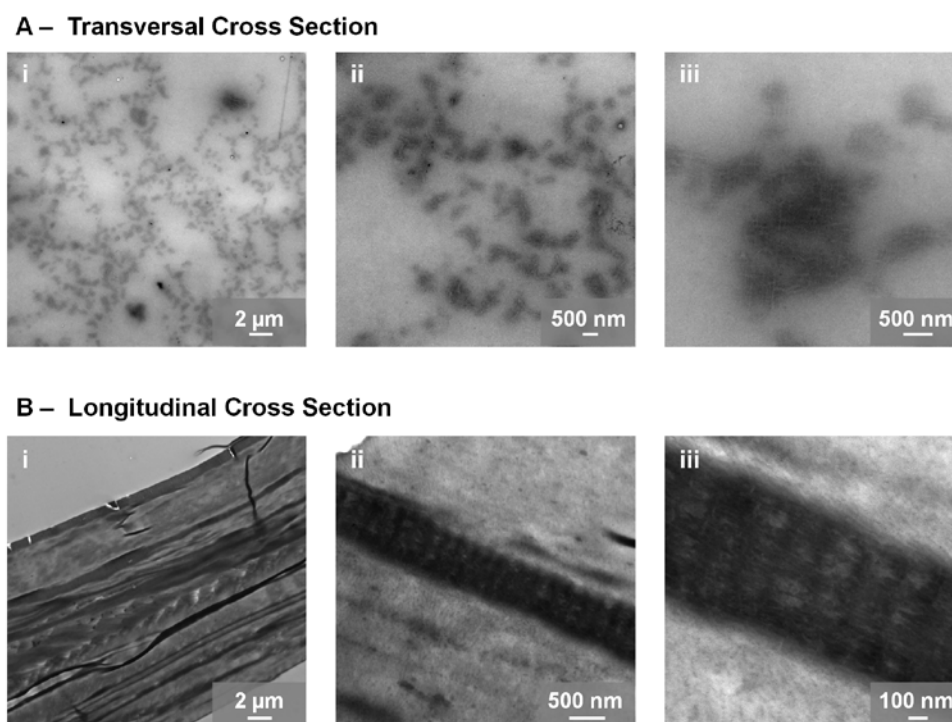
Figure VII.4. Characterization of the nano-structure of the fibrils. Transmission electron micrographs of (A) transversal and (B) longitudinal cross-sections of the hydrogel fibers bundles.

Although well characterized morphologically, peptide-based systems have a limited number of publications regarding the biological performance. Thus, most of the work related to cell alignment in collagen-like systems has been performed typically by culturing cells onto electrospun fibers. Herein we explored the effect of the aligned fibrils on directing the orientation of encapsulated fibroblasts isolated from rat cardiac tissue. A closer system to biological matrices was achieved by covalently incorporating cell adhesive motifs (RGD) into the MeGG backbone (Figure VII.S3 in the appendix of the present chapter). The presence of carboxylic groups on MeGG and of amino groups on CHT will allow introduction of nearly any biomolecule in the fibril system to optimize the biological performance in specific biomedical applications. After dissolving the MeGG-RGD polymer, the cells were dispersed into the solution at physiological temperature (36 ºC), allowed to flow through the PDMS channel and exposed to UV light for the stabilization of the PEC fibrous hydrogel (Figure VII.5.A). The encapsulated cells exhibited viability (Figure VII.5.B) after fiber processing, suggesting that the shear stress induced by the fluidic channel, the UV exposure and the slight acidic pH of the CHT solution did not cause any major deleterious effect on the viability of the fibroblasts. This result suggests that the MeGG provides a protective shield around the encapsulated cells. Confocal microscopy analysis of the encapsulated cells demonstrates that the cells are able to adhere and spread along the fibril direction (Figure VII.5.C). Previous studies from the

literature shown that fibroblasts encapsulated in partially constrained hydrogels, tend to align parallel to the free edges [38]. Accordingly, we hypothesize that the actin filaments of the fibroblasts isolated from rat cardiac tissue preferentially orient along the contact points of the hydrogel fibrils.
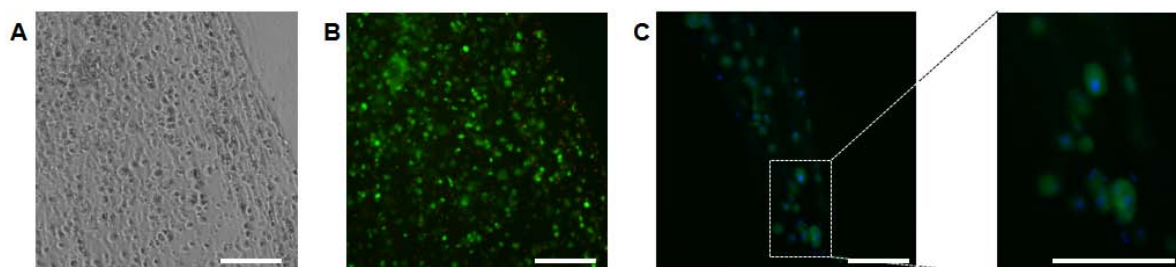

Figure VII.5. Encapsulation of rat cardiac fibroblasts into the fibrous hydrogel. (A) Phase micrograph of the rat cardiac fibroblasts encapsulated into the fibrous hydrogel. (B) Live (green) and Dead (red) staining of encapsulated rat cardiac fibroblasts after 7 days of culture. (C) Cytoskeleton (phalloidin, green) and nuclei (Hoechst, blue) staining of encapsulated rat cardiac fibroblasts after 7 days of culture. Scale bar: 100 µm.

4. CONCLUSIONS

We have described the fabrication of a fibrous hydrogel that replicates the hierarchical structure of natural collagen fibers up to the nanoscale. A simple method that combines the properties of two oppositely charged polyelectrolytes and the use of a fluidic channel to extrude the solution was successfully demonstrated. A fibrous hydrogel was engineered by the combination of the anionic MeGG and the cationic CHT through two confluent PDMS channels. At the channel junction, polymer chains of MeGG interacted with polymer chains of CHT. The engineered structure self-organized into a bundle of microfibrils at the micro-scale. The natural features at the nano-scale of collagen fibers were also replicated into the engineered fibrous hydrogel as demonstrated by the presence of periodic *D*-bands ($D\approx100nm$), although not exactly with the same dimensions. We have proposed a mechanism for the formation of these striations. We hypothesize that, following a similar mechanism than the one occurring in natural fibers, polymeric chains of MeGG and CHT self-assemble linearly and parallelly in a mechanism driven by electrostatic interactions, being the structure stabilized by hydrogen bonds. Furthermore, by this method we showed the viability of encapsulated rat cardiac fibroblasts. Although our work was focused on the mechanism of interaction of CHT and MeGG polyelectrolytes, other polyelectrolyte materials with similar molecular structures may show analogous behavior. From all parameters that might influence this interaction, the polymer charge is probably the most important. We

emphasize the unique property of our photocrosslinkable polymer MeGG allowing to tuning the properties of this material and therefore, to change the properties and the range of possible applications of the fibers. Our bundle of fibers is potentially useful for a variety of systems, mimicking the ultrastructure and hierarchical properties of collagen, from collagen fibers in neural tissues to bone.

REFERENCES

1.   Kim D-H, Lipke EA, Kim P, Cheong R, Thompson S, Delannoy M, Suh K-Y, et al. Nanoscale cues regulate the structure and function of macroscopic cardiac tissue constructs. Proceedings of the National Academy of Sciences of the United States of America 2010;107(2):565-570.
2.   Finlay HM, McCullough L, Canham PB. 3-Dimensional Collagen Organization of Human Brain Arteries at Different Transmural Pressures. J Vasc Res 1995;32(5):301-312.
3.   Weiner S, Wagner HD. The material bone: Structure mechanical function relations. Annual Review of Materials Science 1998;28:271-298.
4.   Prost-Squarcioni C, Fraitag S, Heller M, Boehm N. Functional histology of dermis. Ann Dermatol Venereol 2008;135(1):S5-S20.
5.   Myllyharju J, Kivirikko KI. Collagens and collagen-related diseases. Ann Med 2001;33(1):7-21.
6.   Gelse K, Poschl E, Aigner T. Collagens - structure, function, and biosynthesis. Advanced Drug Delivery Reviews 2003;55(12):1531-1546.
7.   Hodge A, Petruska J. Recent studies with the electron microscope on ordered aggregates of the tropocollagen macromolecule. In: Ramachandran G, editor. Aspects of Protein Structure. London: Academic, 1963. p. 289–300.
8.   Shoulders MD, Raines RT. Collagen Structure and Stability. Annual Review of Biochemistry, 2009. p. 929-958.
9.   Martins A, da Silva MLA, Faria S, Marques AP, Reis RL, Neves NM. The Influence of Patterned Nanofiber Meshes on Human Mesenchymal Stem Cell Osteogenesis. Macromolecular Bioscience 2011;11(7):978-987.
10.   Hwang CM, Khademhosseini A, Park Y, Sun K, Lee S-H. Microfluidic chip-based fabrication of PLGA microfiber scaffolds for tissue engineering. Langmuir 2008;24(13):6845-6851.
11.   Przybyla DE, Chmielewski J. Higher-Order Assembly of Collagen Peptides into Nano- and Microscale Materials. Biochemistry 2010;49(21):4411-4419.
12.   Zhang SM, Greenfield MA, Mata A, Palmer LC, Bitton R, Mantei JR, Aparicio C, et al. A self-assembly pathway to aligned monodomain gels. Nature Materials 2010;9(7):594-601.
13.   Soliman S, Sant S, Nichol JW, Khabiry M, Traversa E, Khademhosseini A. Controlling the porosity of fibrous scaffolds by modulating the fiber diameter and packing density. Journal of Biomedical Materials Research Part A 2011;96A(3):566-574.
14.   Sant S, Hwang CM, Lee SH, Khademhosseini A. Hybrid PGS-PCL microfibrous scaffolds with improved mechanical and biological properties. Journal of Tissue Engineering and Regenerative Medicine 2011;5(4):283-291.
15.   Hwang CM, Park Y, Park JY, Lee K, Sun K, Khademhosseini A, Lee SH. Controlled cellular orientation on PLGA microfibers with defined diameters. Biomedical Microdevices 2009;11(4):739-746.
16.   Hu M, Deng R, Schumacher KM, Kurisawa M, Ye H, Purnamawati K, Ying JY. Hydrodynamic spinning of hydrogel fibers. Biomaterials 2010;31(5):863-869.
17.   Papapostolou D, Smith AM, Atkins EDT, Oliver SJ, Ryadnov MG, Serpell LC, Woolfson DN. Engineering nanoscale order into a designed protein fiber. Proceedings of the National Academy of Sciences of the United States of America 2007;104(26):10853-10858.
18.   Yeates TO, Padilla JE. Designing supramolecular protein assemblies. Curr Opin Struct Biol 2002;12(4):464-470.
19.   Seeman NC. Biochemistry and structural DNA nanotechnology: An evolving symbiotic relationship. Biochemistry 2003;42(24):7259-7269.
20.   Wan ACA, Liao IC, Yim EKF, Leong KW. Mechanism of fiber formation by interfacial polyelectrolyte complexation. Macromolecules 2004;37(18):7019-7025.
21.   Rele S, Song Y, Apkarian RP, Qu Z, Conticello VP, Chaikof EL. D-periodic collagen-mimetic microfibers. Journal of the American Chemical Society 2007;129(47):14780-14787.
22.   Woolfson DN, Ryadnov MG. Peptide-based fibrous biomaterials: some things old, new and borrowed. Current Opinion in Chemical Biology 2006;10(6):559-567.
23.   Tai BCU, Wan ACA, Ying JY. Modified polyelectrolyte complex fibrous scaffold as a matrix for 3D cell culture. Biomaterials 2010;31(23):5927-5935.
24.   Coutinho DF, Sant SV, Shin H, Oliveira JT, Gomes ME, Neves NM, Khademhosseini A, et al. Modified Gellan Gum hydrogels with tunable physical and mechanical properties. Biomaterials 2010;31(29):7494-7502.

25. Oliveira JT, Martins L, Picciochi R, Malafaya PB, Sousa RA, Neves NM, Mano JF, et al. Gellan Gum: A New Biomaterial for Cartilage Tissue Engineering Applications. Journal of Biomedical Materials Research-Part A 2010.

26. de Campos AM, Diebold Y, Carvalho ELS, Sanchez A, Alonso MJ. Chitosan nanoparticles as new ocular drug delivery systems: in vitro stability, in vivo fate, and cellular toxicity. Pharmaceutical Research 2004;21(5):803-810.

27. Hwang CM, Sant S, Masaeli M, Kachouie NN, Zamanian B, Lee SH, Khademhosseini A. Fabrication of three-dimensional porous cell-laden hydrogel for tissue engineering. Biofabrication 2010;2(3).

28. Li LH, Wu JD, Gao CY. Gradient immobilization of a cell adhesion RGD peptide on thermal responsive surface for regulating cell adhesion and detachment. Colloid Surf B-Biointerfaces 2011;85(1):12-18.

29. Khademhosseini A, Eng G, Yeh J, Kucharczyk PA, Langer R, Vunjak-Novakovic G, Radisic M. Microfluidic patterning for fabrication of contractile cardiac organoids. Biomedical Microdevices 2007;9(2):149-157.

30. Ii'ina AV, Varlamov VP. Chitosan-based polyelectrolyte complexes: A review. Applied Biochemistry and Microbiology 2005;41(1):5-11.

31. Lawrie G, Keen I, Drew B, Chandler-Temple A, Rintoul L, Fredericks P, Grondahl L. Interactions between alginate and chitosan biopolymers characterized using FTIR and XPS. Biomacromolecules 2007;8(8):2533-2541.

32. Deng C, Zhang PC, Vulesevic B, Kuraitis D, Li FF, Yang AF, Griffith M, et al. A Collagen-Chitosan Hydrogel for Endothelial Differentiation and Angiogenesis. Tissue Engineering Part A 2010;16(10):3099-3109.

33. Oliveira JT, Santos TC, Martins L, Picciochi R, Marques AP, Castro AG, Neves NM, et al. Gellan Gum Injectable Hydrogels for Cartilage Tissue Engineering Applications: In Vitro Studies and Preliminary In Vivo Evaluation. Tissue Engineering Part A 2009;16(1):343-353.

34. Grasdalen H, Smidsrod O. Gelation of Gellan Gum. Carbohydrate Polymers 1987;7(5):371-393.

35. Buehler M. Molecular architecture of collagen fibrils: A critical length scale for tough fibrils. Current Applied Physics 2008;8:440-442.

36. Franca E, Lins R, Freitas L, Straatsma T. Characterization of Chitin and Chitosan Molecular Structure in Aqueous Solution. J Chem Theory Comput 2008;4:2141–2149.

37. Chandrasekaran R, Millane R, Arnott S, Atkins E. The crystal structure of gellan gum. Charbohydrate Research 1988;175:1-15.

38. Aubin H, Nichol JW, Hutson CB, Bae H, Sieminski AL, Cropek DM, Akhyari P, et al. Directed 3D cell alignment and elongation in microengineered hydrogels. Biomaterials 2010;31(27):6941-6951.

APPENDIX

Supplementary Figure VII.S1

Figure VII.S1 shows a schematic representation of the chemical reaction followed to produce fluorescein-labeled CHT. Fluorescein-CHT was used for analyzing the distribution of CHT throughout the fibrous hydrogel, as depicted in Figure VII.2.
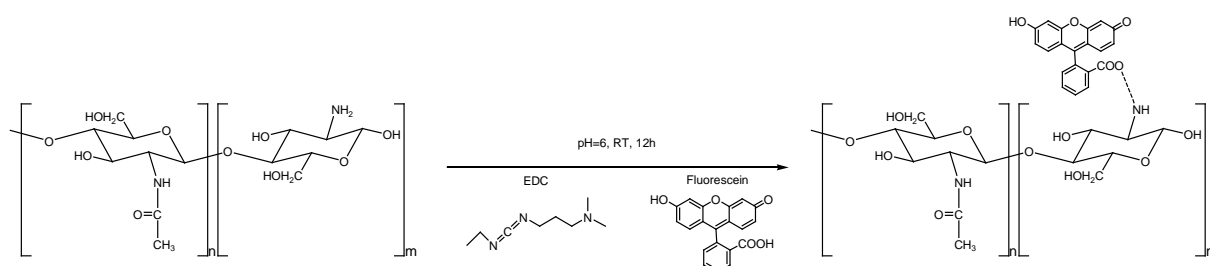
Figure VII.S1. Schematic representation of the chemical reaction for producing fluorescein-labeled CHT (fluorescein-CHT).

Supplementary Figure VII.S2

Zeta potential of CHT and MeGG solutions was measured in order to evaluate the initial charged states of both solutions. The analysis of the charged states of the solutions in their initial states helped on analyzing the interactions between both solutions.

Figure VII.S2. Zeta potential (mV) of the initial solutions of CHT and MeGG.

Supplementary Figure VII.S3

The biofunctionalization of the hydrogel fiber bundle was achieved by covalently attaching RGD motifs to the MeGG backbone. Figure VII.S3.A shows the chemical reaction followed for obtaining MeGG-RGD. X-ray photoelectron spectroscopy (Kratos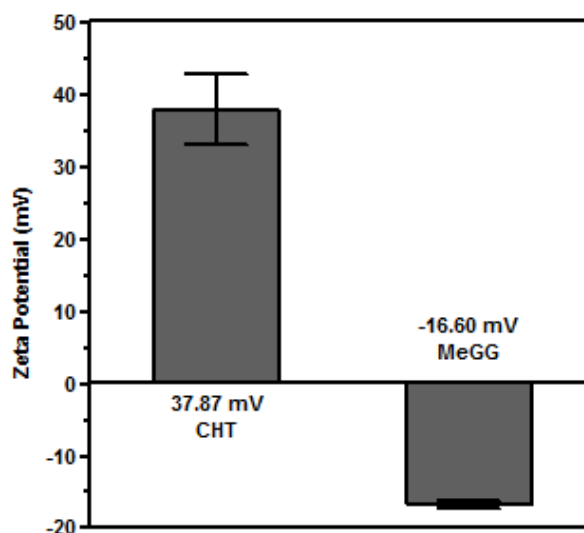 Axis Ultra XPS instrument using a monochromatic Al Kα X-ray source operating at 15 kV and 10 mA) was performed to the modified and non-material in order to evaluate changes in the atomic percentages of carbon, oxygen and nitrogen elements. The elements in the sample surface were identified from a survey spectrum at pass energy of 160 eV. The areas under the specific peaks were used to calculate the atomic percentages. Figure VII.S3.B shows the presence of nitrogen species only in the modified material with RGD, as expected, since plain MeGG does not present any nitrogen group. In order to evaluate the functionality of the modified material, rat cardiac fibroblasts were seeded onto freshly prepared MeGG-RGD hydrogels. Phalloidin/Hoechst staining of the actin filaments and nucleus of the seeded cells showed the presence of a monolayer of rat cardiac fibroblasts on the MeGG-RGD material, while no cells were visualized on the plain MeGG (Figure VII.S3.C). The synthesized material was used for encapsulation of rat cardiac fibroblasts within the hydrogel fibers, as depicted in Figure VII.5.

A

B

XPS elemental analysis

Materials	C_{1s}(%)	O_{1s}(%)	N_{1s}(%)
MeGG	70.59	29.41	
MeGG-RGD	67.18	30.89	1.93

C

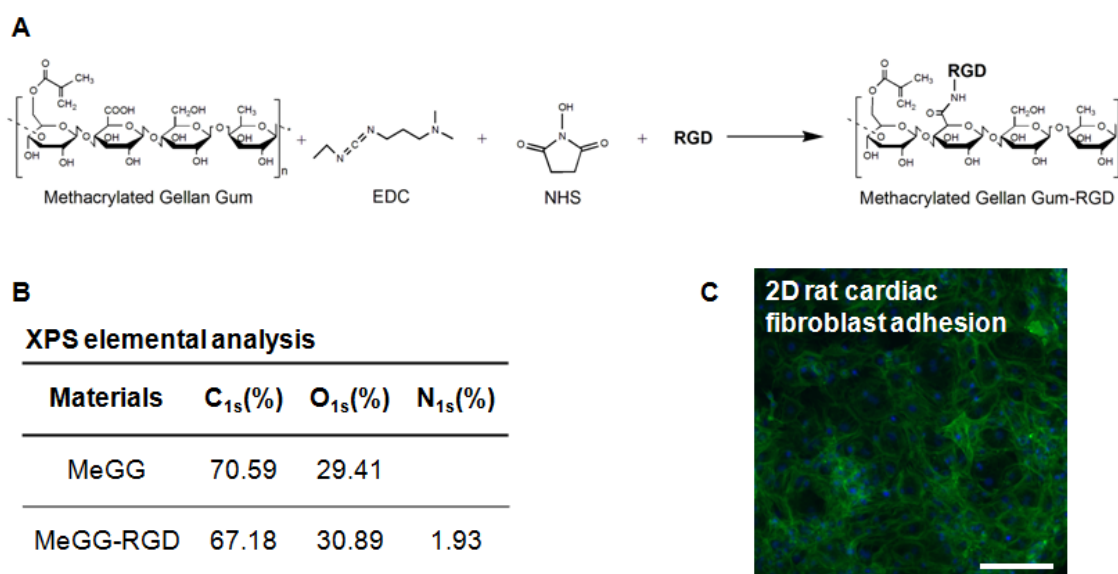**Figure VII.S3.** Synthesis of MeGG-RGD. (A) Chemical reaction. (B) Elemental analysis of modified MeGG-RGD by XPS. (C) Phalloidin and Hoechst staining, respectively, of the actin and nucleus of rat cardiac fibroblasts cultured on the surface (2D) of MeGG-RGD hydrogel after 48 hours of culture (Scale bar: 100 μm).

Section 5

DISCUSSION OF THE THESIS CONCLUSIONS AND OUTLOOK

Chapter VIII

GENERAL CONCLUSIONS AND FINAL REMARKS

Micro and nanofabrication technologies coupled with advances in materials chemistry have allowed for progresses in the development of biomaterials with controlled spatial microenvironments. Top-down approaches have been successful in combining different cues (biochemical, structural and cellular) of tissue microenvironments in a single biomaterial. On the other hand, bottom-up approaches have been fine-tuning the spatial organization of these bioactive cues. In this thesis, several techniques were developed to engineer different aspects of tissue microenvironments. Structural, biochemical and cellular cues were integrated in different biomaterials, yielding novel substrates with improved properties. The reasoning for using such approaches is that by mimicking the native features of the tissue microenvironment, one can match more closely the function of the biomaterial with the function of native tissues.

Micropatterned surfaces have shown to influence the behavior of different cell types, such as cell attachment, migration and differentiation. Thus, the development of biomimetic surfaces that could be used either as membranes or integrated in previously developed scaffolds is of great importance for the success of an implant. In this thesis, biomimetic surfaces at a microscale were developed using a polyester widely studied at the 3B's Research Group. Engineered surfaces of poly(butylene succinate) (PBS) showed to successfully direct the orientation of human adipose stem cells along the micropatterned features of PBS, dictating their orientation. In contrast, cells appeared to be randomly oriented on non-patterned surfaces. Moreover, the ability to microfabricate twenty patterned surfaces with different groove/ridge features indicated the possibility to custom-engineer biomimetic surfaces with different architectures using PBS polymer. This system could potentially be used as an *in vitro* model for studying the biological performance in different patterned surfaces, and the lessons learnt could be incorporated into the design of scaffolds for tissues with specific architectures.

In contrast to inducing a specific cell behavior, some tissue engineering approaches require the protection and delivery of bioactive materials. For that, the production of polymeric microcapsules, capable of engulfing and protecting the encapsulated drug/cell comes as a useful approach. Some of the major hurdles in the fabrication of microcapsules are that: 1) systems are optimized for specific materials/applications, 2) it is difficult to obtain reproducible spherical capsules, and 3) it is complex to obtain, using the same system, microcapsules with different sizes. In this thesis, a system based on the use of two distinct

phases was applied for the production of reproducible microcapsules with diameters ranging from 270 to 600 μm, simply by changing the system parameters. The automated system allowed for the permanent formation and stabilization of the microcapsules in the same system, without requiring external intervention. The potential of the system for different applications was further demonstrated by encapsulating fluorescent beads, cell suspensions (NIH-3T3 cells) and cell aggregates (pseudo-islets of MIN6 cell aggregates) into gellan gum (GG) microcapsules. GG is a polysaccharide that has been studied at the 3B's Research Group for different tissue engineering applications. Studies *in vivo* with this polymer have indicated that it is a good candidate especially for cartilage regeneration applications.

In the previous, as well as in the majority of the existent strategies in tissue engineering, once implanted, hydrogels might have an inconsistent behavior. Most of the hydrogels studied have an ionotropic behavior, which means that their physical structure is dependent on the amount and type of ions present in the surrounding environment. Thus, when implanted, the strong bonds previously established for their formation could be disrupted and replaced by weaker ones, leading to the hydrogel disintegration. To solve this problem, GG was chemically modified in order to incorporate C=C bonds, making this material amenable to be crosslinked by ultraviolet light (UV) and thus to be microfabricated. The modification was accomplished by using methacrylic anhydride (MA), yielding a methacrylated gellan gum (MeGG) hydrogel crosslinkable not only by physical but also by chemical mechanisms. As a result, hydrogels with highly tunable mechanical, swelling and degradability properties could be produced by selecting the appropriate crosslinking mechanisms of the hydrogel. Moreover, the physiologically compatible crosslinking methods used make this hydrogel a good candidate for a wide range of tissue engineering applications.

Blending two materials comes as a useful strategy for some applications since it gives the possibility of taking advantage of the properties of both materials. Thus, in this thesis, MeGG was combined with a polysaccharide with opposite charge, resulting in a polyelectrolyte complex (PEC) with the properties of both polymers. Chitosan (CHT) was the selected natural polymer, given its high availability and reported biodegradability by enzymes. Similarly to what is observed with the ionotropic materials, once implanted, PEC hydrogels might lose their structural stability, if for instance, the pH of the implantation site decreases below the pKa value of the anionic polymer. Given this, the combination of CHT with MeGG, gave the possibility to stabilize the PEC structure by photocrosslinking MeGG. The ability to microfabricate these MeGG-CHT PEC hydrogels conferred additional stability and enabled the production of microgels with different shapes and sizes. Encapsulated rat cardiac fibroblasts remained viable, showing the potential of these PEC hydrogels to be used for different biomedical applications either as injectable systems or as building blocks for modular tissue engineering. Moreover, understanding the mechanisms behind MeGG-CHT

PEC hydrogel formation allows not only to tune the properties of the system for specific applications, but also to predict the behavior of systems where materials with similar properties are used. Controlling the degree of complexation, the interactions at a molecular level and the crosslinking of MeGG, would thus allow the development of customized hydrogels for different biomedical applications.

The integration of biochemical, cellular and structural cues within the same system was achieved by further processing MeGG-CHT PEC hydrogel through the combination of fluidics technology and materials chemistry. Cell adhesive motifs (RGD peptides) were covalently bonded to the MeGG backbone, in order to produce biomaterials with improved bioactive properties, demonstrating the potential to incorporate nearly any biomolecule to the system. The interaction of MeGG and CHT lead to the formation of a PEC hydrogel within a PDMS channel. The extrusion of this PEC resulted in the formation of a fibrous hydrogel with a hierarchical organization and structure similar to the collagen fibers in the human tissues in which cells were able to elongate. This similarity was achieved not only at a microscale, by the assembly into a bundle of microfibrils, but also at a nanoscale, through the presence of the typical periodic _D_-bands of collagen fibers. Although several systems based on the assembly of peptides have already been used for the fabrication of systems with this level of organization, they usually require laborious and expensive processes. In this thesis, a system based on easily available polysaccharides was reported that allows to promptly engineer these complex micro/nanostructures. Understanding the mechanism behind the formation of this fiber bundle allows not only tuning the system properties (polymer charges through variation of pH and degree of methacrylation/crosslinking of MeGG) in order to fabricate biomaterials for specific tissues/applications but also to predict the behavior of other polymers with similar molecular structures that might be relevant for other applications. However, further studies on the biological function of the system should be taken in order to fully evaluate the importance of the spatial organization over the function of the biomaterials.

The present thesis incrementally expanded the current scientific knowledge on the engineering of biochemical, structural and cellular cues onto biomaterials. Most of all, the work reported on this thesis shows that the combination of bottom-up and top-down approaches for the fabrication of micro and nanostructured materials can lead to the production of biomaterials with enhanced properties. However, it is still unclear the minimum level of spatial organization necessary to achieve fully functional biomaterials. The challenge lies on combining the focus of engineering and biology within the same approach. The best way to achieve this is to make use of the great advances made in microfabrication of biomaterials to answer important specific biological questions.